AD NUMBER
AD377973
CLASSIFICATION CHANGES
TO: unclassified
FROM: confidential
LIMITATION CHANGES
TO: Approved for public release, distribution unlimited
FROM: Distribution: Further dissemination only as directed by Federal Aviation Administration, Washington, DC, Jan 1964, or higher DoD authority.
AUTHORITY
FAA ltr, 10 Oct 1972; FAA ltr, 10 Oct 1972

CONFIDENTIAL

SUPERSONIC TRANSPORT

VOLUME A-V

AERODYNAMIC REPORT

LOCKHEED-CALIFORNIA COMPANY • A DIVISION OF LOCKHEED AIRCRAFT CORPORATION

JANUARY 15, 1964/LR 17324 LAC 410066

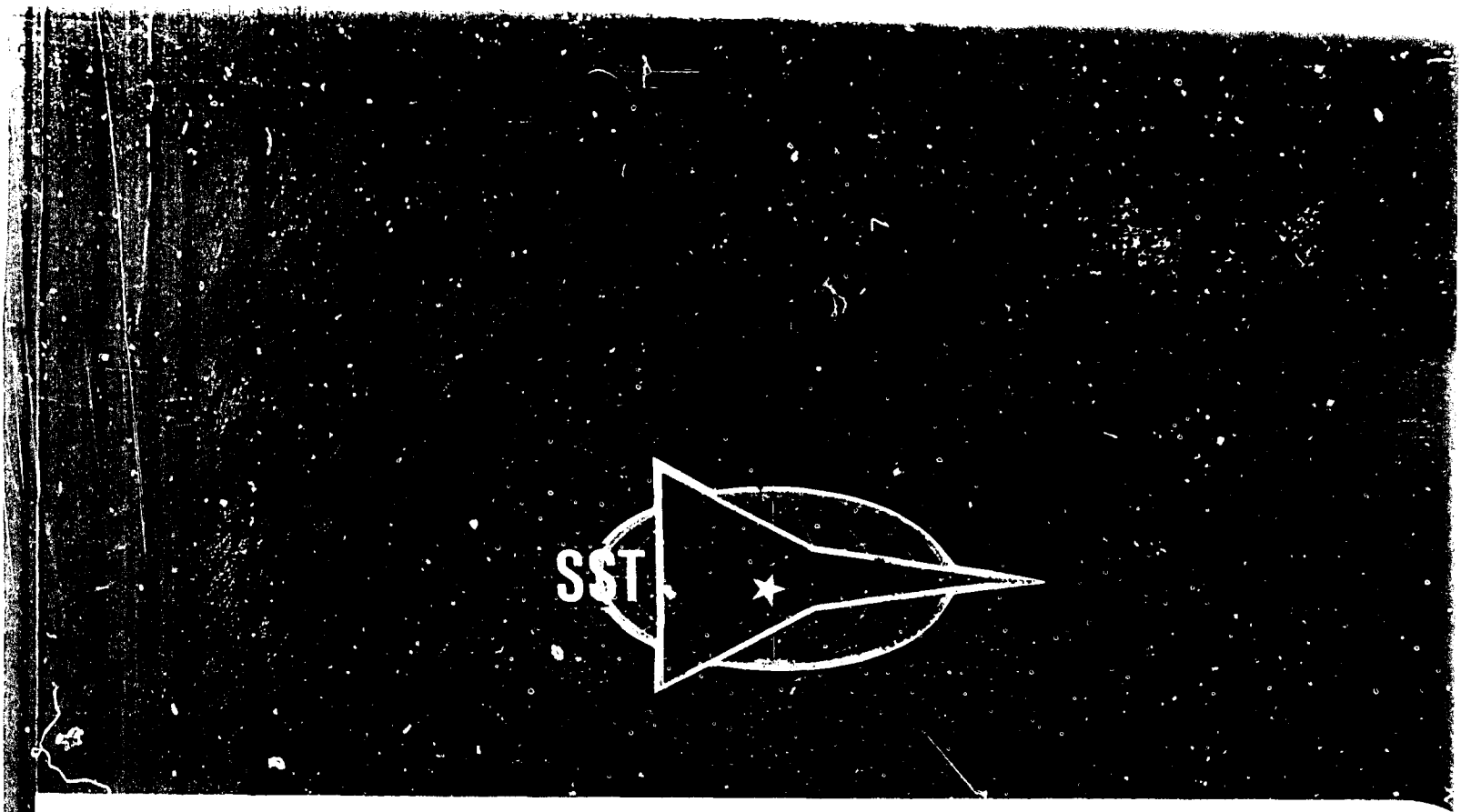

proposal for the

DEVELOPMENT OF A COMMERCIAL SUPERSONIC TRANSPORT

LR 17324 LAC 410066 /15 JANUARY 1964/LOCKHEED • CALIFORNIA COMPANY/BURBANK

CONFIDENTIAL

SECURITY MARKING

The classified or limited status of this report applies to each page, unless otherwise marked.
Separate page printouts MUST be marked accordingly.

THIS DOCUMENT CONTAINS INFORMATION AFFECTING THE NATIONAL DEFENSE OF THE UNITED STATES WITHIN THE MEANING OF THE ESPIONAGE LAWS, TITLE 18, U.S.C., SECTIONS 793 AND 794. THE TRANSMISSION OR THE REVELATION OF ITS CONTENTS IN ANY MANNER TO AN UNAUTHORIZED PERSON IS PROHIBITED BY LAW.

NOTICE: When government or other drawings, specifications or other data are used for any purpose other than in connection with a definitely related government procurement operation, the U. S. Government thereby incurs no responsibility, nor any obligation whatsoever; and the fact that the Government may have formulated, furnished, or in any way supplied the said drawings, specifications, or other data is not to be regarded by implication or otherwise as in any manner licensing the holder or any other person or corporation, or conveying any rights or permission to manufacture, use or sell any patented invention that may in any way be related thereto.

NOTICES

When Government drawings, specifications, or other data are used for any purpose other than in connection with a definitely related Government procurement operation, the United States Government thereby incurs no responsibility nor any obligation whatsoever; and the fact that the Government may have formulated, furnished, or in any way supplied the said drawings, specifications, or other data, is not to be regarded by implication or otherwise as in any manner licensing the holder or any other person or corporation, or conveying any rights or permission to manufacture, use, or sell any patented invention that may in any way be related thereto.

All distribution of this document is controlled. In addition to security requirements which apply to this document and must be met, it may be further distributed by the holder only with specific prior approval of:

Director of Supersonic Transport Development
Federal Aviation Agency
Washington, D. C. 20553

The distribution of this report is limited because it contains technology identifiable with items excluded from export by the Department of State (U. S Export Control Act of 1949, as amended).

February 4, 1964

ERRATA

VOLUME A-V AERODYNAMIC REPORT

1. Page 1-10, Figure 1-7:
   Change ordinate: RANGE-NAUTICAL MILES
   to: PAYLOAD-1000 LB.

2. Page 3-5, Figure 3-6:
   Change: ⊙ CONFIGURATIONS INVESTIGATED FOR STABILITY AND CONTROL
   to: NOTE - CONFIGURATIONS INVESTIGATED FOR STABILITY AND CONTROL:
   ⊙ GEAR DOWN
   ⊙ GEAR UP

3. Page 3-16, Table 3-6, opposite last item in Table, Turbine - in temperature °F (cruise), right-hand column under Wright Turbojet:
   Change: 2200
   to: 2000

4. Page 4-25, Table 4-5, bottom section:

   Change: $\left(\frac{L}{D}\right)_{max} = .613$ to: $\left(\frac{L}{D}\right)_{max} = 7.50$

   Change: $\frac{\Delta C_D}{C_L^2} = 7.50$ to: $\frac{\Delta C_D}{C_L^2} = .613$

5. Page 4-35, add figure number and title:

   FIGURE 4-45 TRANSONIC LONGITUDINAL STABILITY

6. Page 6-29, Figure 6-26, add second line to title:

   (DESCENT, OPERATIVE ENGINES AT FLIGHT IDLE)

7. Page 7-3, Figure 7-3, lower figure (M = 2.5 case)
   Add correction note: Due to a tracing error, Δ P overpressure as shown is incorrect and reads .15 psf high for all weights and altitudes shown for M = 2.5 case.

LOCKHEED CALIFORNIA COMPANY

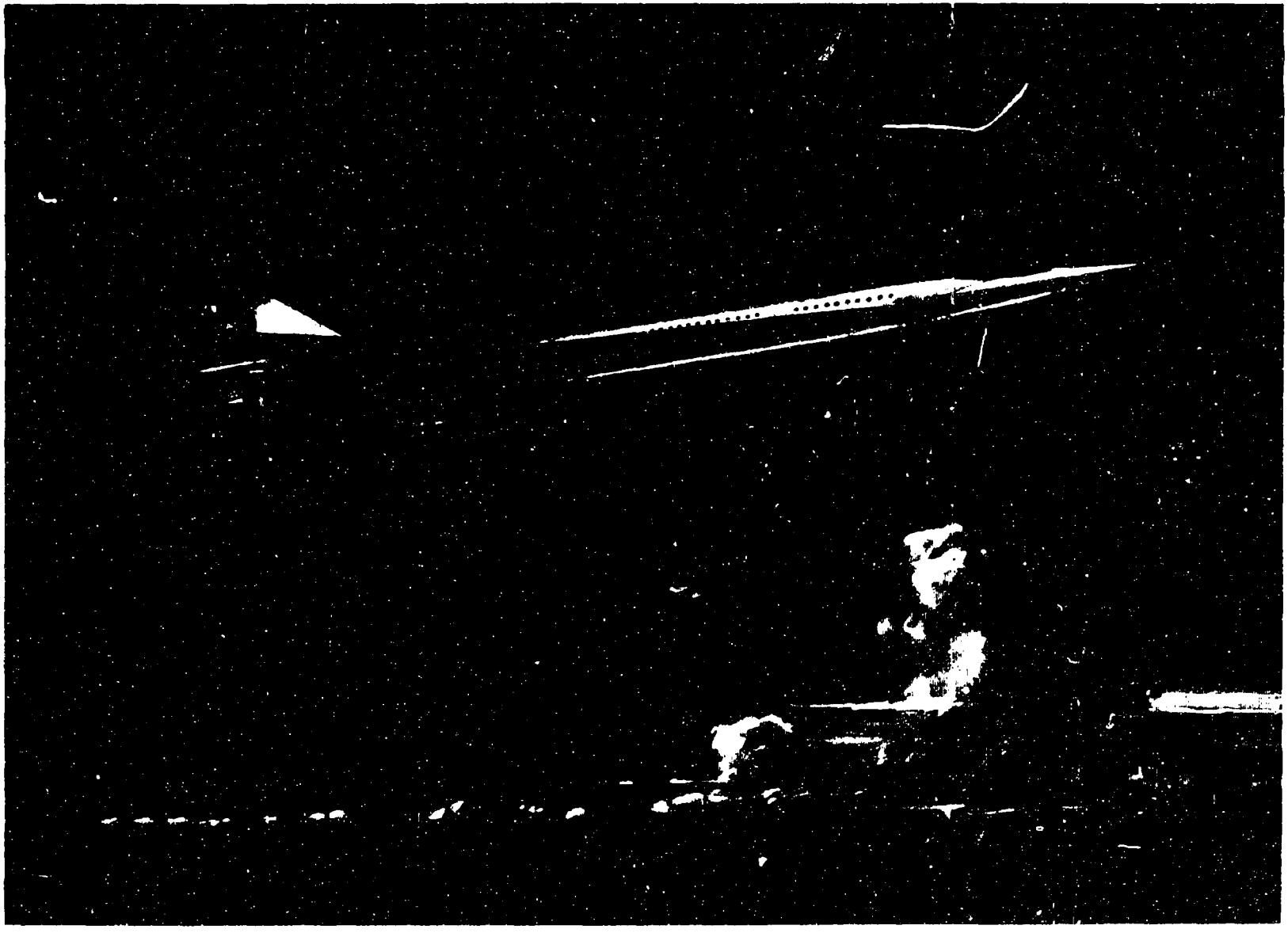

FOREWORD

Lockheed-California Company is pleased to submit this report as a portion of its proposal for the Development of a Commercial Supersonic Transport. The proposal is in response to the Federal Aviation Agency Request for Proposals, dated 15 August 1963, as amended by Addendum I, dated 14 October 1963, and Addendum II, dated 29 November 1963.

All volumes comprising the proposal are prepared in accordance with the FAA Request for Proposals, the Addenda, and the guidance resulting from the Bidders' Briefing on 5 September 1963.

Title and content of each proposal volume are in accordance with the Proposal Format of the RFP. For the convenience of the reviewer, section and subsection titles throughout the volumes are followed by the appropriate RFP reference number in parentheses.

The reports making up the total proposal are listed below, with the title of this volume printed in boldface type:

Volume	*Title*	*Lockheed Report No.*
I	Summary (5.0)	17319
A-I	Airframe Work Statement (3.2.1)	17320
A-II	Model Specification (3.2.2)	17321
A-III	Aircraft Description (3.2.3)	17322
A-IV	Structural Report (3.2.4 – 3.2.5)	17323
A-V	**Aerodynamic Report (3.2.6 – 3.2.8)**	**17324**
A-VI	Propulsion Report (3.2.9)	17325
A-VII	Systems Report (3.2.10 – 3.2.16)	17326
A-VIII	Ground Support Equipment Report (3.2.17)	17327
A-IX	Test and Certification Plan (3.2.18 – 3.2.20)	17328
A-X	Aircraft Mockup and Design Engineering Inspection Plan (3.2.21)	17329
M-I	Management (4.1 – 4.3)	17330
M-II	Management Controls (4.4 – 4.10)	17331
M-III	Product Support Plan (4.11.1 – 4.11.4)	17332
M-IV	Preliminary Production Plan (4.12 – 4.14)	17333
M-V	Development and Production Costs (4.15 – 4.17)	17334
M-VI	Direct Operating Costs (4.18.1 – 4.18.2)	17335
APPENDIX A	Alternate Economic Analysis (4.18.1)	17336

TABLE OF CONTENTS

TABLE OF CONTENTS (Cont)

TABLE OF CONTENTS (Cont)

LIST OF FIGURES

LIST OF FIGURES (Cont)

LIST OF FIGURES (Cont)

LIST OF FIGURES (Cont)

LIST OF FIGURES (Cont)

LIST OF FIGURES (Cont)

LIST OF FIGURES (Cont)

LIST OF FIGURES (Cont)

LIST OF TABLES

SECTION 1 SUMMARY

This report presents the aerodynamic characteristics, performance capabilities, and the stability and control of the Lockheed SST offered in response to the FAA Request for Proposal, dated August 15, 1963. The SST reflects eight years of aerodynamic study, involving continuous evaluation of aerodynamic data from all available sources, configuration analyses, specific wind tunnel tests of many design concepts, and integration of results with design, structure, and weight considerations. The fundamental need for airplane simplicity manifested itself as the major conclusion from this intensive effort. As the studies continued, the ways and means for achieving simplicity emerged.

During these investigations, more than one configuration concept proved capable of doing the SST job. In the final analysis, however, the concept offering the best combination of simplicity of design, maintenance, and operation characteristics will provide the least program risk and cost together with increased safety. The ability of the SST to employ a simple concept and provide the performance, handling qualities, and boom characteristics required for safe, economical supersonic operation is shown in this report.

The SST employs a large fixed wing of double delta planform, four individual underwing nacelles and a single aft fuselage vertical tail. The airplane does not incorporate either a canard or horizontal tail. The general arrangement is shown in Figure 1-1. A complete airplane description is given in Section 3. The unique feature of the design is the double delta planform, and it is this feature which has been exploited aerodynamically to achieve the ultimate in simplicity. This planform offers structural efficiency that allows for practical employment of large wing areas, and therefore light wing loadings. The large area provides improved lift-drag ratios; the light wing loadings and substantial ground effect obviate the need for high lift devices. The planform shape minimizes aerodynamic center shift over the Mach number range, and provides smooth transonic area progression curves that benefit both drag and sonic boom characteristics. The vortex flow field generated by the double delta shape enhances the directional stability characteristics. This planform provides these aerodynamic improvements with simple, structurally reliable fixed geometry.

Since the concept of the double delta supersonic transport is a recent development, availability of experimental data has not been extensive. For this reason detailed low speed and high speed wind tunnel tests have been conducted as part of this proposal to establish the findings discussed above. The aerodynamic data from these tests are presented in Section 4 of this report. The advantages of the double delta wing are demonstrated by these data.

These wind tunnel results indicate that the aerodynamic potential of this type of wing geometry has not yet been fully developed. Tests conducted to assess the benefits of using camber and twist to improve cruise L/D and trim drag characteristics indicate that while gains have been achieved in the wind tunnel to date, additional improvements can be obtained with further development testing. Current status wind tunnel results do not reflect the full capability of the airplane that can be expected by devoting continued research and development during Phase II. In Section 4 the aerodynamic characteristics as they are established to date, and those that can be realized at the end of the Phase II study program are shown and discussed. The performance characteristics of Section 5 and the stability and control characteristics of Section 6 are based on the developed airplane characteristics available by the end of Phase II.

All engines offered by the major U.S. engine companies were considered for the SST. Studies indicated a preference for the fan-type engine, because of operational flexibility and superiority in subsonic flight and airport noise characteristics. Three principal engine candidates were selected, the Pratt and Whitney JT11F-4 turbofan, the General Electric GE4/F6A turbofan and the Curtiss Wright TJ70A4 turbojet. These three powerplants offered the best overall potential after considering weight, performance, and

GL-823 CHARACTERISTICS

POWER PLANT - PRATT & WHITNEY JTF-9 @ 50,400 LBS. THRUST S.L.S

WEIGHTS

WRIGHT EMPTY	182,778 (190,575 OWE)
DESIGN USEFUL LOAD	259,425
DESIGN GROSS WRIGHT	450,000

	WING BASIC DELTA	WING TOTAL	VERTICAL TAIL
SPAN (IN.)	1392	1392	511 (FROM ℄ THRU TIP)
AREA (SQ. FT.)	7000	8370	578
ASPECT RATIO	1.72	1.61	44°
TAPER RATIO	.032	.036	.259
ROOT CHORD (IN.)	1327	2185	702
TIP CHORD (IN.)	121.5	121.5	182
M.A.C. (IN.)	892		538

CONTROL SURFACES

	ELEVATOR	INBD. ELEVON	OUTBD. ELEVON	AILERON	RUDDER (TOTAL)
SPAN (IN.)	94	88	99	124	270
AREA (SQ. FT.)	105	98	72	58	259.5
DEFLECTION LIMITS (DEG)	-30, +25	-35, +25	-35, +25	± 25	± 25

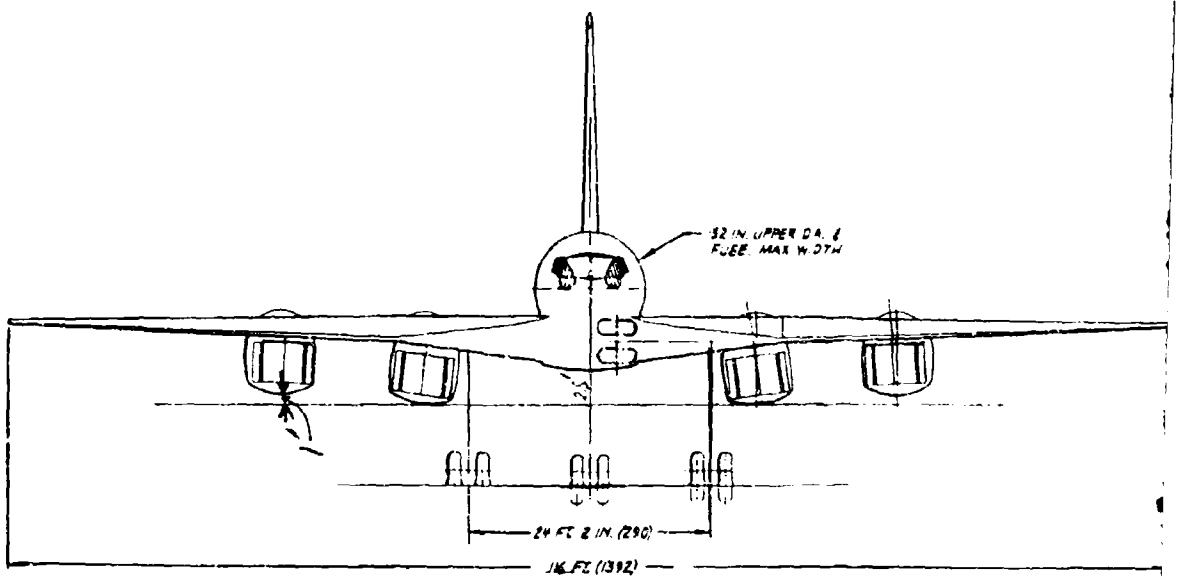

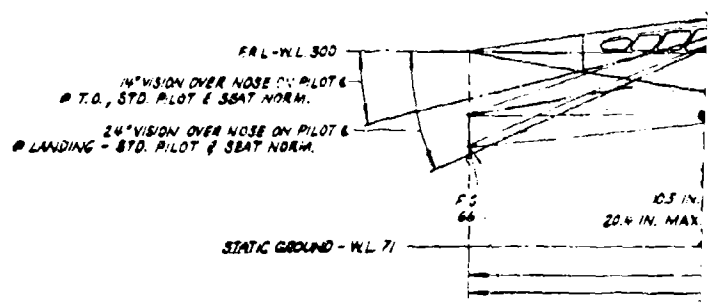

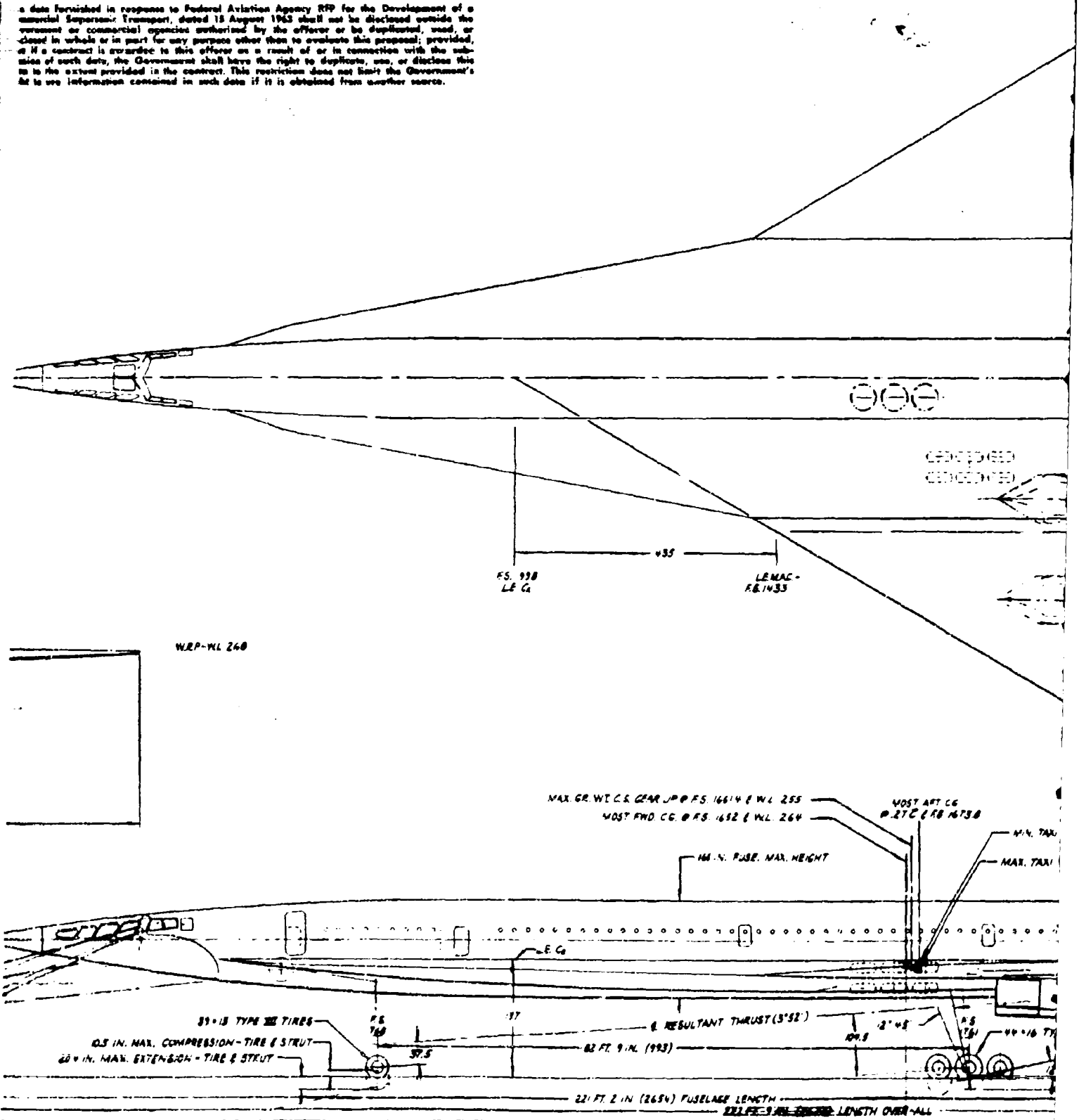

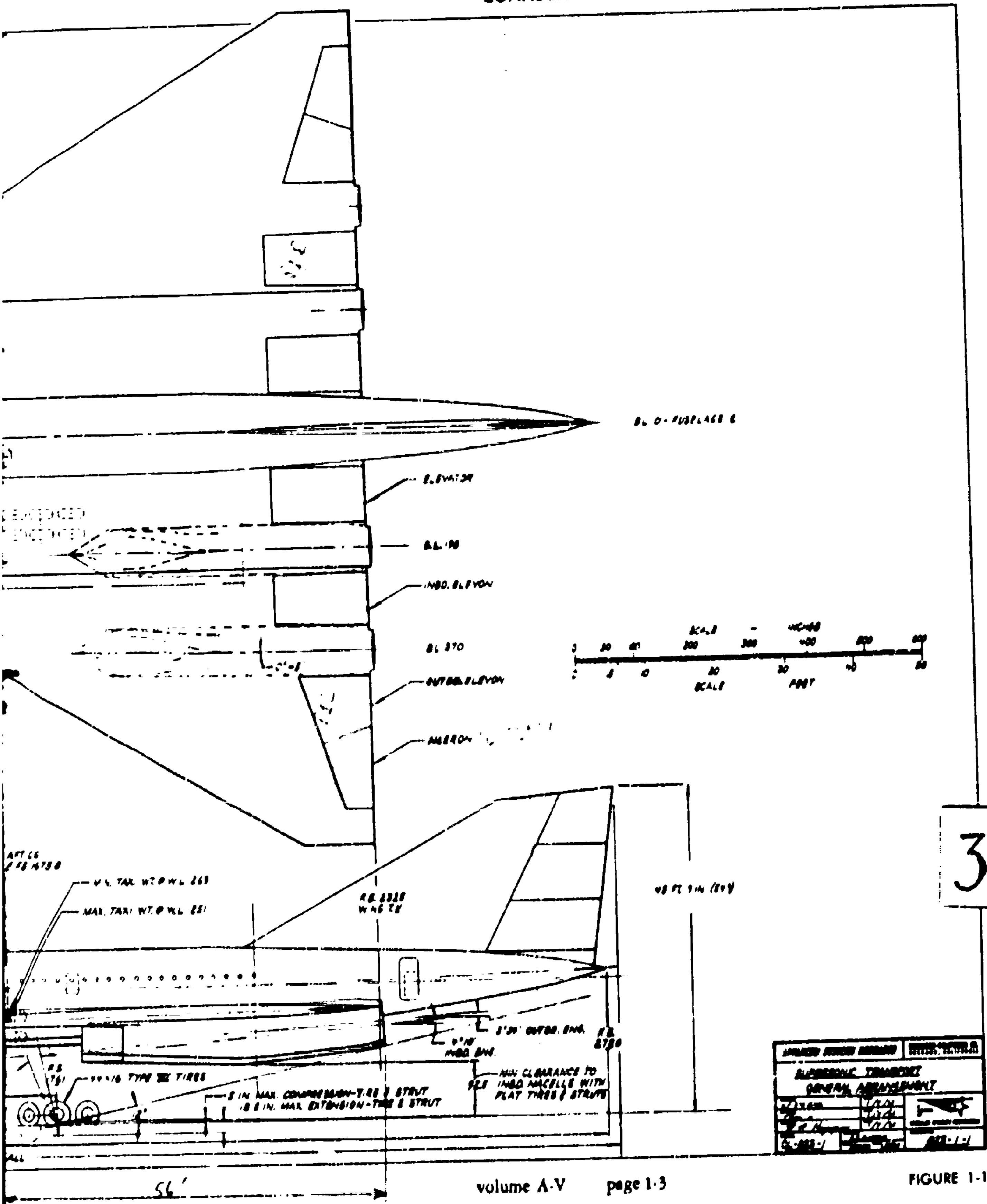
ELEVATOR
INBD. ELEVON
B.L. 370
OUTBD. ELEVON
AILERON
SCALE
FEET
MAX. TAXI WT. @ W.L. 251
MIN. CLEARANCE TO
INBD NACELLE WITH
FLAT TIRES & STRUTS
SUPERSONIC TRANSPORT
GENERAL ARRANGEMENT
56'

FIGURE 1-1

3

development status. Because of the podded nacelle installation for the SST, any of these powerplants can be readily adopted.

Range-payload capabilities achieved with these three powerplants are summarized in Figure 1-2, and are shown using the current status aerodynamic characteristics as substantiated by the wind tunnel.

It is noted that at the design range of 3,470 nautical miles (4,000 statute miles), the basic current status airplane, with the Pratt and Whitney JT11F-4 engine, carries approximately 10,000 pounds of payload. With the General Electric GE4/F6A engine, the payload is increased to 13,000 pounds, and with the Curtiss-Wright TJ70A-4 engine to 38,000 pounds. Despite the indicated performance superiority of the Curtiss-Wright engine and the modes. advantage of the General Electric engine, this proposal is based on the use of the Pratt and Whitney JT11F-4 engine. This engine, with more than 5 years of development experience on the full scale J-58, is used for reasons of reduced program development risk, more assured schedule reliability, and the more conservative, proven status of the engine today.

The range-payload capabilities of the SST, based on the developed status of the airplane at the end of the Phase II period, are shown in Figure 1-3. These data are derived on the basis of improvements that can be realized by continued development in the areas of aerodynamic drag, structural weight, equipment weight, engine specific fuel consumption, and engine weight. The expected improvements in these areas are all realistic values and do not require any state-of-the-art breakthroughs to accomplish. For example, the expected improvement in supersonic L/D at Mach 3.0 is only .25 and the improvement in subsonic L/D is .60. Further work on structural and equipment weights is expected to yield a 5 percent improvement in weight empty. In addition, due to the conservative approach taken by the engine manufacturer in regard to engine turbine operating temperatures and engine weights, an improvement in cruise specific fuel consumption in the order of 1.5 to 2.0 percent appears feasible and a weight improvement of 5 percent is a possibility.

At the design range of 3,470 nautical miles (4,000 st mi), the SST, at its design take-off gross weight of 450,000 pounds, has the capability of transporting 30,000 pounds of payload, using 198,400 pounds of block fuel. The international interior maximum payload of 45,875 pounds can be flown to ranges up to 3,020 nautical miles. With full fuel load, a payload of 17,000 pounds can be transported 3,850 nautical miles.

Typical performance items for the SST along the design flight profile are given in Figure 1-4. Climb to acceleration altitude is conducted at 360 knots CAS. Climb and acceleration is accomplished along a 2 psf boom intensity profile, passing through 43,000 feet altitude at Mach 1.2. Initial cruise starts at 70,000 feet, where the initial ground boom level will be 1.5 psf. Boom intensity decreases along the maximum range climb-cruise profile, with 1.2 psf produced at the end of cruise altitude of 77,000 feet. Descent is conducted at 330 knots CAS down to an altitude of 55,000 feet and 320 knots CAS at lower altitudes. Reserve fuel corresponds to the allowances desired by the FAA Request for Proposal.

Analysis of the effects of cruise speed on economic considerations has led to the choice of Mach 3.0 cruise for the SST. The effects of lower cruise Mach number on range-payload characteristics for a given take-off gross weight airplane are shown in Figure 1-5. For cruise at Mach 2.6 and a range of 3,470 nautical miles, 9,000 pounds of payload must be off-loaded; at Mach 2.2, more than 30,000 pounds. These numbers include effects on empty weight due to cruise Mach number change. When these dramatic losses in payload capability are compounded with reductions in block speed, substantial increases in operating costs are incurred, and increased airplane size as a means for restoring payload capability is indicated. Attempts to recover losses by increasing airplane size actually reduces the economy further. Increased first cost and amplification of the sonic boom problem further deteriorate the operating economics at lower speed. To fully exploit the fundamental high speed cruise concept of the supersonic transport, and to provide the highest payload and most economical airplane, cruise at Mach 3 is clearly indicated.

The design flight profile is conducted using zero wind, standard day conditions, and a climbing cruise technique in accordance with the FAA Request for Proposal. Effects of off-design operation of the SST at a takeoff gross weight of 450,000 pounds, with 30,000 pounds of payload and full reserve fuel are as follows; Constant altitude cruise at an altitude equivalent to the average climb-cruise altitude (74,000 feet) will decrease range by 50 nautical miles. Opera-

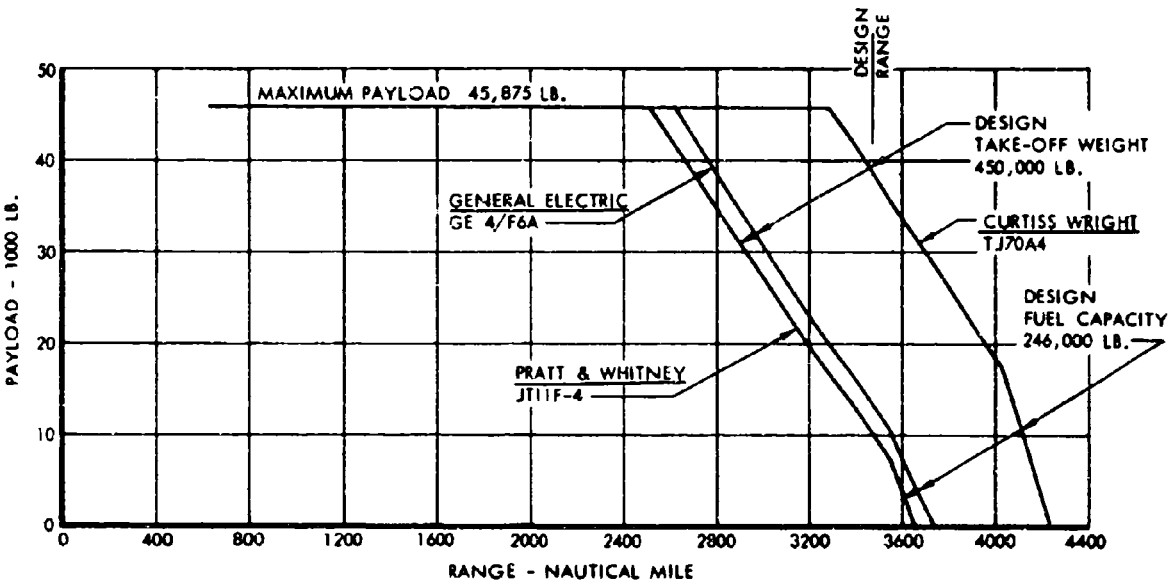

FIGURE 1-2 CURRENT STATUS RANGE—PAYLOAD WITH ALTERNATE ENGINES

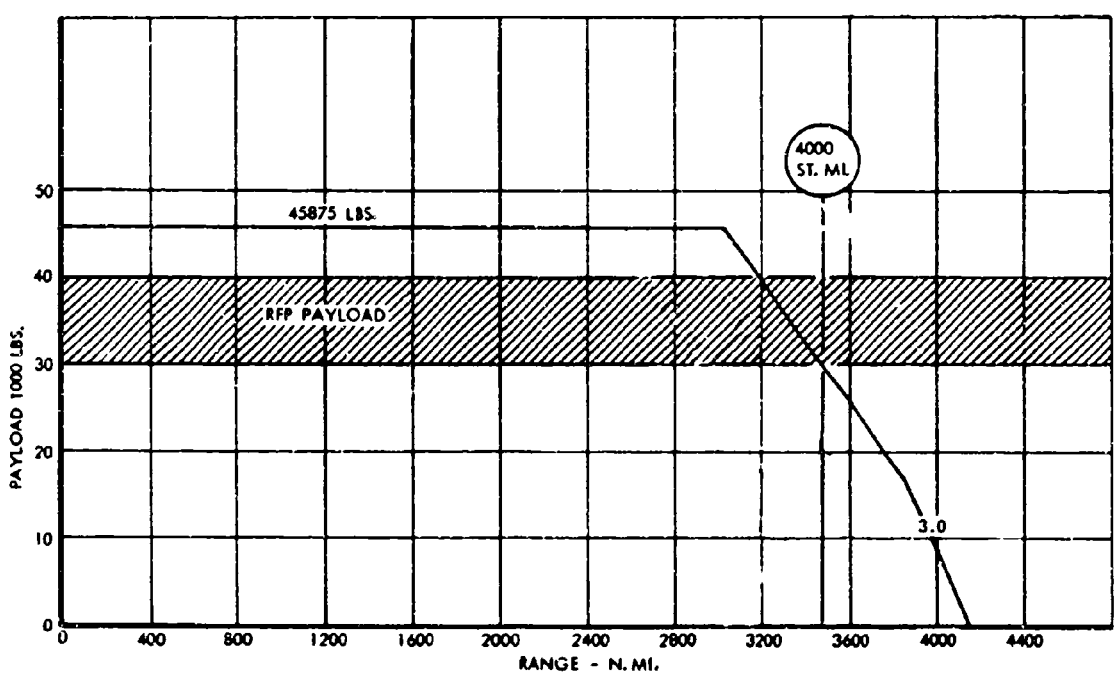

FIGURE 1-3 RANGE-PAYLOAD OF PHASE II DEVELOPED, MACH 3.0 SST

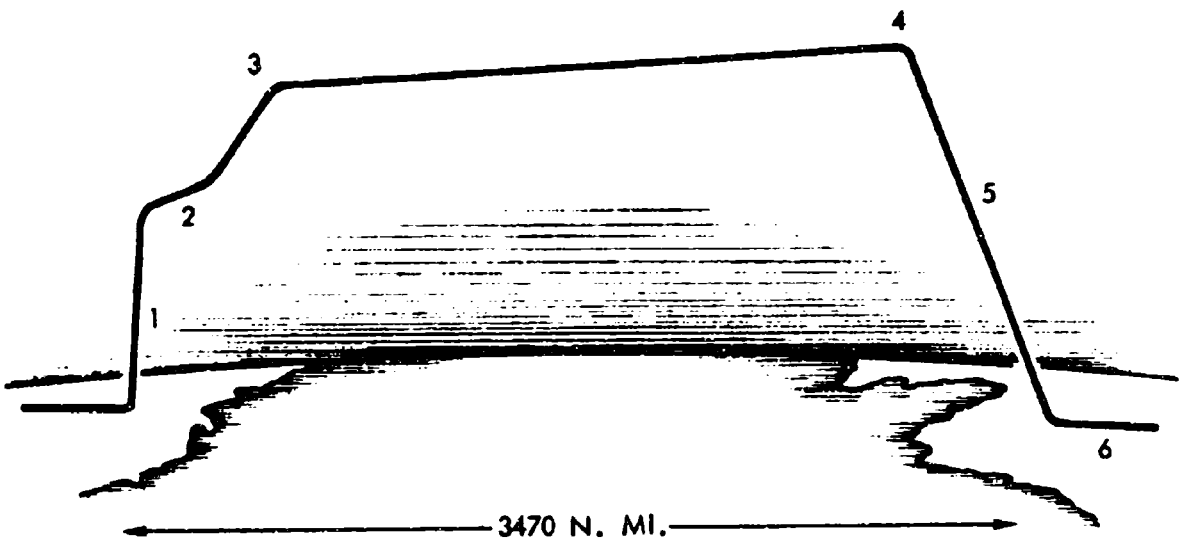

1 SUBSONIC CLIMB @ 360 KNOTS
CAS MINIMUM DUCT BURNING

2 TRANSONIC ACCEL @ 2 PSF BOOM
OVERPRESSURE MAXIMUM DUCT BURNING

3 INITIAL CRUISE @ 70,000 FEET ALTITUDE 1.5 PSF
BOOM OVERPRESSURE PARTIAL DUCT BURNING

4 FINAL CRUISE @ 77,000 FEET 1.2 PSF BOOM
OVERPRESSURE PARTIAL DUCT BURNING

5 DESCENT @ 330 TO 320 KNOTS CAS
PARTIAL DRY POWER

6 RESERVES DEFINED BY FAA
REQUEST FOR PROPOSAL

FIGURE 1-4 DESIGN FLIGHT PROFILE

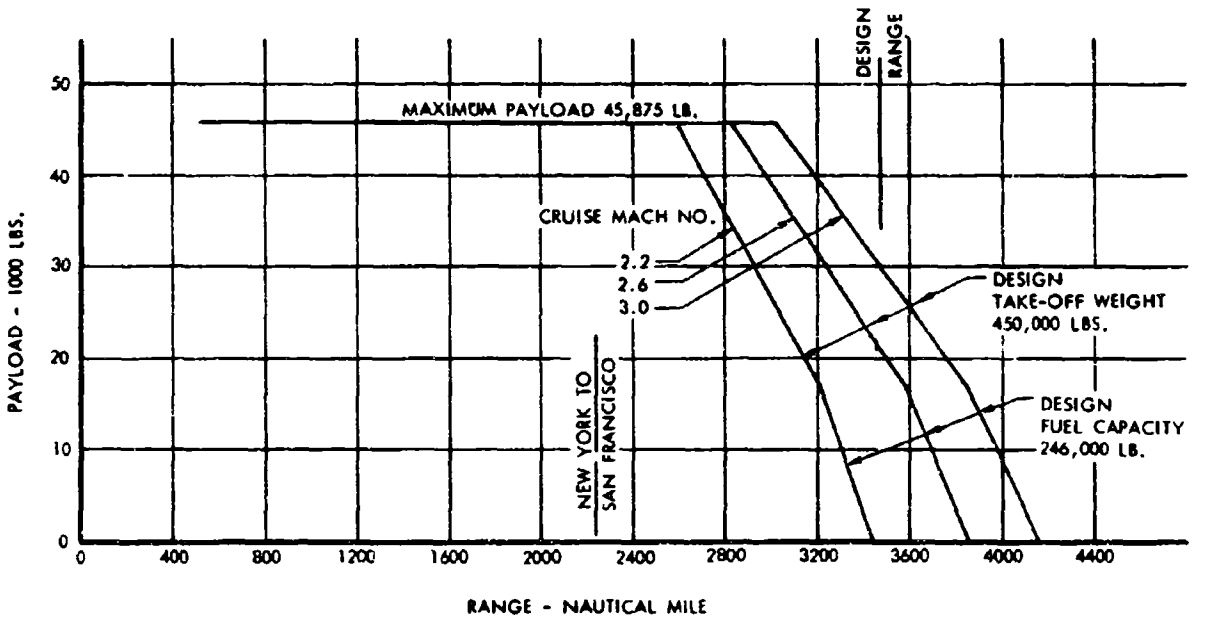

FIGURE 1-5 EFFECT OF CRUISE SPEED ON RANGE-PAYLOAD CAPABILITY

tion at 4,000 feet above or below 74,000 feet will decrease the range by approximately 100 nautical miles. It is seen that the range losses are small, indicating favorable airplane operation flexibility. These range losses are readily restored by use of a small fraction of the reserve fuel.

The design flight profile for the SST follows a 2 psf boom overpressure speed-altitude schedule through the transonic acceleration phase of the flight. The effect of following higher and lower boom intensity profiles on payload-range characteristics is given in Figure 1-6. For long range overwater flights, the use of a 2.5 psf profile over the ocean will provide a range increase of 120 nautical miles. For domestic transcontinental operation, profiles following a 1.7 psf overpressure can be used without off loading payload. The light wing loading and low aspect ratio of the double delta configuration will provide a buffet boundary margin that will allow unlimited selection of sonic boom acceleration altitudes.

Subsonic performance is summarized in Figure 1-7. For a typical ferry-range flight, where subsonic operation for long ranges might be conducted, 15,000 pounds of payload can be transported 3,500 nautical miles.

Using the FAA Request for Proposal emergency reserve fuel definition, the SST can continue the flight assignment to its destination after a midpoint single-engine failure by continuing the flight at either Mach 3 or subsonic cruise speeds. A total range of 3,850 nautical miles can be achieved assuming a single engine failure, and 3,650 nautical miles can be accomplished at subsonic cruise speeds after failure of two engines at the design range midpoint. Total range after a midpoint cabin decompression is 3,730 nautical miles.

Additional performance characteristics and detailed data for each segment of the flight profile are presented in Section 5.0.

The proposed SST utilizes takeoff and landing field lengths that are less than the target numbers desired by the FAA Request for Proposal. At the design takeoff gross weight of 450,000 pounds, the FAA field length required is 9,750 feet operating from a sea level runway at standard plus 15°C temperature conditions. This takeoff runway length is realized using a noise abated reduced power level, so that 112 pndb noise levels are never exceeded at a distance around the runway one mile from the runway centerline. When noise conditions permit, maximum power can be utilized to reduce the above takeoff field length to 8,150 feet.

Landing distance at a normal landing weight of 254,600 pounds is 6700 feet on a wet runway. The FAA dry runway field length is 7050 feet at this operating weight. During approach, the ground noise level one mile from the end of the runway is 112 pndb. Touchdown speed is 134 knots.

Because of the high installed thrust to weight ratio the SST easily meets all takeoff and landing climb gradient requirements. Further discussion and more detailed evaluation of airport performance characteristics are presented in Section 5.

The flying qualities of the SST are exceptional. The airplane demonstrates positive static stability margins both longitudinally and directionally under all flight condition.

Longitudinal control is excellent and sufficient control power is available to bring the airplane to the takeoff attitude well before the takeoff speed. No control power degradation due to miss-trim or runaway trim is incurred for any practicable situation. Lateral and directional control are sufficient to provide a minimum engine out control speed of 123 knots as compared with a landing approach speed of 138 knots and a takeoff rotation speed of 147 knots. Sufficient margins on control capability are available in all flight conditions in conjunction with adequate control system redundancy such that flight safety is retained even in the event of a dual control system failure. The reliability analysis indicates that a dual control system failure on a single flight is estimated to occur once in 50,000,000 flight hours.

The dynamic stability characteristics of the aircraft without damping augmentation of any kind are such that the aircraft is safely flyable under all flight conditions. A damper failure, therefore, should not result in an aborted flight. A pitch damper and a yaw damper are desirable, however, to enhance passenger comfort and to minimize crew fatigue in cruise. A roll damper may prove desirable to minimize the roll to yaw ratio during the landing approach. F-104 experience indicates that a roll damper will enhance rough weather operation although the dutch roll mode in the landing approach is inherently heavily damped without damping augmentation of any kind.

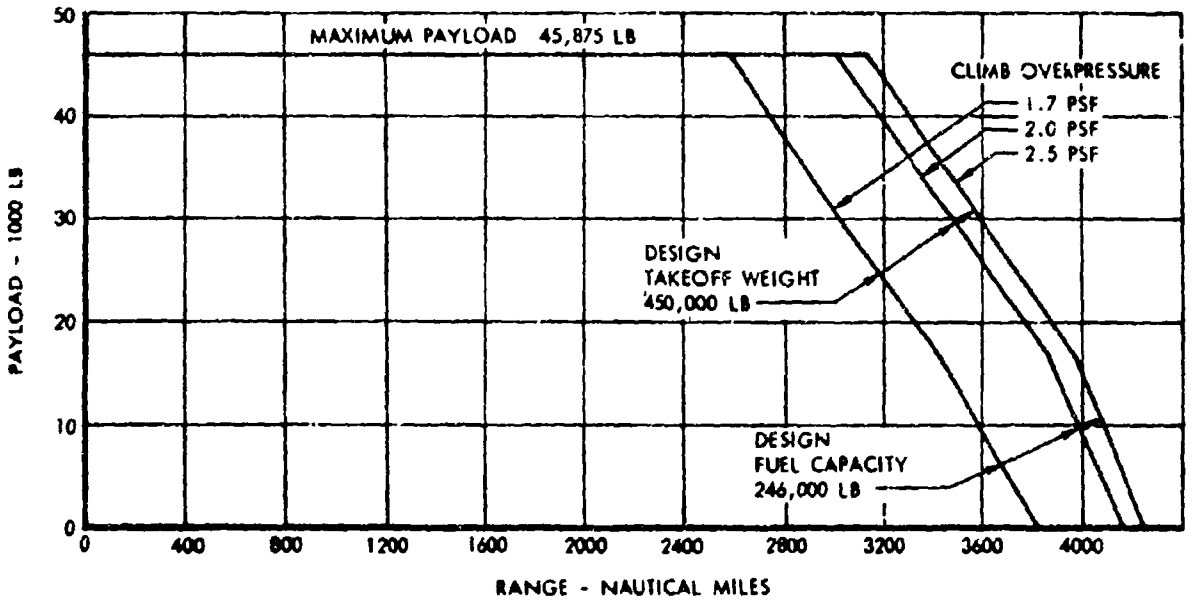

FIGURE 1-6 EFFECT OF CLIMB SONIC BOOM INTENSITY LIMIT ON RANGE-PAYLOAD CAPABILITY

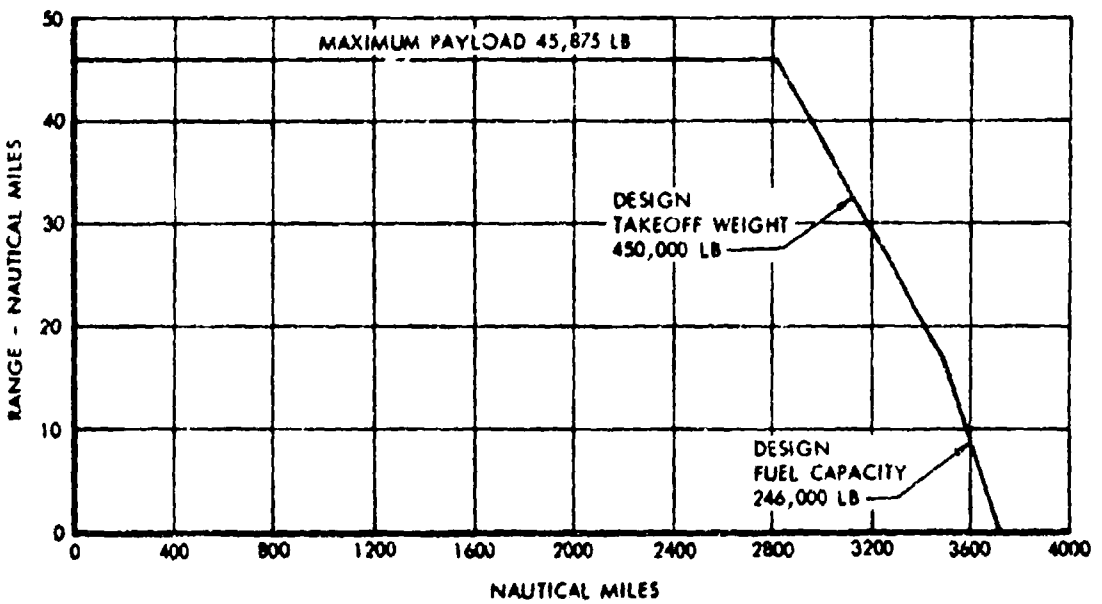

FIGURE 1-7 RANGE-PAYLOAD CAPABILITY AT MACH 0.91

Operating speeds for take-off and landing have at least a 20 percent margin over minimum flight speed. This minimum speed is based on a maximum angle of attack of 20 degrees and does not represent a physical stall speed. The lift characteristics above this angle are linear and lift coefficients 40 to 50 percent greater than at 20° angle of attack can be obtained. This means that even at minimum flight speed it will be possible to achieve maneuver load factors of 1.4 to 1.5 g's. At V_2 climb out and at approach speeds the gust and maneuvering load factor margins are more than double the levels realized by current jet aircraft.

Additional details regarding airplane handling qualities are presented in Section 6.

Analysis of sonic boom and airport noise characteristics are given in Section 7.

SECTION 2 INTRODUCTION

The proposed SST airplane culminates eight years of configuration development of the supersonic transport concept, involving analysis of numerous designs employing many different wing planforms, tail positions, forebody shapes, and engine arrangements. Promising configurations resulting from these studies were evaluated in the wind tunnel using low and high-speed models such as shown in Figure 2-1. During these studies, it was apparent that the most successful SST configuration must meet the following objectives and incorporate aerodynamic design refinements that would solve, or at least alleviate, these potential problem areas:

1. Achieve high aerodynamic efficiency (L/D) without undue structural penalty in order to provide good flight performance.
2. Minimize the aerodynamic center shift to alleviate the trim drag problem.
3. Provide weight and balance characteristics that will minimize sensitivity to off-loaded fuel and payload.
4. Alleviate the sonic boom characteristics.
5. Provide satisfactory airport operation in terms of field lengths, speeds, and noise.
6. Achieve the foregoing objectives without compromising the aircraft handling qualities.

Studies initiated in 1957 included evaluations of numerous wing shapes and airplane configurations, as shown in Figure 2-2. Analyses highlighted the sensitivity of wing structural weight to the overall performance capability and suggested the adoption of the light structural weight trapezoidal wing, Figure 2-3. Further development, however, indicated that the stability characteristics of this type of configuration were not satisfactory.

These findings led to the canard-delta configuration, Figure 2-4, which provided improved pitching moment characteristics and decreased aerodynamic center shift. Using relatively thin airfoil sections and moderate wing loadings, this airplane became an attractive design from the performance standpoint, realizing high cruise lift-drag ratios with a structurally efficient wing design.

Two unattractive features remained with this type of configuration. Thin airfoil sections and moderate wing loadings did not provide sufficient wing fuel volume, necessitating storage of fuel in the aft fuselage. As a result, the weight and balance characteristics were deficient, with large center-of-gravity travel caused by off-loaded fuel or payload. In addition, the sonic boom characteristics were aggravated by the volume and lift shape parameters which could not be adjusted to follow the ideal distributions. A solution to the balance problem was achieved by employing an adjustable area canard which could shift the airplane aerodynamic center position to follow the shifts in center of gravity due to off-loaded fuel or payload.

The folding canard-delta configuration was not considered to be the airplane that provided solutions to all the problems. Sonic boom characteristics were far from predicted lower-bound levels. The adjustable area canard, together with a wing employing leading and trailing edge flaps, represented undesired complexity. The weight and balance problem was not completely resolved, since off-loaded payload required preselected seating arrangements.

Concurrent studies, represented by the low-speed model photo in Figure 2-5 were made. The inboard sections of the wing were extended forward to form a bat, resulting in a double-delta planform shape. The increased wing root chords increased wing volume, reduced structural wing weight because of increases in beam depth, and improve the volume and lift parameters related to sonic boom characteristics. By increasing substantially the amount of fuel stored in the wing, improvements in airplane balance were realized.

Low-speed tunnel tests indicated that the stability characteristics of this configuration were poor. The destabilizing influences of both a canard and bat were detrimental to longitudinal stability characteristics.

WING-TAIL COMBINATIONS

NACELLE INSTALLATION

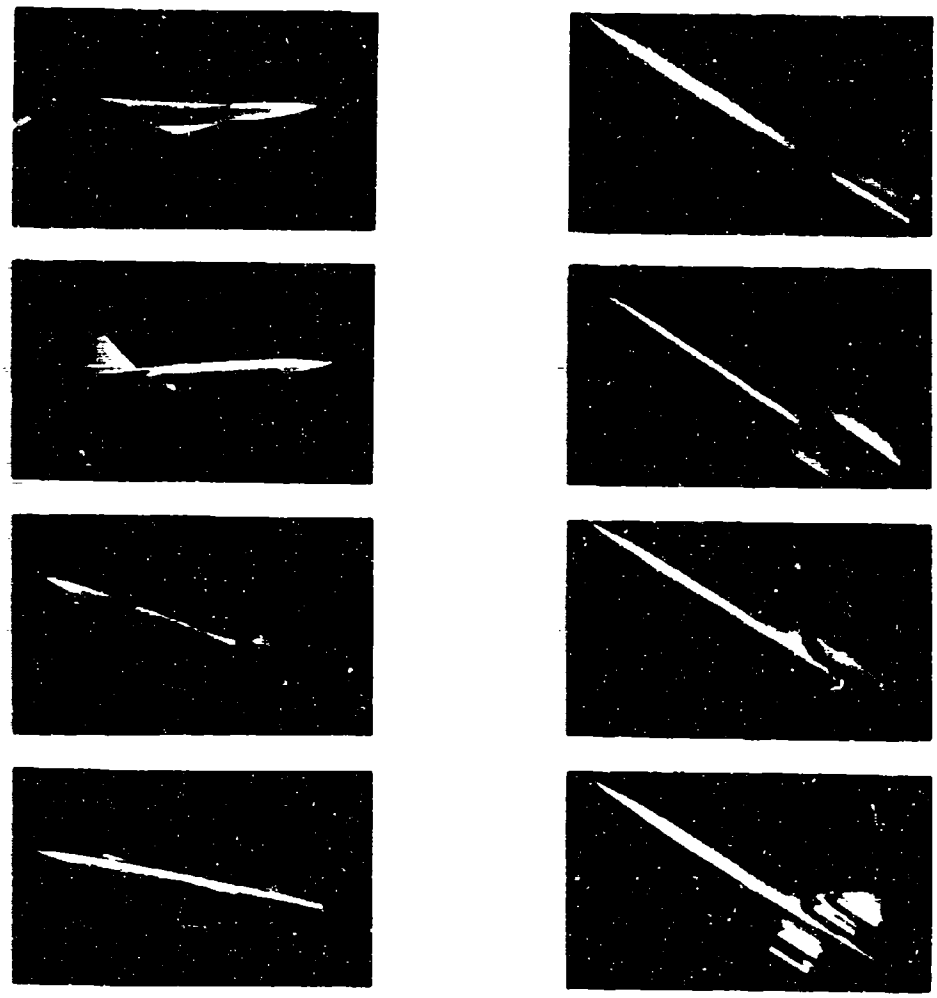

FOREBODY-CANOPY SHAPES

FIGURE 2-1 SST WIND TUNNEL MODELS

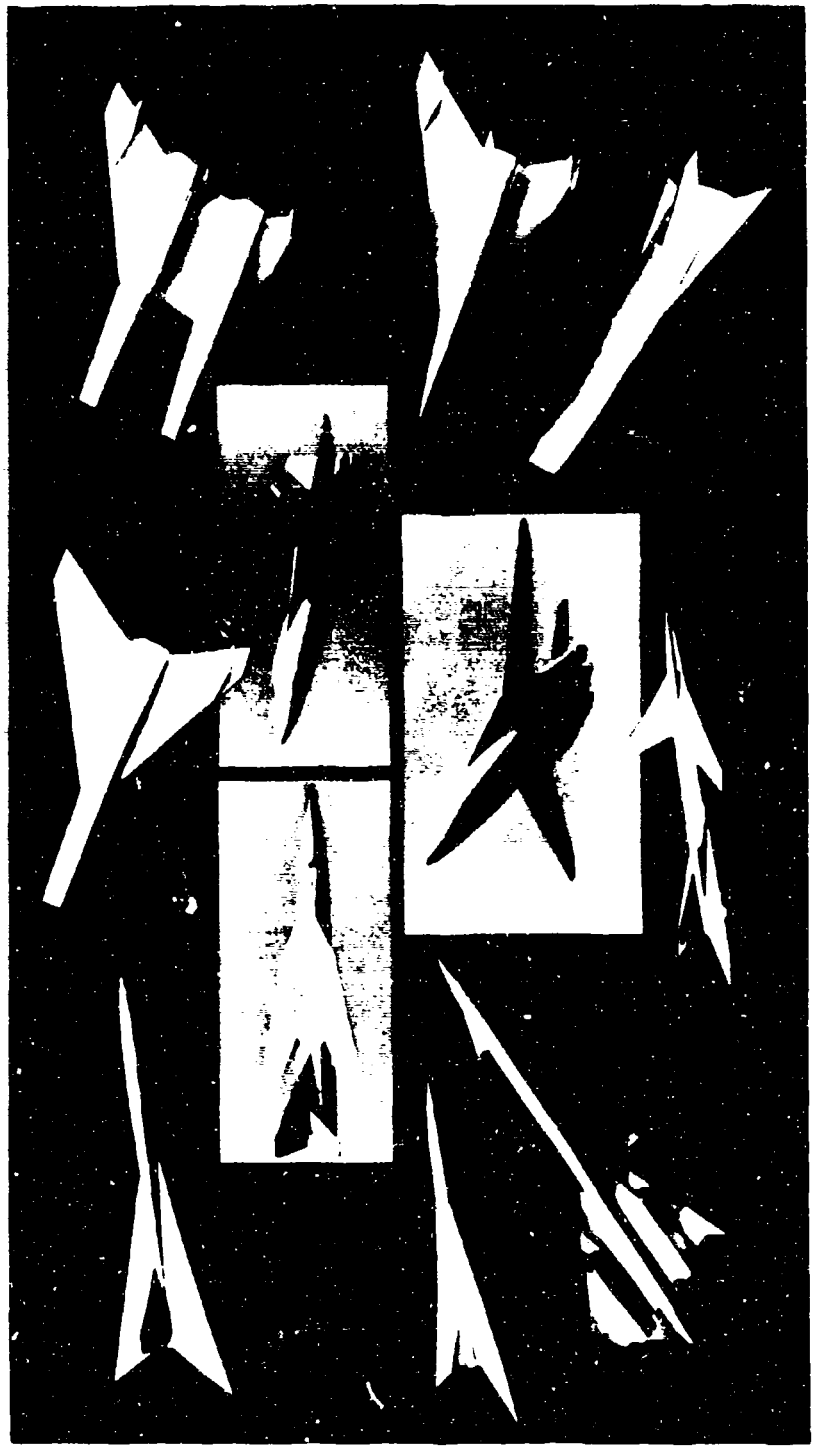

FIGURE 2-2 SST WING PLANFORM STUDIES

FIGURE 2-3 TRAPEZOIDAL WING MODEL

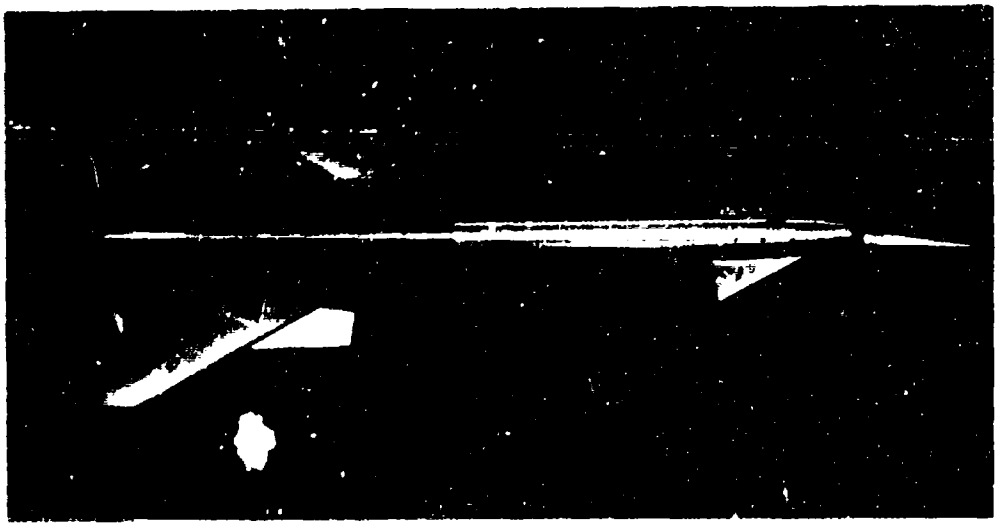

FIGURE 2-4 CANARD-DELTA MODEL

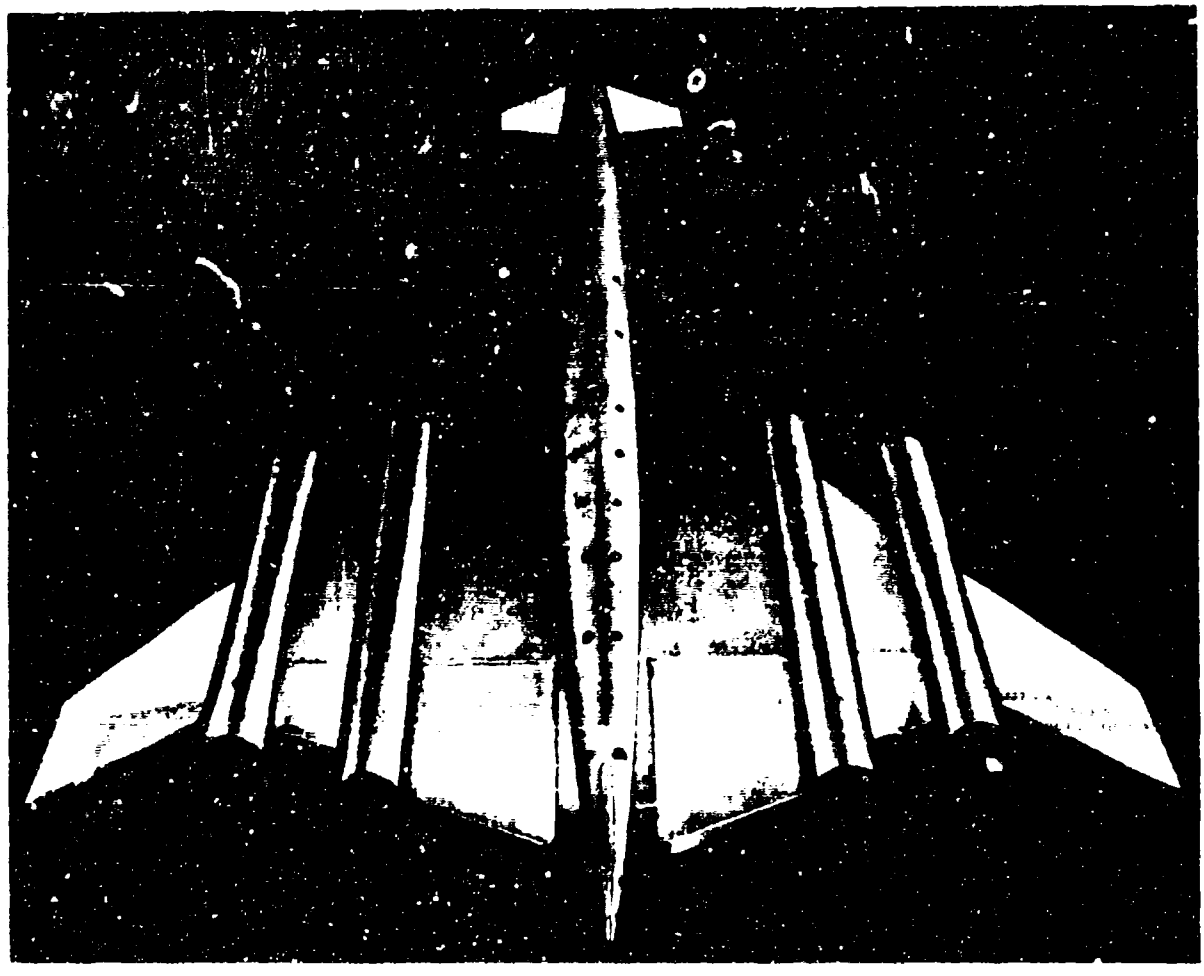

FIGURE 2-5 CANARD-DOUBLE DELTA MODEL

The complex flow field generated by the mixing of forebody, canard, bat, and wing vortices produced undesirable non-linearities to both longitudinal and directional stability data.

Elimination of the canard surface alleviated these problems. It was recognized that additional increases in inboard wing chord lengths, so that the bat extended forward on the fuselage forebody, would improve the aerodynamic behavior of the configuration.

A systematic experimental investigation was conducted to evaluate a series of wing and bat, or double-delta planforms. Low and high-speed models with wings of 50, 60 and 70 degrees of sweep, and bat sizes having 80 and 83 degrees of leading edge sweep were fabricated as shown in Figure 2-6. Primary emphasis was placed on evaluating the potential of achieving a planform shape having linear pitch characteristics and small aerodynamic center shift due to Mach number. Results are summarized in Figure 2-7.

Tests revealed that the 50 degree wing in combination with various bats did not give the desired linear stability characteristics. The 70 degree wing was tested only at low speed. Studies were halted because the low-speed lift curve slope was extremely low and the high dihedral effect could be a potential problem area. The 60 degree wing with an 80 degree bat provided the desired objectives.

Additional tunnel tests of this 80 – 60 double-delta wing indicated substantial aerodynamic improvements in many areas. Because of the favorable area progression distributions, transonic drag rise was reduced considerably. In addition, computed sonic boom signatures were lowered. The vortex flow patterns generated by the double delta provided favorable sidewash flow at the vertical tail and produced high directional stability levels at high airplane angles of attack, at both low speed and high speed.

Low-speed lateral control power was not degraded at approach angles of attack because boundary layer growth was eliminated by vortex flow. Dihedral effect in cruise at Mach 3.0 and in low-speed approach was low enough to permit damper inoperative operation with satisfactory lateral-directional flight characteristics.

The improvements in structural design and wing weight offered by the double-delta planform made it possible to consider substantial increases in wing area. The larger wing provided gains in lift-drag ratio, operation at higher cruise altitudes so cruise sonic boom over-pressures are reduced and light wing loadings for takeoff and landing, thus assuring achievement of satisfactory airport performance characteristics.

For these reasons, the 80 – 60 degree double-delta planform was adopted. Two second series models were constructed, Figure 2-8, and extensive tunnel tests were made. The results from these tests form the basis upon which the predicted performance and stability characteristics presented in this report are made. Results of the tunnel tests are included in Section 4 of this report.

In support of the development of the SST, a supplementary wind tunnel program was conducted to evaluate canopy shape and drag penalties at supersonic speeds. For these tests, larger scale forebody models were utilized, as shown in Figure 2-9. Results of these are summarized in Figure 2-10. This experimental evaluation led to the decision that the only satisfactory means for providing acceptable pilot visibility requires use of a movable geometry forebody. To minimize the high-speed drag penalty with a fixed forebody, the canopy shape must be compromised so severely that low-speed approach visibility is unsatisfactory, particularly with regard to minimum-weather visual landings. Therefore, the weather-vision nose indicated in Figure 2-11 has been adopted.

As part of the SCAT study program, detailed evaluations were made of other wing planform concepts. The fixed and variable geometry arrow wing concepts (SCATs 4 and 15) were found to have excessive structural weight penalties that severely compromised the high aerodynamic efficiency of these designs. Results of the program indicated that the variable-sweep configuration had more potential.

Continued study of the variable sweep airplane, since the completion of the SCAT program, has verified that this concept represents a different approach to the design problem, and leads to a totally different kind of airplane. Reductions in wing area are needed to relieve the weight penalty for variable geometry and the result is an airplane having high wing loadings, elaborate high-lift devices, moderate supersonic lift-drag ratios, and lower cruise altitudes. When compared with the variable sweep wing planform concept, the following advantages are offered by the proposed fixed geometry airplane:

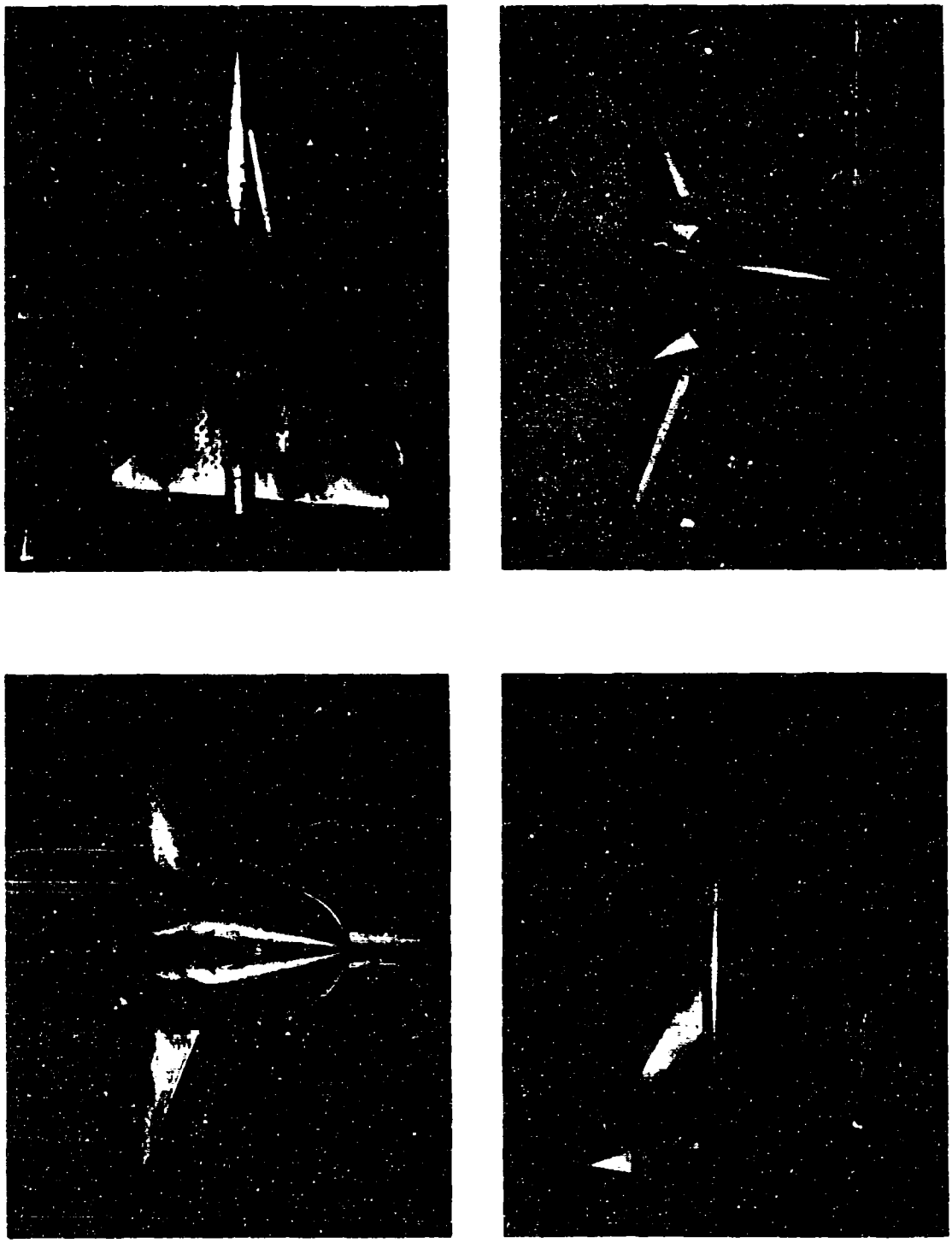

FIGURE 2-6 DOUBLE DELTA WIND TUNNEL MODELS

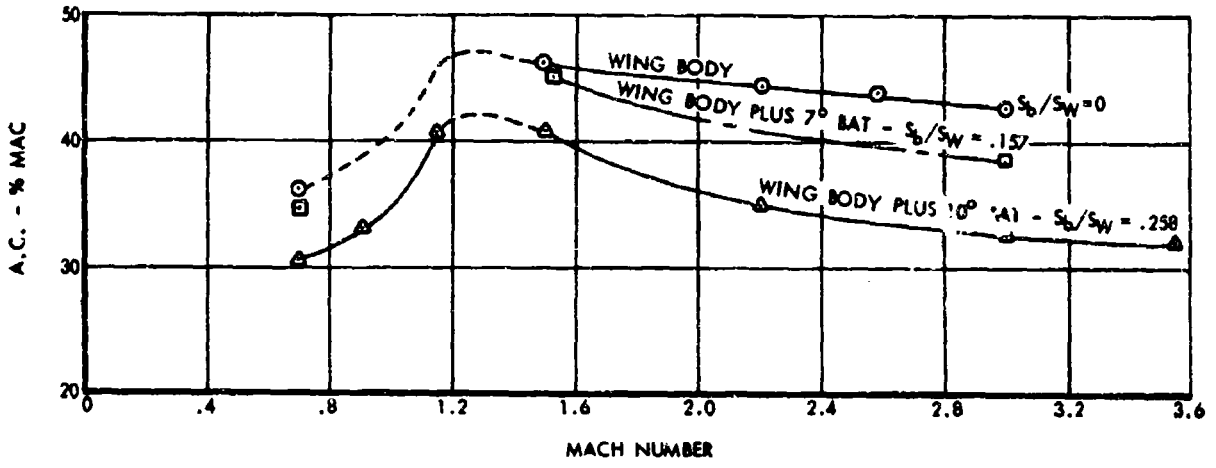

FIGURE 2-7 EFFECT OF WING GEOMETRY ON AERODYNAMIC CENTER LOCATION

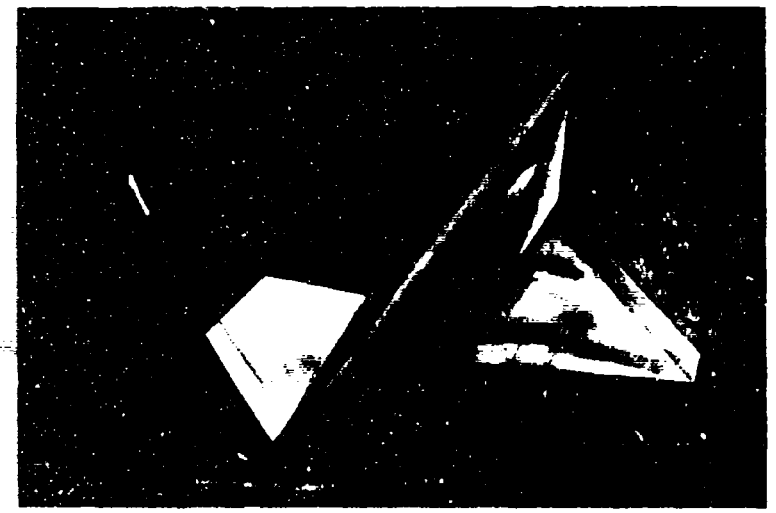

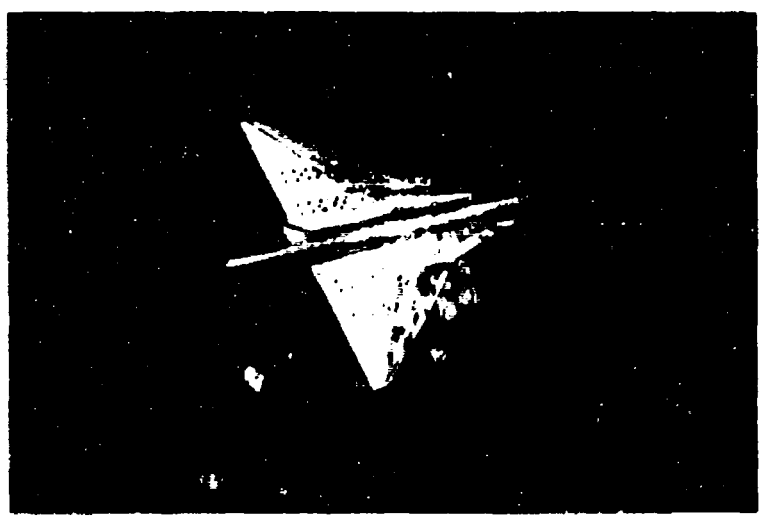

FIGURE 2-8 SECOND SERIES WIND TUNNEL MODELS

FIGURE 2-9 FOREBODY WIND TUNNEL MODELS

FORWARD FUSELAGE BODY STUDIES

CONFIGURATION	OVER-NOSE VISION	Δ SUPERSONIC DRAG COUNTS	Δ L/D	Δ RANGE - N. MI.
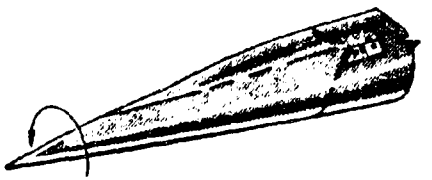 ROTATING NOSE	10 DEGREES	0	0	0
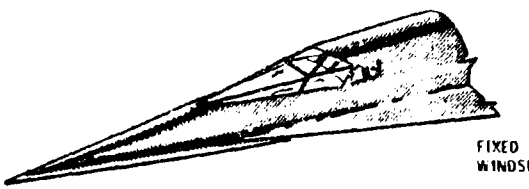 FIXED WINDSHIELD	14 DEGREES	3.5	-.18	-100
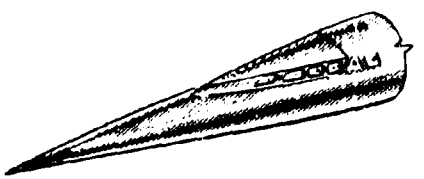 RETRACTABLE WINDSHIELD FAIRING	13 1/2 DEGREES	2.5	-0.12	-70
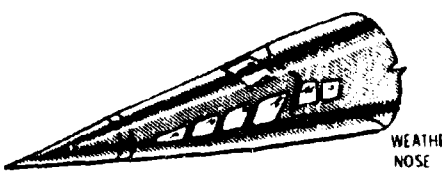 WEATHER-VISION NOSE	23 DEGREES	0	0	0

FIGURE 2-10 FORWARD FUSELAGE BODY STUDIES

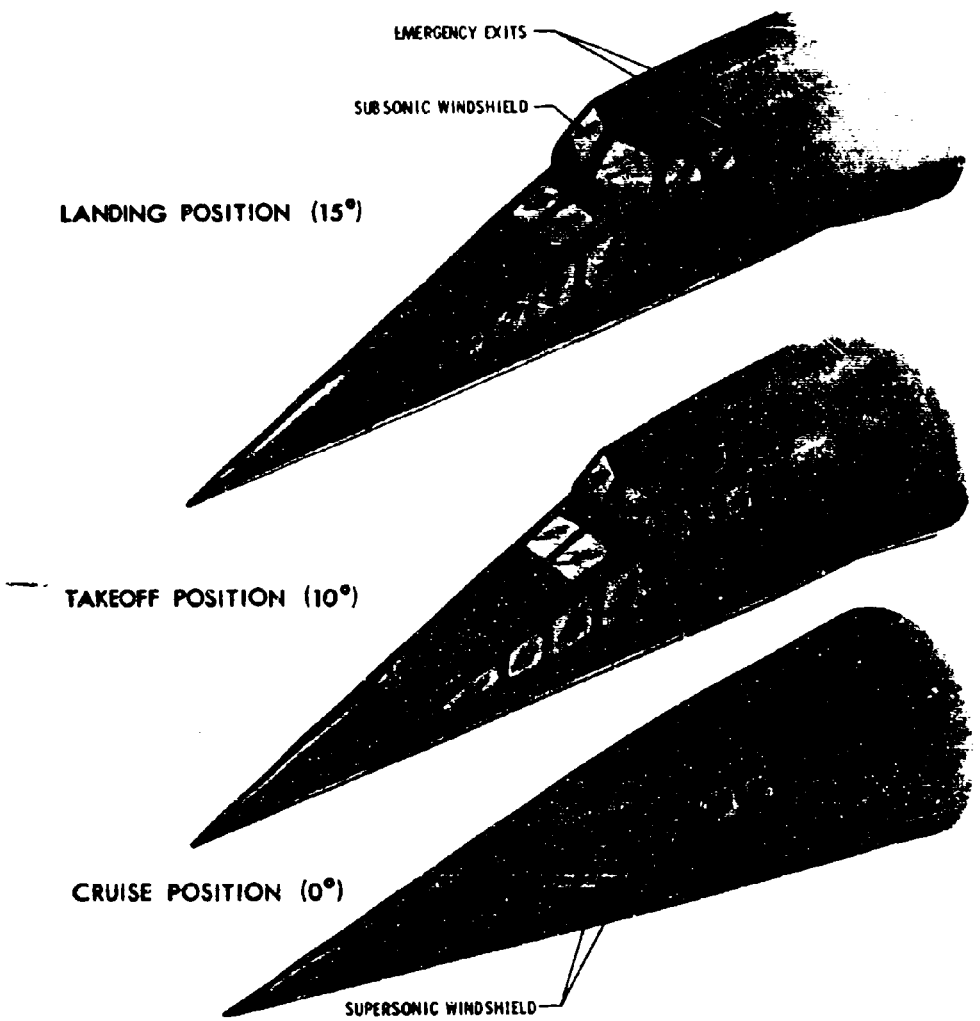

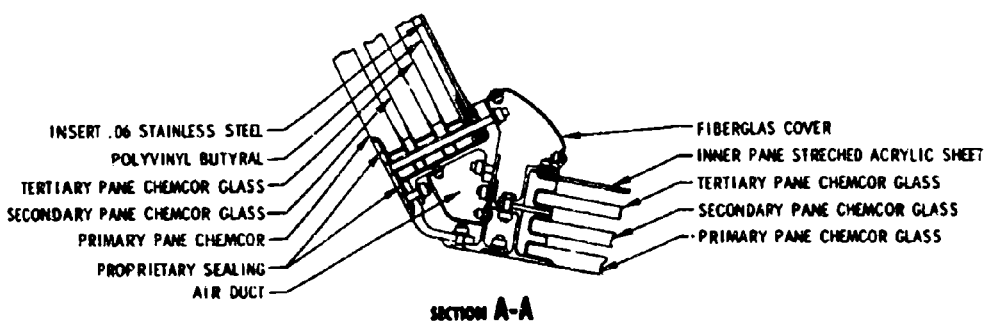

SECTION A-A

FIGURE 2-11 WEATHER VISION NOSE

a. Lighter weights

b. Lower sonic booms

c. Simplicity of design

d. Simplicity of operation and maintenance

e. Less development risk

f. Lower costs

For these reasons, this proposal offers the fixed wing concept supersonic transport. This configuration reflects a design evolution resulting from eight years of study. Significant milestones accomplished during these studies are illustrated by the series of model photographs presented in Figure 2-12. The performance and handling qualities predicted for the SST are presented in the following sections, together with a complete presentation of substantiating wind tunnel data and data analysis.

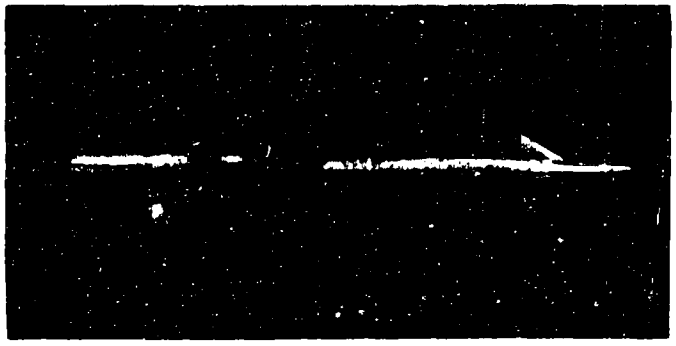

1958

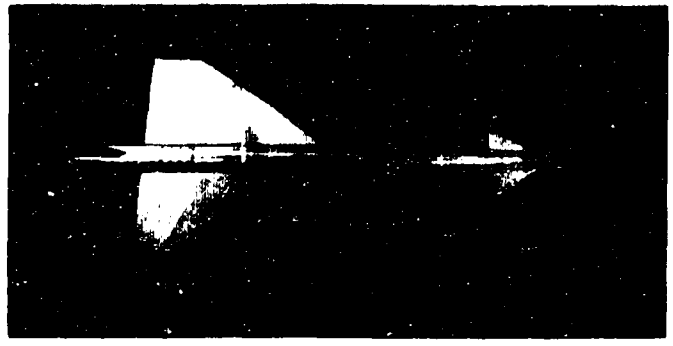

1960

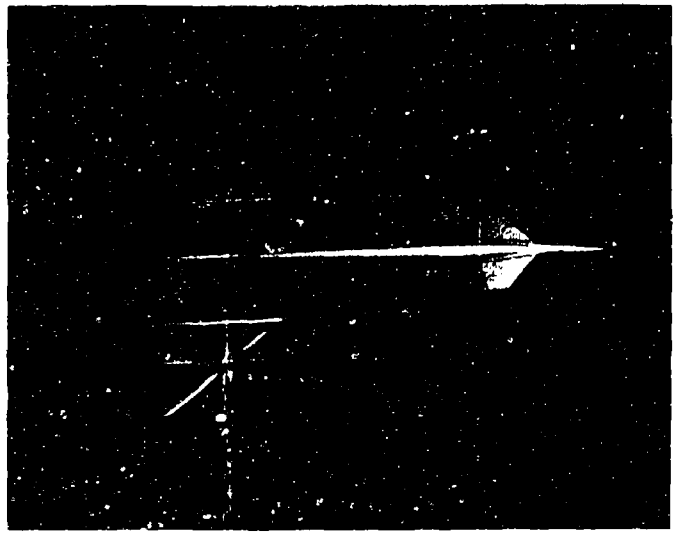

1962

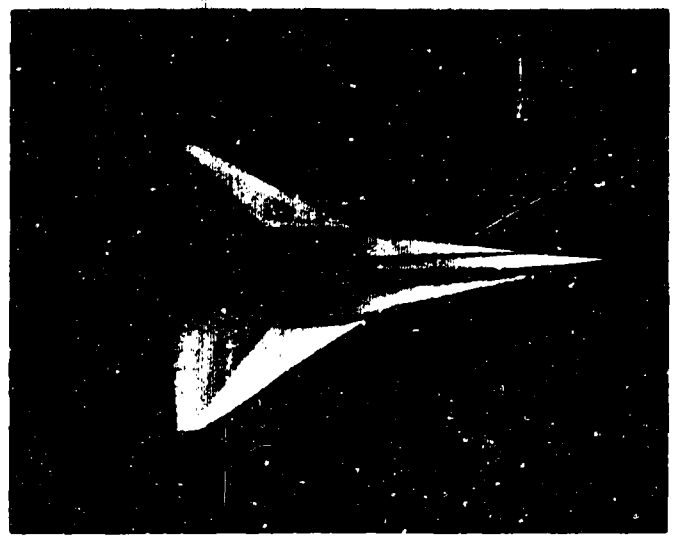

1963

FIGURE 2-12 CONFIGURATION SUMMARY

SECTION 3 PHYSICAL CHARACTERISTICS AND FLIGHT CRITERIA (3.2)

This section of the report presents the basic geometric, weight, flight criteria, and propulsion characteristics of the SST which have been used during the evaluation of the performance capabilities presented in Section 5, and the stability characteristics presented in Section 6.

3.1 AIRPLANE DESCRIPTION (3.2.3)

The SST is a four-engine fixed geometry transport designed for cruise at Mach 3.0, employing a tailless double-delta wing planform. The wing is cambered and twisted to provide high lift-drag ratio and minimum trim drag. Engines are mounted in individual nacelles below the wing, and utilize two dimensional vertical wedge external compression inlets. A single vertical tail is mounted on the aft end of the fuselage.

Wing span is 116 feet and overall airplane length is 222 feet. Total wing area is 8,370 square feet, providing a maximum takeoff wing loading of 54 psf.

Direct vision is achieved using a movable weather-vision nose that provides acceptable visibility in supersonic cruise flight with good flight compartment noise characteristics, and no drag penalty. Extremely good visibility in subsonic operation is achieved by lowering the nose to expose a conventional transport type windshield.

Longitudinal, directional, and lateral control is provided by conventional trailing edge flaps. Four separate wing control surfaces are arranged along the span; the three inboard elements function as elevators; and the three outboard segments serve as ailerons. The tip aileron functions only with gear down at subsonic speeds. There are no high-lift devices.

The powerplant adopted for the SST is the Pratt and Whitney JT11F-4 ducted fan engine, having an uninstalled sea level static thrust of 50,400 pounds. The airplane can, with minor modification, adopt either the General Electric or Curtiss Wright powerplants.

A three-view drawing of the SST is shown in Figure 1-1. An isometric view showing the landing gear and nacelle installation is given in Figure 3-1. A summary of the pertinent physical characteristics following the requested FAA Request for Proposal tabulation is given in Table 3-1.

3.1.1 PHYSICAL CHARACTERISTICS (3.2.6)

TABLE 3-1 TABULATED DATA

Wing	
Span	116 ft.
Area (Total wing)	8370 sq. ft.
Area (Basic Delta, Reference)	7000 sq. ft.
Mean Aerodynamic Chord (Basic)	892 in.
Aspect Ratio (Total)	1.62
Aspect Ratio (Basic)	1.92
Taper Ratio (Total)	.056
Taper Ratio (Basic)	.092
Root Chord (Total)	2185 in.
Root Chord (Basic)	1327 in.
Sweep Angle, Leading Edge	80,60 deg.
Sweep Angle, ¼ Chord Line	76.2, 52.5 deg.
Dihedral Angle	0 deg.
Airfoil Section, Root	Parabolic arc
Airfoil Section, B.L. 230	Parabolic arc
Airfoil Section, Tip	Parabolic arc
Airfoil Thickness Ratio, Root	.027
Airfoil Thickness Ratio, B.L. 230	.030
Airfoil Thickness Ratio, Tip	.045
Angle of Incidence to FRL, Root	0 deg.
Angle of Incidence to FRL, B.L. 230	−1 deg.
Angle of Incidence to FRL, Tip	−1 deg.
L.E. MAC (Basic) @ F.S.	1433.5
Vertical Tail	
Span (FRL to theoretical tip)	311 in.
Area (Total)	978 sq. ft.
Area (Exposed)	741 sq. ft.
Mean Aerodynamic Chord (Total)	508 in.

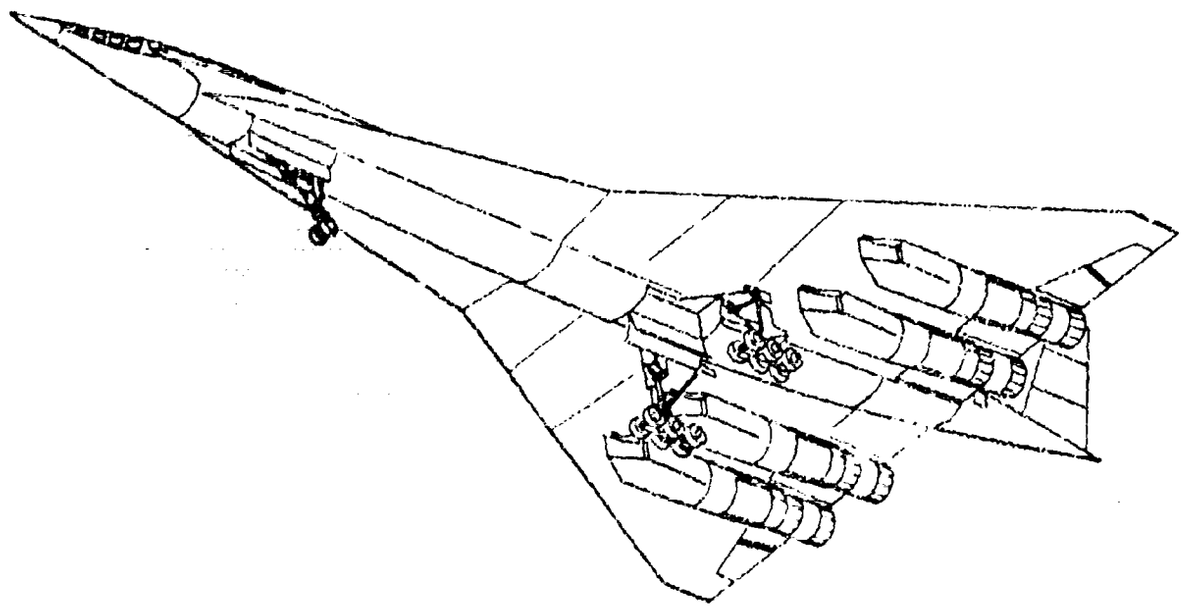

FIGURE 3-1 ISOMETRIC VIEW OF THE SST

Mean Aerodynamic Chord (Exposed)	452 in.
Aspect Ratio (Total)	.687
Aspect Ratio (Exposed)	.638
Taper Ratio (Total)	.248
Taper Ratio (Exposed)	.282
Sweep Angle, Leading Edge	62 deg.
Sweep Angle, ¼ Chord Line	55.2 deg.
Airfoil Section	Parabolic arc
Airfoil Thickness Ratio, Root	.030
Airfoil Thickness Ratio, Tip	.035
L.E. Mac @ F.S. (Total)	2207 in.
L.E. Mac @ F.S. (Exposed)	2267 in.
V_{crp}	.0635
Rudder, Upper	
Span	92 in.
Area	67.5 sq. ft.
Mean Chord	106 in.
Distance, FRL to Inboard End	223.5 in.
Distance, FRL to Outboard End	315.5 in.
Deflection Limits	±25 deg
Rudder, Center	
Span	93 in.
Area	92.5 sq. ft.
Mean Chord	143 in.
Distance, FRL to Inboard End	130.5 in.
Distance, FRL to Outboard End	223.5 in.
Deflection Limits	±25 deg.
Rudder, Lower	
Span	81.5 in.
Area	99.5 sq. ft.
Mean Chord	176 in.
Distance, FRL to Inboard End	49 in.
Distance, FRL to Outboard End	130.5 in.
Deflection Limits	±25 deg.
Elevator	
Span	94 in.
Area/Side	105 sq. ft.
Mean Chord	160 in.
Distance, FRL to Inboard End	62 in.
Distance, FRL to Outboard End	156 in.
Deflection Limits	−30, +25 deg.
Elevon, Inboard	
Span	88 in.
Area/Side	98 sq. ft.
Mean Chord	160 in.
Distance, FRL to Inboard End	240 in.
Distance, FRL to Outboard End	328 in.
Deflection Limits	−35, +25 deg.
Elevon, Outboard	
Span	99 in.
Area/Side	72 sq. ft.
Mean Chord	109 in.
Distance, FRL to Inboard End	412 in.
Distance, FRL to Outboard End (at ℄ hinge)	526 in.
Deflection Limits	−35, +25 deg.
Aileron	
Span	124 in
Area/Side	58 sq. ft.
Mean Chord	73 in.
Distance, FRL to Inboard End (at ℄ hinge)	526 in.
Distance, FRL to Outboard End	684 in.
Deflection Limits	±25 deg.
Wetted Area	
Fuselage	6850 sq. ft.
Nacelles (4)	2680 sq. ft.
Wing	11910 sq. ft.
Vertical Tail	1482 sq. ft.

3.2 AIRFRAME AREA PROGRESSION CURVES (3.2.6)

The area progression buildup for $M = 1.0$ is presented in Figure 3-2. The components are shown separately in Figure 3-3. Figure 3-4 presents the buildup for $M = 3.0$. The Mach 3.0 area progression represents an average of the areas intercepted by the Mach planes as they rotate about the Mach cone. Figure 3-5 shows the component average areas at $M = 3.0$.

Non-dimensionalized area progressions for sonic boom computation are derived and presented in Section 7 and are shown in Figure 7-5. The sonic boom areas were formed by the Mach plane tangent to the Mach cone at its lower intersection with the plane of symmetry.

The area distributions are characteristics of smooth, high fineness-ratio forebodies. The moderate forebody slopes are a direct result of the gradual axial addition of wing area to fuselage area. The nacelle area peaks aft of the wing-fuselage area peak, thus avoiding an abrupt buildup to maximum area.

3.3 WEIGHT AND BALANCE CHARACTERISTICS (3.2.6)

The SST has been designed for a maximum take-off gross weight of 450,000 pounds. The passenger and cargo compartment arrangements permit variations

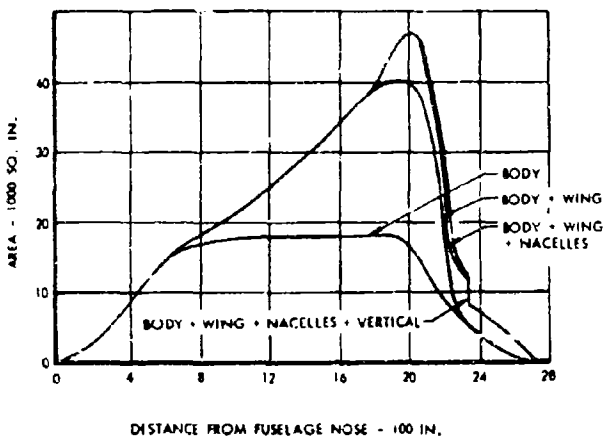

FIGURE 3-2 COMPLETE AIRPLANE AREA PROGRESSION, M = 1.0

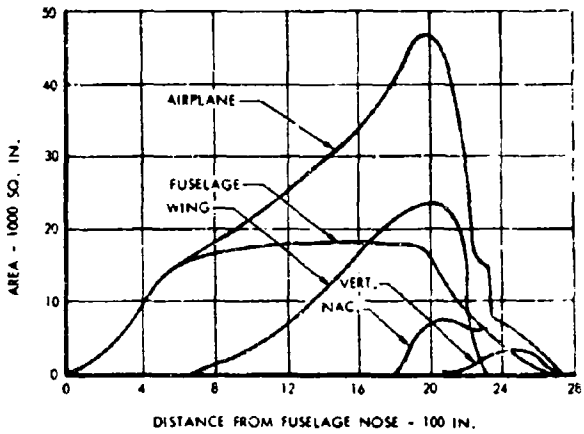

FIGURE 3-3 AIRFRAME COMPONENT AREA PROGRESSION, M = 1.0

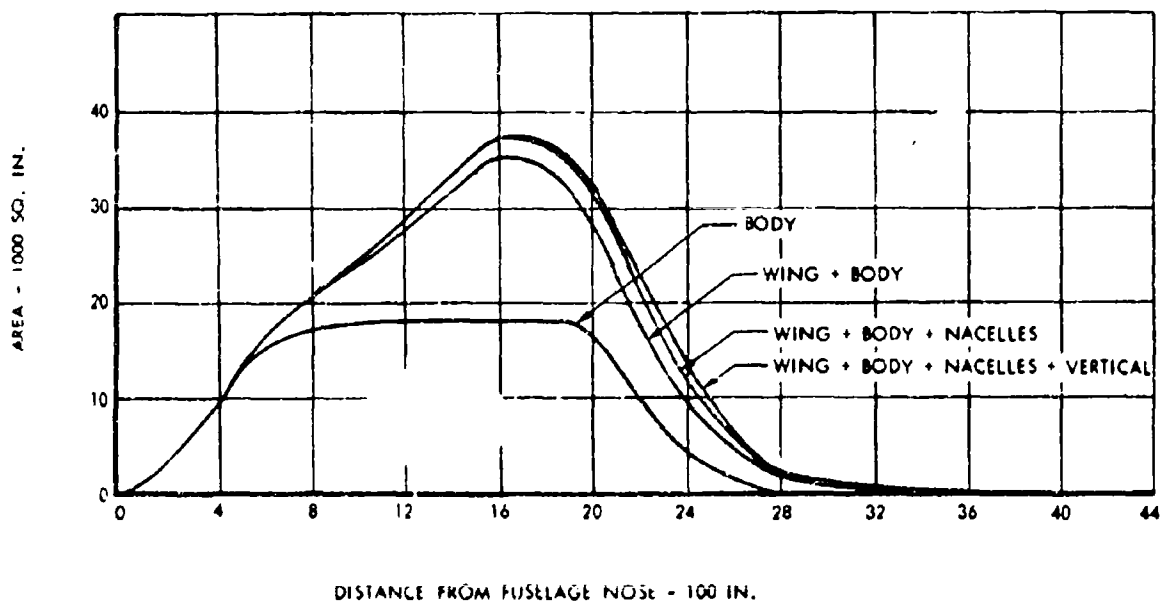

FIGURE 3-4 COMPLETE AIRPLANE AREA PROGRESSION, M = 3.0

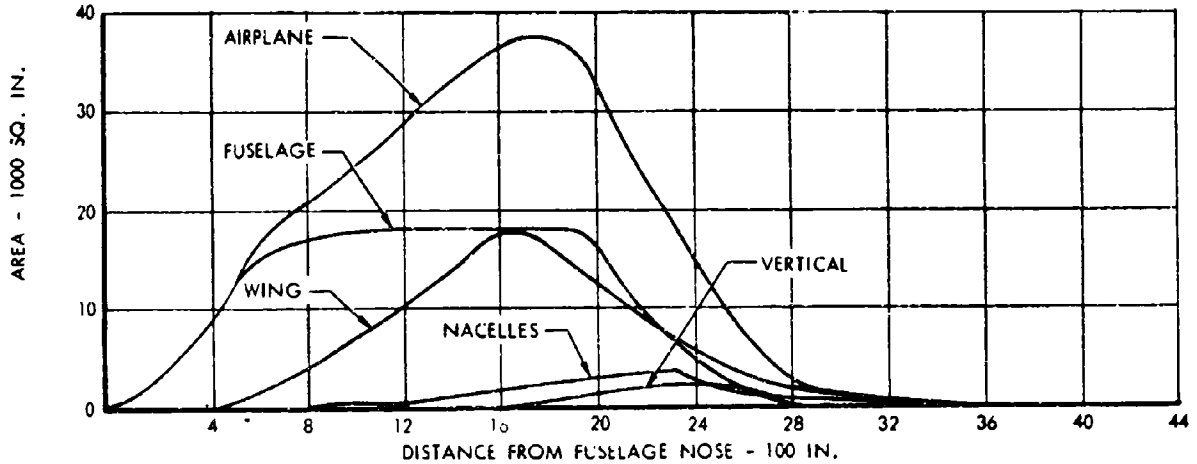

FIGURE 3-5 AIRFRAME COMPONENT AREA PROGRESSION, M = 3.0

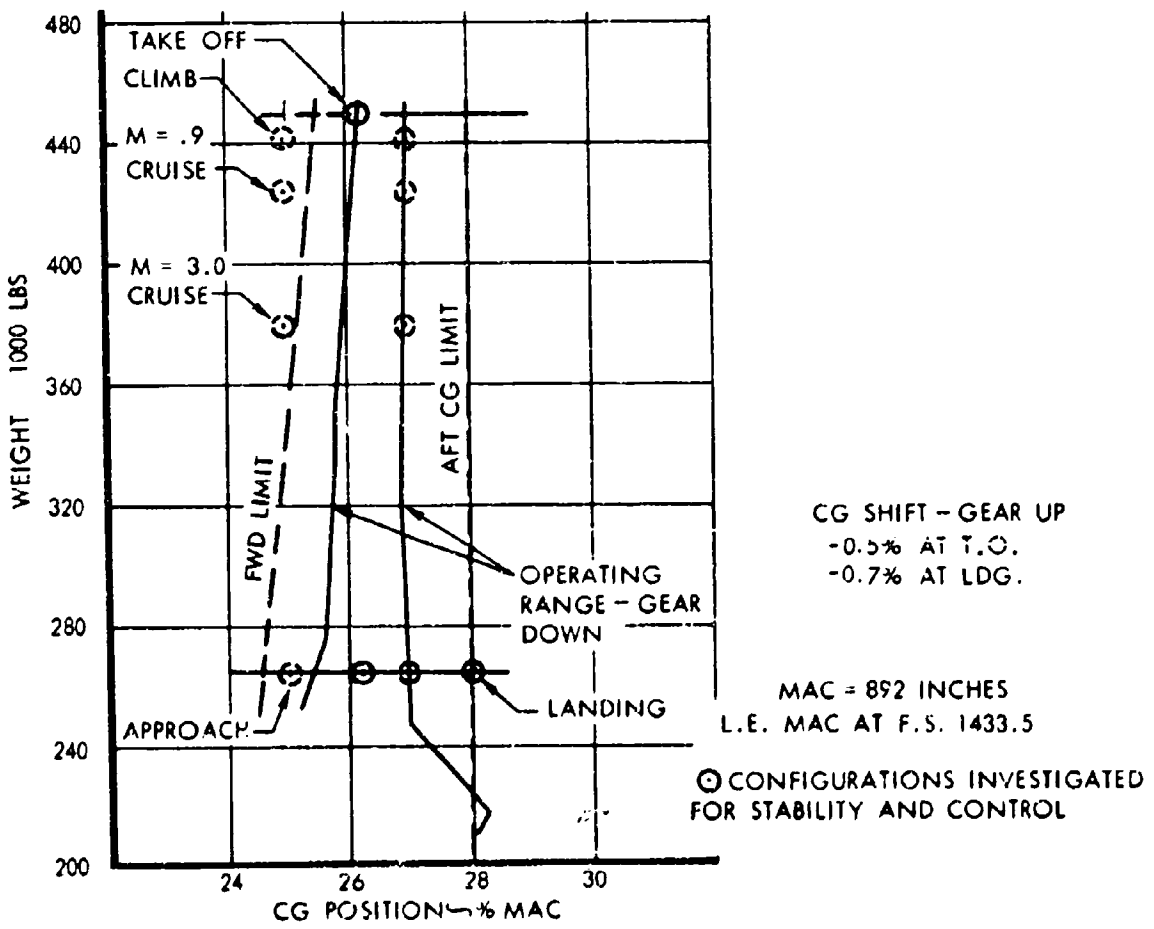

FIGURE 3-6 AIRPLANE CENTER OF GRAVITY ENVELOPE

in payload capacity up to a space limited 45,875 pounds. Possible alternate interior and high density seating arrangements are discussed in detail in Volume A-III. Design weights are summarized in Table 3-2.

TABLE 3-2 DESIGN GROSS WEIGHTS

Manufacturer's Weight Empty, lbs.	See Table 3-3 and 3-4
Maximum Ramp Weight, lbs.	453,000
Maximum Take-Off Weight, lbs.	450,000
Maximum Landing Weight, lbs.	280,000
Maximum Zero Fuel Weight, lbs.	240,000
Operating Weight Empty, lbs	See Table 3-3 and 3-4
Maximum Fuel Capacity, U.S. Gals.	37,846

For performance analysis, the design range mission is conducted with 30,000 pounds of payload. For this loading disposition, operating weight empty is 189,880 pounds, and total fuel is 233,120 pounds. Loading conditions are presented in Table 3-3. The data of Table 3-4 shows the loading condition for a 192 passenger interior arrangement, designated alternate one.

TABLE 3-3 125 PASSENGER LOADING CONDITION

Manufacturers Weight Empty, lbs		182,344
Operating Equipment — Total, lbs		7,536
Crew and Crew Baggage, lbs	1205	
Passenger and Service Equipment, lbs	2833	
Overwater Equipment, lbs	1278	
Unusable Fuel and Oil, lbs	2060	
Usable Oil, lbs	160	
Operating Weight Empty, lbs		189,880
Payload — Total, lbs		30,000
Passengers (125) and Baggage, lbs	25000	
Cargo, lbs	000	
Weight less Fuel, lbs		219,880
Fuel Reserve, lbs		34,530
Landing Weight, lbs		254,410
Fuel Burned, lbs		198,590
Ramp Weight, lbs		453,000

TABLE 3-4 192 PASSENGER LOADING CONDITION ALTERNATE ONE

Manufacturers Weight Empty, lbs		182,778
Operating Equipment — Total, lbs		7,797
Crew and Crew Baggage, lbs	1,205	
Passenger and Service Equipment, lbs	3,069	
Overwater Equipment, lbs	1,303	
Unusable Fuel and Oil, lbs	2,060	
Usable Oil, lbs	160	
Operating Weight Empty, lbs		190,757
Payload — Total, lbs		40,128
Passengers (192) and Baggage, lbs	40,128	
Cargo, lbs	—	
Weight Less Fuel, lbs		230,703
Fuel Reserve, lbs		36,000
Landing Weight, lbs		266,703
Fuel Burned, lbs		186,297
Ramp Weight, lbs		453,000

Figure 3-6 presents the forward and aft center-of-gravity limits established for the SST. Also indicated is the operating range of actual center-of-gravity positions obtained with various fuel and payload loadings. The circles shown on the figure represent specific weight and center-of-gravity positions which have been investigated to establish handling quality characteristics.

Airplane moments of inertia data versus gross weight are shown in Figure 3-7.

3.4 FLIGHT CRITERIA (3.2.6)

3.4.1 DESIGN SPEEDS

Design cruise and dive speed-altitude variations are indicated in Figure 3-8. Considerations leading to the adoption of these speeds are discussed in Volume A-IV, Section 2.2, where it is shown that adequate margins over normal operating speeds are provided to allow for system malfunctions and possible inadvertent upsets.

The operational speed-altitude variations to be followed during a normal flight profile are also presented in Figure 3-8. This schedule utilizes calibrated airspeeds and constant Mach number where possible, so the pilot can readily follow the prescribed schedule.

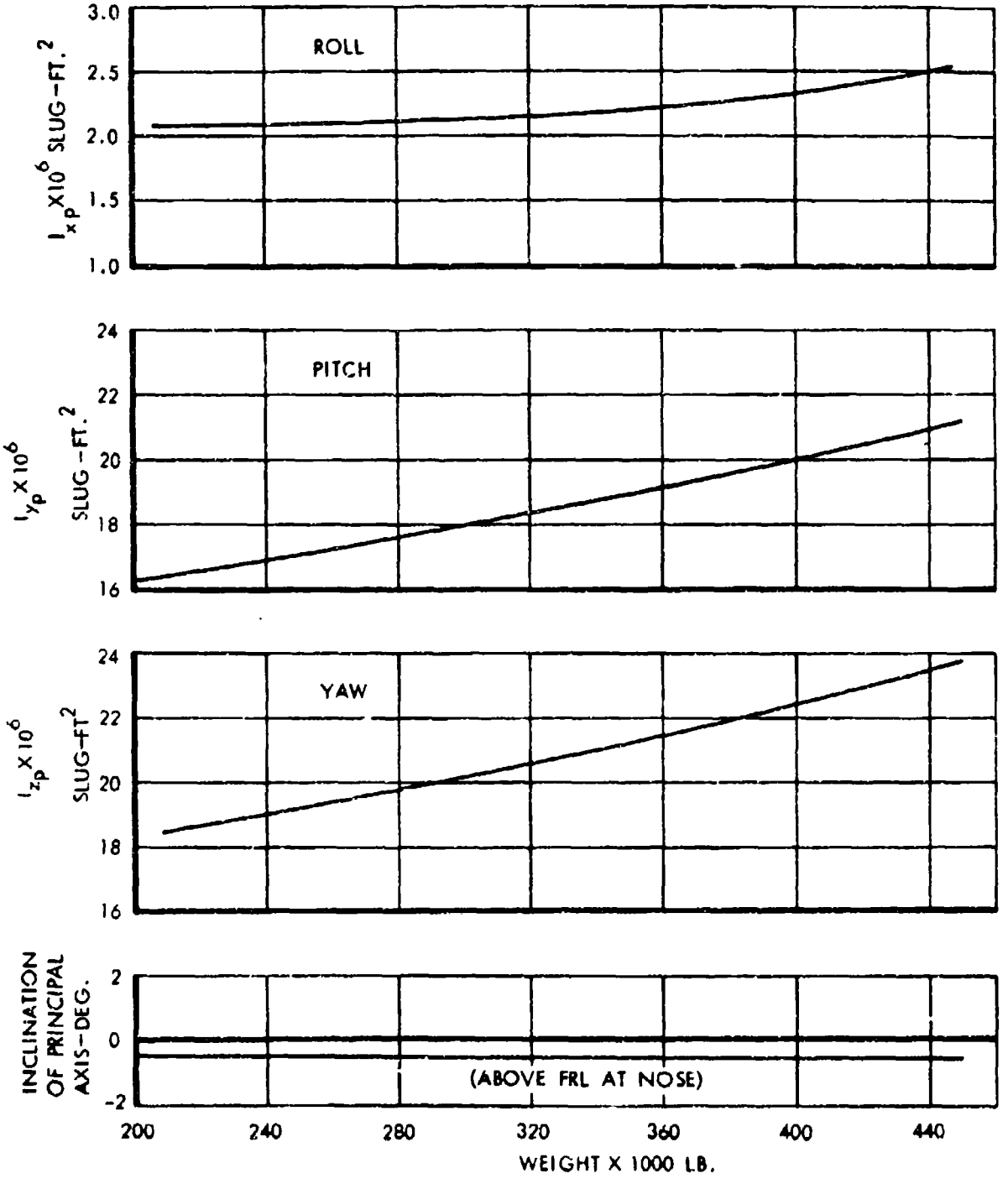

FIGURE 3-7 INERTIA CHARACTERISTICS

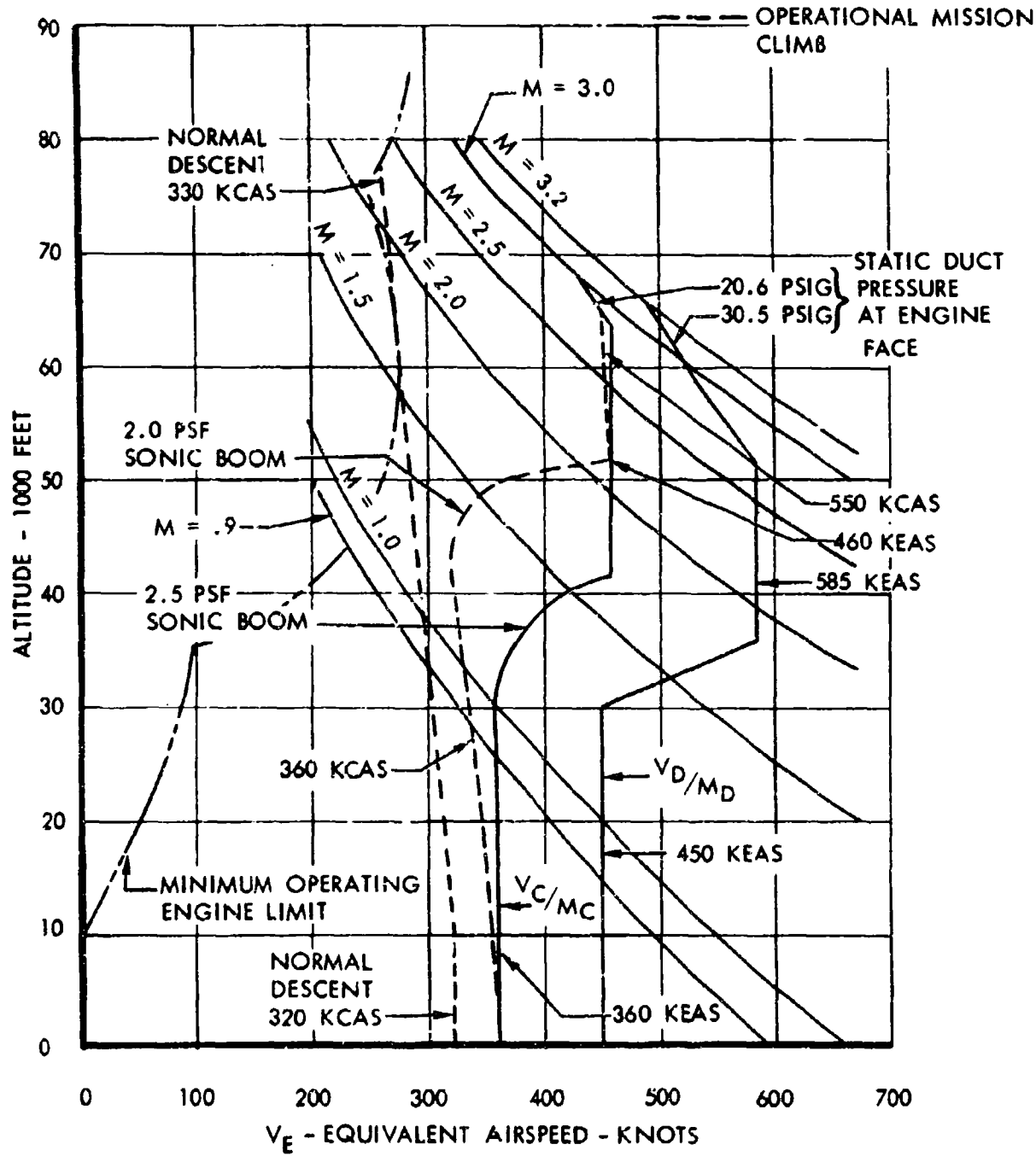

FIGURE 3-8 DESIGN SPEED VERSUS ALTITUDE

In the transonic regime, a constant 2 psf sonic boom profile is followed.

Design placard speeds for landing gear extension and lowering of the weather-vision nose are summarized in Table 3-5. It should be noted that subsonic cruise operation can be conducted with the weather-vision nose lowered to the intermediate position. The main landing gear can be lowered below Mach .90 to improve emergency descent rates.

TABLE 3-5 DESIGN PLACARD SPEEDS

Landing Gear	
Main Gear—Retraction	250 KEAS
—Extension	360 KEAS or $M = 0.90$
Nose Gear—Retraction and Extension	250 KEAS
Weather Vision Nose	
10° Position	360 KEAS or $M = 0.90$
15° Position	250 KEAS or $M = 0.50$

3.4.2 MANEUVER LOAD FACTORS (3.2.6)

Design maneuver load factor diagrams are presented in Figure 3-9, showing the variations in allowable load factors as a function of speed and altitude. Further discussion of these diagrams is presented in Section 2.2 of Volume A-IV.

3.4.3 MINIMUM SPEED BOUNDARIES (3.2.6)

A stick shaker warning device is incorporated to limit angle of attack to 20 degrees from M=0 to M= 0.3, then varying linearly to 10 degrees at $M = 1.3$, and constant at 10 degrees above $M = 1.3$. At low speeds the shaker action initiates at 17 degrees with maximum intensity at 20 degrees, and at high speeds the initiation is at 8 degrees with maximum intensity at 10 degrees. The effect of the shaker boundary on the maneuvering load factor is presented on Figure 3-9.

Based on experience with low aspect ratio highly swept wings, it is believed that no buffet boundary limits will be imposed on the SST within the limits shown in Figure 3-9. This capability provides added flexibility in selecting cruise altitudes to alleviate sonic boom, and freedom for the operator to select transonic acceleration altitudes.

3.4.4 DESIGN MISSION PROFILE (3.2.6)

Flight load spectra and analysis are based on the five flight profiles described in Figures 3-10 to 3-14. Included are short, medium, and long range supersonic flight profiles, a short range subsonic mission, and a check flight profile. Discussion of fatigue load spectra and analysis for these profiles is given in Paragraph 2.2 of Volume A-IV.

3.5 PROPULSION CHARACTERISTICS

The candidate engine for powering the SST was chosen after reviewing the offerings of all three U.S. engine companies. Potential capability of each engine was assessed in terms of performance, availability, schedule, cost and risk. Three candidate engines were selected, the P&W JT11F-4, the G.E. 4/F6A, and the CW TJ70A-4 engines. From this list, the Pratt & Whitney JTIIF-4 ducted fan powerplant is presented as the basic engine, since it evolves from an existing turbojet powerplant having five years of development effort and should involve less risk and better assurance with regard to schedules and availability. Further discussion of engine characteristics is presented in Volume A-VI.

Characteristics of the JT11F-4, GE 4/F6A and TJ70A4 engines are summarized in Table 3-6.

Performance analysis presented in Section 5 is based on the JT11F-4 powerplant. The performance characteristics realized using the General Electric GE 4/F6A and the Curtiss Wright TJ70A-1 engines are shown in Figure 1-2. Any of these engines can be utilized by the SST with the more advanced versions offering greater payload-range capability.

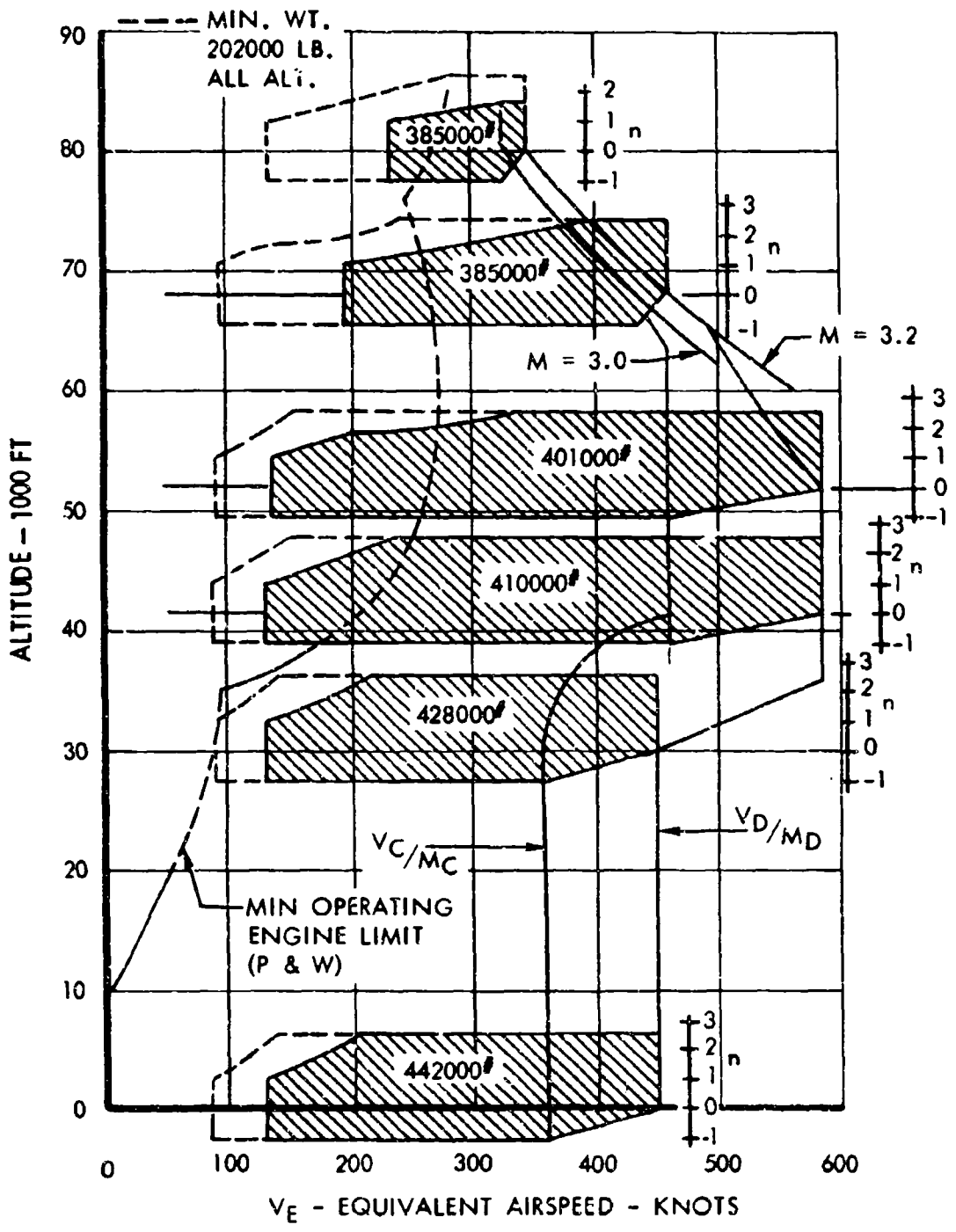

FIGURE 3-9 AIRSPEED—LOAD FACTORS—DIAGRAM

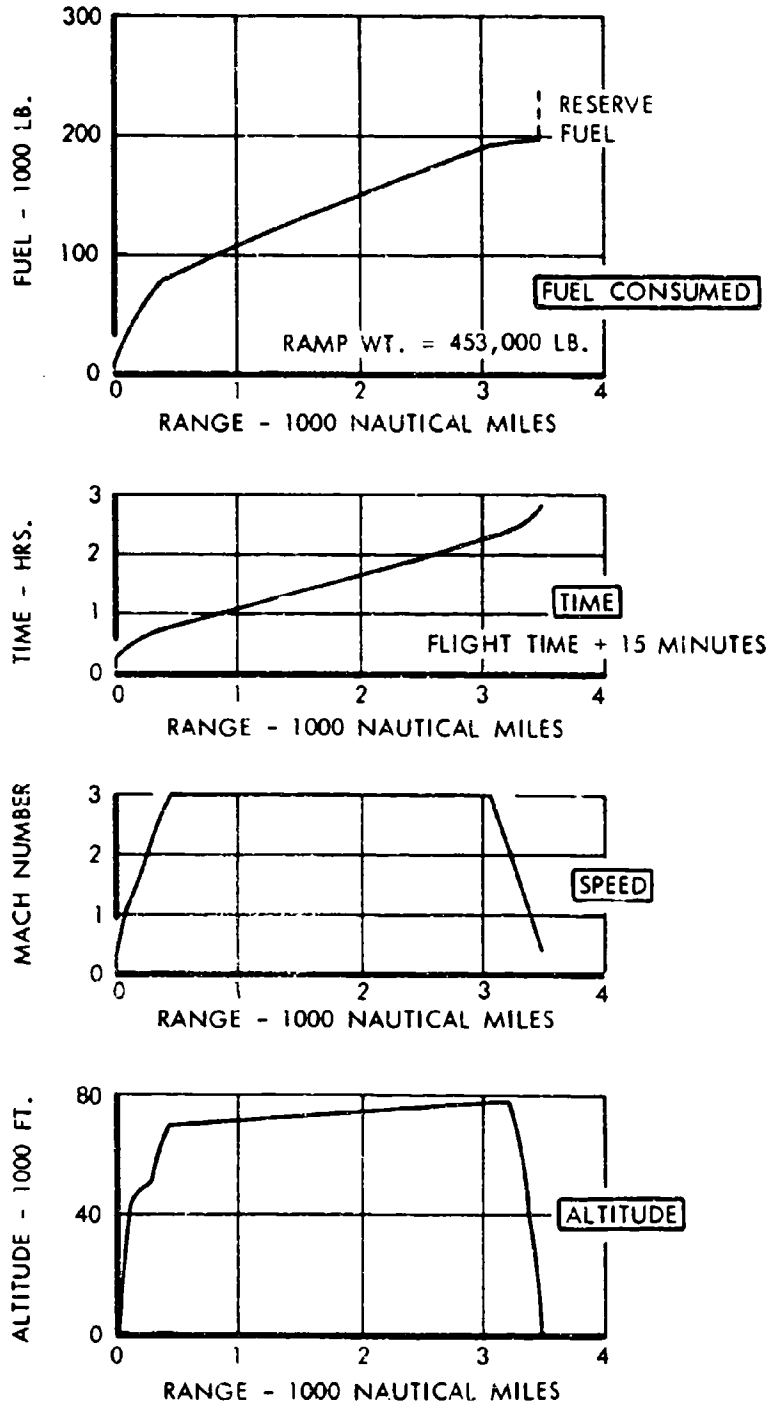

FIGURE 3-10 DESIGN FLIGHT PROFILE – TAKE-OFF GROSS WEIGHT 450,000 LB.

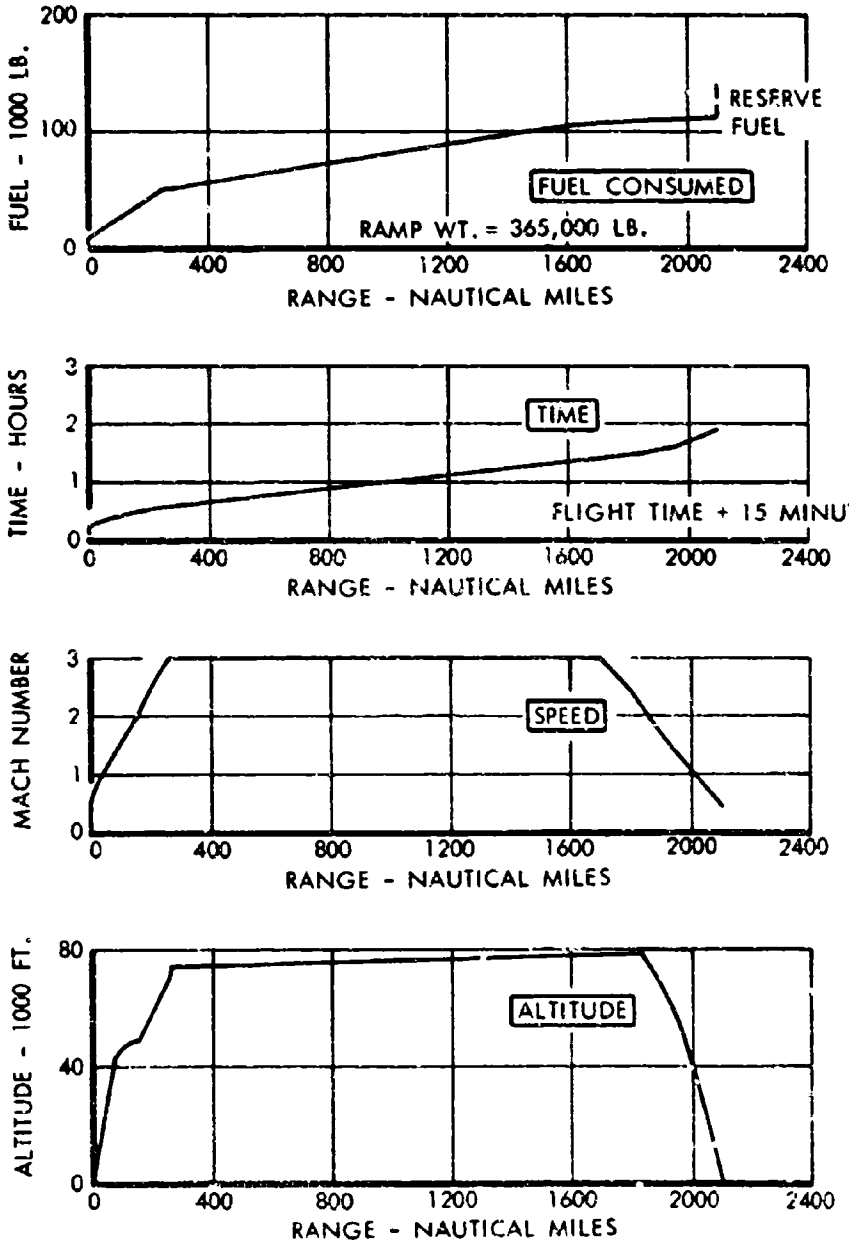

FIGURE 3-11 2100 NAUTICAL MILE FLIGHT PROFILE — TAKE-OFF GROSS WEIGHT 362,000 LB.

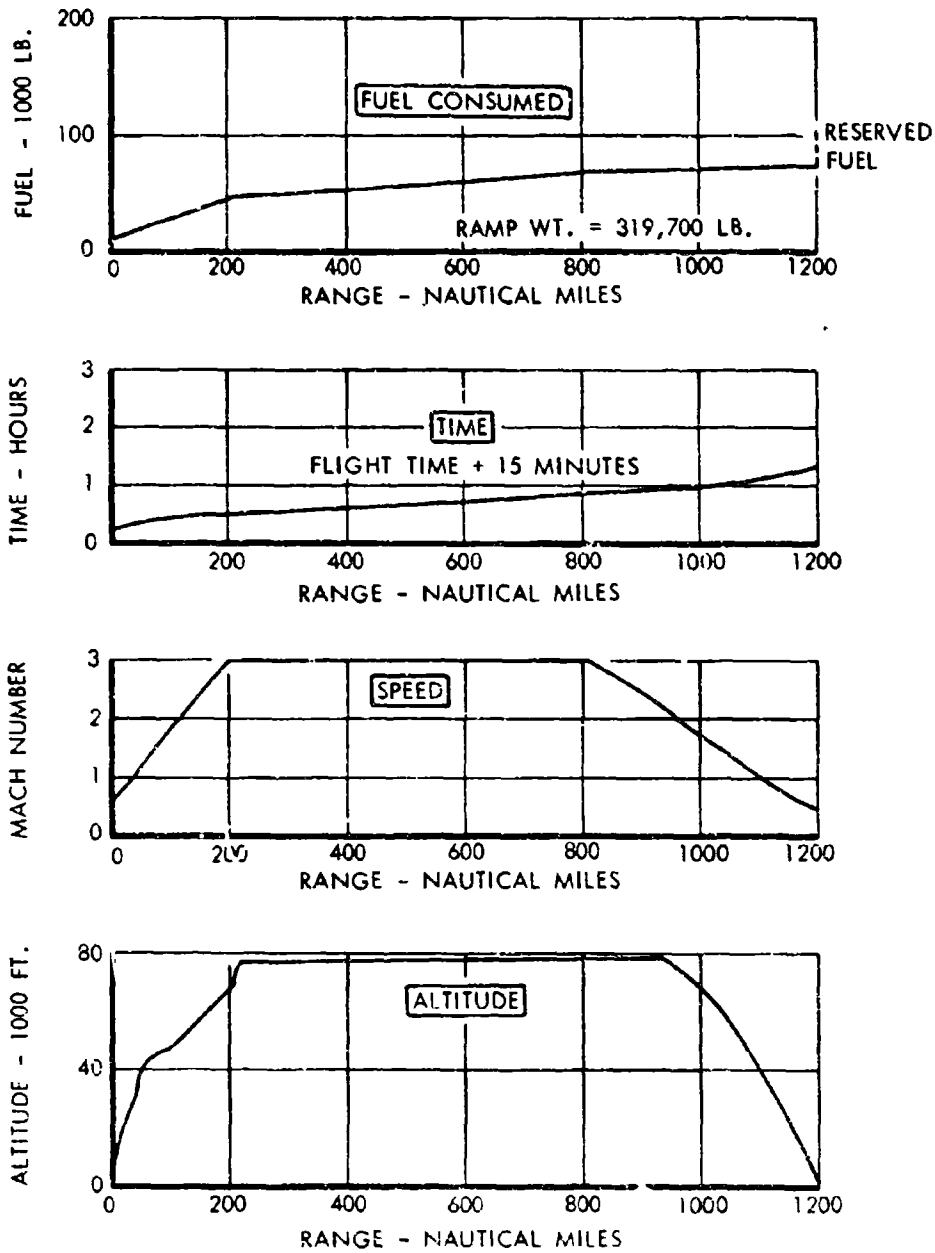

FIGURE 3-12 1200 NAUTICAL MILE FLIGHT PROFILE – TAKE-OFF GROSS WEIGHT 316,700 LB.

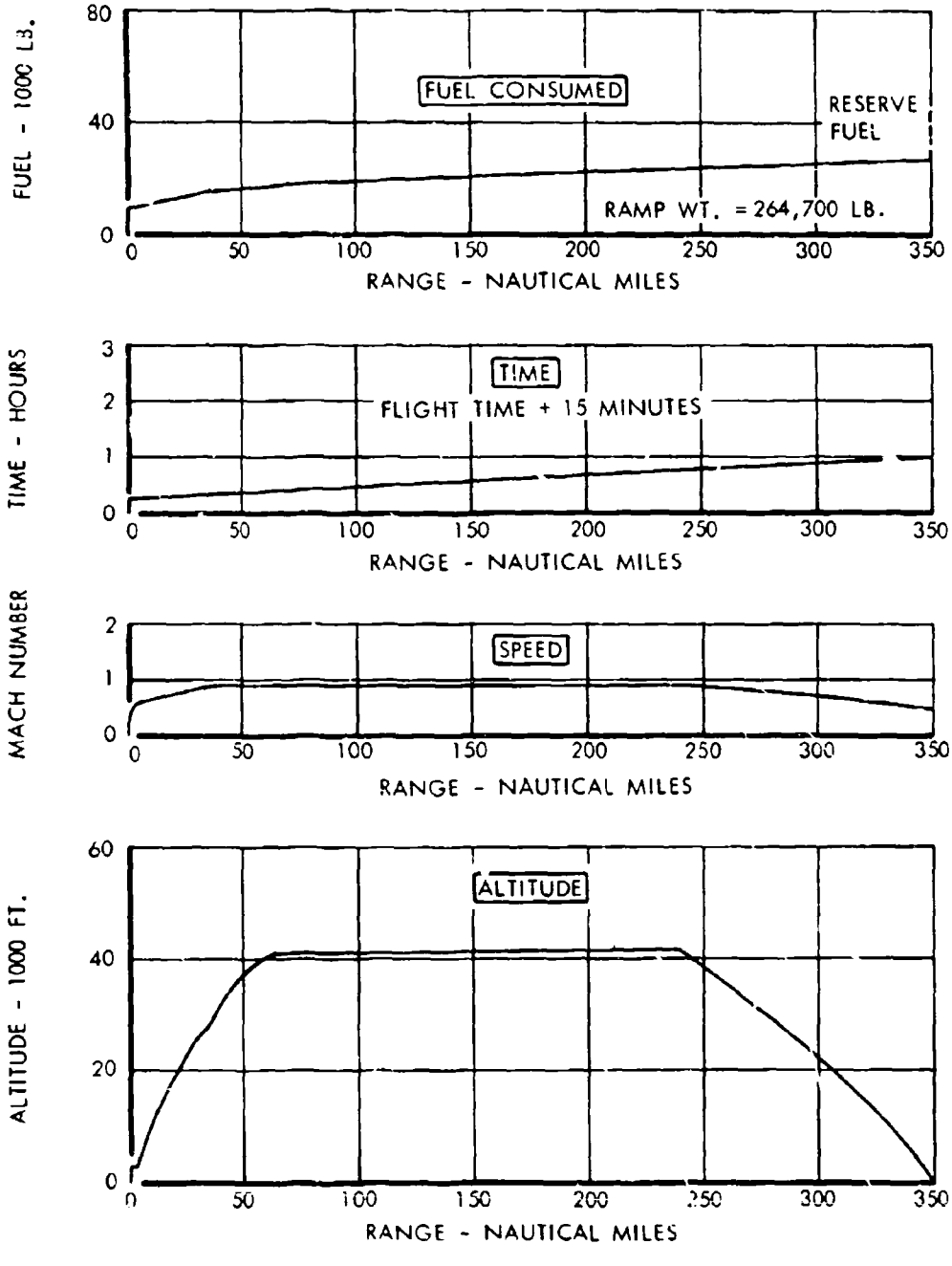

FIGURE 3-13 350 NAUTICAL MILE FLIGHT PROFILE— TAKE-OFF GROSS WEIGHT 261,700 LB.

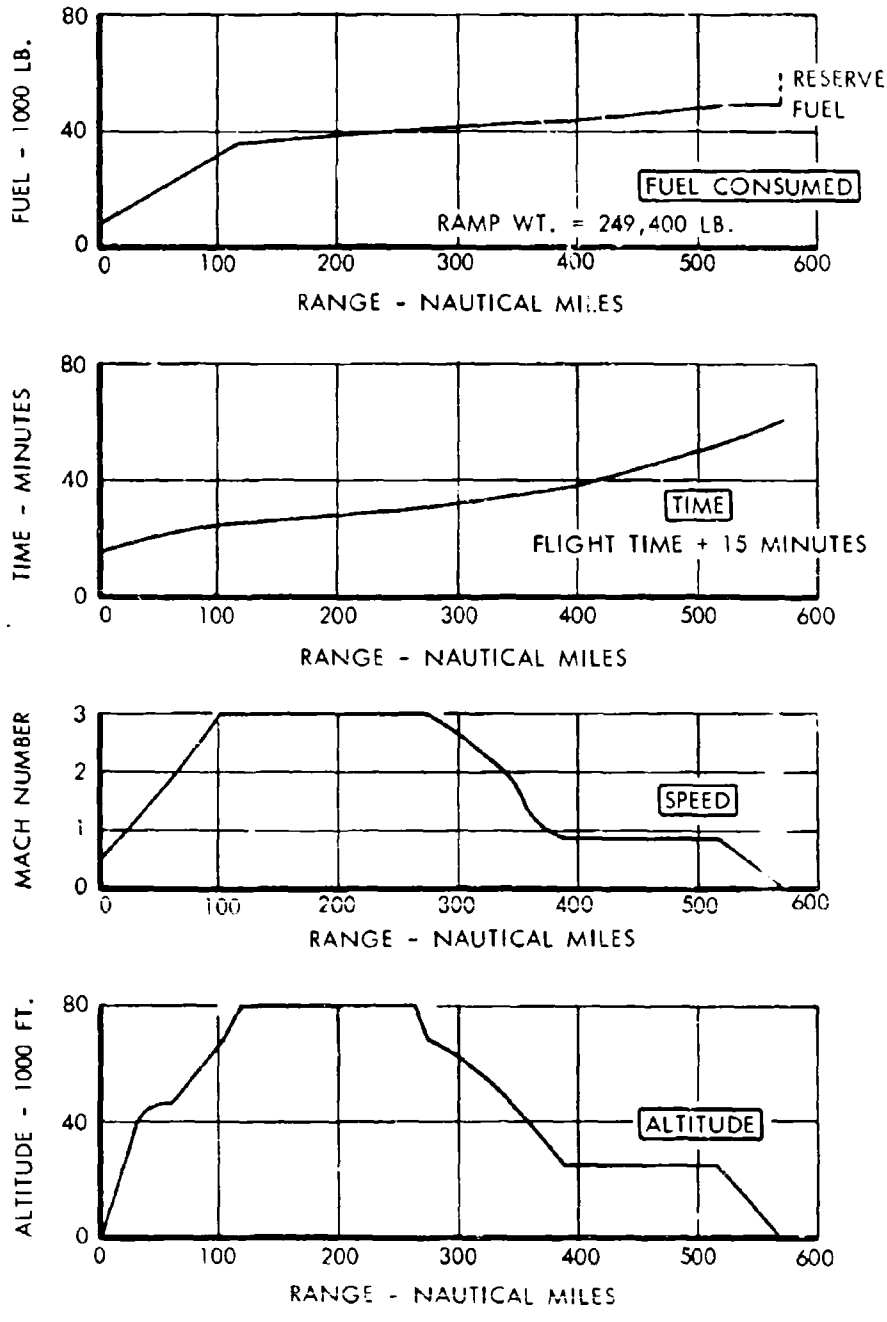

FIGURE 3-14 PILOT TRAINING AND CHECK FLIGHT PROFILE – TAKE-OFF GROSS WEIGHT 246,400 LB.

TABLE 3-6 ENGINE CHARACTERISTICS

	Turbofans		*Turbojet*
	Pratt & Whitney	*G.E.*	*Wright*
	JT11F-3/4	GE4/F6A	TJ70A4
Thrust, Sea Level Static*	50,400	49,700	54,700
Weight, lb.	9355/9605	8370/8620	7000
$\frac{\text{Thrust}}{\text{Weight}}$ Mach 3.0 Design*	5.2	5.8	7.8
Sea Level Static Airflow* lbs/sec	640	600	600
Mach = 3.0, Specific Fuel Consumption, 10,000 lb Thrust, 75,000 ft Altitude	1.77	1.77	1.50 (max. cruise = 7800 lbs T)
Mach 1.2, Maximum Thrust 43,000 ft Altitude	18,200	19,800	17,800
Mach 0.9, Specific Fuel Consumption, 6700 lb Thrust, 36,150 ft Altitude	1.06	1.00	.97
Mach 0.5, Specific Fuel Consumption, 4750 lb Thrust, 15,000 ft Altitude	1.23	1.18	1.18
Turbine-in Temperature °F (Cruise)	1900	2200	2200

**Uninstalled Values*

SECTION 4 AERODYNAMIC DATA (3.2.6)

Substantiation and summaries of all basic aerodynamic characteristics are presented in this section, including descriptions of models and test facilities, results obtained from wind tunnel tests, analysis and interpretation of these wind tunnel tests, correlation with other appropriate results, and extrapolation techniques employed.

Also included in this section is a proposed wind tunnel schedule that will serve to continue the present program and provide further substantiation and refinement of the SST airplane.

4.1 WIND TUNNEL MODELS

The proposed SST configuration incorporates several aerodynamic refinements of the basic delta wing planform shape that result in reduced drag and improved stability characteristics. This new wing geometry, which can be described as a twisted and cambered double-delta wing, was developed as a result of extensive wind tunnel tests as discussed in Section 2. Performance and handling qualities for the SST are based primarily on these wind tunnel data. The final low-speed and high-speed models shown in Figure 4-1 closely simulate the final airplane configuration, and data from these models form the principal basis for evaluating the basic aerodynamic data.

Low-speed data were obtained in a continuous, closed circuit 8 foot x 12 foot subsonic tunnel, using a 1/30 scale fork-mounted model. Flow conditions for most tests were at 180 miles per hour (80 psf dynamic pressure) giving an operating Reynolds number of 11×10^6 based on body length. Six component data were recorded, and tufts and oil-lamp black were used to assist in flow visualization studies. Low-speed tests provided static stability derivatives and control effectiveness. The drag due to lift characteristics at subsonic speeds are determined from the results of subsonic tests in the Rye Canyon facility. This facility, which operates subsonically at Reynolds numbers of 31 million based on fuselage length or 14 million based on exposed wing MAC is preferable for this purpose to the 8 foot x 12 foot tunnel, which operates at Reynolds numbers approximately one third as large. All low-speed airplane configurations were tested, including effects of landing gear extension, weather-vision nose position, and presence of the ground. Pitch data were examined beyond the maximum proposed airplane flight attitude for all configurations. A total of 313 pitch and yaw runs were conducted using the final low-speed model.

High-speed wind tunnel data were conducted in the Rye Canyon Research facility, using the 4 foot x 4 foot blow-down tunnel. Complete model data were obtained from Mach numbers of .40 to .70 and 1.5 to 3.6 using the supersonic test section, and from .90 to 1.2 using the porous wall transonic test section. Variations in operating pressure permitted test Reynolds number variations from 20×10^6 to 85×10^6 based on body length. The model employed for final aerodynamic testing was 1/60 scale, sting mounted, and fabricated of aluminum and steel.

For both the low and high-speed models, the air passage duct through the nacelles was rectangular over the nacelle length, to facilitate internal drag measurement and help maintain full-flow duct operation. Aerodynamic coefficients for both the low-speed and high-speed model data are based on the reference area shown in Figure 4-2. All aerodynamic analyses in this report are also based on this reference area.

In the presentation of the wind tunnel data, there are figures indicating the effects of changes in airplane geometry such as landing gear extension, control surface deflection, or adjustment of the weather-vision nose. In some instances, the model tests were conducted before some of the details of the final airplane configuration were selected and the effects are evaluated on intermediate model configurations. These tests were used to obtain the incremental changes due to gear or nose position, and the increments were applied as corrections to the final model geometry data. Since no large model configuration changes were ever adopted, this procedure is considered to be valid.

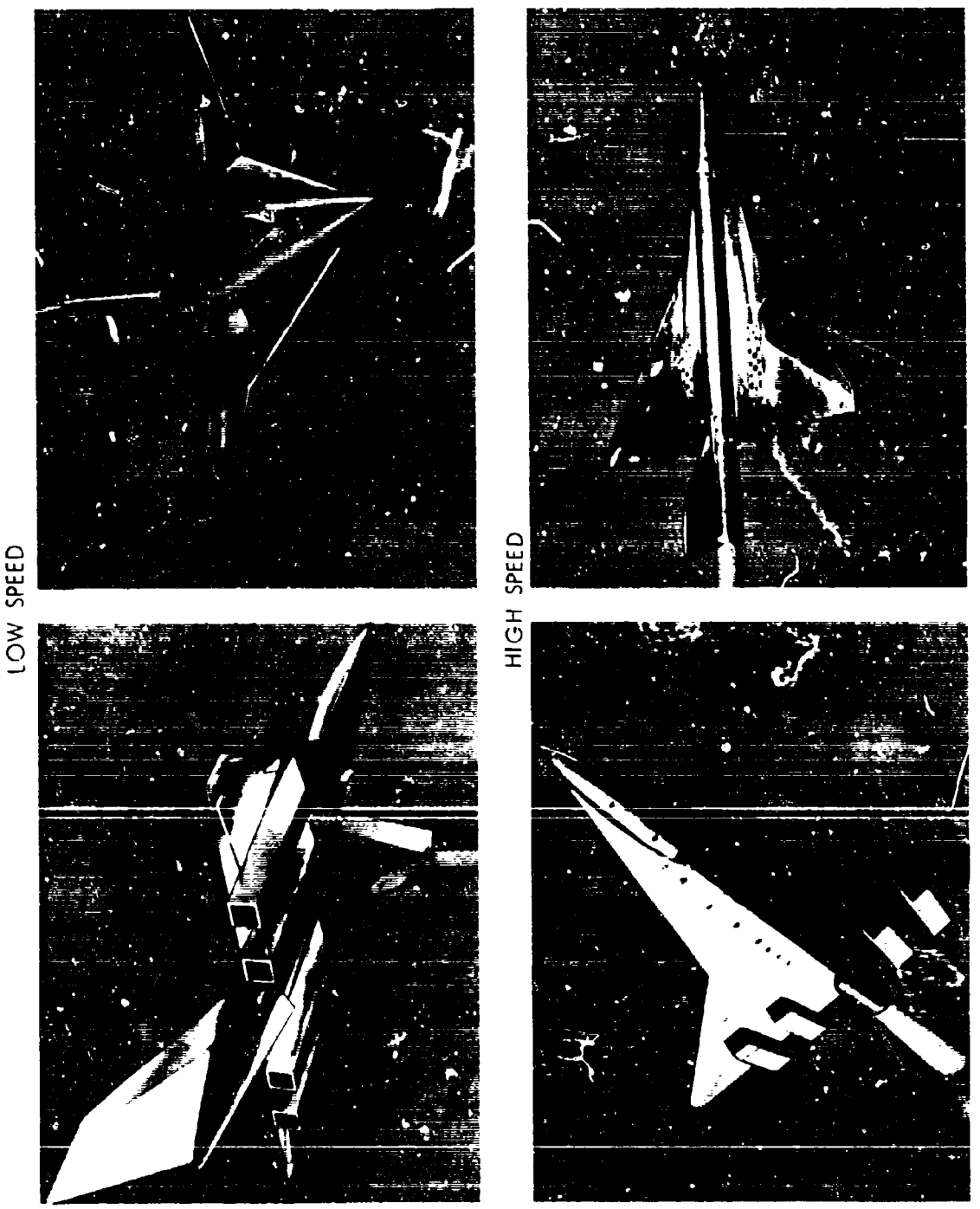

FIGURE 4-1 LOW SPEED AND HIGH SPEED WIND TUNNEL MODELS

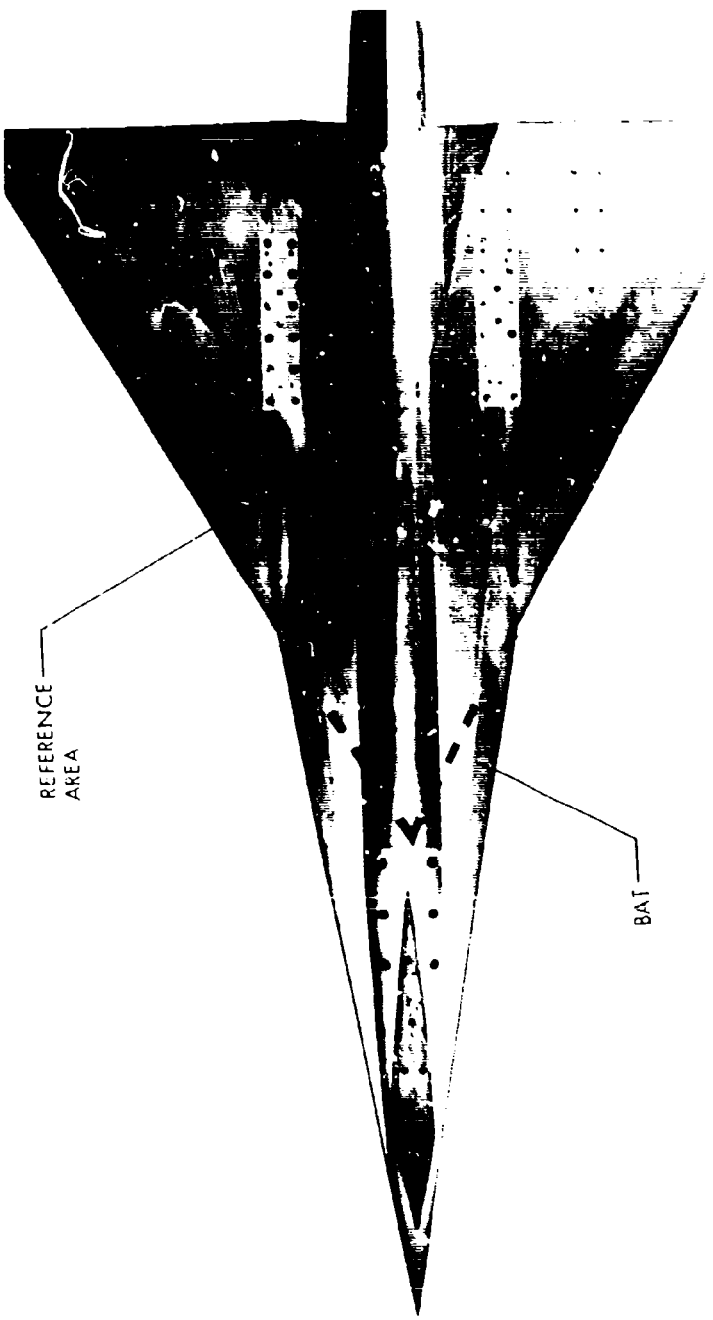

FIGURE 4-2 WING REFERENCE AREA

4.2 DRAG ESTIMATION

The drag estimation for the SST is based on wind tunnel test data obtained in the Rye Canyon high-speed test facility from scale models of the SST configuration. Theoretical methods and NASA test information are used to correlate the measured data and to permit extrapolation to full-scale flight conditions. This section presents the wind tunnel test information and provides the required substantiation of the drag data used in the calculation of the SST performance characteristics.

4.2.1 WING-BODY DRAG

Typical drag polars for the wing body configuration of the SST are shown for a range of Mach numbers between 0.73 and 3.0 in Figures 4-3 through 4-8. These data were obtained in the Rye Canyon high-speed test facility on a 1/60th scale model at a fixed Reynolds number of 10 million per foot. This is equivalent to a Reynolds number of 31 million based on the actual length of the model fuselage. The maximum lift-to-drag ratios measured under these conditions are indicated on Figures 4-3 through 4-8 and range from 11.5 at Mach 0.91 to 7.9 at Mach 3.0.

In order to apply the wing-body data to the drag estimation of the SST, it is necessary to be able to separate the wing and body effects on a rational basis. Since the method of model construction did not permit the testing of the body alone, the body effects are separated by analytical techniques. The means for substantiation of the analytical methods is afforded by a series of tests of forebody shapes. No question of afterbody drag arises in the analysis of either the wing-body data or the forebody data, since in each case the afterbody was cylindrical and the base drag was removed experimentally.

The fore-body drag data are presented in Figure 4-9 for fineness ratio 6.0 and 7.5 Sears Haack nose shapes tested at Mach numbers between 0.7 and 3.0 at Reynolds numbers equivalent to 57 million based on the fuselage length. Figure 4-9 indicates that simple theoretical methods provide an accurate estimation of total forebody drag both at subsonic speeds and throughout the supersonic speed range. The forebody pressure drag at supersonic speeds is estimated from the relation,

$$C_{D_F} = \frac{4.7}{F^2}$$

where:

C_{D_F} = pressure drag coefficient based on frontal area

$$F = \frac{2 \times \text{forebody length}}{\text{forebody diameter}}$$

This relation is derived from the linearized theory for parabolic arc nose shapes and predicts the pressure drag to be independent of Mach number. At transonic speeds, a peak pressure drag approximately 30 percent higher than the supersonic level is usually obtained as is indicated in Figure 4-9. The skin friction drag is estimated by the Sommer and Short T' method as described in Reference 4-1 for smooth flat plates increased by 10 percent to account for the thinning of the boundary layer on the three dimensional nose shape. The total drag estimated by this procedure is seen to be in very close agreement with the test data in the Mach range for which the data are available. It is of interest to note that the maximum departure of the test data from the estimate, 0.0008 C_{D_F}, corresponds to a value of drag coefficient based on wing area of only approximately 0.0001 for the SST. The fact that the estimation procedure is successful for bodies of different fineness ratio which, in addition, have different ratios of surface area to frontal area indicates that the separate estimates of friction drag and pressure drag are reliable. These methods are used to separate the wing and body effects in the zero-lift wing-body drag data presented in Figure 4-12.

All available zero-lift wing-body drag data from the SST model test program are plotted in Figure 4-12 as a function of Mach number on a large scale. These data are taken from drag polars as typified by Figures 4-3 through 4-8. The same Mach range is encompassed and the number of re-run and check points are indicated. The resolution of the tunnel data appears to be very good with departures from the mean fairing of less than 0.0002 drag coefficient based on the reference wing area of 7,000 square feet. All data presented in Figure 4-12 were obtained at a Reynolds number of 10 million per foot or 31 million based on the model fuselage length.

The turbulent skin friction drag for the wing-body combination which is shown in Figure 4-12 is estimated by the Sommer and Short T' method of Reference 4-1 with an assumed recovery factor of 0.9. In the case of the fuselage, the flat plate drag coefficient from Reference 4-1 is increased by 10 percent to allow

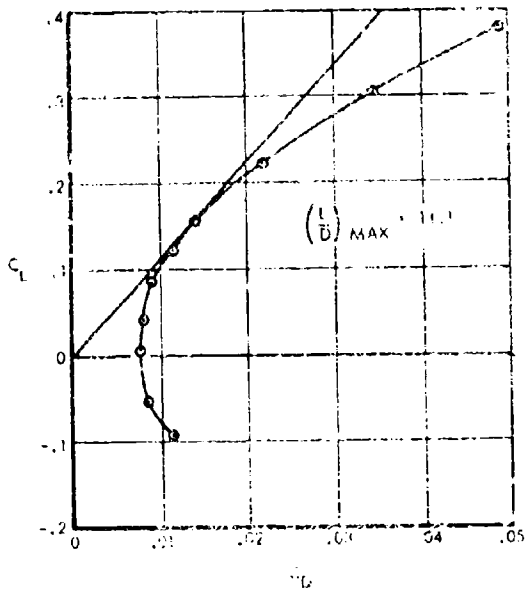

FIGURE 4-3 WING-BODY WIND-TUNNEL DRAG POLAR, M = .73

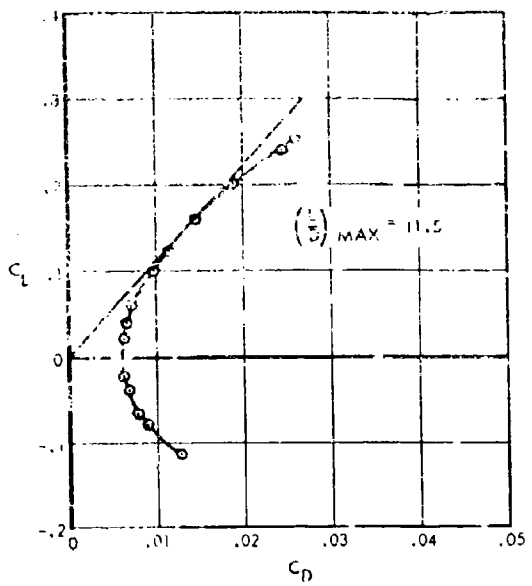

FIGURE 4-4 WING-BODY WIND-TUNNEL DRAG POLAR, M = .91

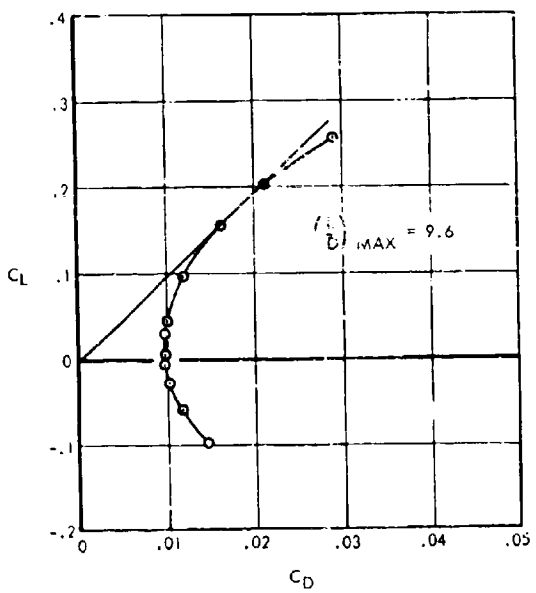

FIGURE 4-5 WING-BODY WIND-TUNNEL DRAG POLAR, M = 1.18

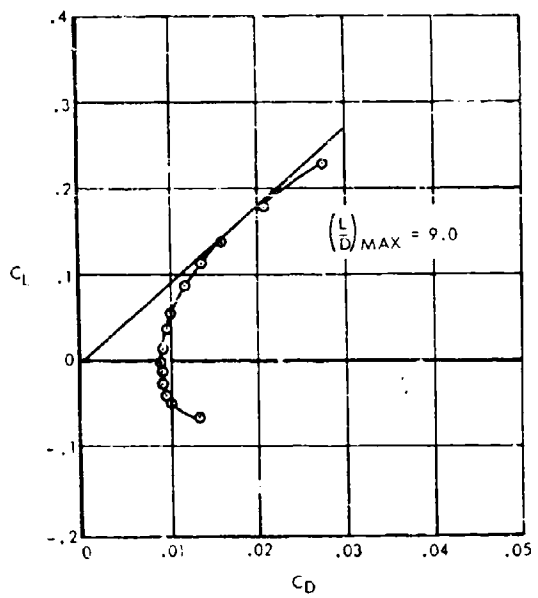

FIGURE 4-6 WING-BODY WIND-TUNNEL DRAG POLAR, M = 1.51

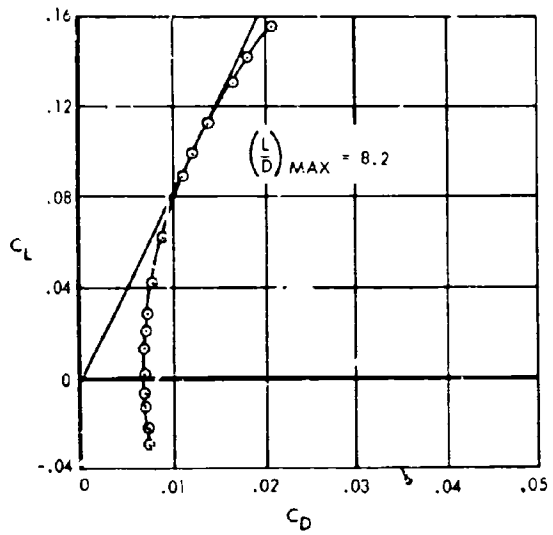

FIGURE 4-7 WING-BODY WIND-TUNNEL DRAG POLAR, M = 2.6

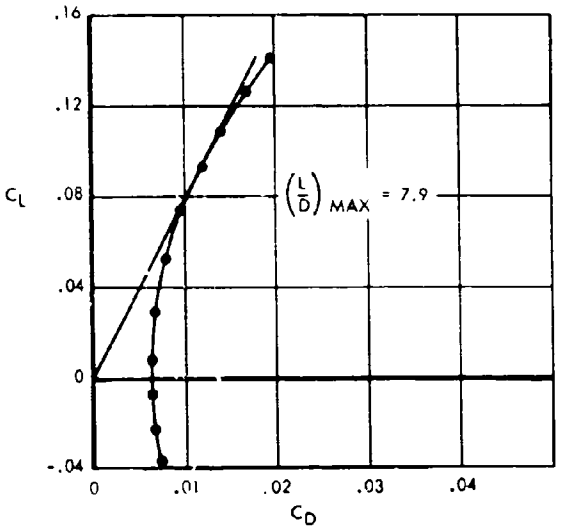

FIGURE 4-8 WING-BODY WIND-TUNNEL DRAG POLAR, M = 3.0

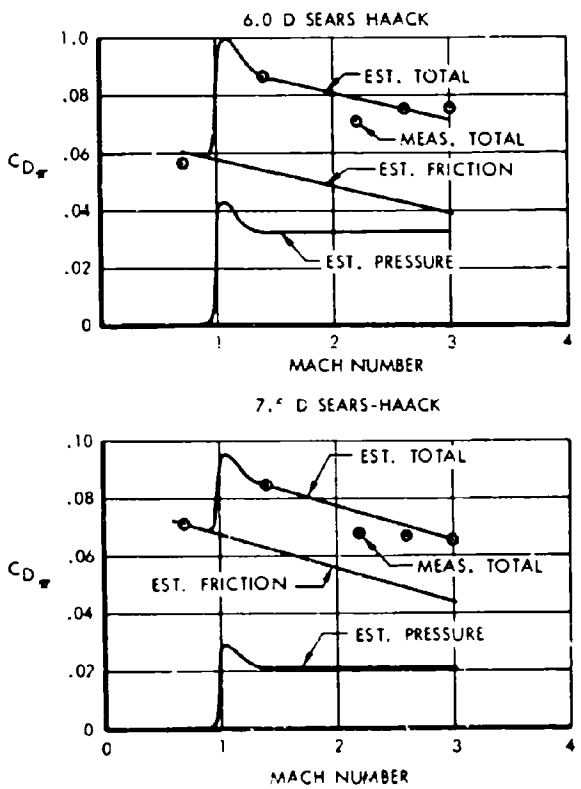

FIGURE 4-9 FORE-BODY DRAG

for the thinning of the boundary layer in three dimensional flow. That the flow is fully turbulent at the test Reynolds numbers is demonstrated by the typical data in Figure 4-13 shown for $M = 2.6$ and $M = 3.0$. No evidence of typical transition characteristics is indicated at Reynolds numbe of 30 million or above corresponding to the Reynolds number range of Figure 4-12.

The difference between the measured total drag and the friction drag is plotted on the lower part of Figure 4-12 as the wing and fuselage pressure drag. The fuselage forebody pressure drag is estimated for the 8.5 fineness ratio nose shape of the SST model by the procedure outlined previously. The pressure drag of the exposed wing is obtained by subtracting the forebody pressure drag from the total pressure drag of the wing-body combination.

The mean thickness ratio of the exposed model wing is defined by a strip integration in the following manner:

$$\left(\frac{t}{c}\right)_{av} = \sqrt{\frac{\int_{Fuse.\ Side}^{Tip} \left(\frac{t}{c}\right)^2 c\, dy}{Exposed\ Plan\ Area}}$$

For the wind tunnel model wing, this average thickness ratio is found to be equal to 0.0244.

The SST wing is cambered and twisted similar to the model wing, but incorporates parabolic arc sections rather than the hexagonal and diamond sections used on the wind tunnel model. The airfoil sections used on the inboard extended chord bat are aerodynamically equivalent for both applications. The outer panel which incorporates a parabolic arc section represents 52 percent of the exposed wing area. The wing pressure drag is adjusted for airfoil section type in proportion to the magnitude of the two-dimensional section-shape parameter and the area affected. That is, the model-wing data are multiplied by the factor $.48(1.0) + .52\,(5.33/4.16) = 1.147$. The SST wing thickness ratios vary from 2.7 percent at the centerline, to 3.0 percent at the crank, to 4.5 percent at the tip and the physical thickness varies linearly from station to station. The average thickness ratio of the exposed wing, computed as described previously is 3.03 percent. The model-wing pressure drag is increased by an additional factor equal to the square of the ratio of the thickness ratios or $(3.03/2.44)^2 = 1.545$. The total adjustment factor is then the product of the shape factor and the thickness factor or $1.147 \times 1.545 = 1.78$. This adjustment is made in Figure 4-14 which shows the variation with Mach number of the SST wing pressure drag based on exposed plan area. The use of exposed area is necessary in this case, since the nacelles of the SST blanket a large part of the wing and the net exposed drag-producing area is less relatively for the SST than for the wind-tunnel model without nacelles.

4.2.2 VERTICAL TAIL PRESSURE DRAG

No attempt was made to obtain a measurement of the pressure drag of the vertical tail during the wind tunnel program, since the magnitude of the drag increment is of the same order as the resolution capability of the wind tunnel. It is felt that analytical estimates of pressure drag are in this case more meaningful. The thickness ratio of the vertical tail varies from 3.0 percent at the root to 3.5 percent at the tip and has an average value of 3.12 percent. The pressure drag of the vertical tail is assumed to be the same as that for the wing on the basis of exposed area.

4.2.3 FUSELAGE PRESSURE DRAG

The SST fuselage has the double-bubble shape sketched in Figure 4-15. For the purpose of drag estimation, it is necessary to know how the fuselage contours are developed. For the upper bubble, the forebody shape is generated from a Sears Haack profile of 8.5 length to diameter ratio and 148 inch maximum diameter joined to the 132 inch diameter cylindrical fuselage. The afterbody shape is generated similarly from an 8.0 length to diameter ratio Sears Haack profile with a maximum diameter of 148 inches. The lower bubble is essentially one-half of a complete closed Sears Haack body with an effective diameter of 10.37 feet and a fineness ratio of 21.7 based on total fuselage length. For the actual SST fuselage, the basic afterbody shape is shortened by 5 feet and refaired. For the purpose of drag estimation, this shortening is not considered either in the wave drag or the friction drag, since the net effect of this change to the rear of the fuselage is very small.

The pressure drag of the forebody and afterbody of the upper bubble is computed from the relation $C_{D_F} = 4.7/F^2$ discussed under Section 4.2.1. The

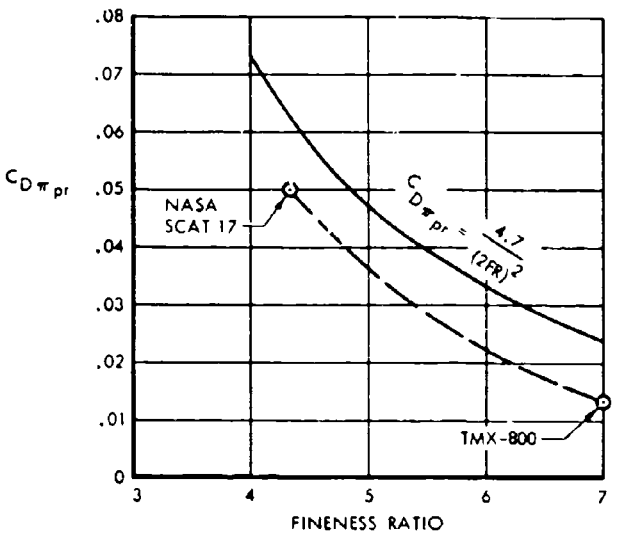

FIGURE 4.10 EFFECT OF FINENESS RATIO ON AFTERBODY DRAG, M = 3.0

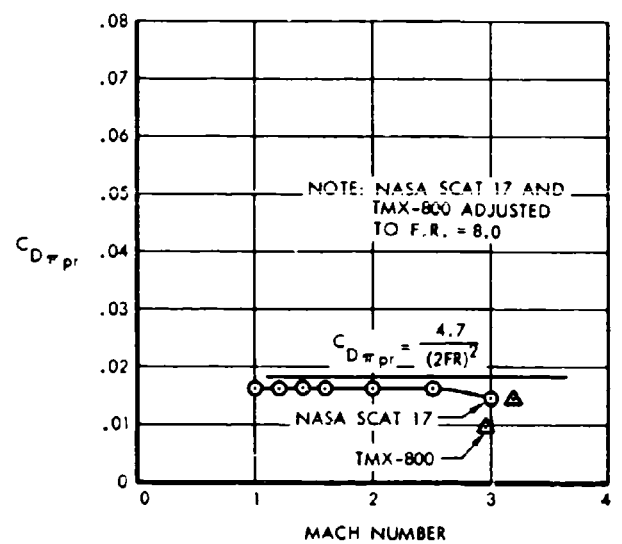

FIGURE 4-11 EFFECT OF MACH NUMBER ON AFTERBODY DRAG, FR = 8.0

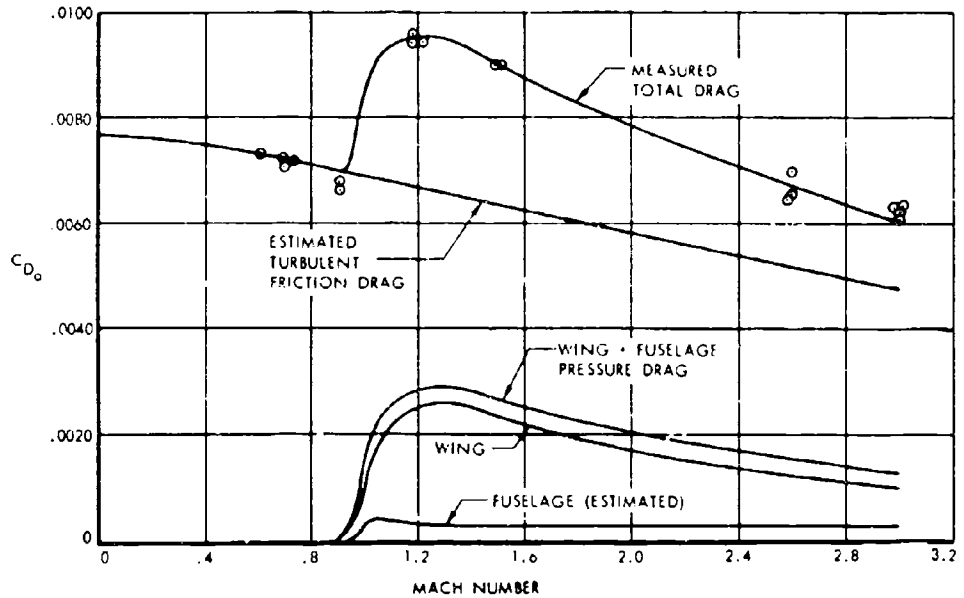

FIGURE 4-12 WIND-TUNNEL ZERO-LIFT DRAG

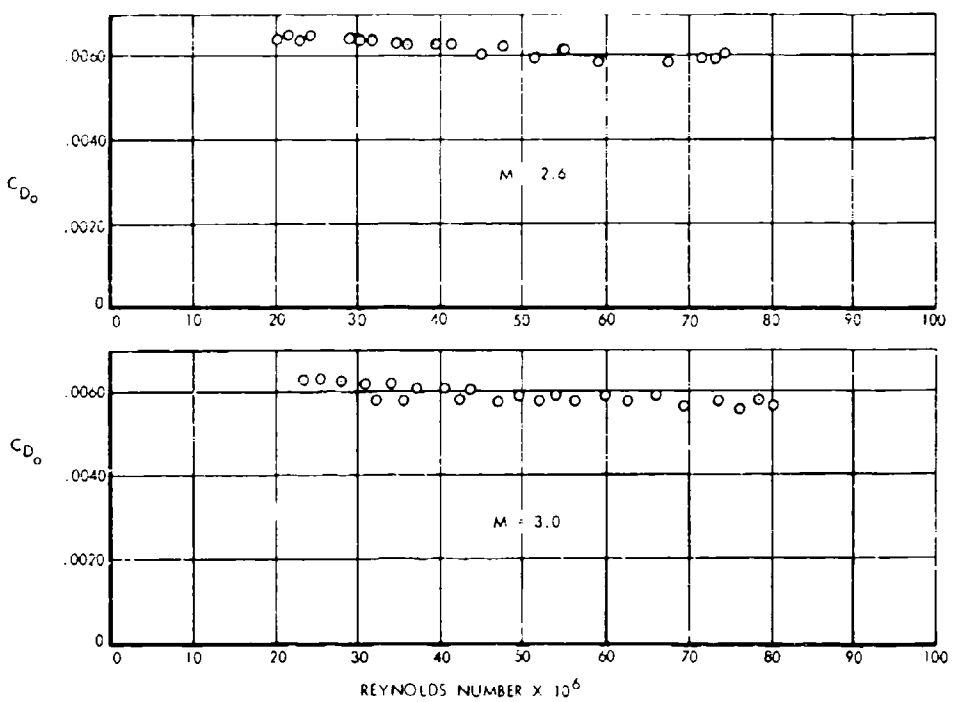

FIGURE 4-13 EFFECT OF REYNOLDS NUMBER ON WING-BODY DRAG

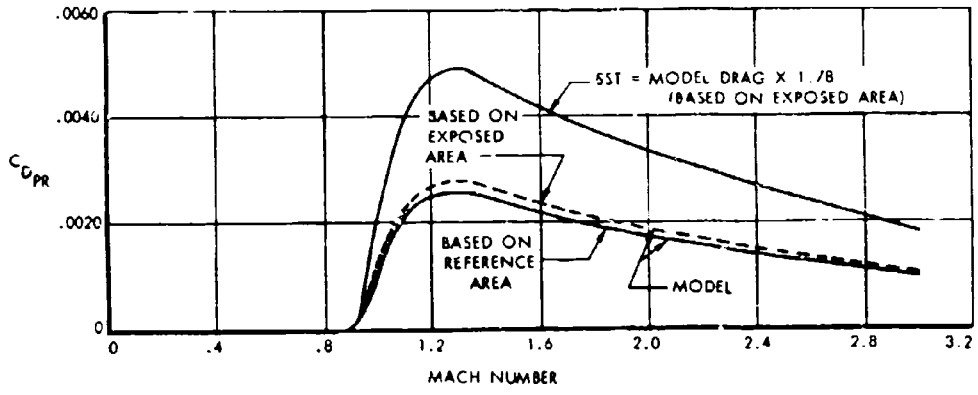

FIGURE 4-14 WING PRESSURE DRAG

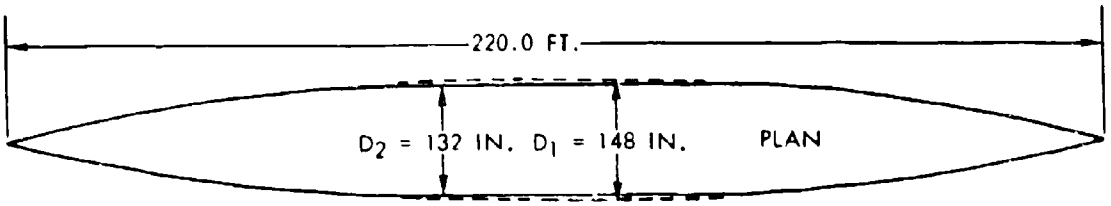

FOREBODY: 8.5 D_1 SEARS-HAACK SHAPE INTERSECTING A CYLINDER WITH DIAMETER D_2 = 132 IN.

AFTERBODY: 6.0 D_1 SEARS-HAACK SHAPE INTERSECTING A CYLINDER WITH DIAMETER D_2 = 132 IN.

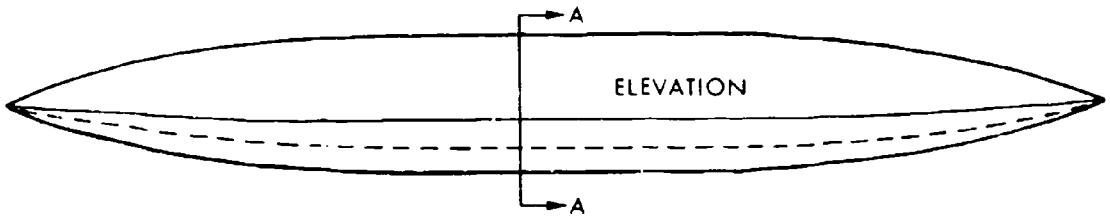

(WIDTH AND HEIGHT INCREASED FOR CLARITY)

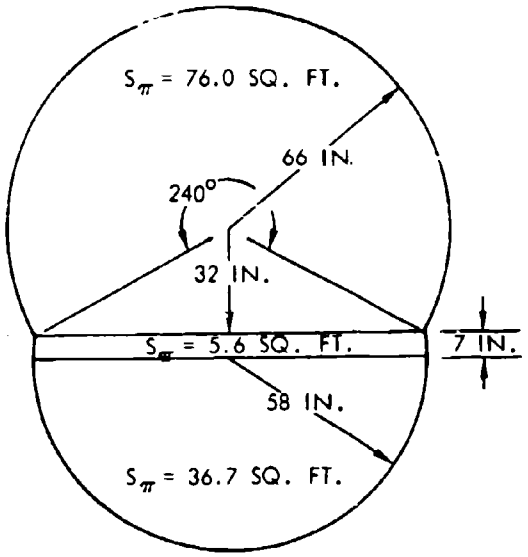

SECTION A-A
(TO SCALE)

FIGURE 4-15 SST FUSELAGE CONTOURS

proper area, S_π, is 119.3 square feet corresponding to the full 148 inch basic diameter from which the shapes are developed. The drag is computed only for the exposed periphery of the upper bubble. The drag of the afterbody is considered to be equal to the drag of a forebody of identical shape in keeping with the well-known reversibility theorem. Since the afterbody is separated from the forebody by almost 100 feet, the effect of forebody interference on the afterbody drag is considered to be negligible. The available afterbody drag data from References 4-2 and 4-3 are assembled in Figures 4-10 and 4-11 and indicate that this method of estimating afterbody drag is conservative. The pressure drag coefficient of the upper bubble based on the wing reference area is found to be:

$$C_{D_{PR}} = \frac{4.7}{F^2}\frac{S_\pi}{7000}\frac{\theta}{360}$$

or

$$C_{D_{PR}} = 4.7\left[\left(\frac{1}{17}\right)^2 + \left(\frac{1}{16}\right)^2\right] \times \frac{119.3}{7000} \times \frac{240°}{360°} = .00039$$

For a symmetric, closed Sears Haack body the expression for pressure drag based on frontal area is

$$C_{D_{F_{PR}}} = \frac{10.7}{F^2}$$

The pressure drag of the lower bubble is computed for the lower half of a closed Sears Haack shape including forebody interference as follows:

$$C_{D_{PR}} = \frac{1}{2}\frac{10.7}{(21.7)^2} \times \frac{84.4}{7000} = .00014$$

The total fuselage pressure drag coefficient based on the wing reference area is then equal to .00053, or when based on fuselage frontal area is equal to .032. This value is plotted in Figure 4-16 as a function of Mach number. The fuselage drag is essentially constant throughout the supersonic speed range of the SST, but as shown in Figure 4-16 is expected to peak at transonic speeds to a value approximately 30 percent greater than the supersonic level.

4.2.4 NACELLE PRESSURE DRAG

The pressure drag of all four nacelles based on the wing reference area is shown as a function of Mach number in Figure 4-17 and is developed analytically. The drag of the cowl lips is determined by the method of characteristics throughout the Mach number range. The drag of the slightly curved nacelle mid-body and afterbody is determined by means of two-dimensional linearized theory to avoid the lengthy characteristics analysis and is expected to be conservative. The pressure drag of the nacelle is due principally to the cowl lips. For example, at Mach 3.0, the cowl lip drag coefficient is equal to 0.00033 and only 0.00017 is attributed to the rest of the nacelle.

Verification of the estimated nacelle pressure drag at high supersonic speeds is provided in Figure 4-17. The drag of the wing and body combination, with all four nacelles installed, is compared with the drag of the wing and body alone taken from Figure 4-12. The additional friction drag due to the nacelle installation including the external drag, internal drag, and the decrease in wing drag due to blanketing is estimated as shown. To this drag is added the estimated base drag due the total of 1 square inch model scale nacelle base area. The base drag is determined from Figure 16-11 of Reference 4-4. The sum of these two drag items is seen to constitute the total nacelle drag increment at subsonic speeds. At Mach 2.6 and 3.0 subtraction of this sum from the total drag is seen to leave a residual pressure drag of approximately 0.0005. This pressure drag is compared with the estimated data in the lower part of Figure 4-17. Nacelle drag was also determined in the wind-tunnel at Mach numbers of 1.2 and 1.5 but are not presented, since the mass flow ratios indicated that the flow was choked with excessive spillage.

4.2.5 BOUNDARY LAYER DIVERTER PRESSURE DRAG

The pressure drag of the boundary layer diverters is based on the experimental data reported in Reference 4-5 for an included wedge angle of 16 degrees. The pressure drag coefficient based on the diverter wedge frontal area is shown as a function of Mach number in Figure 4-18. The low values of diverter pressure drag shown in Figure 4-18 are the result of the ability to incorporate in the nacelle design a diverter with relatively small wedge angles as compared with the included wedge angles of as much as 40 degrees which it is sometimes necessary to employ. It is noteworthy that Reference 4-5 shows that the diverter pressure drag coefficient is considerably less than would be expected on the basis of computed two-dimensional pressure coefficients.

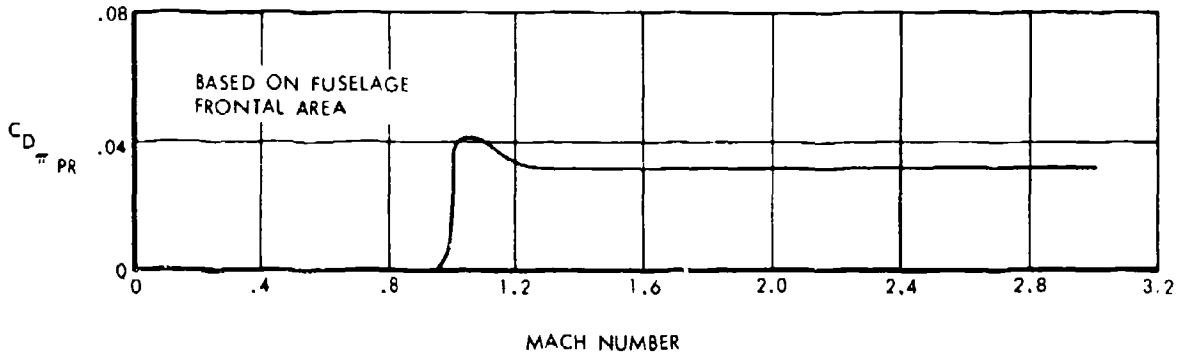

FIGURE 4-16 FUSELAGE PRESSURE DRAG

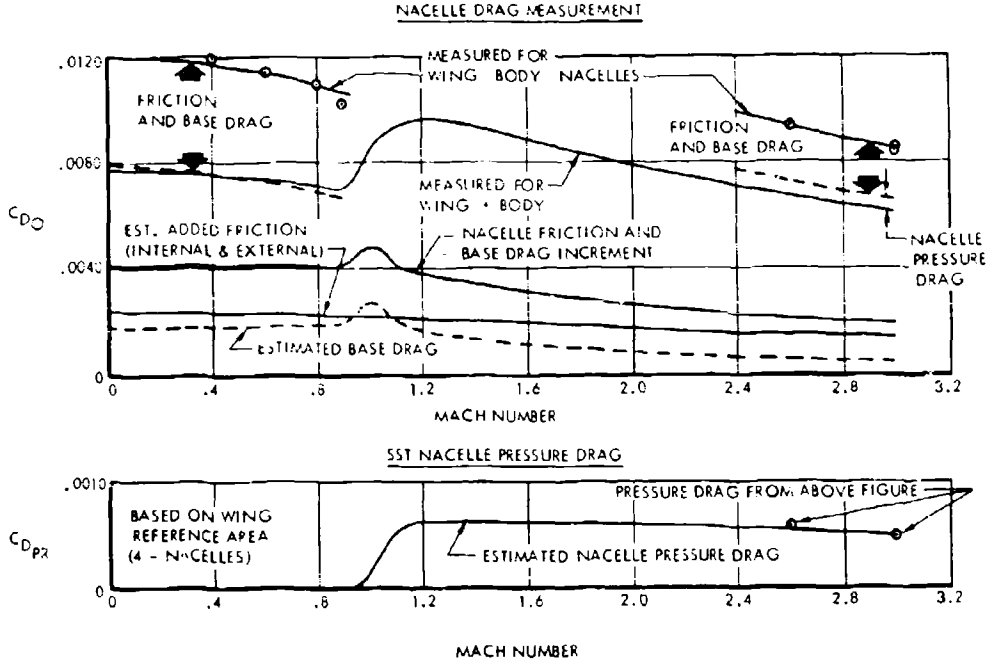

FIGURE 4-17 NACELLE PRESSURE DRAG

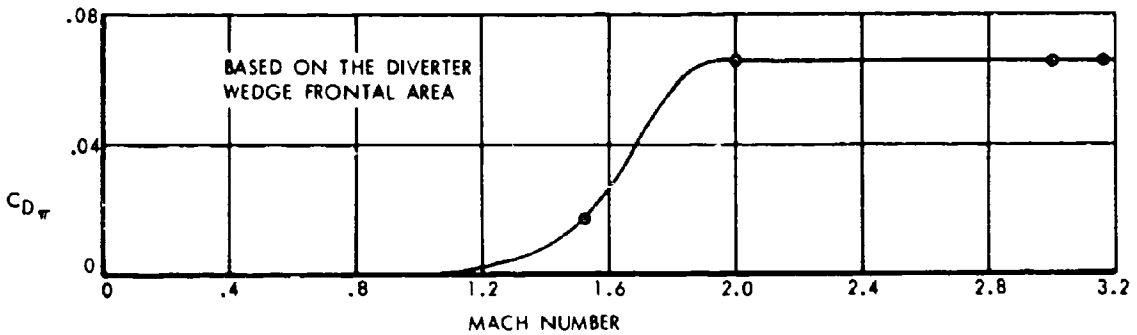

FIGURE 4-18 BOUNDARY LAYER DIVERTER PRESSURE DRAG

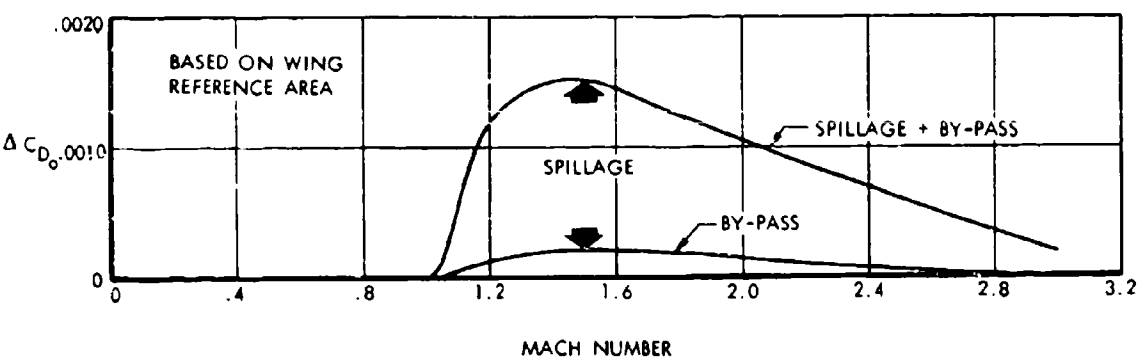

FIGURE 4-19 ENGINE AIR-INDUCTION SYSTEM DRAG

4.2.6 ENGINE AIR-INDUCTION SYSTEM DRAG

The incremental zero-lift drag arising in the engine air induction system due to spillage and by-pass effects is presented in Figure 4-19 as a function of Mach number. The method of calculation and the substantiation of these results are discussed fully in the Propulsion Report, Volume A-VI.

4.2.6.1 Drag Due to Air Conditioning Air

Air for cabin air conditioning and ventilation is taken aboard at the rate of 150 pounds per minute. The drag due to the momentum of this air is measurable at high speeds. For example the associated drag is 225 pounds at Mach 3.0. This air, however, passes through a heat exchanger before leaving the cabin and the added energy makes possible a partial recovery when the air is ejected from the airplane in the stream direction. It is estimated that the net drag at Mach 3.0 is 90 pounds corresponding to a pressure drag coefficient of 0.00003, which is included in the drag estimate. At lower Mach numbers this drag item is negligible.

4.2.7 SKIN FRICTION DRAG

The skin friction drag of the SST is found by summing the individual skin friction drags of the various aircraft components as a function of Mach number and altitude with consideration of the particular Reynolds number of each individual component. The Sommer and Short T' method is used as described in Reference 4-1 which shows that this method more closely correlates the available experimental data than any of the other methods investigated. In the application of the Sommer and Short T' method to the SST, a recovery factor of 0.9 is assumed for the calculations. The average flat plate skin friction coefficients determined in this way are shown as a function of Reynolds number and Mach number in Figure 4-20.

The results in Figure 4-20 are used directly in calculating the average skin friction coefficients for the wing, tail, nacelles, and boundary layer diverters. Reference 4-5 shows that the skin friction drag coefficients of diverters such as are used in the SST design are readily predictable by compressible flat plate theory. In the case of the fuselage, the computed flat plate friction coefficients are increased by 10 percent to account for the increased friction effect due to the thinning of the boundary layer on the forebody in axisymmetric flow. The characteristic lengths used for the computation of Reynolds number are: for the wing and tail, the mean aerodynamic chord of the exposed panels; for the fuselage, the basic length of 225 feet; for the nacelles, the distance from the cowl lip to the jet exit; and for the boundary layer diverters, the total run of the diverter air which corresponds to the local wing chord length at the nacelle station.

4.2.8 DRAG DUE TO LIFT

The drag due to lift factor is determined from an analysis of the wind tunnel drag polars such as shown in Figures 4-3 through 4-8, and is plotted as a function of Mach number in Figure 4-21. The present tunnel data indicate that the drag due to lift factor is maintained at a level of 0.30 from subsonic speeds up to a Mach number of 1.2 and increases thereafter with Mach number reaching a value of 0.65 at a Mach number of 3.0.

During the tunnel program, attention was given to the study of twist and camber, leading edge shape, and planform shape in order to effect a reduction in drag due to lift simultaneously with a positive shift in zero-lift pitching moment to reduce the trim drag to a negligible value. Considerable progress has been made toward both of these goals. The trim drag has been held to very low values as will be discussed in a later section. Considerable progress has been made toward the realization of low supersonic drag due to lift values.

Figure 4-21 shows that the theoretical drag due to lift of a 60 degree delta planform which at Mach 3.0 has a value of $\Delta C_D/C_L^2 = 0.707$ which corresponds to $\beta/4$. The double-delta planform of the SST which incorporates a 60 degree clipped delta main wing and a highly-swept forward-delta or bat attains a drag due to lift factor at Mach 3.0 as low as 0.65. The minimum drag due to lift achievable theoretically through the choice of the proper camber and twist distribution appears to correspond to a value of $\Delta C_D/C_L^2$ equal to $\beta/4$ when referred to the total planform. This would indicate that a drag due to lift factor of 0.596 is attainable theoretically for the SST planform. An analytical and experimental approach will be applied during the Phase II program to the attainment of this goal. It is anticipated that the value of $\Delta C_D/C_L^2$ at Mach 3.0 can be reduced at least to 0.61 through continued tailoring of nose shape and camber and twist distributions.

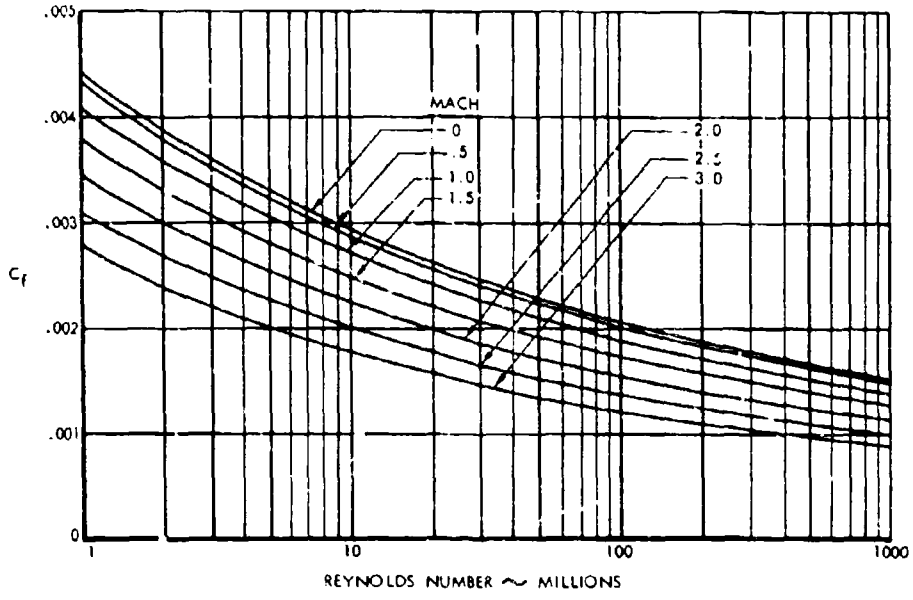

FIGURE 4-20 FLAT PLATE SKIN FRICTION DRAG, SOMMER AND SHORT T' METHOD

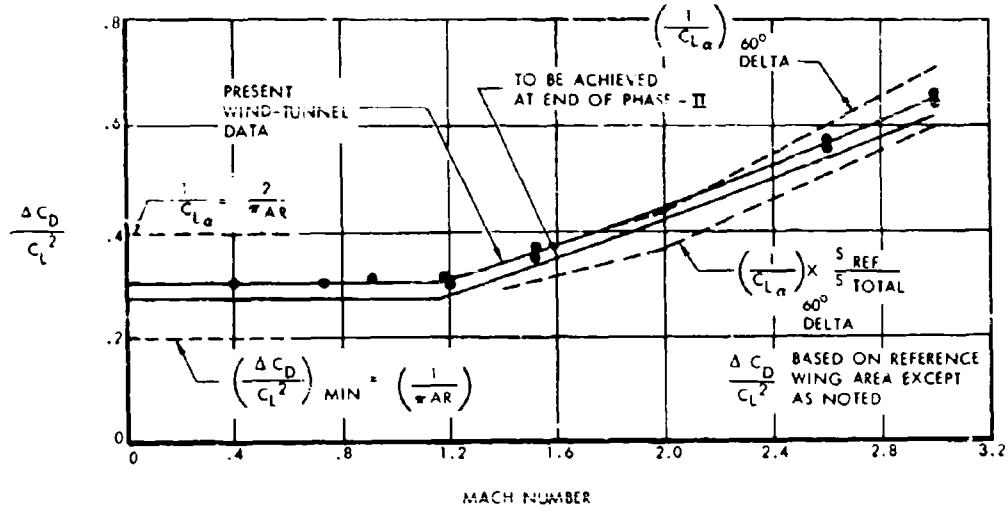

FIGURE 4-21 DRAG DUE TO LIFT

Attention is also directed to the possibilities for drag due to lift improvement at subsonic speeds. Theoretical studies have shown that, for highly-swept low-aspect ratio planforms, the spanwise lift distribution at all chordwise stations is elliptical. This leads to the conclusion that minimum drag due to lift factors corresponding to $1/\pi AR$ are theoretically possible even for highly-swept low-aspect ratio wings if sufficient attention is given to the shape of the leading edge so the theoretical flow conditions can be realized. On the other hand, complete mattention to the requirements of leading edge shape and the use of untwisted or uncambered highly swept deltas, for example, invariably results in the complete loss of leading edge suction. In this case, the resultant force on the wing is normal to the chord plane and the drag due to lift factor $\Delta C_D/C_L^2$ is found to be equal to $1/C_{L_\alpha}$ or $2/\pi AR$. These two extreme conditions of subsonic drag due to lift are illustrated in Figure 4-21. The present wind tunnel data is seen to lie half way in between these extremes. It is evident that there is still the possibility of considerable further reduction in drag due to lift in this speed range also. It is anticipated that a further reduction of at least 10 percent in subsonic drag due to lift can be accomplished during the Phase II effort.

The drag due to lift which is expected to be achieved at the end of Phase II is indicated on Figure 4-21. This variation in drag due to lift is used for all of the performance analysis in this report except where current status results are clearly indicated.

4.2.9 LONGITUDINAL TRIM DRAG

The wind tunnel model elevator effectiveness data are used to derive a longitudinal trim drag factor in terms of the square of the elevator deflection required for trim. The change in drag due to elevator deflection is measured at a constant lift coefficient, so the angle-of-attack increase required with up elevator and the concomitant increase in wing drag is taken into account as well as the basic change in parasite drag due to surface deflection. The available data are plotted as a function of Mach number in Figure 4-22. These values are expected to yield conservative drag estimates, since the wind tunnel model was rigid, whereas the SST wing is flexible and will twist as a function of elevator deflection in such a way as to partially compensate for the effect of elevator deflection on the required trimmed angle of attack.

The variation of the elevator angle required for trim and the resultant trim drag increment are shown as a function of Mach number in Figure 4-23 for both forward and aft center-of-gravity positions. The aft position corresponds to the condition existing during climb and transonic acceleration following a take-off at the design weight of 450,000 pounds.

4.2.10 COMPLETE AIRPLANE DRAG

The drag of the complete airplane is built up from the drag of the component parts which are discussed in detail in the preceding sections; and the method of calculation is illustrated in Tables 4-1 through 4-5 for the key segments of the basic design flight profile. The drag due to lift factors, which are quoted, correspond to those expected to be achieved at the end of Phase II.

TABLE 4-1 MACH .5 DRAG AT 15,000 FEET

Friction Drag: $RN = 2.31 \times 10^6$ per foot

	S_f sq. ft.	L ft.	$RN \times 10^{-6}$	C_f	C_{D_f}
Wing	11910	82.5	190	.00183	.00311
Fuselage	6850	225	520	.00188	.00184
Vertical	1482	37.1	85.6	.00210	.00044
Nacelles	2680	48.0	111	.00198	.00076
Diverters	612	69.0	159	.00189	.00016
Total	23,534				.00631

$(C_f)_{av} = .00188$

Total Drag:

$C_{D_o} = .00631$ $\qquad \left(\frac{L}{D}\right)_{MAX} = 12.12$

$\frac{\Delta C_D}{C_L^2} = .270$ $\qquad (C_L)_{(L/D)_{MAX}} = .1530$

A comparison of the present drag status with that of the Phase II SST is presented in Table 4-6 for the key flight segments. It is noted that the same zero-lift drag and trim drag are assumed in both cases. Potential improvements achievable by wing-body blending to reduce wetted area, for example, are under investigation. The present status drag due to lift is that which has been demonstrated by wind tunnel model tests of the SST. The Phase II SST drag due to lift repre-

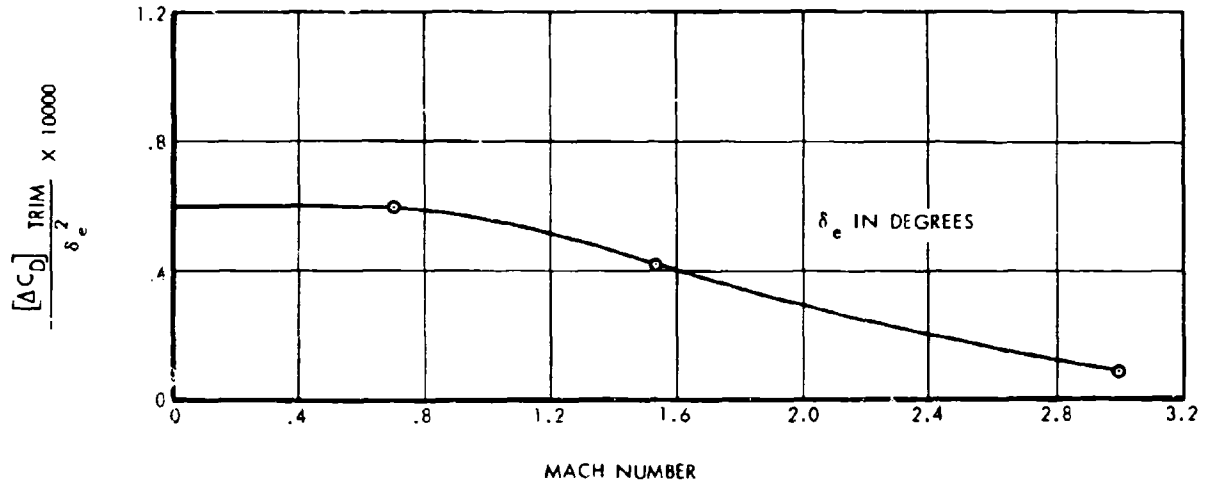

FIGURE 4-22 TRIM DRAG FACTOR

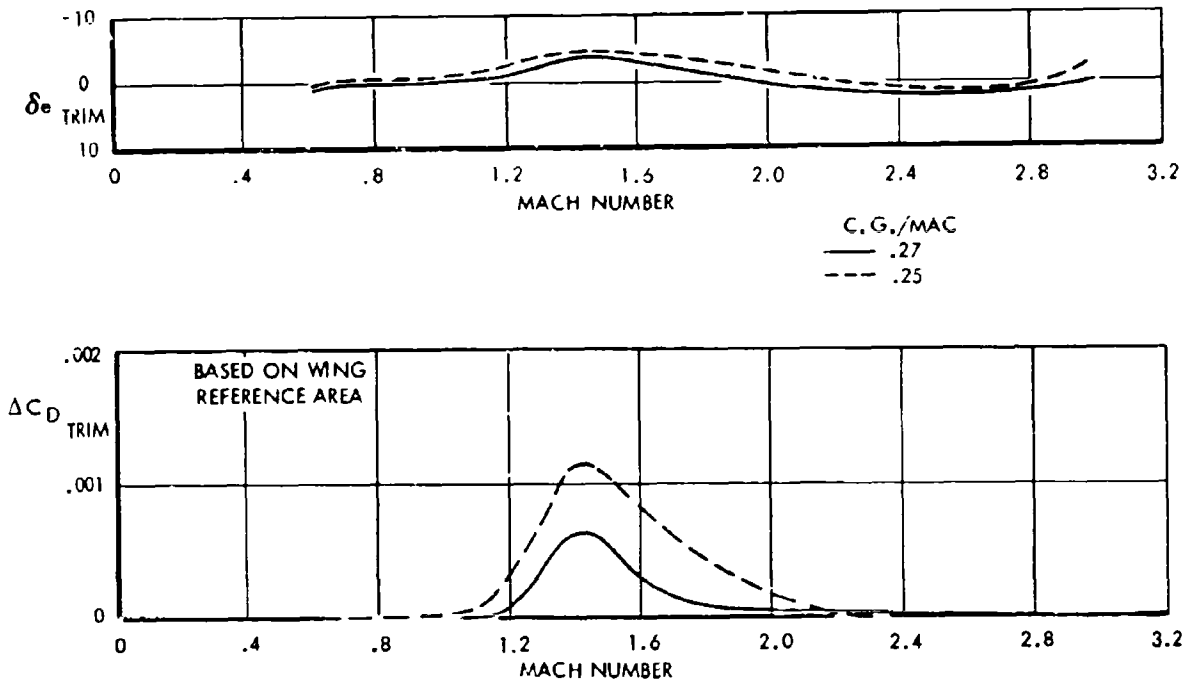

FIGURE 4-23 LONGITUDINAL TRIM DRAG

TABLE 4-2 MACH .9 DRAG AT 30,000 FEET

Friction Drag: $RN = 2.57 \times 10^6$ per foot

	S_f sq. ft.	L ft.	$RN \times 10^{-6}$	C_f	C_{D_f}
Wing	11910	82.5	212	.00172	.00292
Fuselage	6850	225	578	.00167	.00164
Vertical	1482	37.1	95.2	.00192	.00041
Nacelles	2680	48.0	123	.00186	.00071
Diverters	612	69.0	177	.00179	.00016
Total	23,534				.00584

$(C_f)_{AV} = .00174$

Total Drag:

$C_{D_o} = .00584$ $\qquad \left(\frac{L}{D}\right)_{MAX} = 12.60$

$\frac{\Delta C_D}{C_f} = .270$ $\qquad (C_L)_{(L/D)_{MAX}} = .1470$

TABLE 4-3 MACH 1.2 DRAG AT 43,000 FEET

Pressure Drag:

	S_{ref} sq. ft.	C_{D_B}	$C_{D_{PR}}$
Wing	5970	.00470	.00400
Fuselage	118.2	.0340	.00057
Vertical	741	.00470	.00050
Nacelles	154		.00062
Diverters	11.3	.002	.00000
Spillage & By-pass			.00135
Air. Cond. Air Drag			.00000
Total			.00704

Friction Drag: $RN = 1.99 \times 10^6$ per foot

	S_f sq. ft.	L ft.	$RN \times 10^{-6}$	C_f	C_{D_f}
Wing	11910	82.5	164	.00171	.00291
Fuselage	6850	225	448	.00164	.00160
Vertical	1482	37.1	73.6	.00192	.00041
Nacelles	2680	48.0	95.5	.00187	.00072
Diverters	612	69.0	137	.00176	.00015
Total	23,534				.00579

$(C_f)_{AV} = .00172$

Trim Drag: $(\Delta C_D)_{TRIM} = .00010$

Total Drag:

$C_{D_o} = .01293$ $\qquad \left(\frac{L}{D}\right)_{MAX} = 8.31$

$\frac{\Delta C_D}{C_f} = .280$ $\qquad (C_L)_{(L/D)_{MAX}} = .2150$

sents the improvement which is anticipated as the result of further aerodynamic refinement during the Phase II program as is discussed in Paragraph 4.2.8.

The incremental gains in $(L/D)_{max}$ which are expected, are 0.60 at subsonic speeds and 0.25 at Mach 3.0. These increments are included in the performance analysis of the SST presented in this volume.

The zero-lift drag and total drag existing along the flight path during the climb and acceleration to cruise altitude following take-off at the design weight are illustrated in Figure 4-24 for the airplane at the end of Phase II. The maximum lift-to-drag ratios at points along this flight path are illustrated in Figure 4-25 for the present status airplane as well as for the Phase II SST. The variation of trimmed drag coefficient with Mach number and lift coefficient is presented in Figures 4-26 through 4-32 for the range of altitudes and speeds applicable to the operation of the SST. The effect of variations in center-of-gravity position on the trimmed drag coefficient is indicated.

4.2.11 EFFECT OF WEATHER-VISION NOSE

In the preceding sections, no consideration is given to possible effects of lowering the weather-vision nose during subsonic flight. Figure 4-33 shows that the 10 degree down position, which is the maximum used for any condition other than the final landing approach, has no noticeable effect on the subsonic drag characteristics within the normal operating lift coefficient range of the SST. These data were obtained in the low-speed wind tunnel and include the

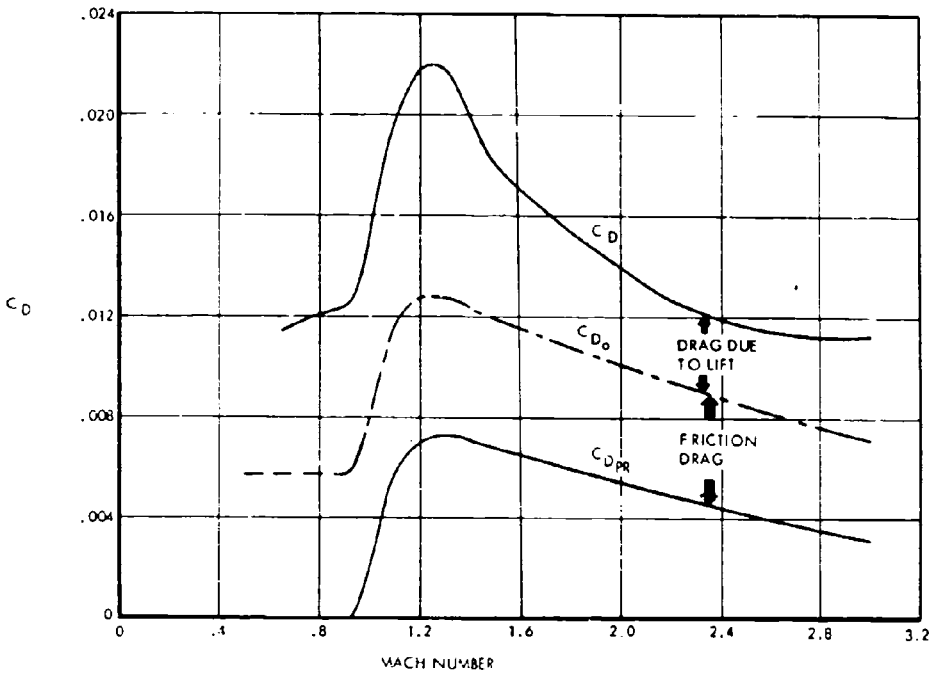

FIGURE 4-24 DRAG VARIATION ALONG FLIGHT PATH

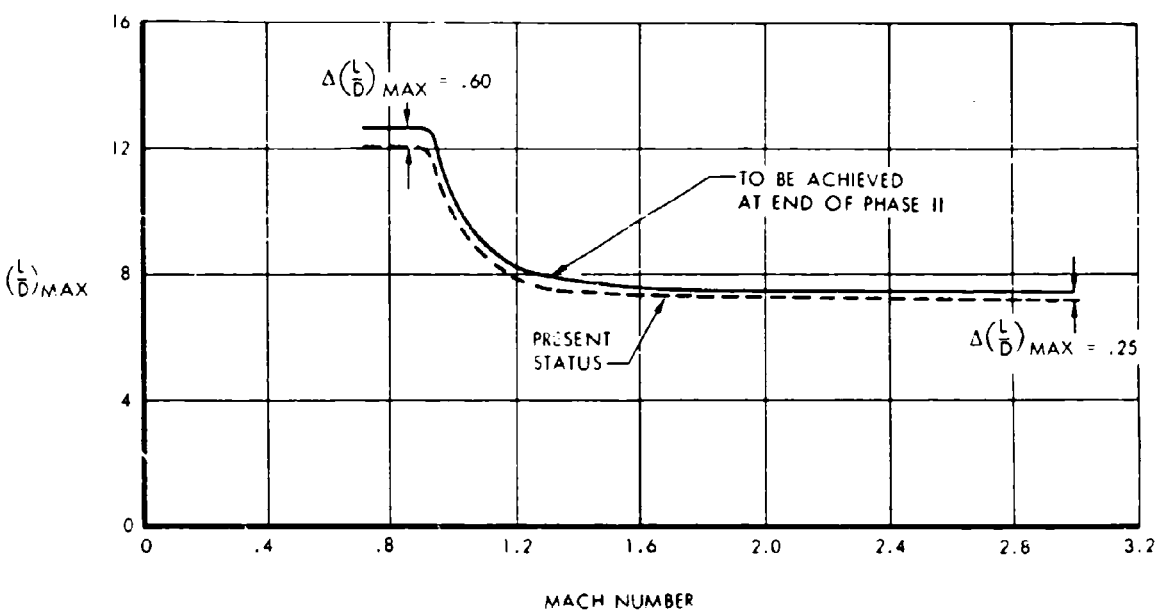

FIGURE 4-25 MAXIMUM $\frac{L}{D}$ ALONG FLIGHT PATH

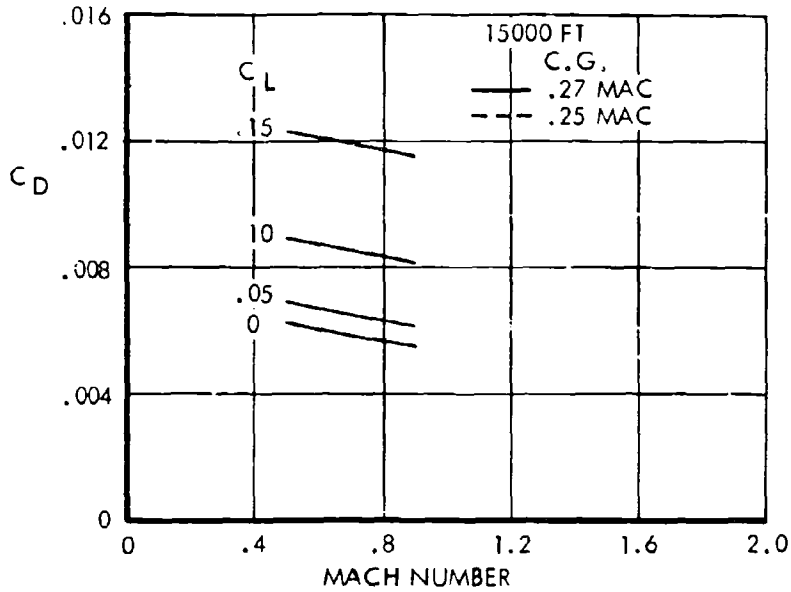

FIGURE 4-26 AIRPLANE TRIMMED DRAG COEFFICIENT, 15,000 FEET

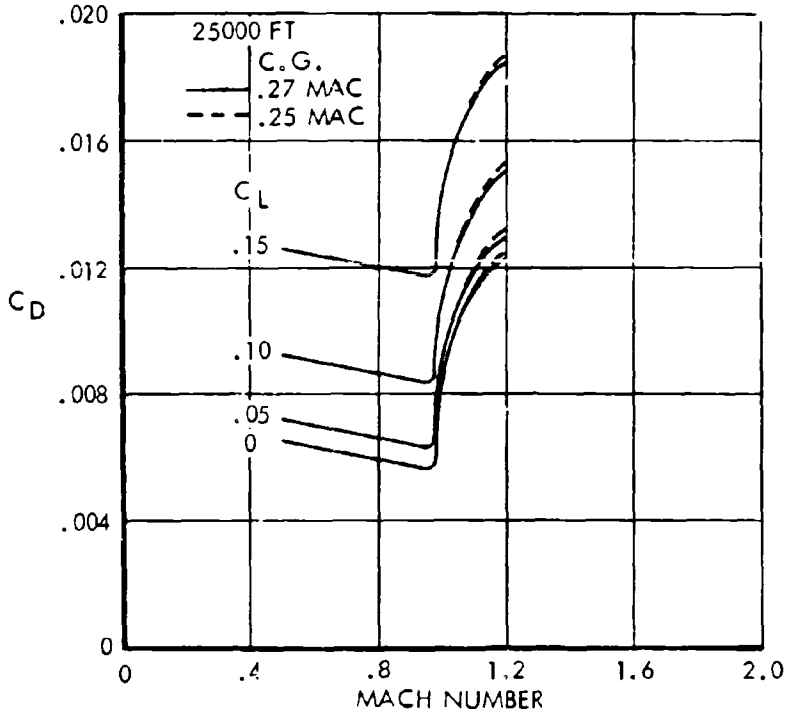

FIGURE 4-27 AIRPLANE TRIMMED DRAG COEFFICIENT, 25,000 FEET

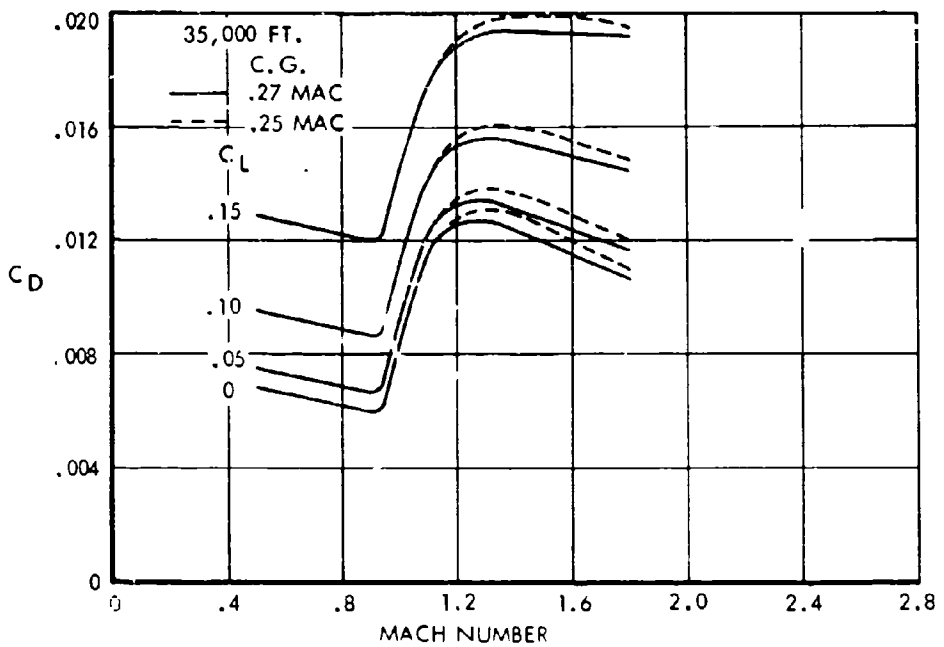

FIGURE 4-28 AIRPLANE TRIMMED DRAG COEFFICIENT, 35,000 FEET

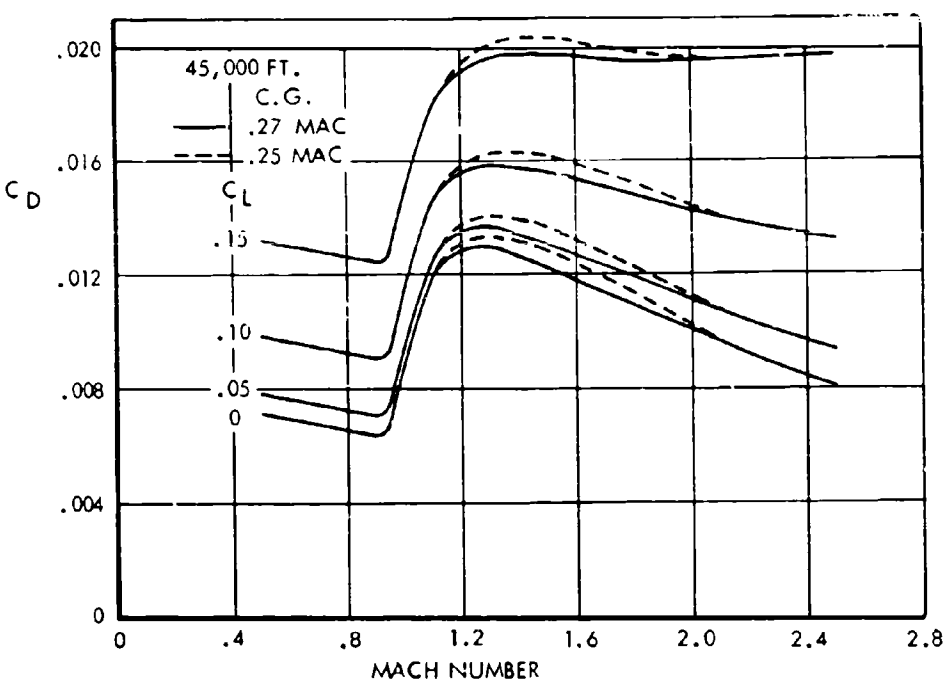

FIGURE 4-29 AIRPLANE TRIMMED DRAG COEFFICIENT, 45,000 FEET

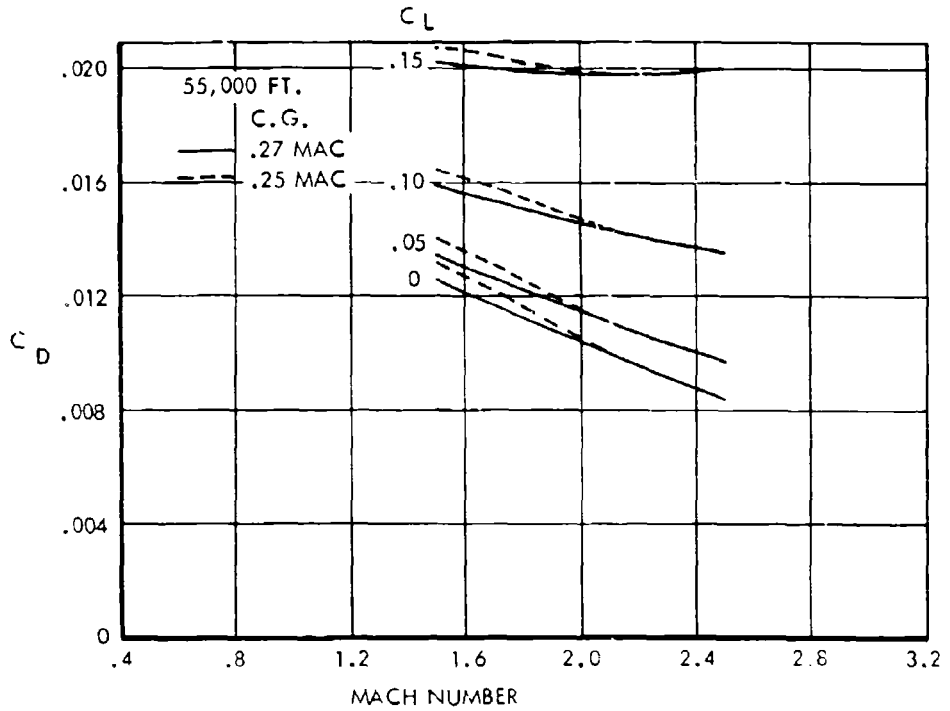

FIGURE 4-30 AIRPLANE TRIMMED DRAG COEFFICIENT, 55,000 FEET

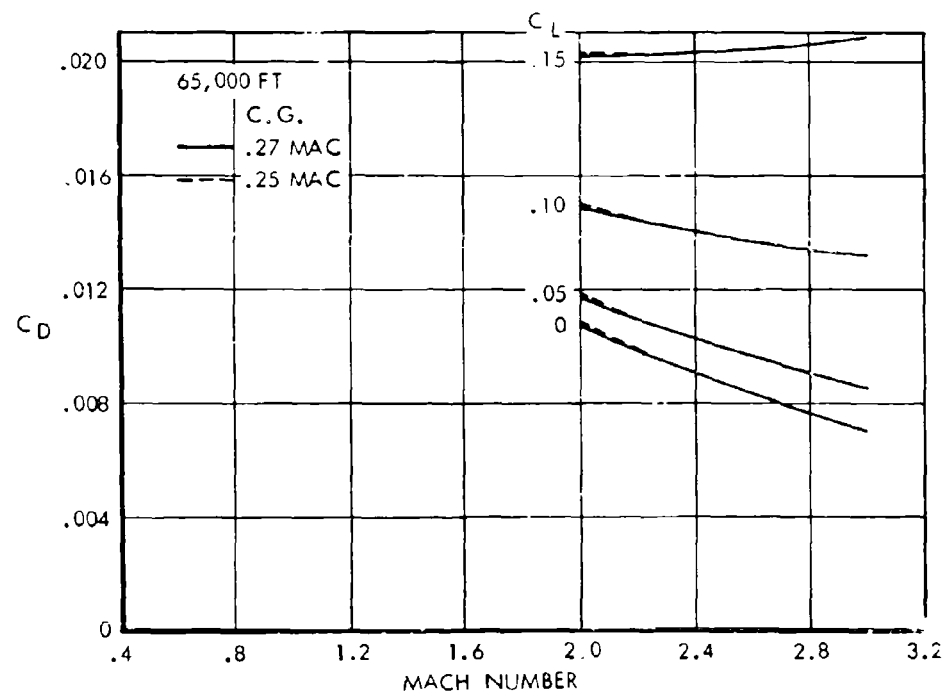

FIGURE 4-31 AIRPLANE TRIMMED DRAG COEFFICIENT, 65,000 FEET

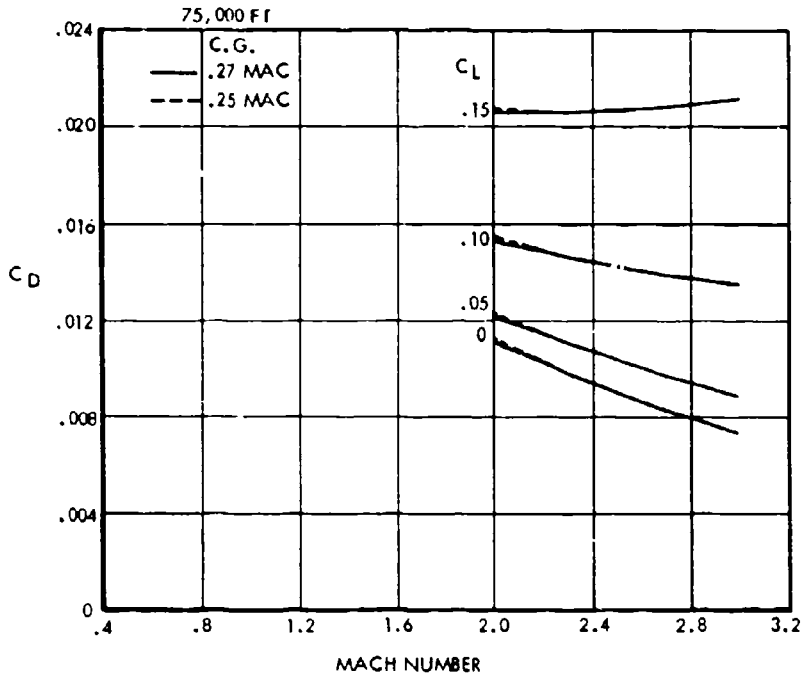

FIGURE 4-32 AIRPLANE TRIMMED DRAG COEFFICIENT, 75,000 FEET

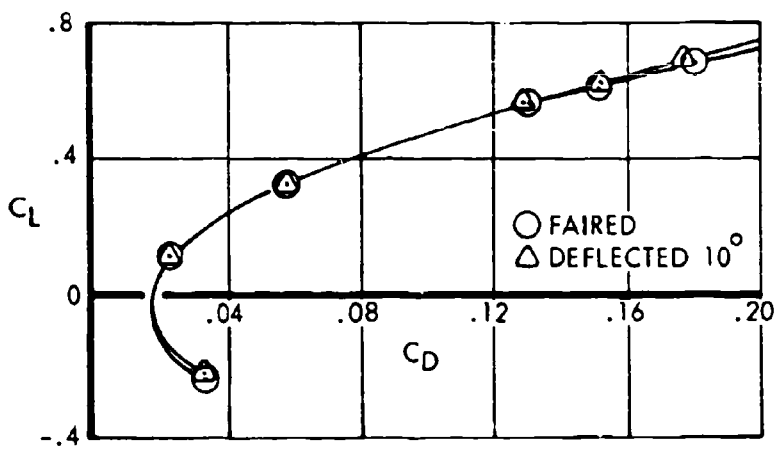

FIGURE 4-33 EFFECT OF WEATHER-VISION NOSE DEFLECTION

TABLE 4-4 MACH 2.0 DRAG AT 51,000 FEET

Pressure Drag:

	S_{π} sq. ft.	$C_{D_{\pi}}$	$C_{D_{PR}}$
Wing	5970	.00335	.00286
Fuselage	118.2	.0320	.00054
Vertical	741	.00335	.00035
Nacelles	154		.00060
Diverters	11.3	.0660	.00011
Spillage & By-pass			.00111
Air Cond. Air Drag			.00000
Total			.00557

Friction Drag: $RN = 2.26 \times 10^6$ per foot

	S_f sq. ft.	L ft.	$RN \times 10^{-6}$	C_f	C_{D_f}
Wing	11910	82.5	186	.00141	.00240
Fuselage	6850	225	508	.00135	.00132
Vertical	1482	37.1	83.8	.00158	.00033
Nacelles	2680	48.0	108	.00152	.00058
Diverters	612	69.0	156	.00144	.00013
Total	23,534				.00476

$(C_f)_{AV} = .00142$

Trim Drag: $(\Delta C_D)_{TRIM} = .00007$

Total Drag:

$C_{D_o} = .01040$ $\qquad \left(\frac{L}{D}\right)_{MAX} = 7.56$

$\frac{\Delta C_D}{C_L} = .420$ $\qquad (C_L)_{(L/D)_{MAX}} = .1573$

TABLE 4-5 MACH 3.0 DRAG AT 75,000 FEET

Pressure Drag:

	S_{π} sq. ft.	$C_{D_{\pi}}$	$C_{D_{PR}}$
Wing	5970	.00182	.00155
Fuselage	118.2	.0320	.00054
Vertical	741	.00185	.00020
Nacelles	154		.00050
Diverters	11.3	.0660	.00011
Spillage & By-pass			.00018
Air Cond. Air Drag			.00003
Total			.00311

Friction Drag: $RN = 1.06 \times 10^6$ per foot

	S_f sq. ft.	L ft.	$RN \times 10^{-6}$	C_f	C_{D_f}
Wing	11910	82.5	87.5	.00122	.00208
Fuselage	6850	225	239	.00116	.00114
Vertical	1482	37.1	39.3	.00140	.00030
Nacelles	2680	48.0	50.9	.00133	.00051
Diverters	612	69.0	73.1	.00127	.00011
Total	23,534				.00414

$(C_f)_{AV} = .00124$

Trim Drag: $(\Delta C_D)_{TRIM} = .00002$

Total Drag:

$C_{D_o} = .00727$ $\qquad \left(\frac{L}{D}\right)_{MAX} = .613$

$\frac{\Delta C_D}{C_L} = 7.50$ $\qquad (C_L)_{(L/D)_{MAX}} = .1084$

effect of the subsonic windshield which is exposed when the weather-vision nose is lowered as illustrated by wind tunnel model photographs in Figure 4-34.

4.2.12 ASYMMETRIC TRIM DRAG

The incremental drag resulting from inoperative engines, including the associated drag resulting from the trim requirements, is illustrated in Figure 4-35 as a function of Mach number and altitude.

4.2.13 TAKE-OFF AND LANDING DRAG POLARS

Drag polars corresponding to the take-off and landing configurations are shown in Figure 4-36 for both at the ground and away from the ground conditions. The drag of the extended landing gear is included and the specific points corresponding to the ground attitude and to the important specific points along the take-off and landing flight paths are indicated. Figure 4-37 shows a photograph of the wind-tunnel model with extended landing gear.

4.3 STATIC LONGITUDINAL STABILITY

Static longitudinal stability considerations are primarily involved with aerodynamic center shift due to lift coefficient and Mach number, and zero lift pitching moments. During the development of the SST,

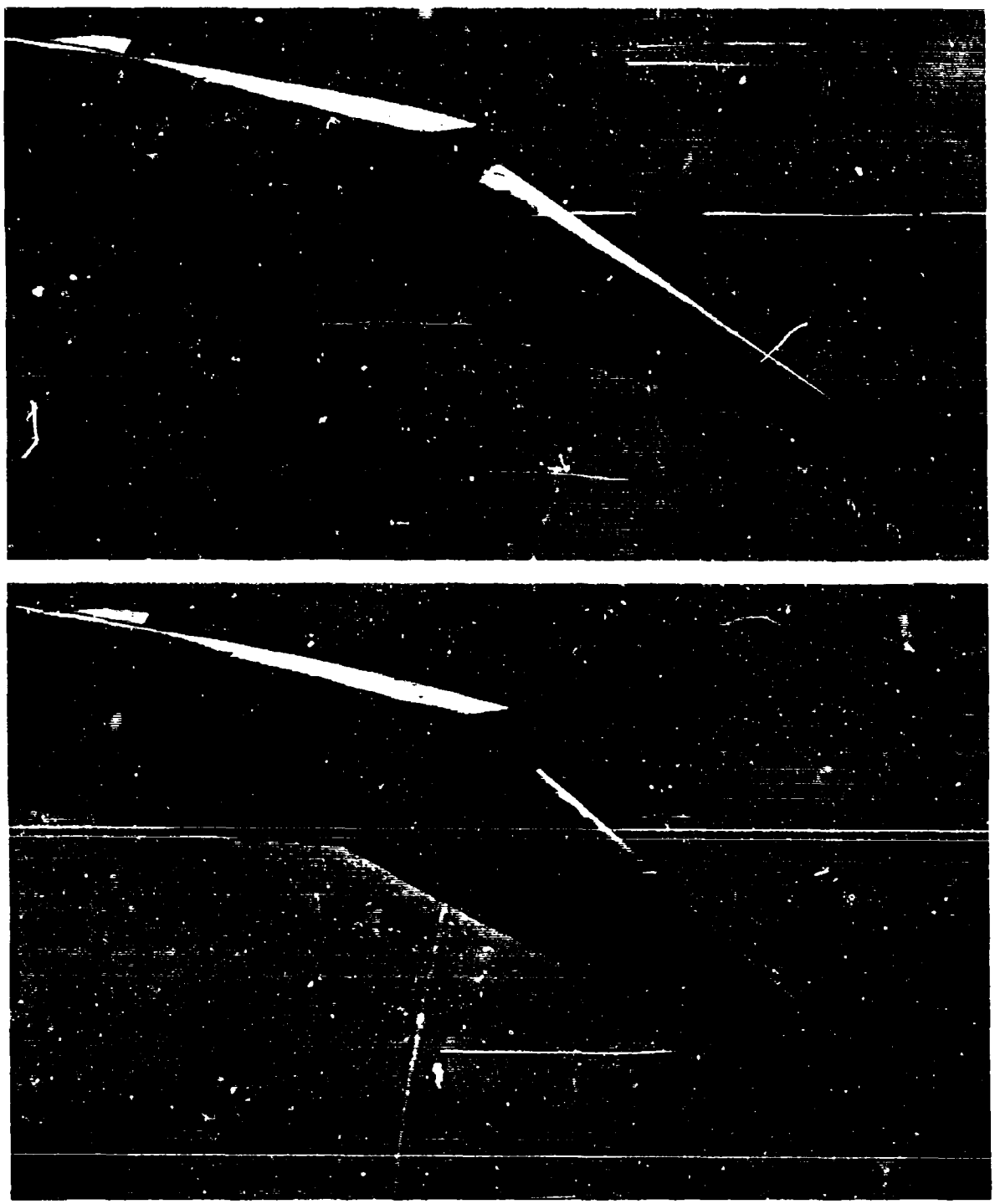

FIGURE 4-34 MODEL WITH WEATHER-VISION NOSE

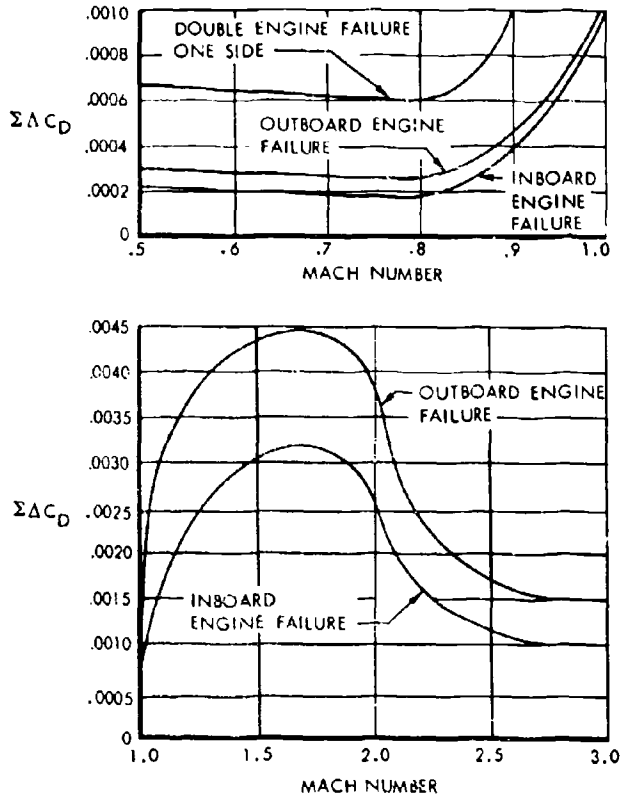

FIGURE 4-35 DRAG WITH INOPERATIVE ENGINES

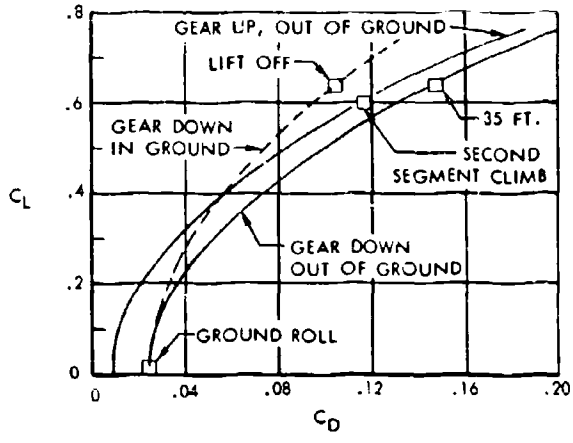

FIGURE 4-36 TAKE-OFF AND LANDING DRAG POLARS

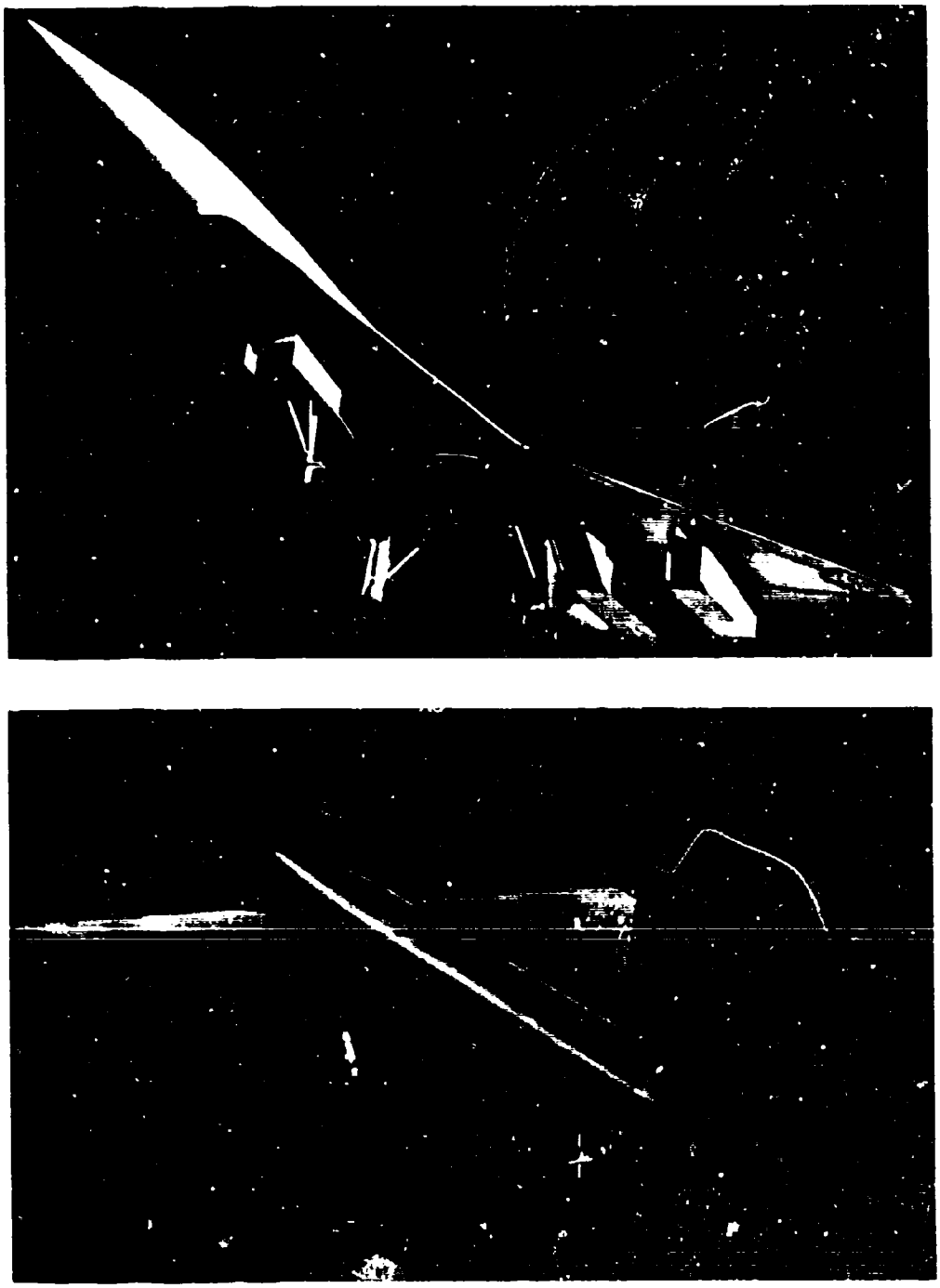

FIGURE 4-37 MODEL WITH GEAR DOWN

TABLE 4-6 TOTAL AIRPLANE DRAG AT KEY POINTS

(Present Status vs. Phase II SST)

			Present Status		Phase II SST	
Mach	*Altitude (ft.)*	$C_{D_0} + (\Delta C_D)_{TRIM}$	$\frac{\Delta C_D}{C_L}$	$\left(\frac{L}{D}\right)_{MAX}$	$\frac{\Delta C_D}{C_L}$	$\left(\frac{L}{D}\right)_{MAX}$
.5	15000	.00631	.300	11.50	.270	12.10
.9	30000	.00584	.300	12.00	.270	12.60
1.2	43000	.01293	.310	7.90	.280	8.31
2.0	51000	.01040	.442	7.38	.420	7.56
3.0	75000	.00727	.650	7.25	.613	7.50

emphasis was given to these characteristics, so both trim drag and stability levels about the operating center-of-gravity locations would be satisfactory throughout the flight regime for all operating weights. The use of the double-delta planform shape and wing camber and twist was found to provide the means needed to meet these requirements.

Low speed longitudinal characteristics are presented in Figure 4-38. As shown, the low-speed aerodynamic center position can be adjusted by making slight changes to the double-delta wing geometry. By means of a slot opening in the bat, or by incorporating a chordwise extension of the wing tip, such as shown in Figures 4.39 and 4.40, the aerodynamic center position for the higher operating C_L range can be shifted four to five percent. This effect can be attributed to changes in the vortex flow behavior. As can be seen in Figure 4.38, the lift and moment characteristics are strongly affected by vortex flow beyond an angle of attack of approxin ly 6 degrees, and slight changes to the wing planform can exert a significant influence on the flow pattern over the wing.

Flow separation near the leading edge is experienced on the thin outboard delta wing panel because the vortex flow field induces high upwash ahead of the leading edge. The presence of local flow separation suggests that Reynolds number may influence the flow characteristics. High Reynolds numbers tests on other wing planform shapes, which have experienced similar vortex flow, have indicated an aft aerodynamic center shift with increasing Reynolds number. Unfortunately, these tests are not directly applicable to the double-delta planform, and are not quantitative enough to permit an evaluation of Reynolds number effect.

A low speed aerodynamic center position at 29.5 percent MAC has been adopted. Continued evaluation of the low-speed longitudinal characteristics are to be conducted during Phase II development to more clearly establish the relationships between planform shape, Reynolds number, and aerodynamic center position.

The low-speed lift curve slope data of Figure 4-38 indicates that the SST wing does not experience a stalled flow in the normal sense, and, therefore, does not define a minimum stall speed. A minimum speed corresponding to an angle of attack of 20 degrees has been selected for the SST. This method of establishing a fictitious stall speed will allow defining take-off and landing speeds as percents above minimum usable speed. For the definition selected, take-off and landing speeds for the SST will be 1.20 or greater than the minimum speed corresponding to 20 degrees angle of attack.

The SST wing planform experiences a large increase in lift due to ground effect, as shown in Figure 4-41. Comparison of these data with large scale delta wind tunnel results of Reference 4-6 is shown in Figure 4-42. It is seen that the addition of the bat amplifies the ground effect since it behaves as a lower aspect ratio wing.

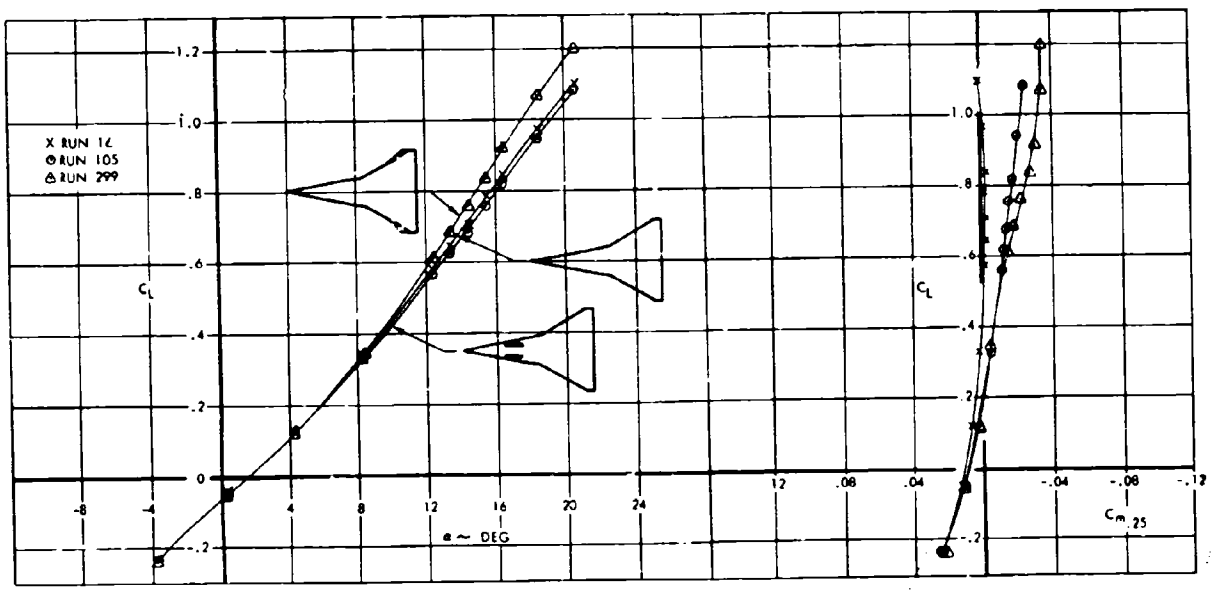

FIGURE 4-38 LOW SPEED LONGITUDINAL STABILITY— EFFECT OF WING PLANFORM

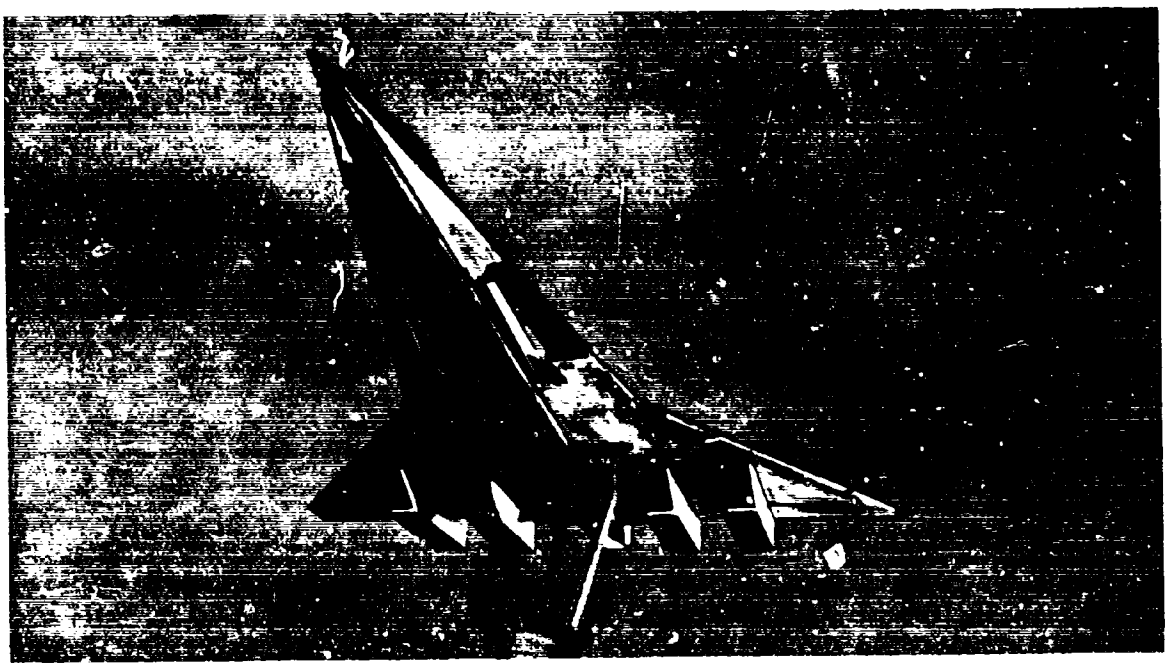

FIGURE 4-39 PICTURE OF BAT SLOTS

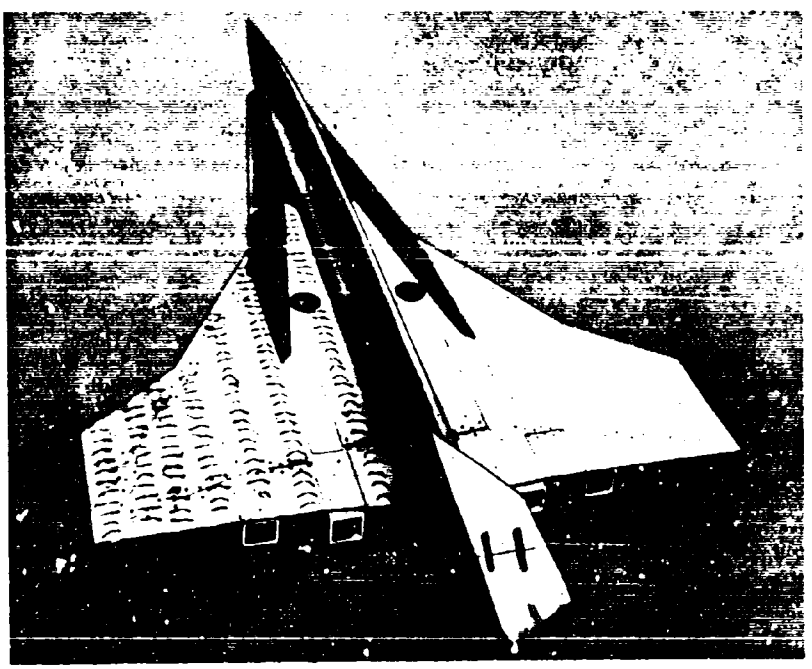

FIGURE 4-40 PICTURE OF TIP EXTENSIONS

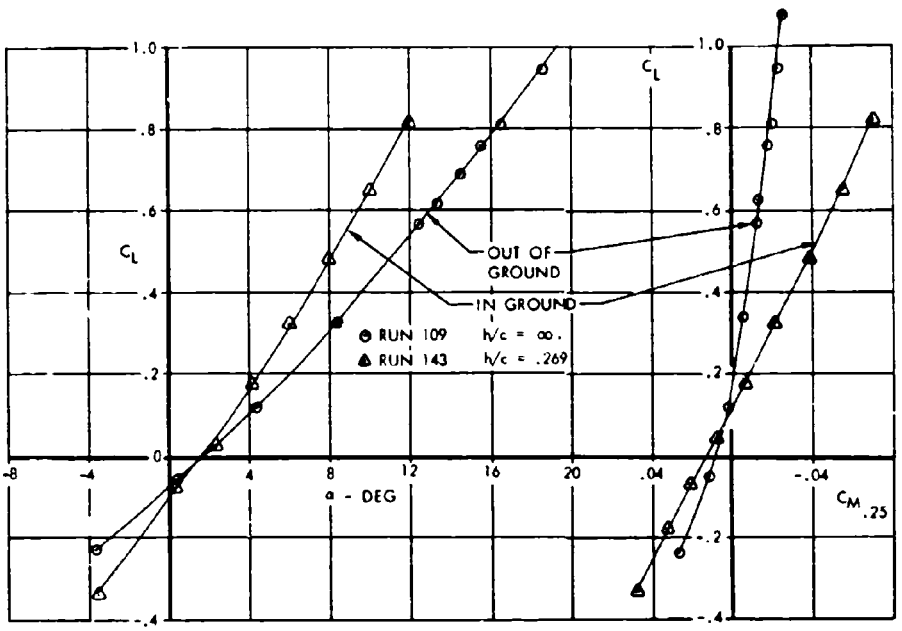

FIGURE 4-41 LOW SPEED LONGITUDINAL STABILITY—EFFECT OF GROUND

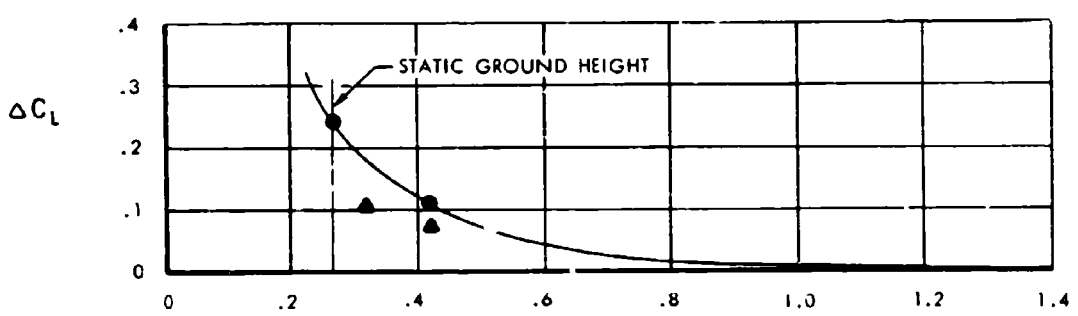

FIGURE 4-42 INCREMENT IN LIFT DUE TO GROUND EFFECT

The ground effect lift increment will help to reduce rate of descent near touchdown, and provide an automatic flare effect that will benefit landing characteristics. This characteristic has been observed on several current aircraft that experience similar large ground effects. Figures 4-43 and 4-44 show that the extension of the landing gear and dropping of the weather-vision nose do not affect the longitudinal stability characteristics. Subsonic and transonic longitudinal stability data are presented in Figure 4-45; similar data at supersonic Mach numbers are presented in Figure 4-46.

All the above data are presented for the cambered and twisted wing shape. One benefit derived from this type of wing can be seen from an inspection of the zero lift pitching moment shown in Figures 4-45 and 4-46. The moment is positive throughout the Mach range and is, therefore, a factor that minimizes trim drag. The effect of wing twist on the zero-lift moment at Mach 3.0 is shown in Figure 4-47, where the twisted wing is compared with data obtained from an untwisted wing of the same planform. Another factor affecting C_{m_0} is forebody shape, as shown in Figure 4-48, which illustrates one adverse effect created by adoption of an external canopy.

Figure 4-49 presents Mach 3 data showing the changes in lift and moment characteristics caused by reducing the mass flow through the left outboard engine to zero.

Longitudinal control effectiveness data are presented in Figure 4-50 for low-speed conditions in and out of ground effect. Control effectiveness is greatly increased because of the presence of the ground.

High speed elevator control effectiveness data is given in Figures 4-51 and 4-52. These data were obtained from the first series model tests, but the flap area/wing area ratio is of similar geometry. To adapt these data to the airplane configuration, control power was assumed to be proportional to flap/wing area. Transonic elevator effectiveness is estimated on the basis of the foregoing low speed and supersonic data and correlation with data measured on a delta wing planform presented in Reference 4-3. The correlated and estimated SST transonic effectiveness is given in Figure 4-53.

4.4 LATERAL-DIRECTIONAL CHARACTERISTICS

Since airplane handling qualities are largely dependent upon realizing satisfactory static stability characteristics, extensive wind tunnel tests were conducted to obtain experimental data that would permit development of a configuration having acceptable stability levels. Lateral-directional considerations involve static directional stability at high angles of attack and high speed, dihedral effect in the approach and cruise regime, and rudder and aileron control power. Wind tunnel tests have been conducted to evaluate these stability parameters. The results are given below to substantiate the stability derivative data used in estimating the handling quality characteristics given in Section 6.

Final vertical tail geometry for the SST was modified slightly from that used for the wind tunnel models, and the wind tunnel stability data must be adjusted for tail volume coefficient differences. The corrections required are small, since the changes in tail volume are as follows:

Low Speed Model Tail Volume Coefficient = .0625

High Speed Model Tail Volume Coefficient = .0720

SST Tail Volume Coefficient = .0635

Specific wind tunnel data results presented in this section are as obtained using the model size vertical tail. In the stability summary, Section 4.7, the stability levels corrected to the airplane tail sizes are shown.

Low-speed directional stability characteristics are presented in Figure 4-54, showing thee ffects of angle of attack. The favorable tail sidewash effects created by the double-delta planform at the higher angles of attack are apparent. No loss in directional stability due to ground effect is indicated by the data in Figure 4-55. As shown in Figures 4-56 and 4-57, the extension of the landing gear and lowering of the weather-vision nose have no significant influence on the directional characteristics. The yawing moment produced by an inoperative outboard engine is indicated in Figure 4-58 for zero and $-5°$ degrees of sideslip, where the nacelle was plugged to reduce the mass flow to zero.

Stability levels at transonic and supersonic Mach numbers are presented in Figures 4-59 to 4-62. The reduction in stability due to increasing angle of attack is small.

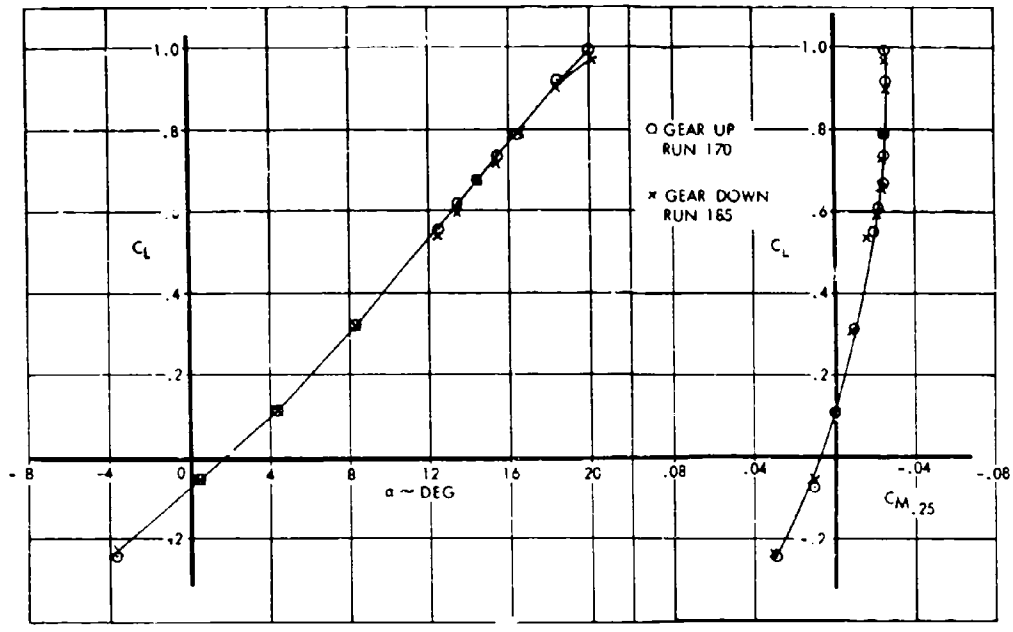

FIGURE 4-43 LOW SPEED LONGITUDINAL STABILITY—EFFECT OF LANDING GEAR

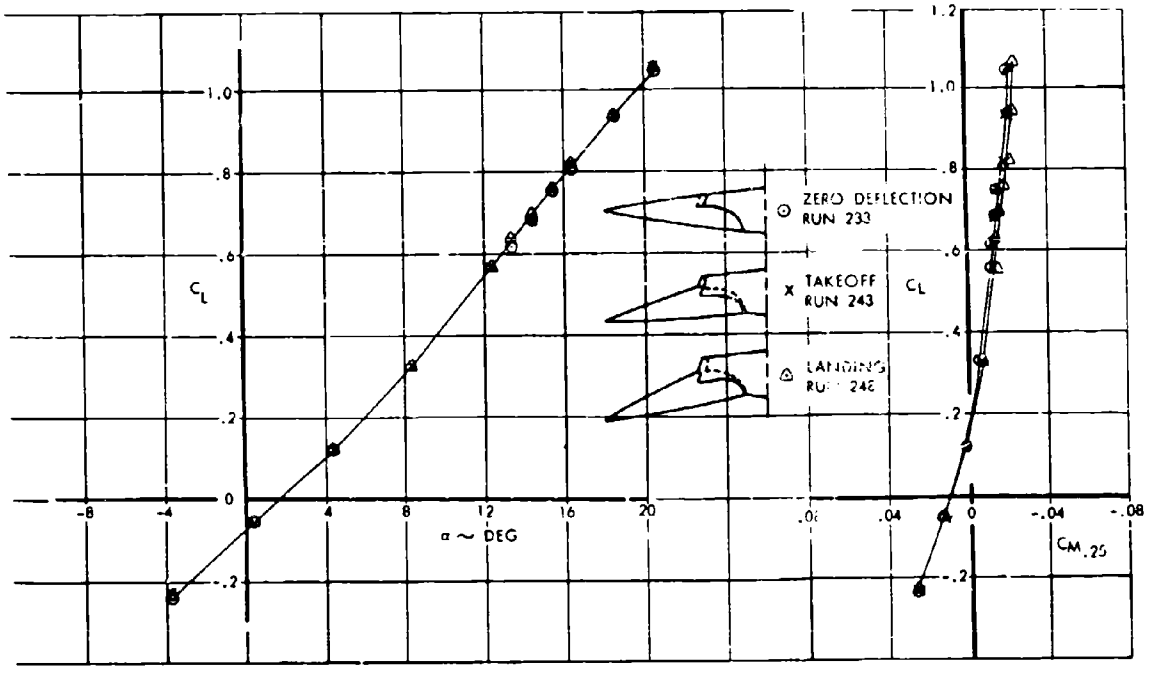

FIGURE 4-44 LOW SPEED LONGITUDINAL STABILITY—EFFECT OF WEATHER-VISION NOSE

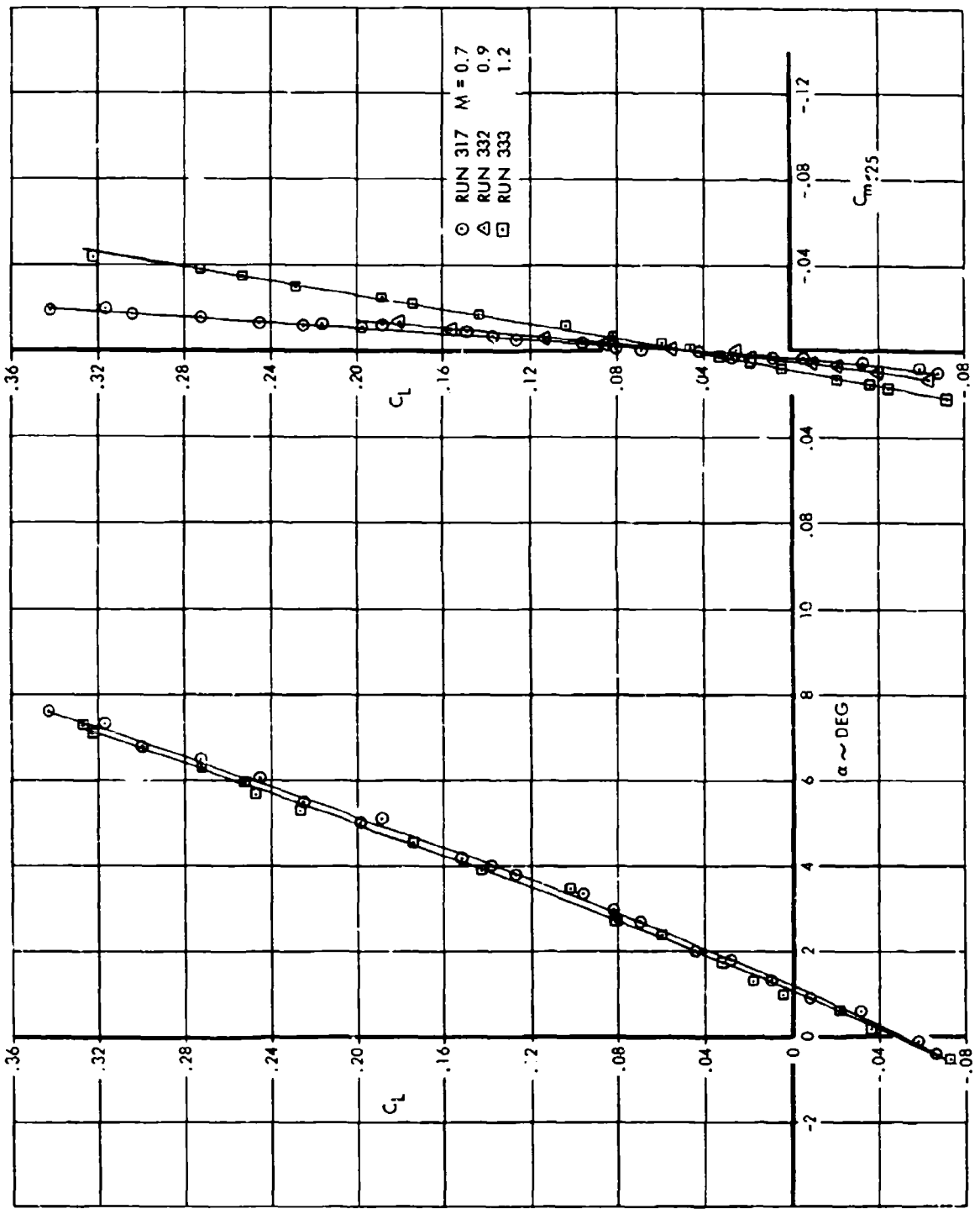
RUN 317 M = 0.7
RUN 332 0.9
RUN 333 1.2
$C_{m_{.25}}$
C_L
$\alpha \sim$ DEG

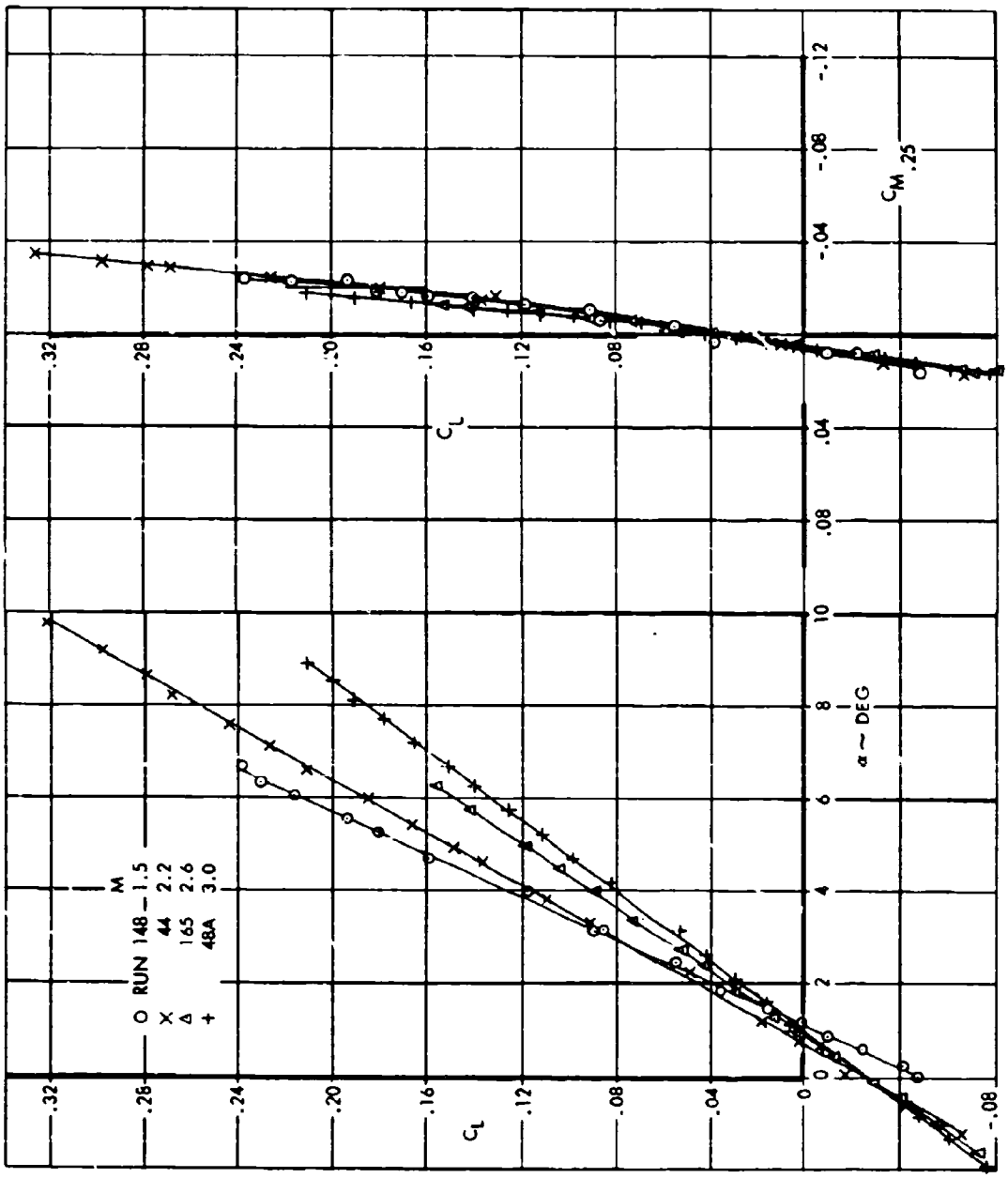

FIGURE 4-46 SUPERSONIC LONGITUDINAL STABILITY

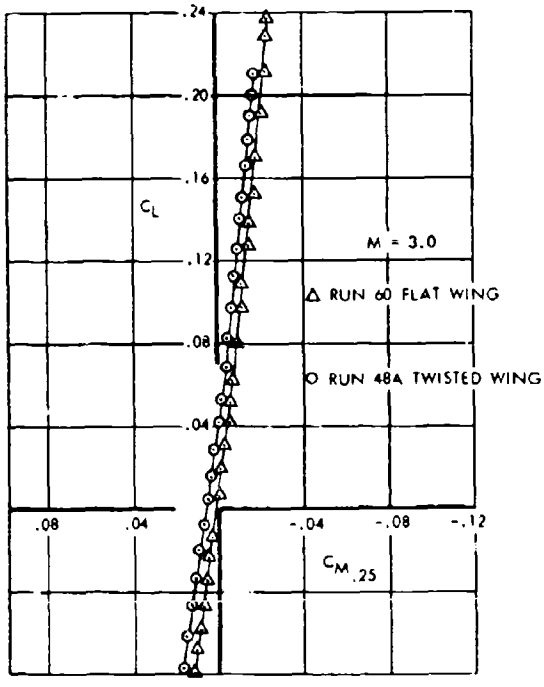

FIGURE 4-47 EFFECT OF WING TWIST ON LONGITUDINAL STABILITY AT MACH 3.0

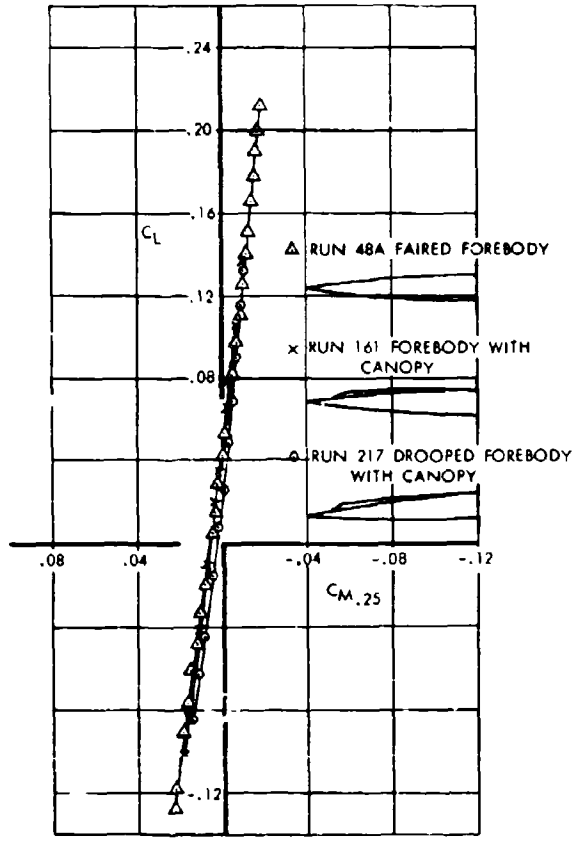

FIGURE 4-48 EFFECT OF FOREBODY SHAPE ON LONGITUDINAL STABILITY AT MACH 3.0

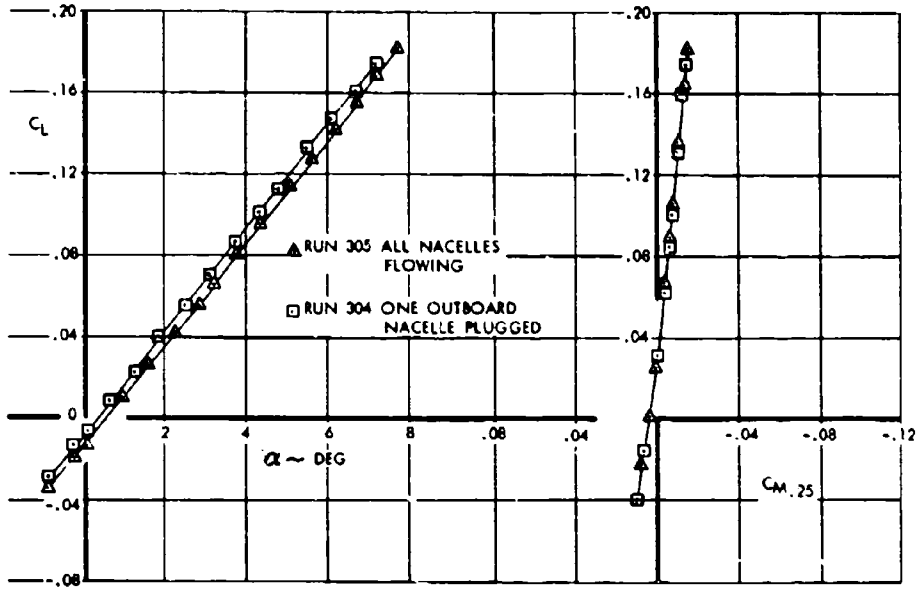

FIGURE 4-49 EFFECT OF SIMULATED ENGINE FAILURE ON MACH 3.0 LONGITUDINAL STABILITY

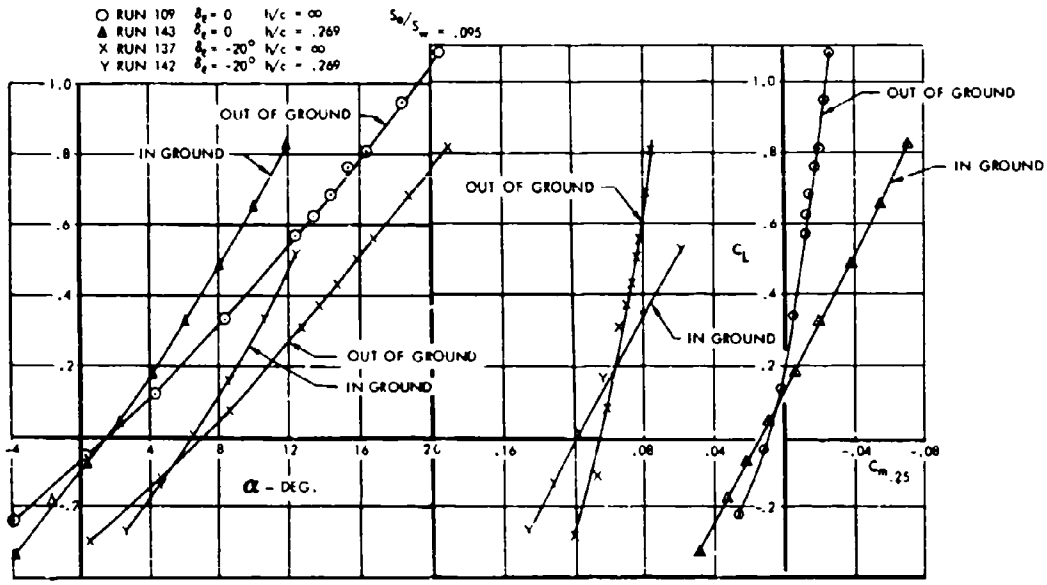

FIGURE 4-50 LOW SPEED ELEVATOR CONTROL POWER

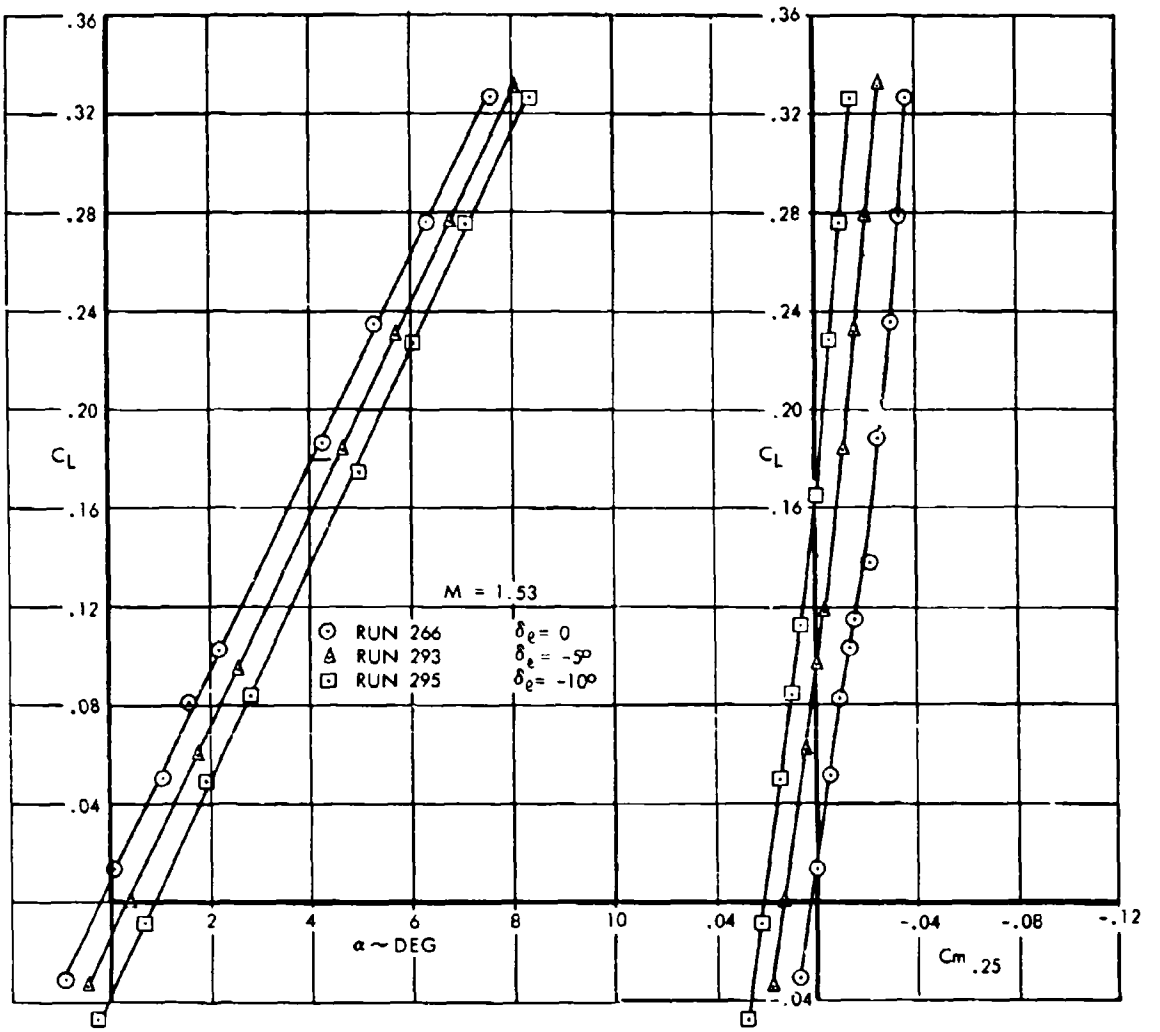

FIGURE 4-51 SUPERSONIC ELEVATOR CONTROL POWER AT MACH 1.5

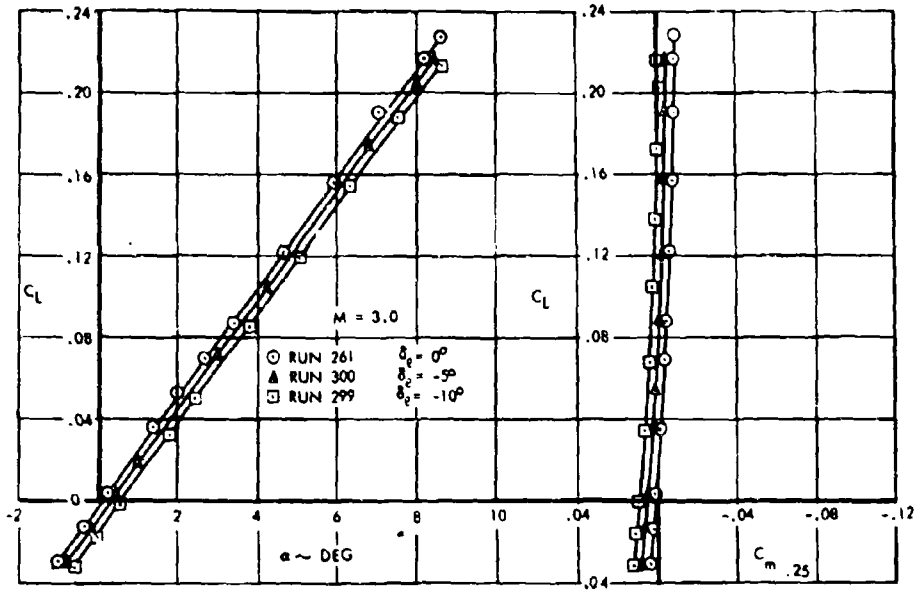

FIGURE 4-52 SUPERSONIC ELEVATOR CONTROL POWER AT MACH 3.0

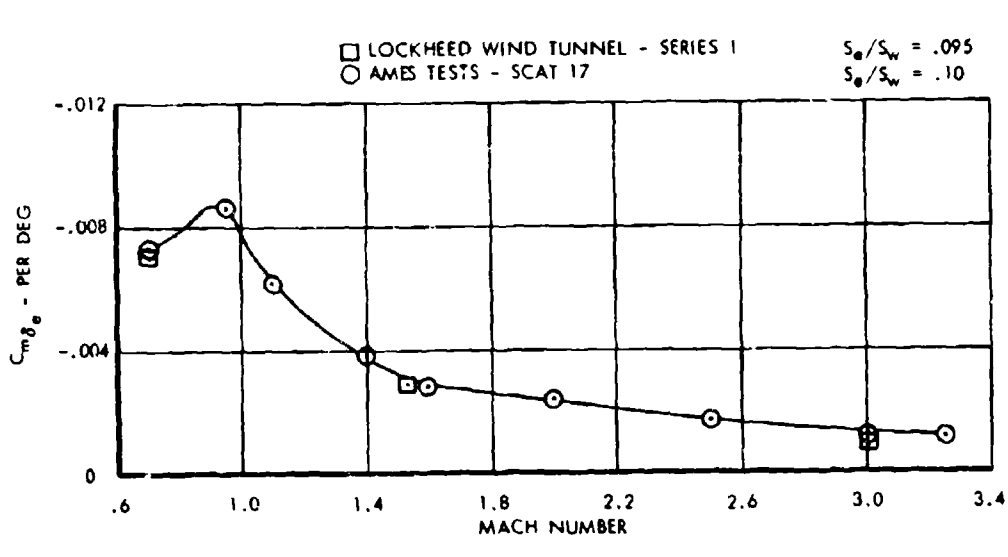

FIGURE 4-53 ELEVATOR EFFECTIVENESS

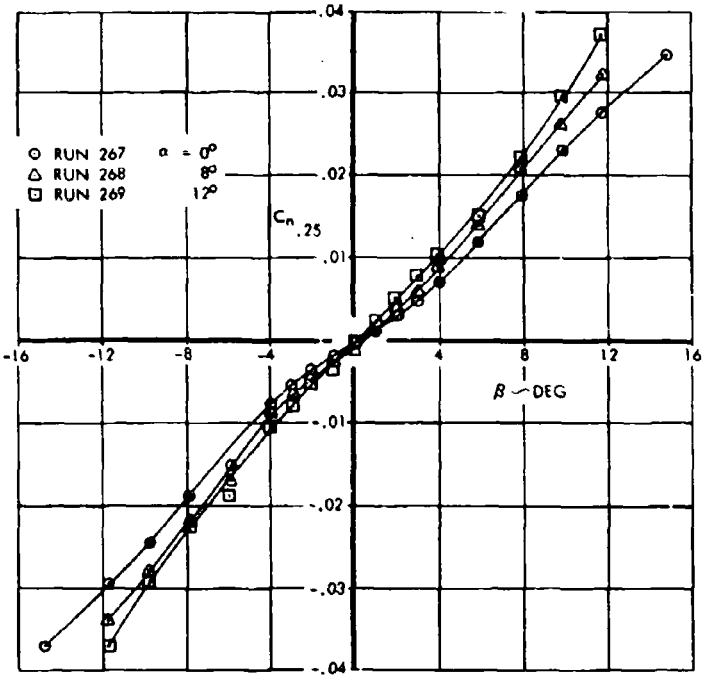

FIGURE 4-54 LOW SPEED DIRECTIONAL STABILITY—EFFECT OF ANGLE OF ATTACK

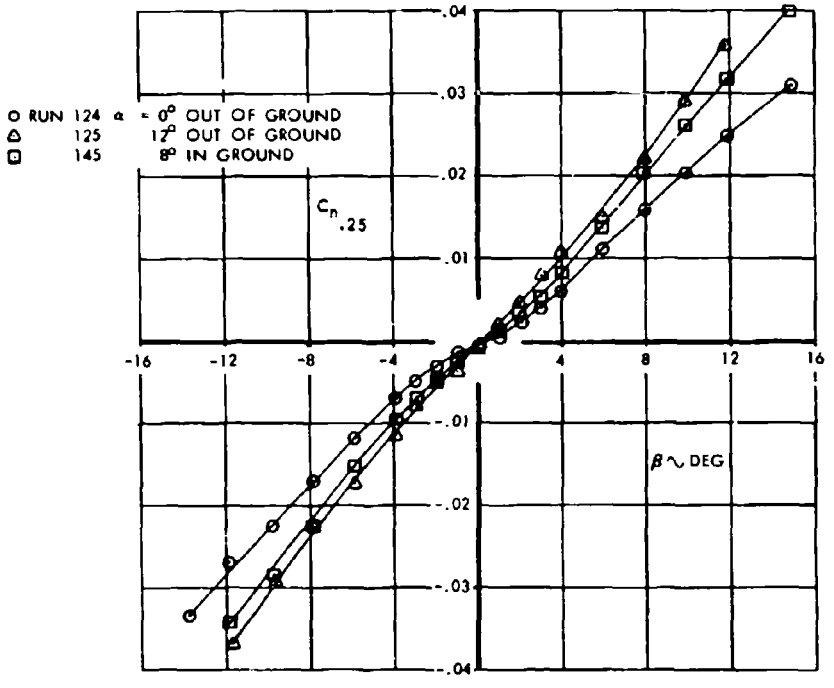

FIGURE 4-55 LOW SPEED DIRECTIONAL STABILITY—EFFECT OF GROUND

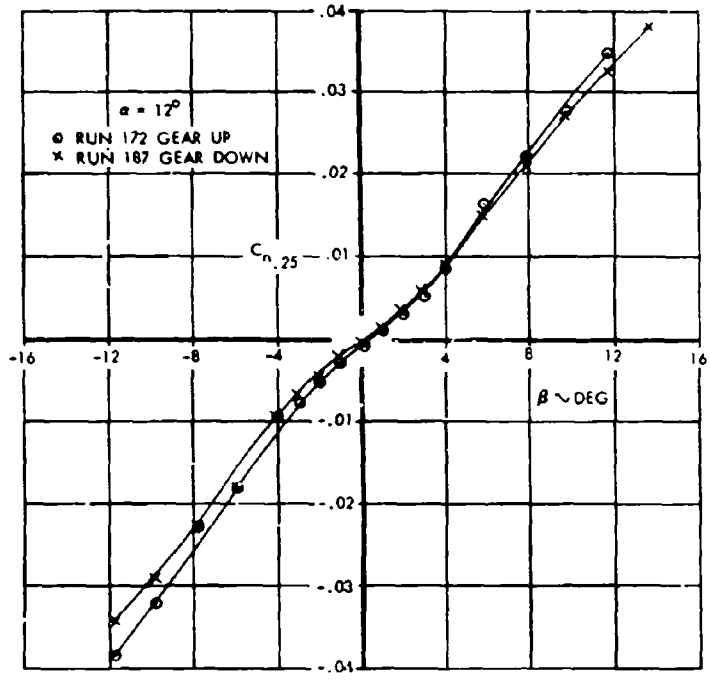

FIGURE 4-56 LOW SPEED DIRECTIONAL STABILITY—EFFECT OF LANDING GEAR

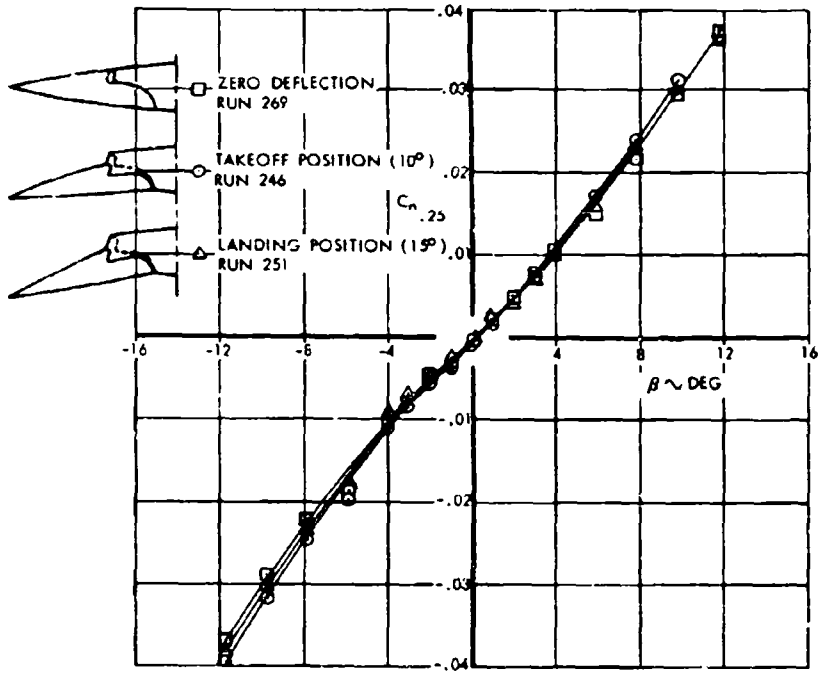

FIGURE 4-57 LOW SPEED DIRECTIONAL STABILITY—EFFECT OF WEATHER-VISION NOSE

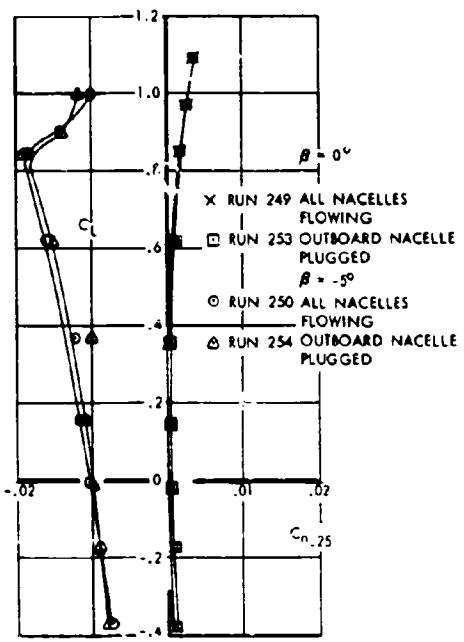

FIGURE 4-58 SIMULATED ENGINE FAILURE EFFECTS ON LOW SPEED DIRECTIONAL STABILITY

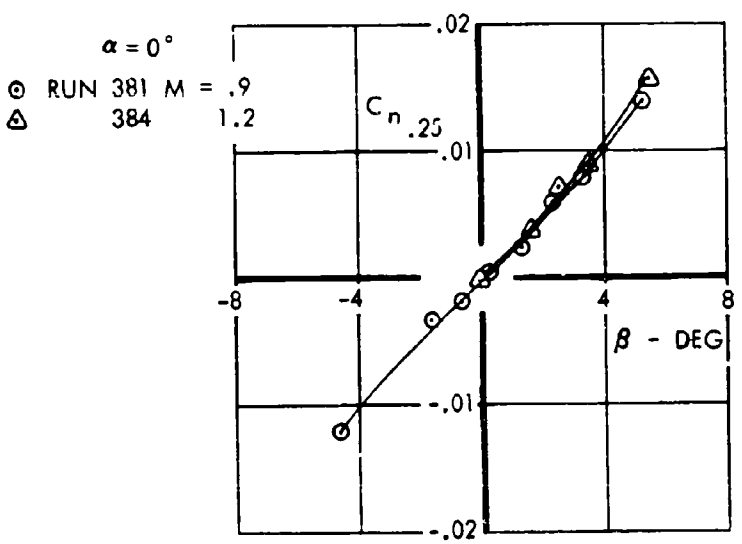

FIGURE 4-59 TRANSONIC DIRECTIONAL STABILITY

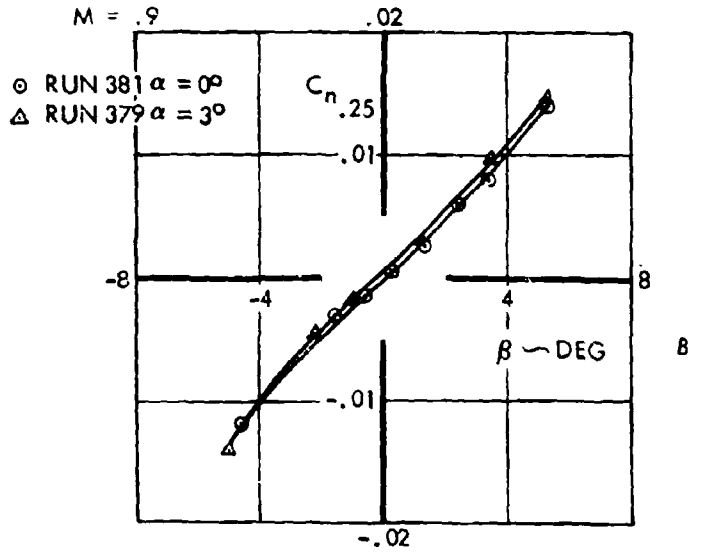

FIGURE 4-60 EFFECT OF ANGLE OF ATTACK ON MACH 0.9 DIRECTIONAL STABILITY

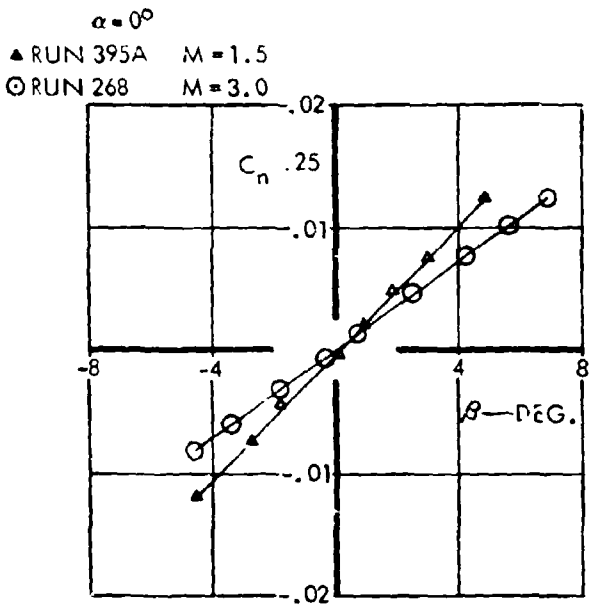

FIGURE 4-61 SUPERSONIC DIRECTIONAL STABILITY

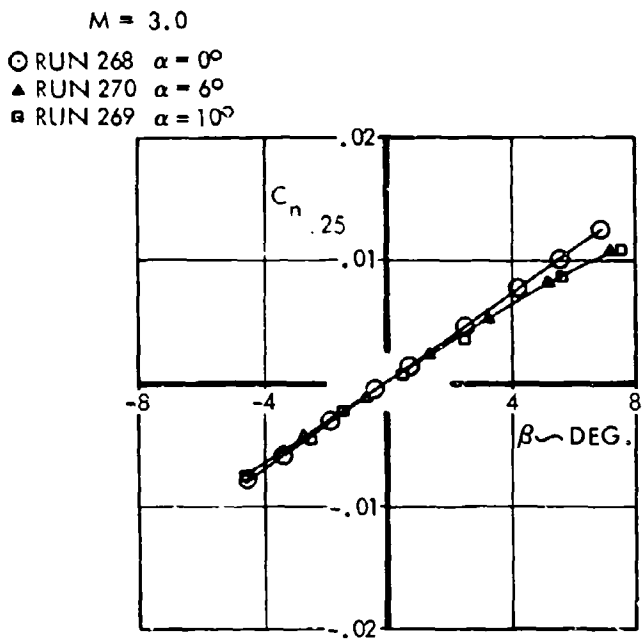

FIGURE 4-62 EFFECT OF ANGLE OF ATTACK ON MACH 3.0 DIRECTIONAL STABILITY

Figure 4-63 summarizes the effects of a ventral mounted below the aft fuselage for Mach 3 conditions. Results indicated that a small favorable contribution was realized from the ventral with nacelles removed. However, a similar contribution was realized from the addition of the nacelles, regardless of whether the ventral was on or off. An interference flow field from the nacelles cancels out the ventral stability increment. Therefore, the ventral has not been incorporated on the SST.

The effects of reducing the mass flow of an outboard engine to zero are presented in Figure 4-64 for Mach 3 conditions. Also shown is the predicted increment in yawing moment, based on data of Reference 4-7. This simulation of an engine failure is far more severe than will be encountered in actual SST operation for reasons discussed in Section 6. However, even under these extreme conditions, the steady state rudder angle required for zero sideslip angle is estimated to be only 6 degrees at the cruise attitude.

Low-speed wind tunnel data showing lateral characteristics are presented in Figures 4-65 and 4-66 showing effects of angle of attack and ground effect. The effects of gear extension and weather-vision nose position are shown to have insignificant effects in Figures 4-67 and 4-68.

A simulation of a low-speed engine failure situation is presented in Figure 4-69, showing that the incremental rolling moment caused by zero mass flow through an outboard duct is small.

Supersonic lateral characteristics are presented in Figures 4-70 and 4-71, showing effects of Mach number and angle of attack. Rolling moments produced by a plugged outboard engine nacelle at Mach 3.0 are shown in Figure 4-72. The estimated increment based on data of Reference 4-7 is also shown.

Low-speed directional control power characteristics are presented in Figure 4-73 for various angles of attack. The effect of partial span rudder deflection is given in Figure 4-74. Figure 4-75 presents supersonic rudder effectiveness data.

The effect of angle of attack on low-speed lateral control power is shown in Figure 4-76. There is no loss in aileron effectiveness at high angles. The effect of sideslip on aileron effectiveness is presented in Figure 4-77. The relative lateral control power of inboard, mid-span, and outboard ailerons at low speed is compared in Figure 4-78. These data indicate that the inboard controls have very poor lateral control power. For this reason, this inboard control is used only as an elevator.

Supersonic lateral control effectiveness, shown in Figures 4-79 and 4-80 were obtained on the first series high speed model. The aileron geometry was similar to the proposed airplane, and the data are considered to be directly applicable.

4.5 HINGE MOMENT CHARACTERISTICS

Control surface hinge moments coefficients were determined using the USAF Stability and Control Methods Handbook for low speed and at Mach 3.0. The variation with Mach number was estimated using the experimental trends indicated in the referenced NASA reports. Figure 4-81 presents the data for the elevator, elevon, and rudder surfaces.

4.6 ROTARY STABILITY DERIVATIVE CHARACTERISTICS

Three general types of data or information were used in obtaining rotary stability derivatives for the SST. The most applicable source of data was taken from forced oscillation tests of geometrically similar models such as found in References 6-13 and 6-14. Data for the primary damping derivatives such as C_{m_q}, C_{l_p} and C_{n_r} were obtained from these sources. When required, these data were corrected for wing and tail planform and fuselage shape. In the absence of complete speed or configuration data from the first type of information, References 6-18 through 6-21 and 6-23 were used as a second type to obtain characteristic trends with speed, shape or angle of attack. This type of data was required on nearly all rotary derivatives. The third general form of information was obtained from theoretical or empirical methods as found in References 6-6, 6-15, 6-16 and 6-22. These sources were used to correlate the test data and extend test results in speed and angle of attack. This latter form of information was required for estimating the "cross-derivatives" such as C_{n_p} and C_{l_r}. Combinations of all sources were used whenever possible to develop the rigid rotary stability characteristics which are presented in Figures 4-82 to 4-84.

$\alpha = 6^{o}$

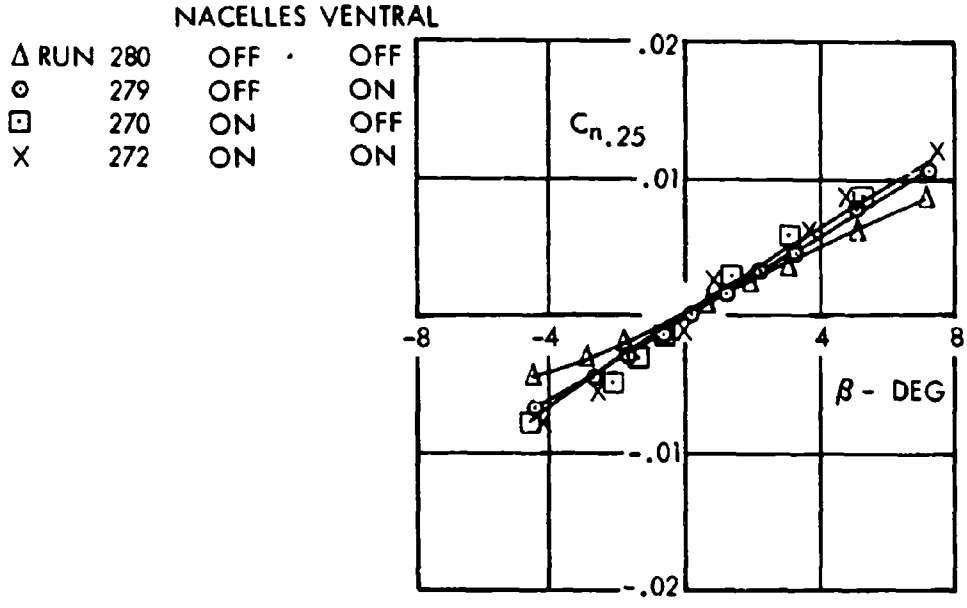

FIGURE 4-63 EFFECT OF A VENTRAL AND NACELLES ON MACH 3.0 DIRECTIONAL STABILITY

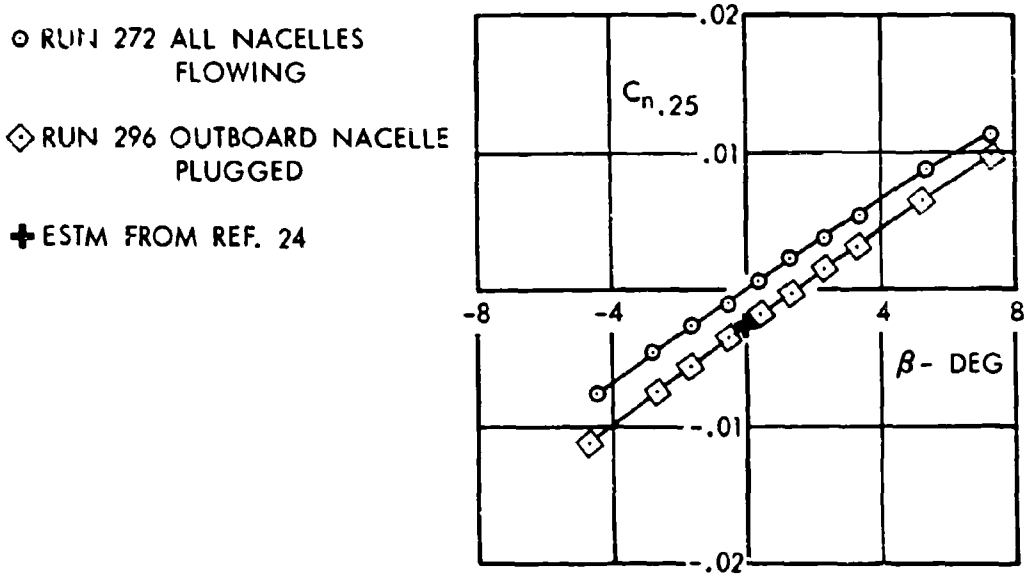

FIGURE 4-64 SIMULATED ENGINE FAILURE EFFECTS ON MACH 3.0 DIRECTIONAL STABILITY

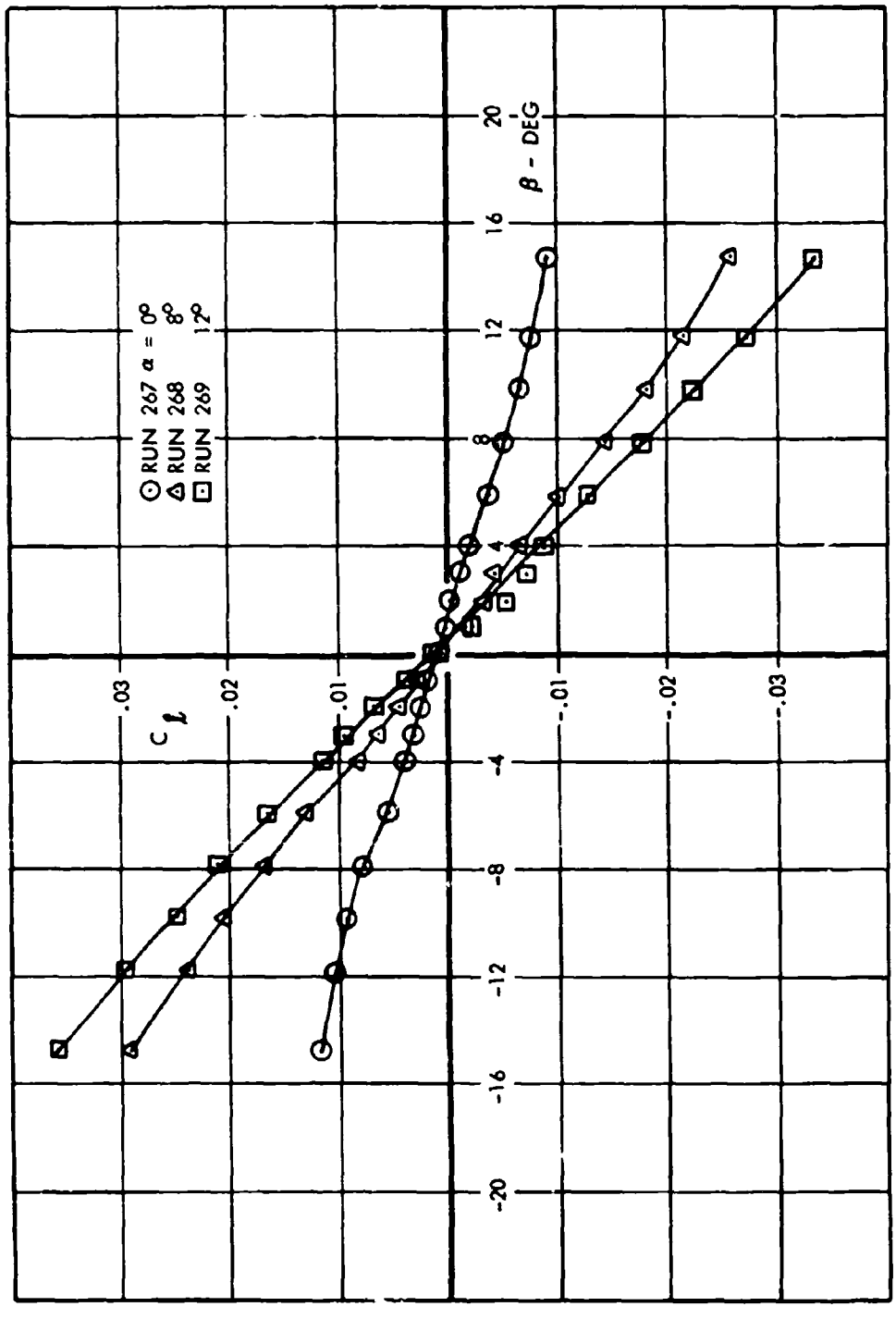

FIGURE 4-65 LOW SPEED LATERAL STABILITY—EFFECT OF ANGLE OF ATTACK

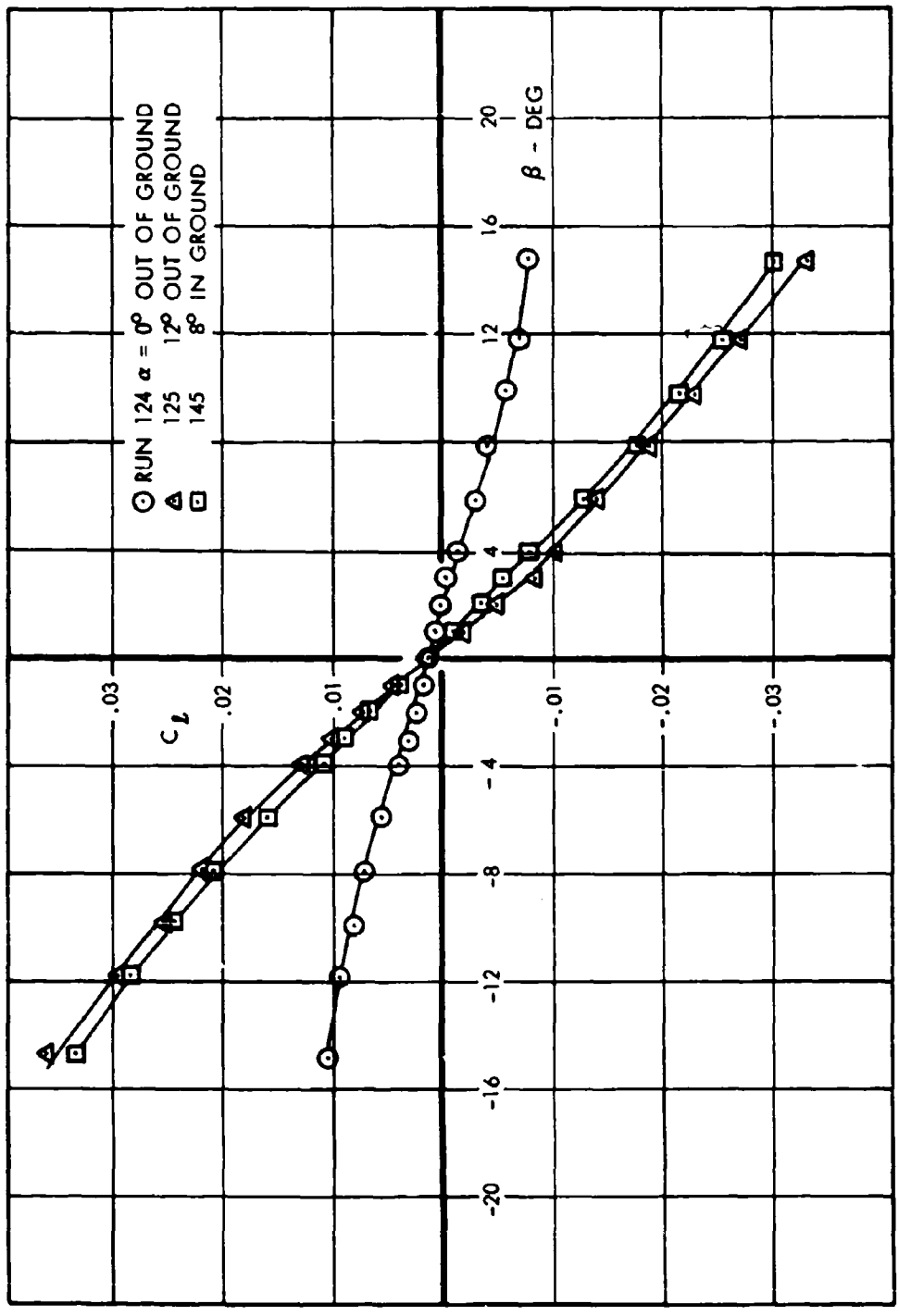

FIGURE 4.66 LOW SPEED LATERAL STABILITY—EFFECT OF GROUND

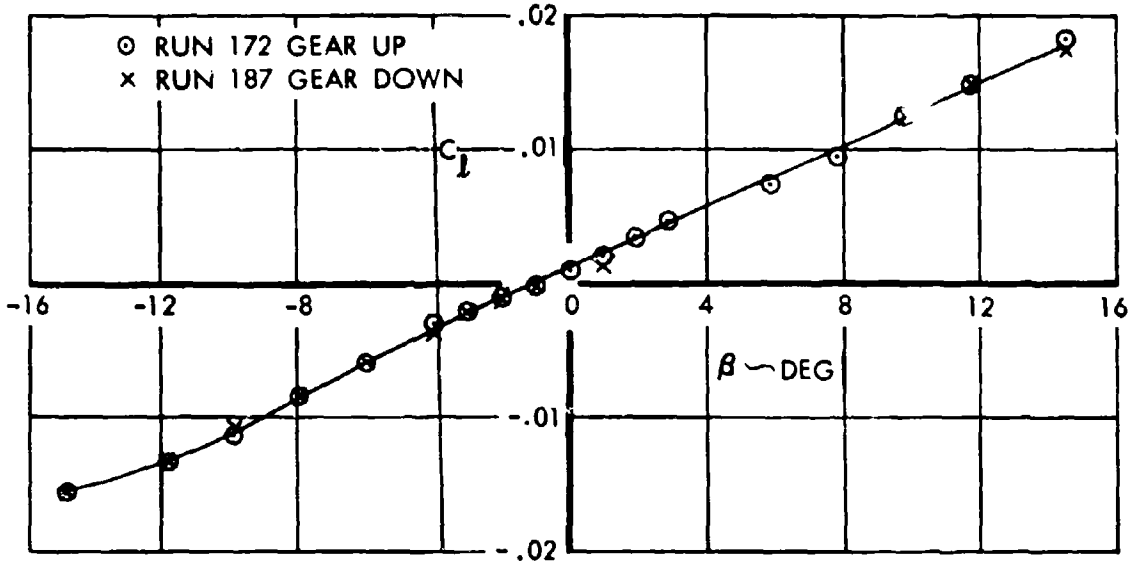

FIGURE 4-67 LOW SPEED LATERAL STABILITY—EFFECT OF LANDING GEAR

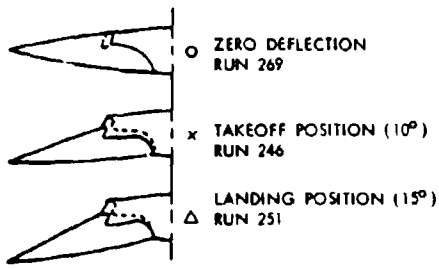

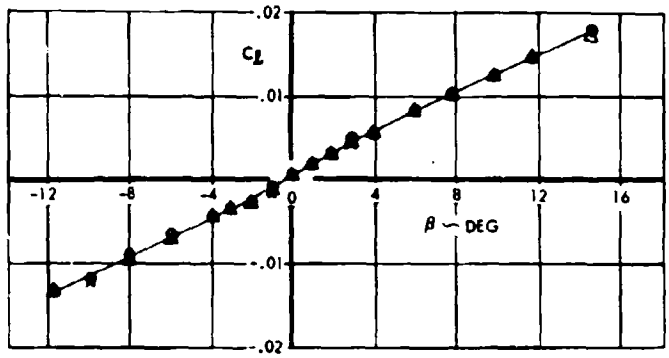

FIGURE 4-68 LOW SPEED LATERAL STABILITY—EFFECT OF WEATHER-VISION NOSE

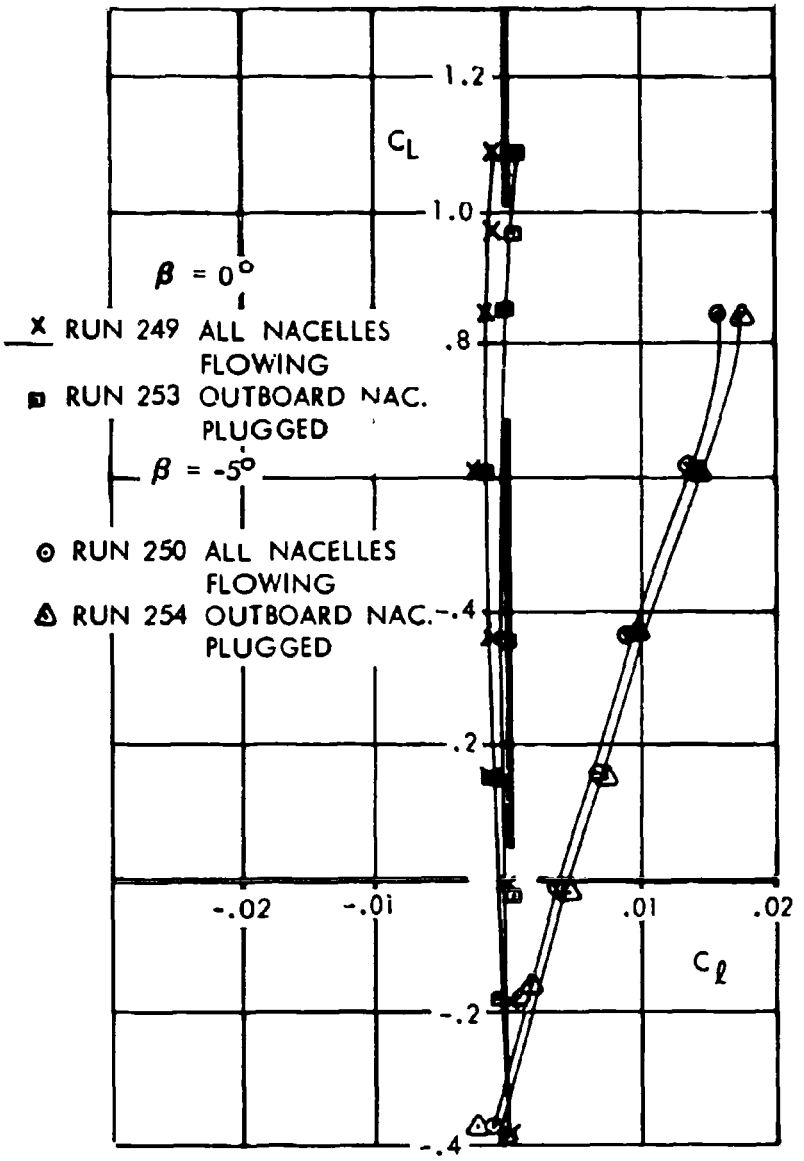

FIGURE 4-69 SIMULATED ENGINE FAILURE EFFECTS ON LOW SPEED LATERAL STABILITY

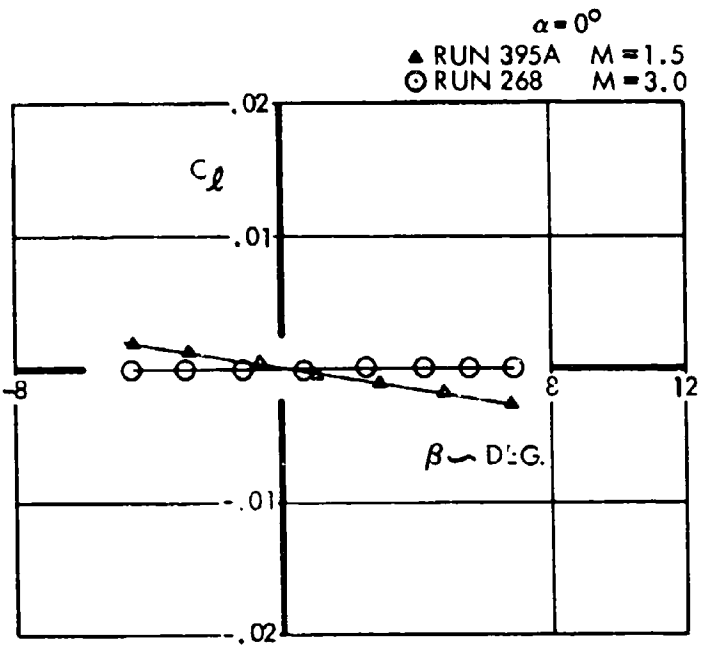

FIGURE 4-70 EFFECT OF MACH NUMBER ON SUPERSONIC LATERAL STABILITY

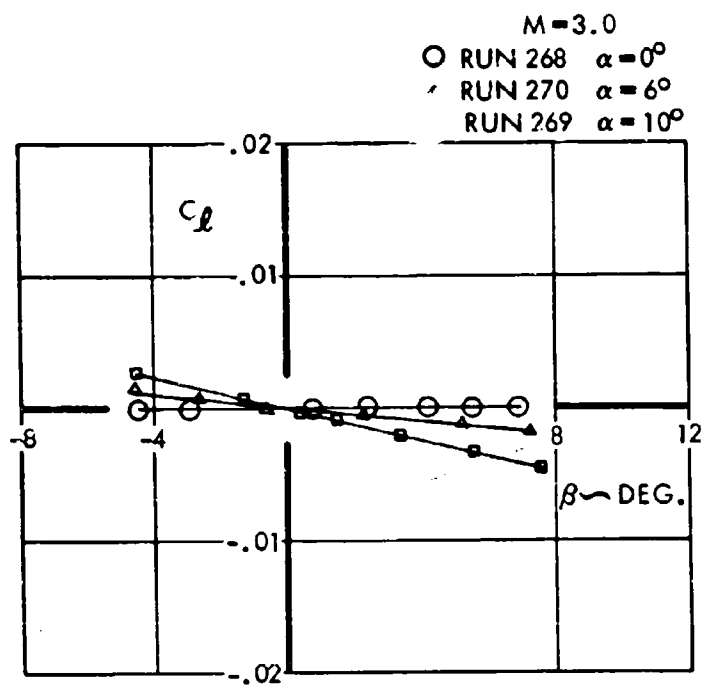

FIGURE 4-71 EFFECT OF ANGLE OF ATTACK ON MACH 3.0 LATERAL STABILITY

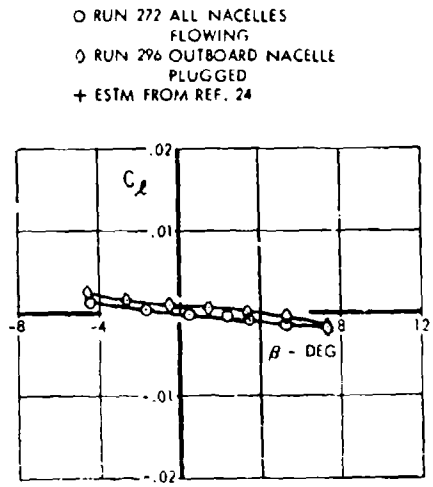

FIGURE 4-72 SIMULATED ENGINE FAILURE EFFECTS ON MACH 3.0 LATERAL STABILITY

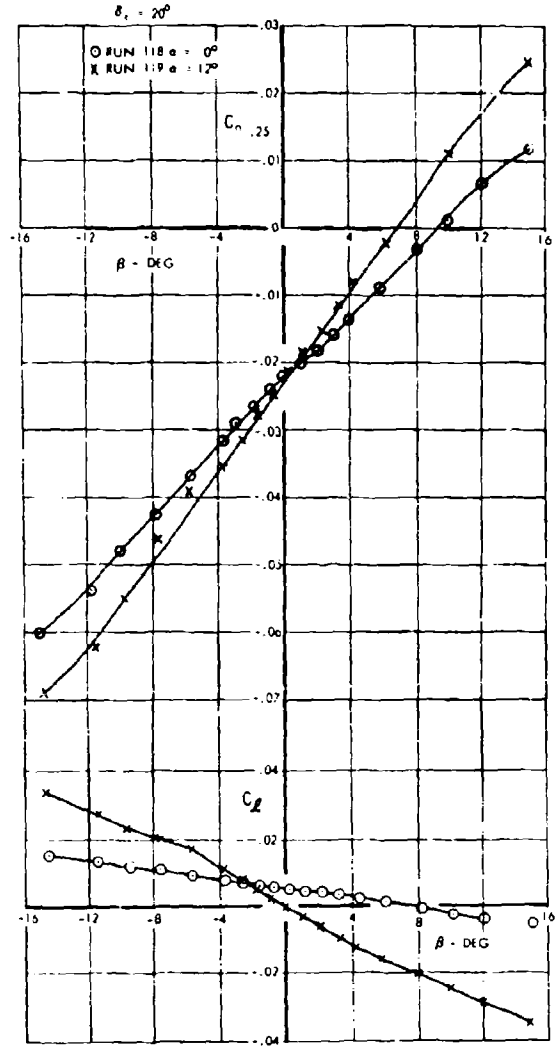

FIGURE 4-73 LOW SPEED DIRECTIONAL CONTROL POWER

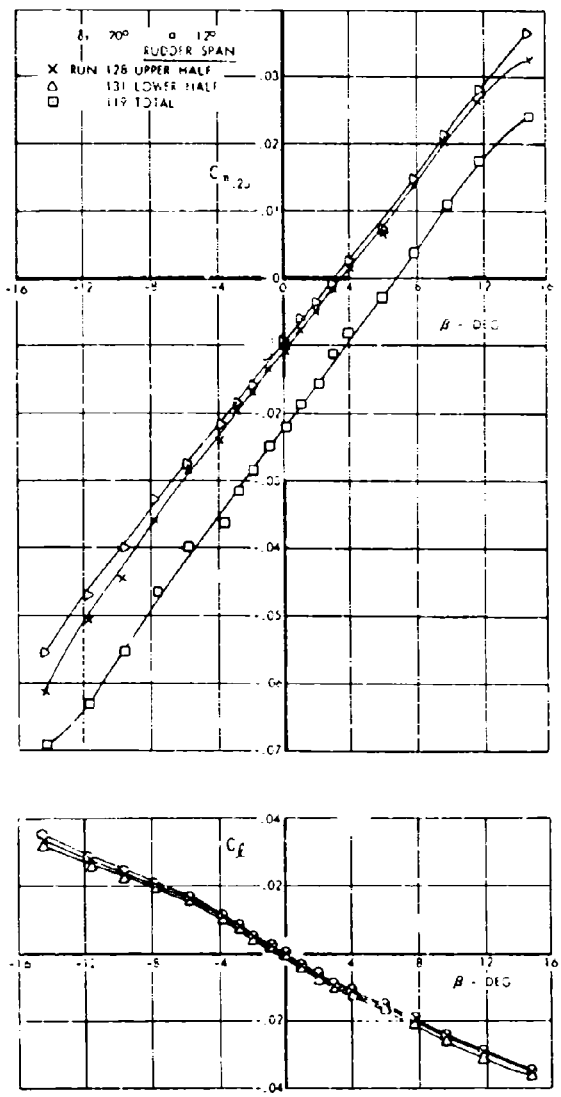

FIGURE 4-74 EFFECT OF PARTIAL SPAN RUDDER DEFLECTION ON DIREC ONAL CONTROL POWER

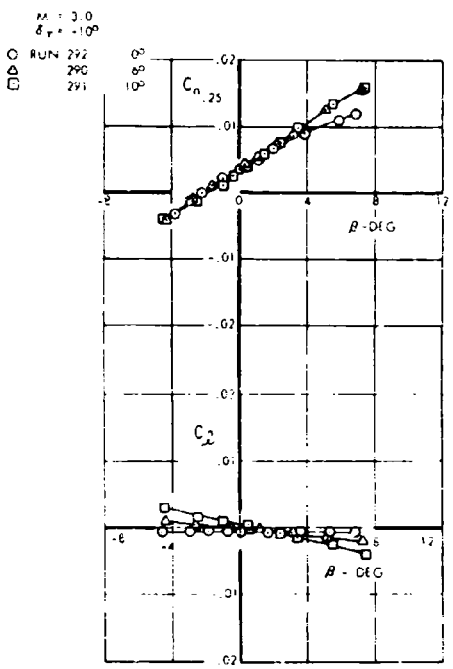

FIGURE 4-75 SUPERSONIC DIRECTIONAL CONTROL POWER

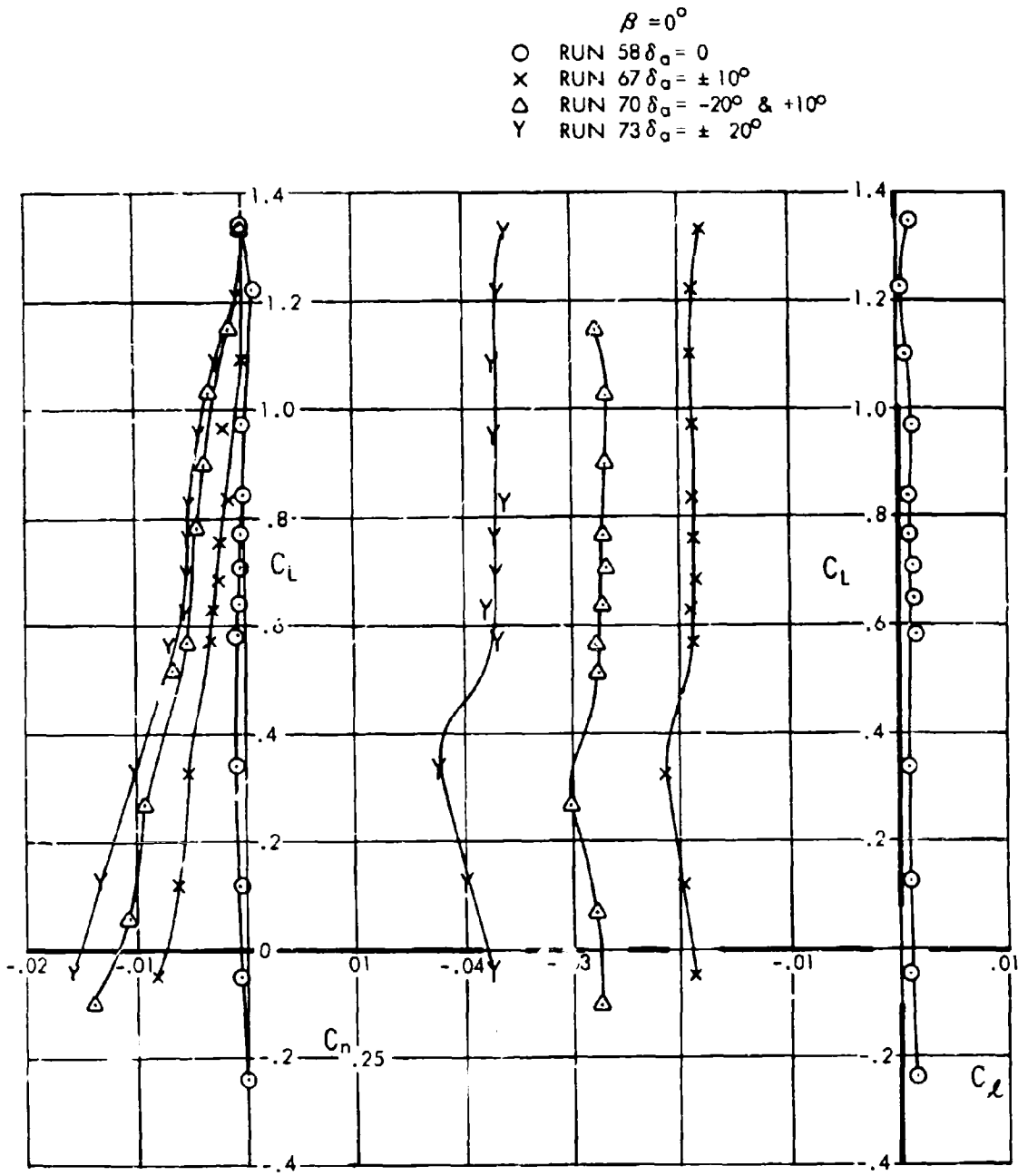

FIGURE . 76 LOW SPEED LATERAL CONTROL POWER

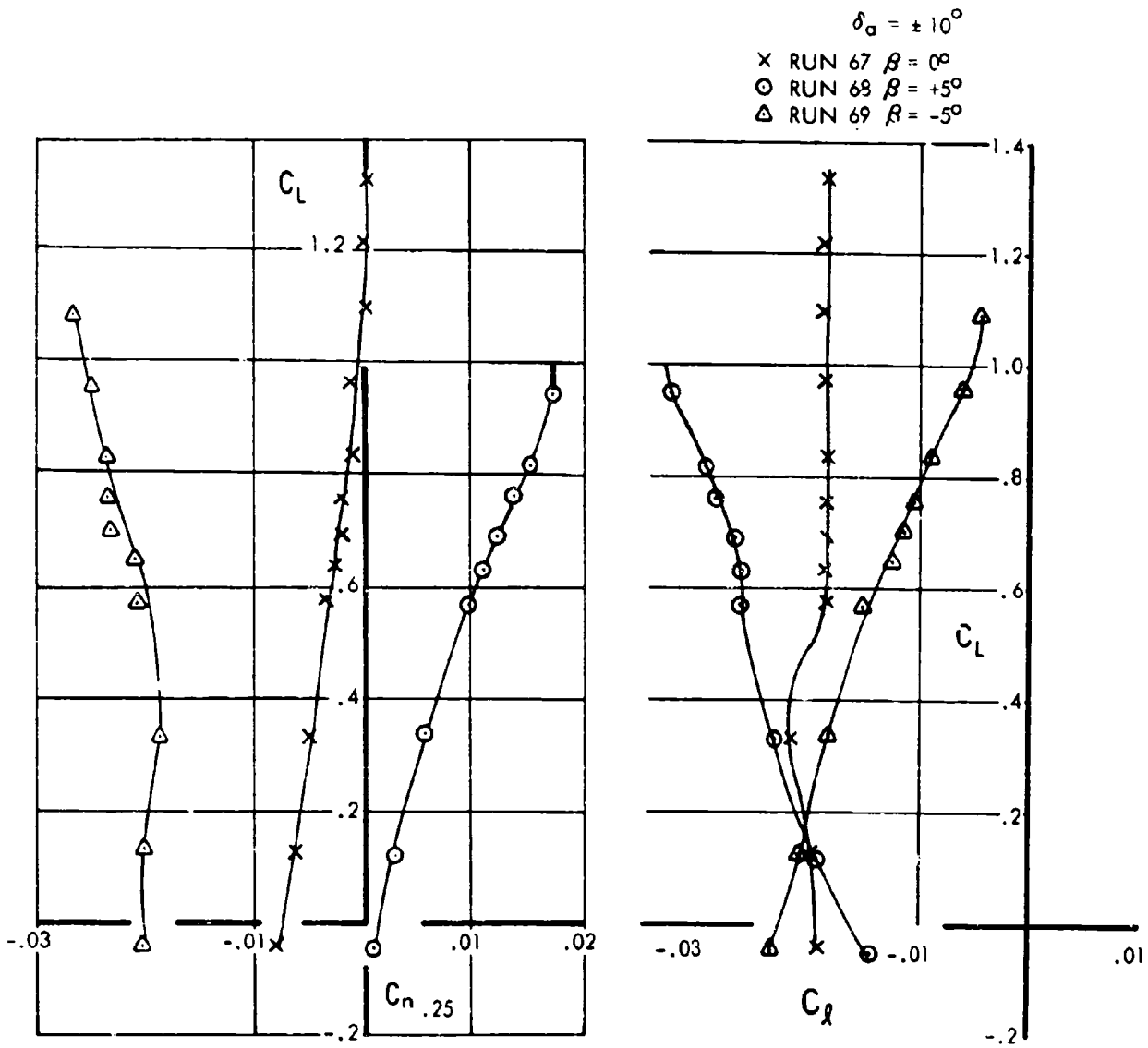

FIGURE 4-77 EFFECT OF SIDESLIP ON LOW SPEED LATERAL CONTROL POWER

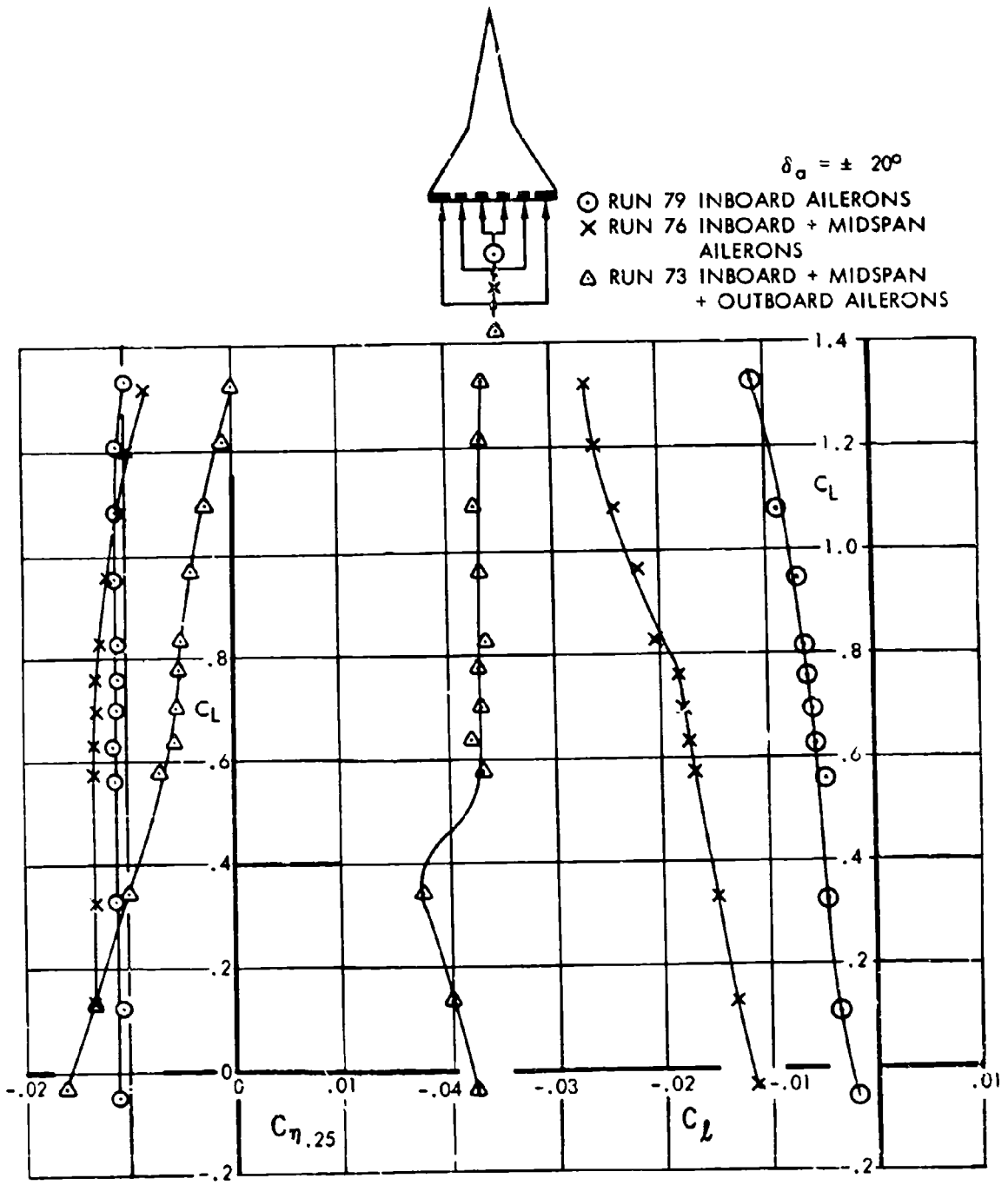

FIGURE 4-78 EFFECT OF AILERON GEOMETRY ON LOW SPEED LATERAL CONTROL POWER

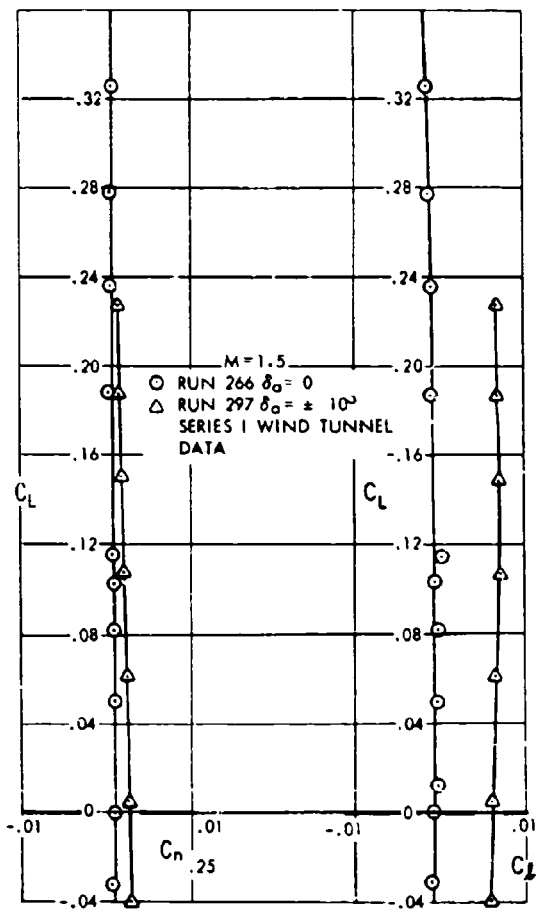

FIGURE 4-79 SUPERSONIC AILERON CONTROL POWER AT MACH 1.5

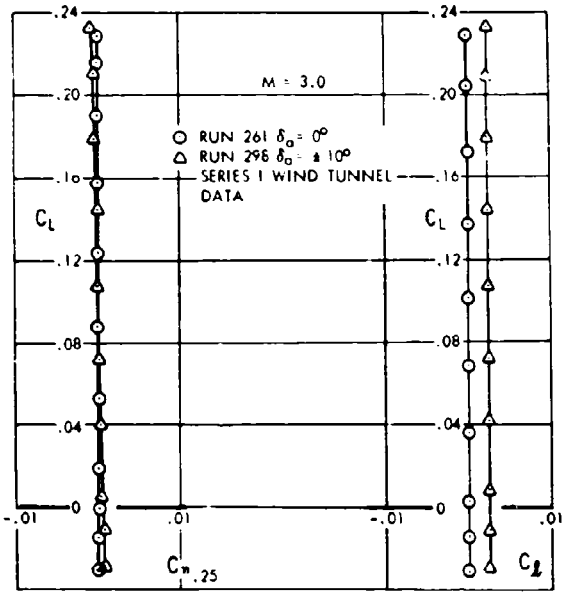

FIGURE 4-80 SUPERSONIC AILERON CONTROL POWER AT MACH 3.0

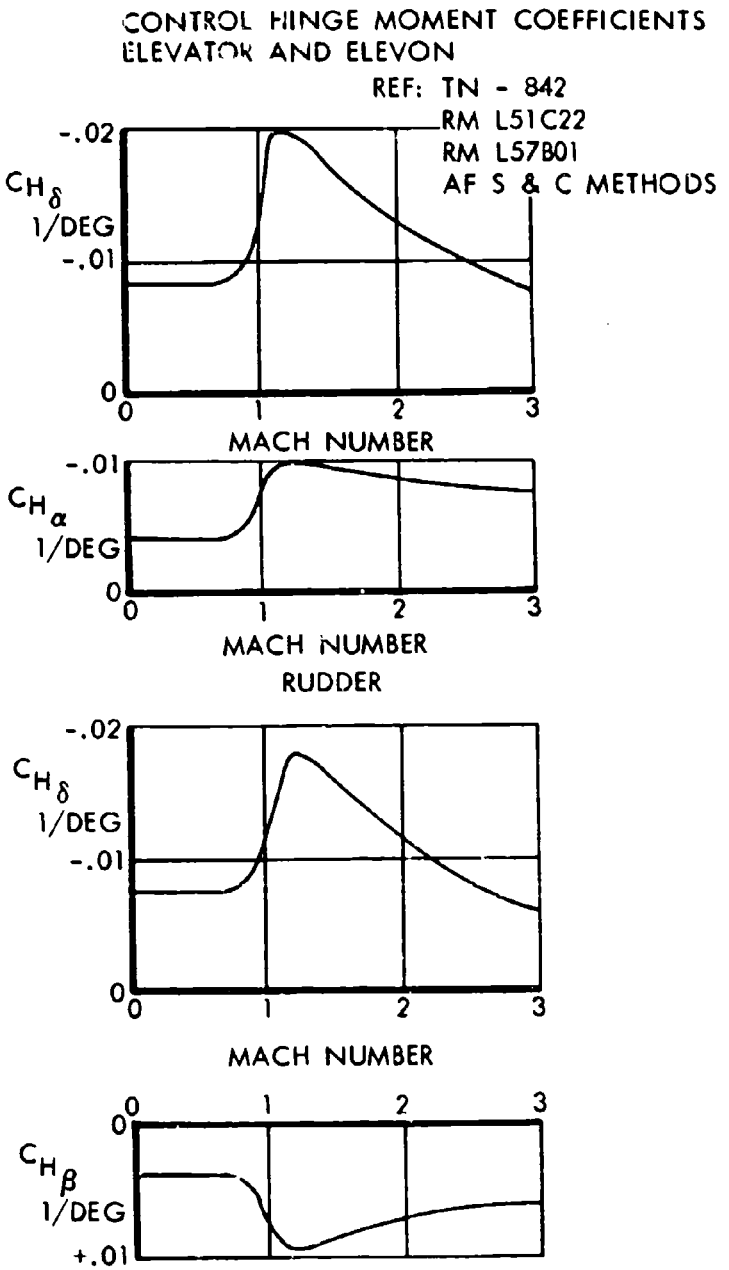

FIGURE 4-81 CONTROL HINGE MOMENT COEFFICIENTS

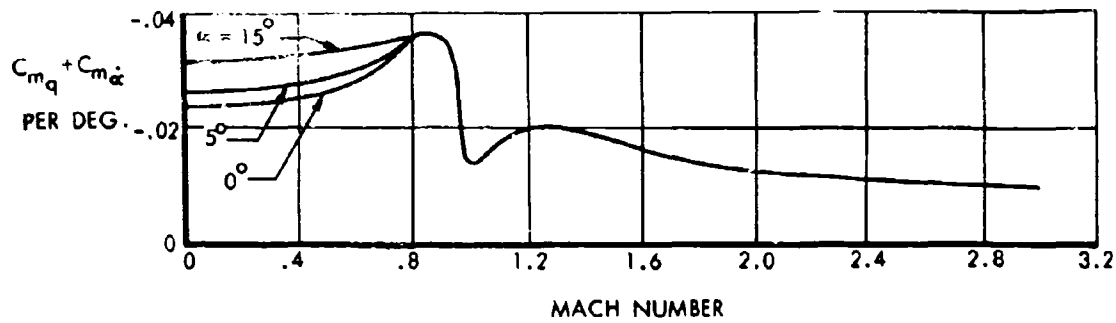

FIGURE 4-82 DAMPING IN PITCH

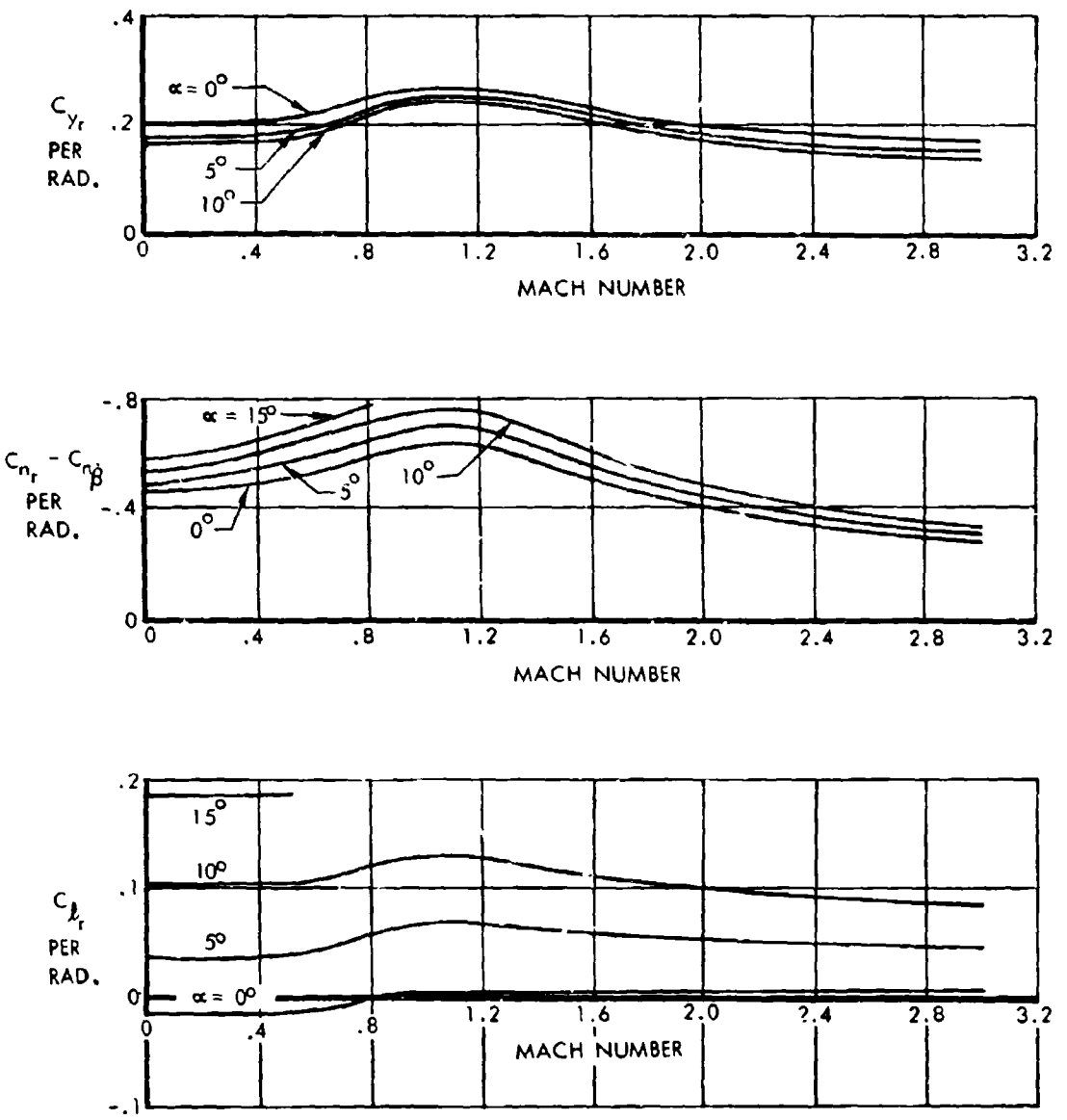

FIGURE 4-83 DAMPING IN YAW

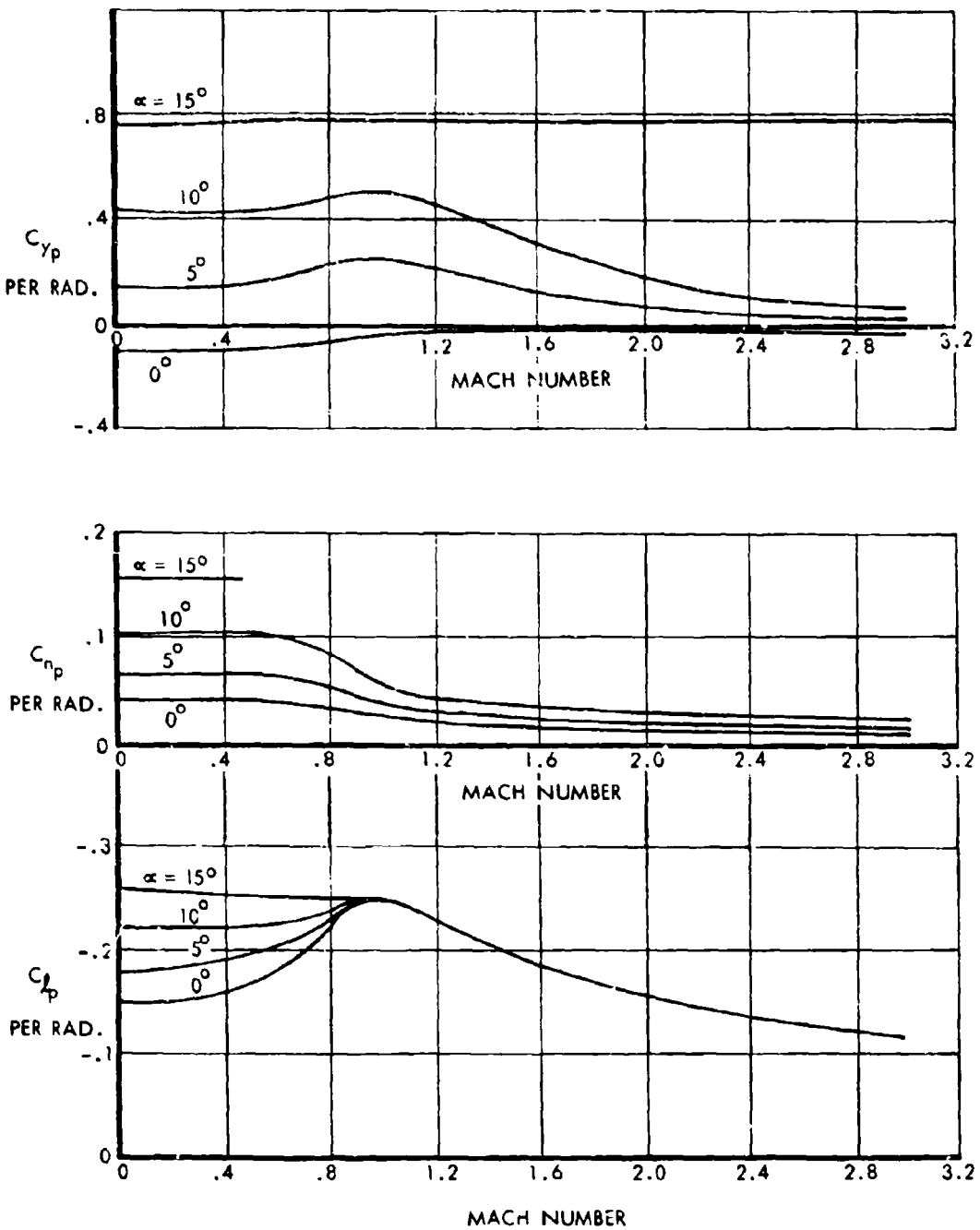

FIGURE 4-84 DAMPING IN ROLL

4.7 SUMMARY OF BASIC AERODYNAMIC DATA

Lift and drag characteristics used for performance analysis, and stability and control derivatives used for handling quality evaluations are summarized in this section. These data are derived from the wind tunnel results previously presented but include corrections for Reynolds number and small geometry differences between model and airplane. These summary data also incorporate the predicted aerodynamic improvements that will be achieved at the end of the Phase II study program. Drag characteristics are presented in Figure 4-85, giving the variation of zero lift drag, C_{D_0}, drag due to lift, $\Delta C_D/C_L^2$, and lift-drag ratio, L/D, with Mach number. These values reflect full-scale estimates, with all drag penalties for propulsion, trim and miscellaneous items included. The data clearly indicated a low transonic drag rise increment and high maximum lift-drag ratios which are a result of the cambered and twisted double-delta wing planform shape. Trimmed drag polar curves are presented in Figure 4-86 for typical subsonic, transonic and supersonic cruise Mach numbers. The low-speed drag polar presented in Figure 4-87 is applicable for all low speed flight regimes, since the SST does not employ either leading or trailing edge high-lift devices. Increments in drag for landing gear extension and inoperative engine operation are noted on Figure 4-87.

Basic static longitudinal stability parameters are summarized in Figures 4-88 to 4-90. Figure 4-90 presents the rigid wing aerodynamic center shift and positive zero lift pitching moment characteristics for several C_L ranges. The effects of flexibility on aerodynamic center, discussed in Section 6, are illustrated for one g flight along the flight profile in Figure 4-91. Rigid wing longitudinal control effectiveness is summarized in Figure 4-92. The effects of flexibility for any particular flight condition are considered separately and are discussed in Section 6.

Rigid wing lateral-directional characteristics as a function of Mach number are presented in Figure 4-93. The relatively high directional stability at high airplane attitudes can be attributed to favorable sidewash created by the bat. Rudder control effectiveness and lateral control power characteristics are summarized in Figures 4-94 and 4-95. Effects of flexibility are considered in Section 6.

4.8 WIND TUNNEL PROGRAM (3.2.6)

The speed-altitude spectrum of the SST is new to commercial aviation and there is little background of military experience from which to draw knowledge. Therefore, it will be necessary to lean heavily on laboratory testing to provide simulation of the SST flight environment. The proposed wind tunnel program has been conceived with the belief that thorough testing is mandatory to assure an optimum design for this new flight regime. It is preliminary in nature and will finally be established following consultation with FAA personnel.

Both contractor and NASA tunnel facilities will be utilized to support the program. Initial developmental type testing will be carried out in the contractor's wind tunnels. Multi-purpose models will be utilized where advisable. As noted in the Master Program Plan, most models will be tested several times during the program.

The aerodynamic concept features a relatively new type of wing planform shape which has not yet received extensive theoretical and experimental study by industry and government facilities. From the analyses and wind tunnel evaluations conducted to date, significant aerodynamic improvements have been achieved in many key areas, potential improvements have been indicated in others, and still other areas of potential improvement remain unexplored. The proposed program continues this developmental type testing to assure an optimum final configuration.

The wind tunnel test plan is outlined below. A corresponding test schedule has been coordinated with the Master Program Plan presented in Volume M-I. This wind tunnel schedule is presented for reference in Figure 4-96. The testing will support essentially all of the technical activities. In particular, the vital areas of aerodynamic configuration development, airloads and temperature distribution, engine inlet and exhaust system development, and flight dynamics will utilize the wind tunnel tests.

A close liaison with NASA personnel will be maintained throughout the program. This is considered especially important during the initial phases of the work. NASA's experience with the SST flight regime through many years of wind tunnel testing and the X-15 flight program will be utilized in developing the model configurations and planning the tests.

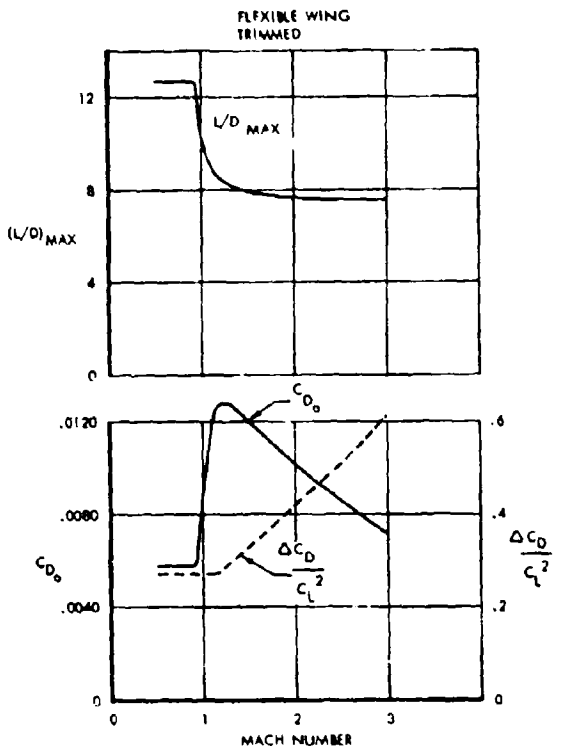

FIGURE 4-85 SUMMARY OF BASIC DRAG DATA

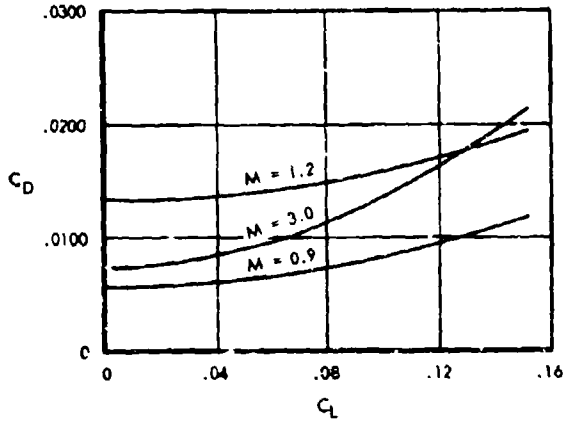

FIGURE 4-86 FULL SCALE CRUISE DRAG POLARS

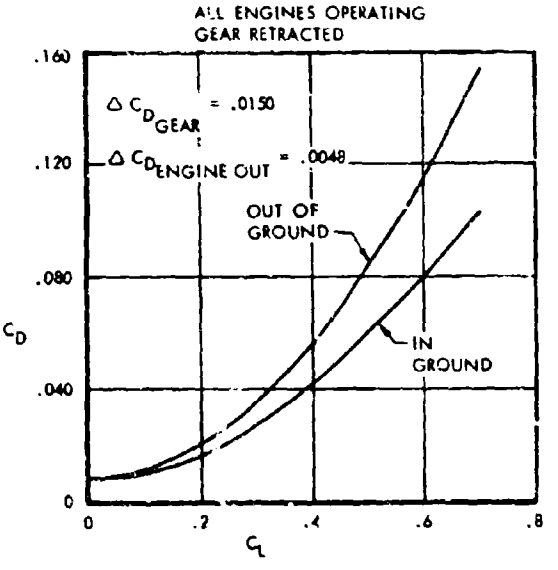

FIGURE 4-87 FULL SCALE LOW SPEED DRAG POLAR

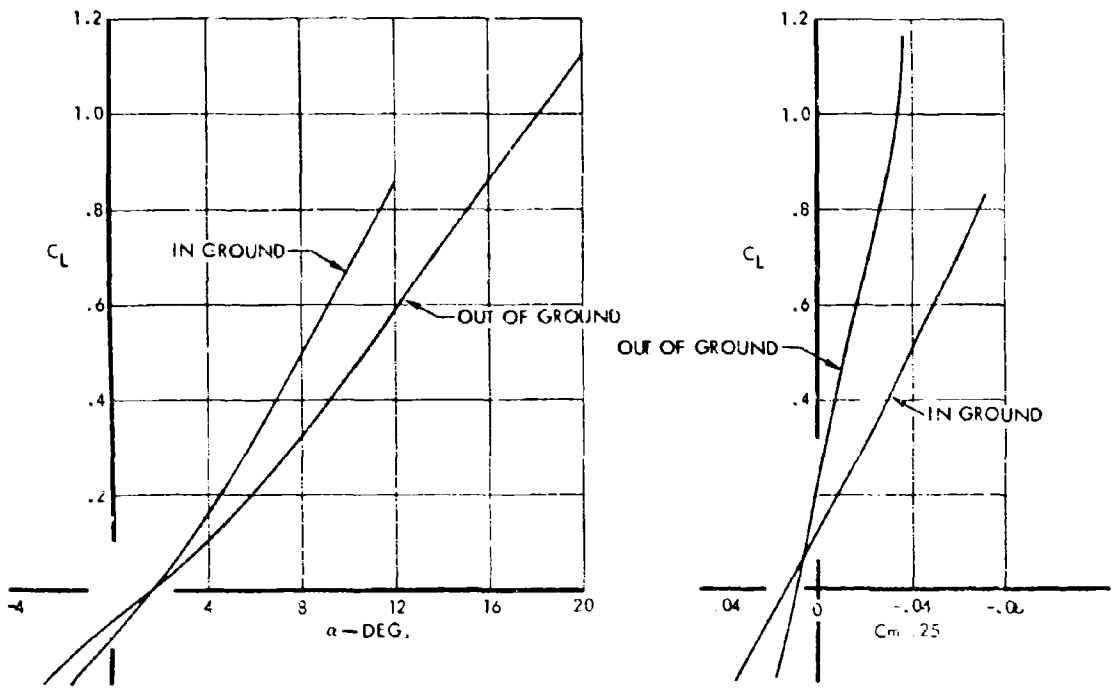

FIGURE 4-88 SUMMARY OF LOW SPEED LONGITUDINAL CHARACTERISTICS

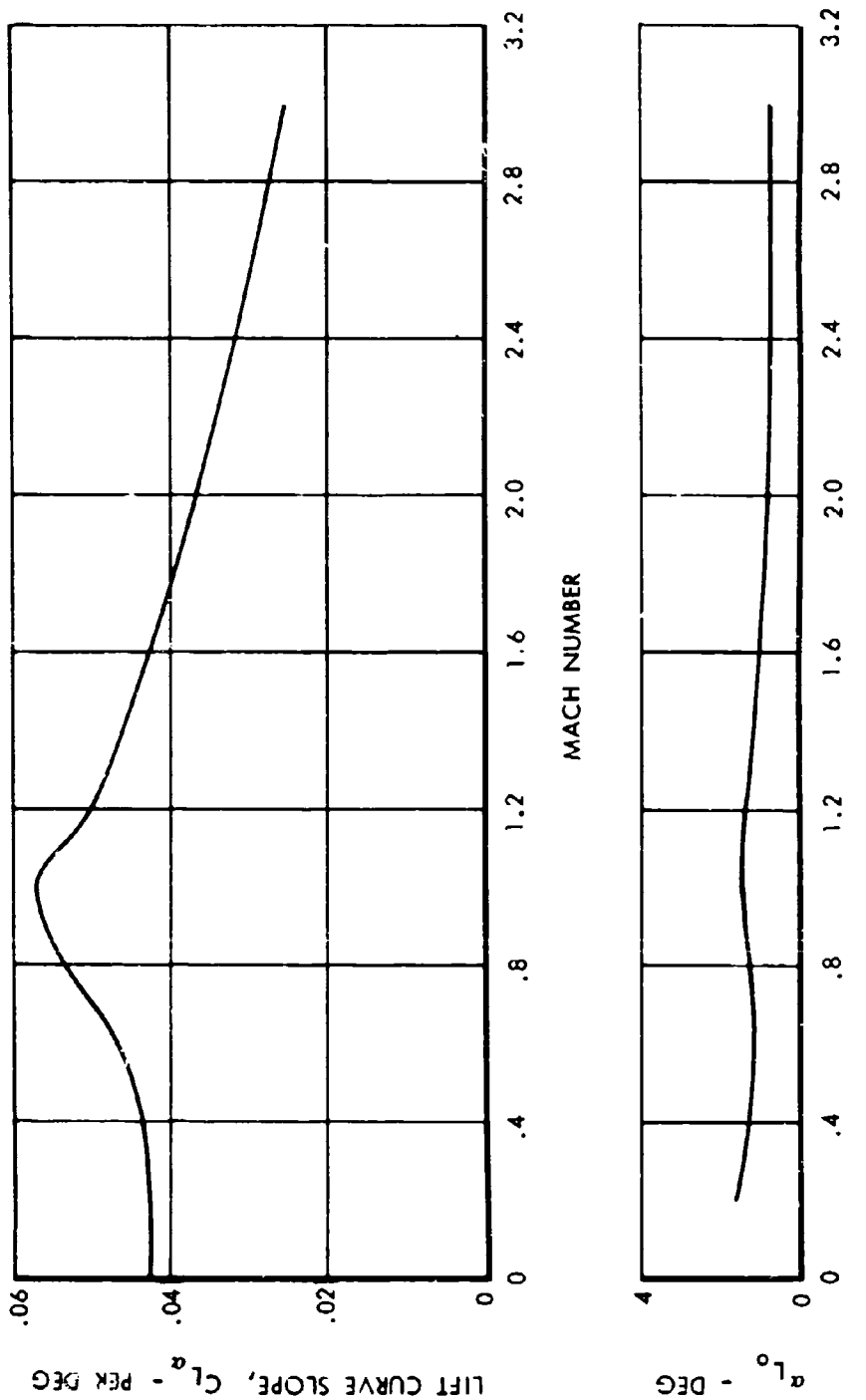

FIGURE 4-89 RIGID AIRPLANE LIFT CHARACTERISTICS SUMMARY

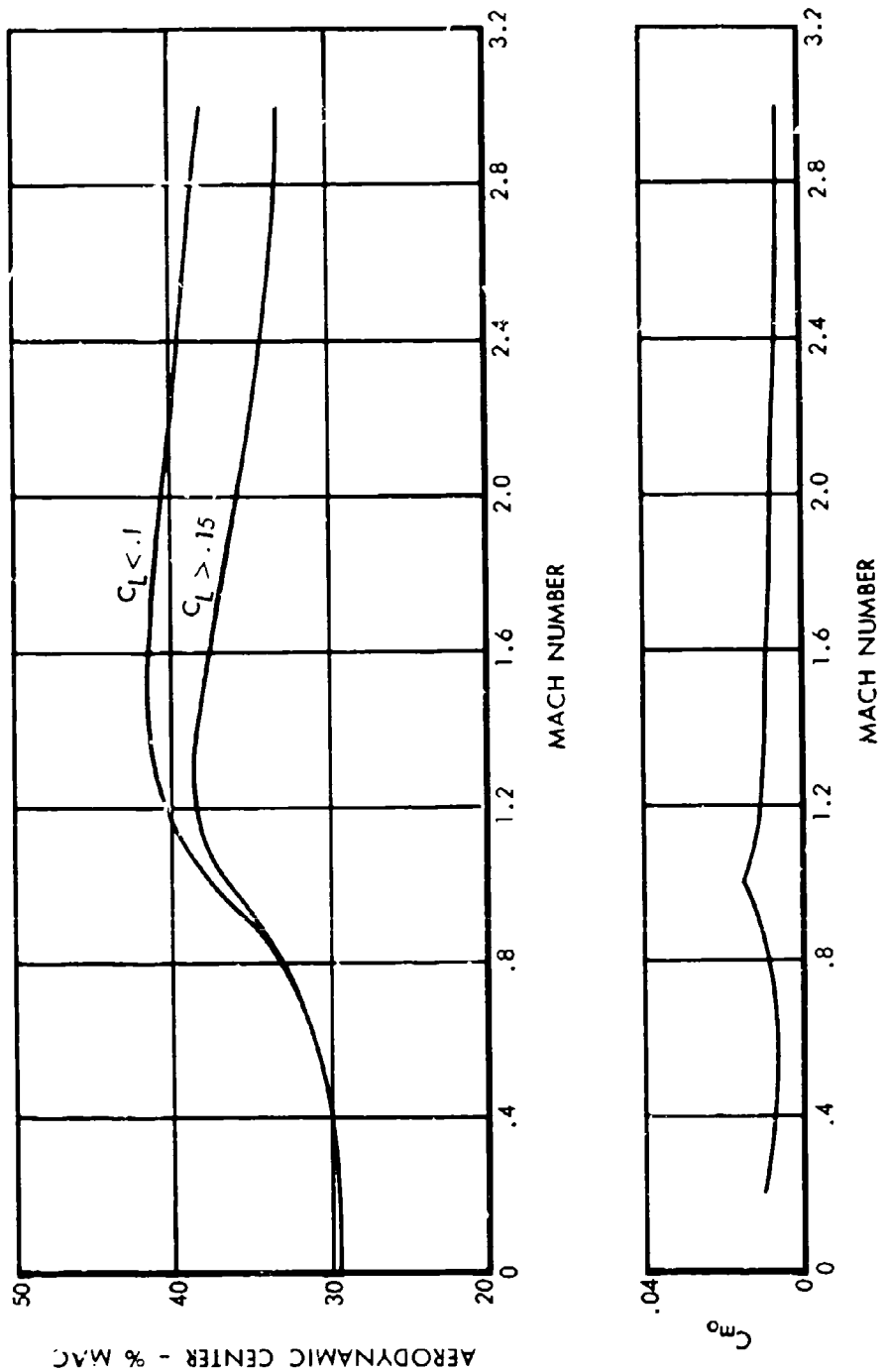

FIGURE 4-90 RIGID AIRPLANE AERODYNAMIC CENTER CHARACTERISTICS SUMMARY

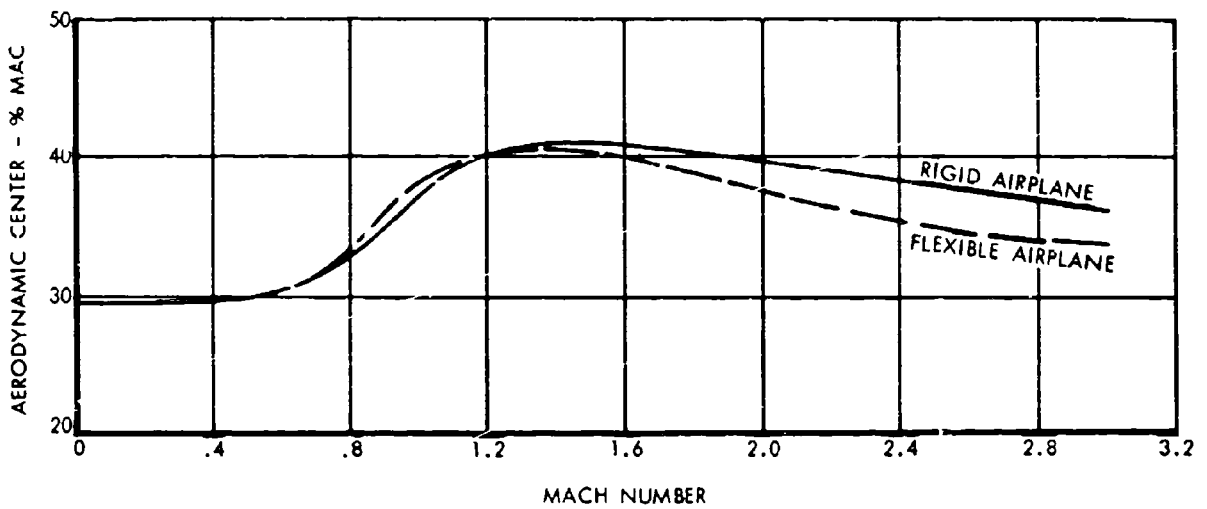

FIGURE 4-91 EFFECTS OF FLEXIBILITY ON THE AERODYNAMIC CENTER MOVEMENT FOR FLIGHT PROFILE

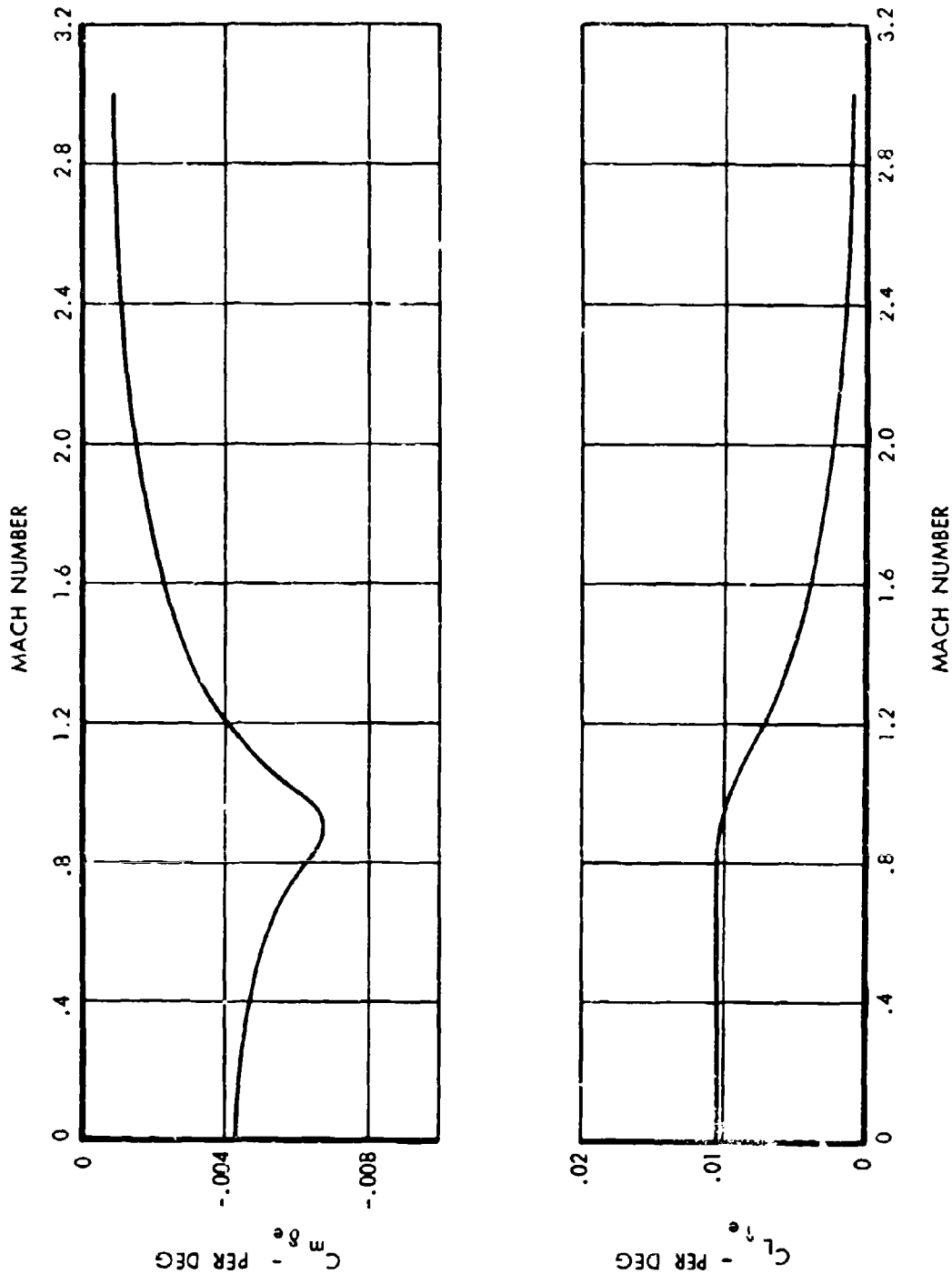

FIGURE 4-92 RIGID AIRPLANE LONGITUDINAL CONTROL CHARACTERISTICS SUMMARY

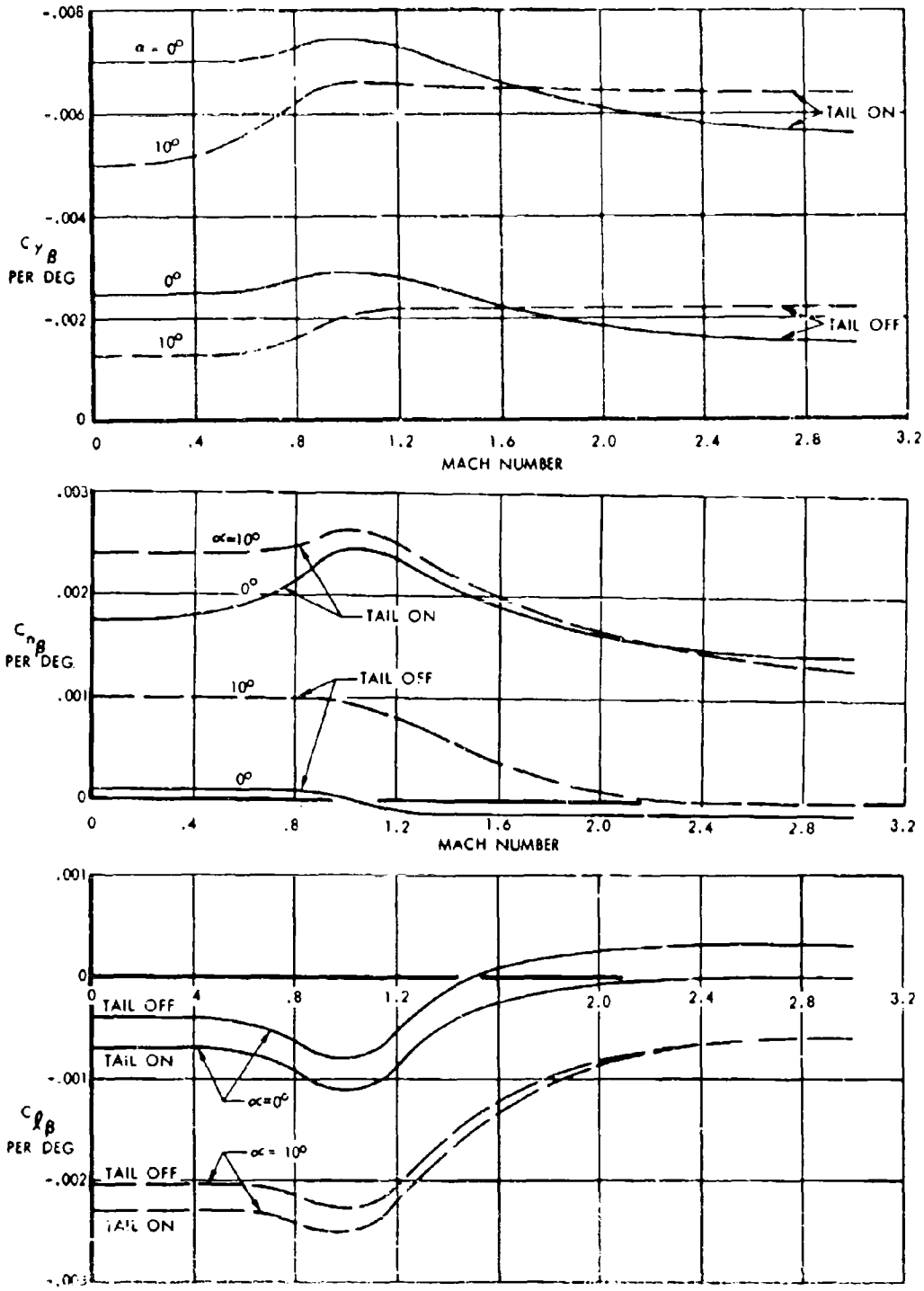

FIGURE 4.93 RIGID AIRPLANE LATERAL-DIRECTIONAL CHARACTERISTICS SUMMARY

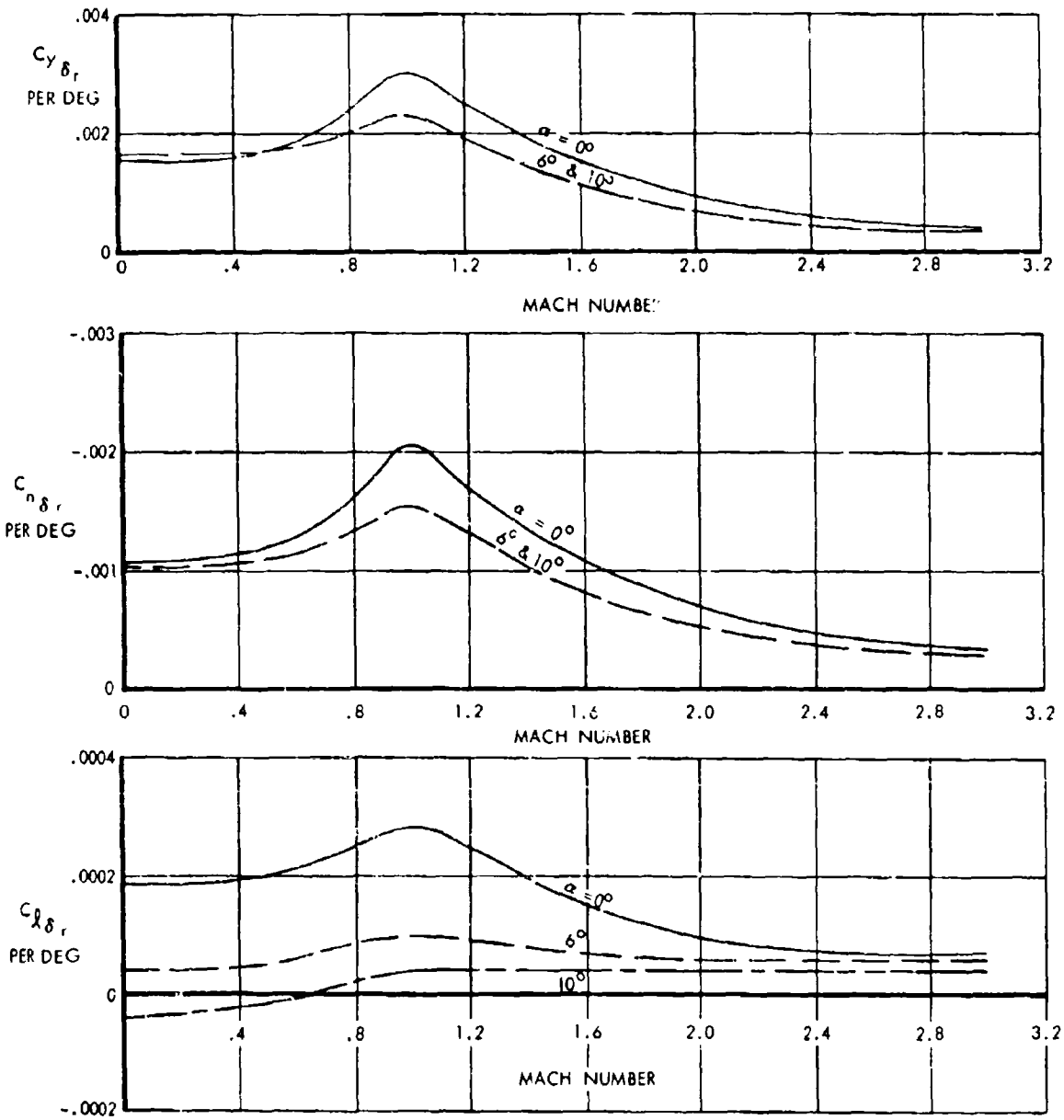

FIGURE 4-94 RIGID AIRPLANE DIRECTIONAL CONTROL CHARACTERISTICS SUMMARY

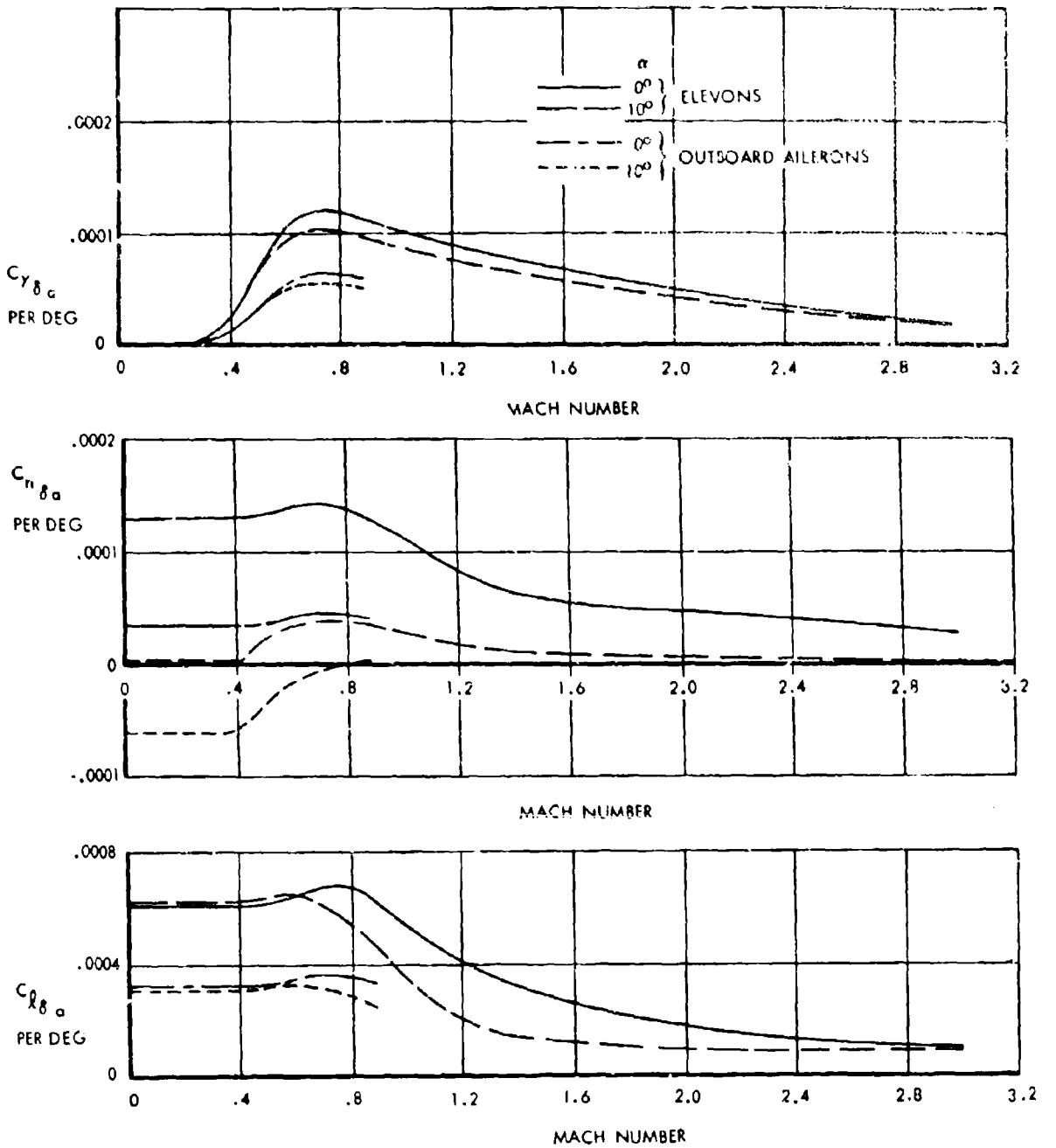

FIGURE 4-95 RIGID AIRPLANE LATERAL CONTROL CHARACTERISTICS SUMMARY

PHASE II WIND TUNNEL PR...

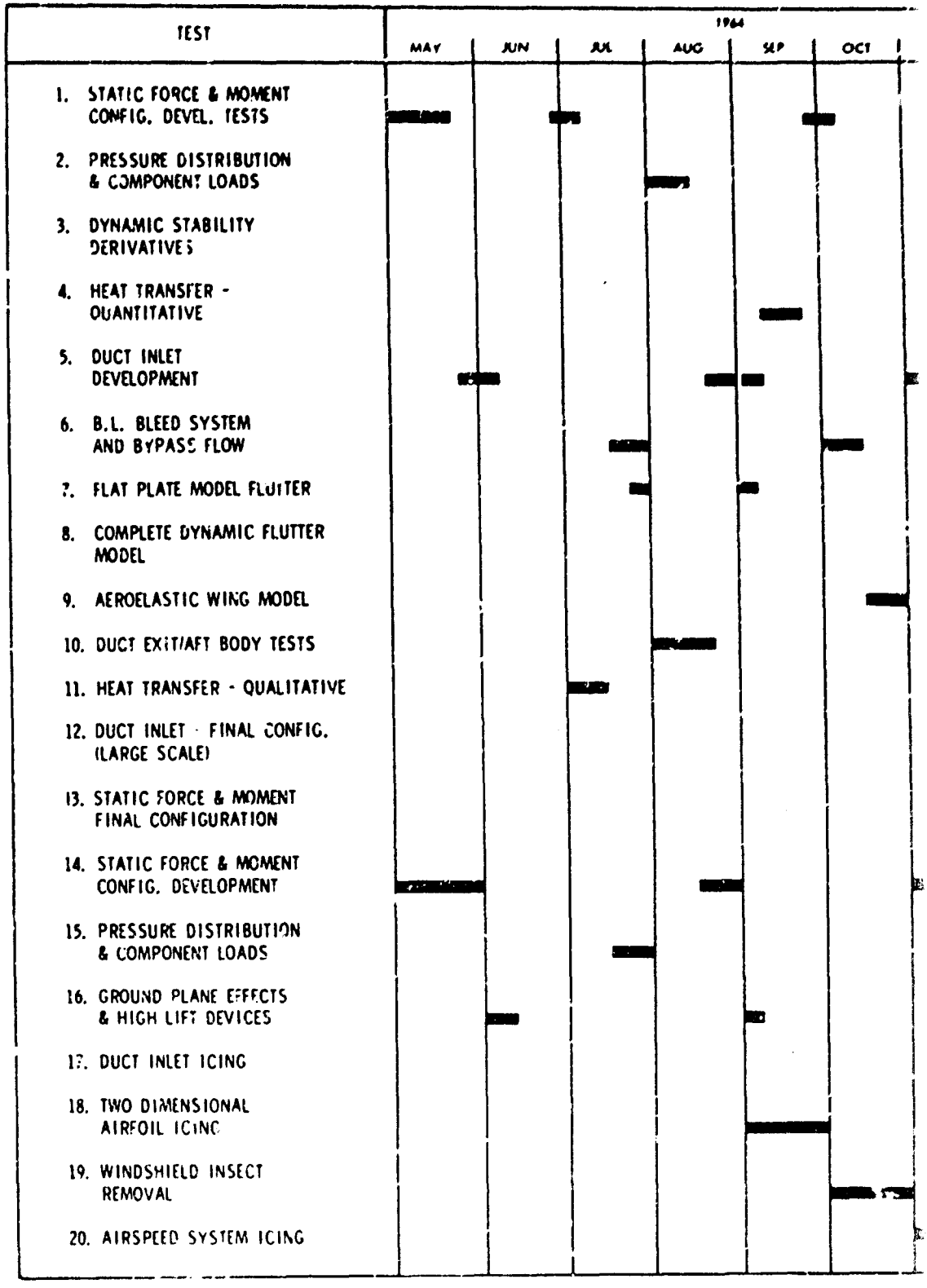

FIGURE 4-96 PHASE II

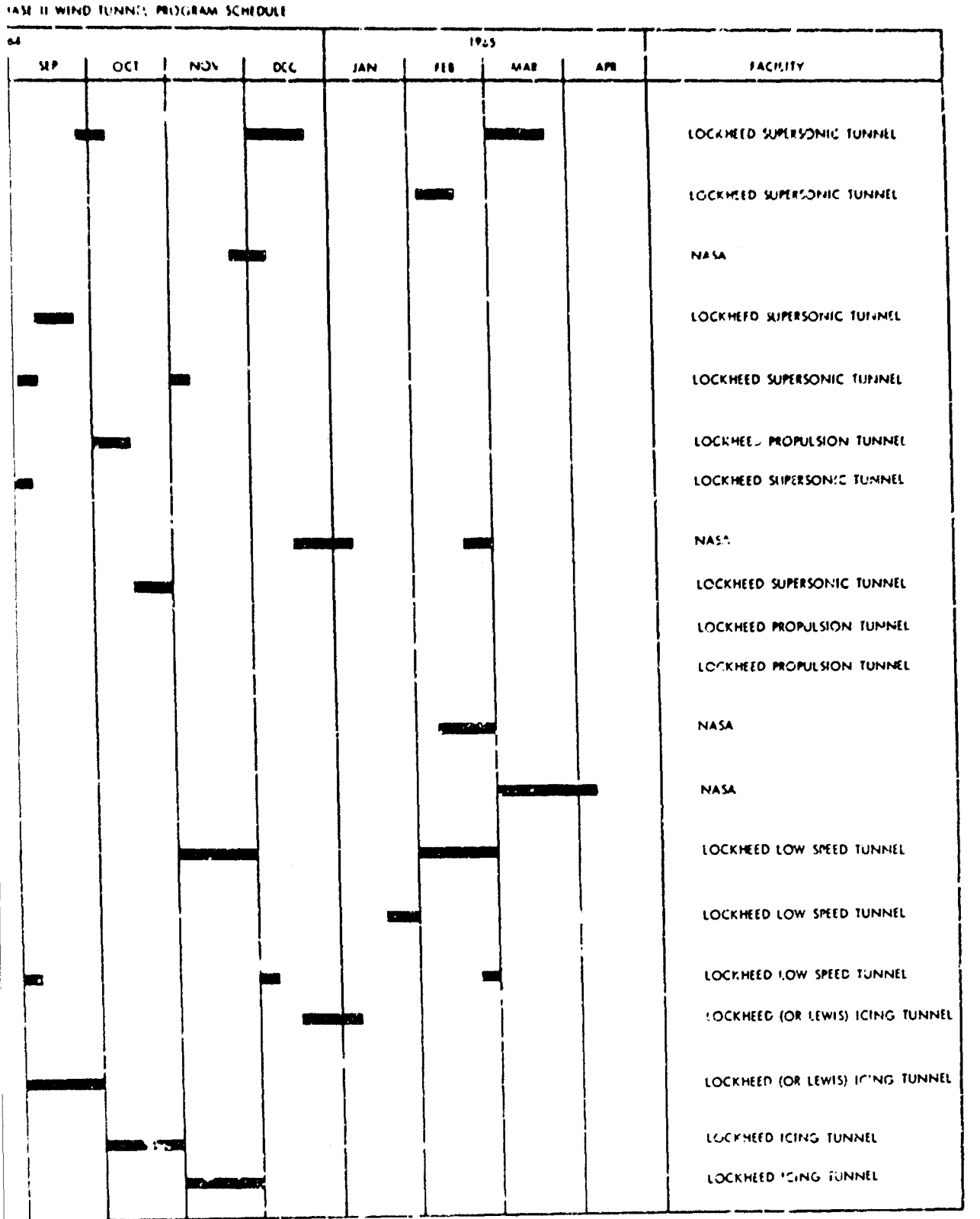

CONFIDENTIAL

26 PHASE II WIND TUNNEL PROGRAM

(2)

4.8.1 AERODYNAMIC CONFIGURATION DEVELOPMENT TESTS

The aerodynamic configuration will be optimized through a series of wind tunnel tests covering the complete Mach number range of the airplane. Several models will be involved. Tests will include low speed tests in and out of ground effect and at angles of attack from −10 ◦ + 40 degrees. Basic measurements will include lift, drag, and the static stability and control derivatives. The low speed tests will include evluation of various devices to improve take-off and landing performance and low speed flight characteristics. These tests will be conducted in the Lockheed 8 x 12 ft. low speed wind tunnel. The model will be designed to permit evaluation of component effects in classic model buildup studies. Items will include nacelles, fuselage afterbody and vertical tail.

Configuration development at high Mach number will be carried out in the Rye Canyon 4 ft. supersonic wind tunnel. Mach number will range from high subsonic through transonic to Mach 3.0. Measurements will include lift, drag, and the static stability and control derivatives. Elevon hinge moment measurements may be included in these tests pending further consideration. Development tests will be carried out in the tunnel on the wing planform arrangement, spanwise thickness distribution, spanwise camber and twist distribution, and chordwise camber distribution. Smiliar tests of nacelle geometry and location effects will also be carried out.

Several tunnel entries with these models will be involved in the configuration development and the test data will support the basic aerodynamic analysis. The high Reynolds number capability of the supersonic tunnel will permit evaluation of the effects of Reynolds number on certain critical aerodynamic parameters such as drag due to lift as it is affected by leading edge radius and camber.

A refined model of the final configuration, as developed from the above testing, will be built for the NASA unitary tunnel complex. It will be of a relatively large scale and constructed to allow complete model buildup in the tunnel for evaluation of the separate component effects. The final lift, drag and static stability and control derivatives will be generated from these tests. The size of the model will permit attention to small detail. Use of all three tunnels of the unitary complex is anticipated for this model in Phase II.

Following development of the aerodynamic configuration, a model will be constructed to permit measurement of the dynamic stability derivatives. These tests will be conducted in a NASA facility and will include measurements of the damping in pitch, yaw and roll, and the rotary stability derivatives. Measurements will be carried out over the design Mach number range. A single test series is anticipated for this model in Phase II.

4.8.2 AIRLOAD TESTS

Basic airloads will be determined through wind tunnel tests of pressure distribution models. These models will also incorporate strain gage supported components where advisable to permit direct measurement of loads. Such items will include landing gear doors, the variable geometry forebody, and certain elements of the nacelle inlet and exhaust system. Two models are anticipated for this work; a low speed model designed for testing in the 8 x 12 ft. low speed tunnel, and a high speed model designed for tests in the Rye Canyon 4 ft. supersonic wind tunnel. Two tunnel entries for each model are planned. The first entry will be early in the program to permit preliminary measurement of the loads, and the second entry later in the program with the final configuration. These tests are discussed further in Volume A-IV, Paragraph 2.3.5.

4.8.3 HEAT TRANSFER TESTS

Two heat transfer models are planned for tests in the Rye Canyon 4 ft. supersonic wind tunnel. The first model will be of small scale and will utilize the heat sensitive paint technique to qualitatively establish heat patterns. From this information regions of significant flow interference and shock impingement will be determined and utilized in the design of a quantitative heat transfer model.

The quantitative model will be designed to evaluate heat transfer rates over critical areas of the airframe. The use of the insulated plug technique is planned. Tests will be conducted over the upper Mach number regime. A single tunnel entry for each of the heat transfer models is anticipated. These tests are discussed further in Volume A-VII, Paragraph 6.4.

4.8.4 ENGINE INLET AND EXHAUST DEVELOPMENT TESTS

Engine inlet configuration development testing will be carried out in the Rye Canyon 4 ft. supersonic wind tunnel utilizing a model of the engine air intake system, including the variable ramp and bypass systems. The inlet will be optimized by evaluating the effects of subsonic diffuser geometry, bleed configuration, diverter arrangement, and cowl lip angles. The model will include, where appropriate, a segment of the adjacent wing planform to assure a proper matching of the inlet flow field. Mach number for these tests will range from high subsonic to Mach 3.0. Extensive pressure distribution measurements will be taken over the cowl lips, inlet ramp, and across the engine face. Flow distortion at the engine face will be carefully studied in these tests. Sufficient data will be taken to permit design of the inlet control system. Several tunnel entries are anticipated for this model.

A large scale model of the final duct inlet configuration is planned for tests in the NASA unitary tunnel complex. The tests will be conducted over the significant Mach number spectrum. The model will include a scaled operational version of the actual inlet control system. The primary purpose of these tests will be to measure inlet recovery characteristics and flow distortion at the engine face, and to permit evaluation of the inlet control system.

Small scale tunnel tests on bleed and other aerodynamic subsystems are planned for the Lockheed Propulsion Tunnel. Where significant, these tests may be conducted at elevated stream stagnation temperatures to provide thermodynamic simulation.

4.8.5 FLUTTER TESTS

Initial flutter testing will be carried out on a series of simple semi-span solid aluminum models of the wing planform to check the flutter aerodynamics used in the initial flutter analysis. These models will have provisions for simulating fixed mass items such as engine nacelles. A similar model of the vertical tail will be tested. Tests will be conducted over a Mach number range from 0.8 to 3.0 in the Lockheed 4 ft. supersonic wind tunnel. Two or three tunnel entries are planned for this model.

A complete airplane flutter model will be tested in the 8 x 12 ft. low speed tunnel. It will have appropriate mass, stiffness and dynamic pressure scaling for high subsonic flight conditions of the full scale vehicle, but Mach effects will not be represented. However, the relative simplicity of the subsonic model and the ease with which it can be modified makes it a very useful tool for experimental flutter analysis. Two tunnel entries for this model are anticipated.

The initial flutter analysis performed on the early configurations will be checked by tests of a complete dynamically similar model in a suitable NASA facility. The model will be designed to provide simulation of all signicant modes of the wing, fuselage and vertical tail. The model influence coefficient and vibration characteristics will be determined prior to the wind tunnel tests. Test conditions will cover the total Mach number range. Flutter testing is discussed further in Volume A-IV, Paragraph 3.2.

4.8.6 ICING TESTS

The extreme sweep angle of the wing makes prediction of ice accretion difficult. Therefore, wing panel icing tests are planned. These tests will be carried out in the Lewis Laboratory or the Lockheed icing tunnels. The shape and degree of ice accumulation during takeoff, descent, and loiter operations will be evaluated from these tests. A single tunnel entry for this model is anticipated. Aerodynamic testing to determine the effects of ice buildup on the flight characteristics will be carried out to complete the evaluation.

Engine inlet tests similar to those noted above for the wing will likewise be carried out in the Lewis or Lockheed icing tunnel. Susceptibility of the engine inlet to icing and the resulting effects on internal flow will be studied, and the need for ice protection determined. A single tunnel entry is anticipated for this work. These tests are discussed further in Volume A-VII, Section 7.

4.8.7 SECONDARY SYSTEM TESTS

The need for testing various air intake and exhaust configurations necessary for primary and secondary subsystems has not yet been determined. However, it is likely that some special testing will be needed in this area. This is particularly true in those cases where supersonic exhaust involving thrust recovery will be utilized.

Ice protection for the pressure pickups for the air data system has not been determined. If analysis shows tests to be necessary they may be carried out in the Lockheed icing tunnel.

4.9 REFERENCES

4-1. Peterson, John B., Jr.: A Comparison of Experimental and Theoretical Results for the Compressible Turbulent Boundary Layer Skin Friction with Zero Pressure Gradient. NASA TN D-1795, March 1963.

4-2. Whitcomb, Richard T., Patterson, James C., Jr., and Kelly, Thomas C.: An Investigation of the Subsonic, Transonic, and Supersonic Aerodynamic Characteristics of a Proposed Arrow-Wing Transport Airplane Configuration. NASA TM X-800, January 1963.

4-3. Anon: NASA SCAT Feasibility Study Results, 1963.

4-4. Hoerner, Sighard F.: Fluid-Dynamic Drag, 1958.

4-5. Stitt, Leonard E. and Anderson, Bernard H.: Friction and Pressure Drag of Boundary-Layer Diverter Systems at Mach Number of 3.0. NASA TM X-147, 1960.

4-6. Koenig, David G., Brady, James A., Page, V. Robert: Large Scale Wind Tunnel Tests at Low Speed of a Delta Winged Supersonic Transport Model in the Presence of the Ground. NASA TM X-644.

4-7. Gnos Vernon A, Kurwowski Richard L.: Effect of Off-Design Inlet Mass Flow upon Static Stability of a Delta Winged Configuration with a Canard Control and Pylon Mounted Nacelles for Mach Numbers from 0.65 to 3.50. NASA TM X-658.

SECTION 5 AIRPLANE PERFORMANCE (3.2.7)

5.1 INTRODUCTION

This section of Volume A-V presents operational data on the SST for all phases of flight. Basic payload-range information, including block speeds and block fuels, are shown together with the effect of such other operational factors as constant altitude cruise, non-standard enroute temperatures, and wind. In addition, the effect of variations in acceleration sonic boom levels from the specified value of 2.0 pounds per square foot are shown. Subsonic operating information at various altitudes, and the capabilities of the airplane under various emergencies requiring completion of the flight at subsonic speeds, are shown. Specifically, both single engine and multiple engine failures are considered. In addition, information is presented on climb performance, cruise nautical miles per pound, normal and emergency descent, and holding fuel consumption.

The body of operational data presented is that of the supersonic transport as it will be at the end of Phase II, when actual production orders would be taken. Some elements of the performance basis of the airplane and the weight of both the airframe and engine are somewhat better than can be completely substantiated by wind tunnel and design analysis data at this time.

In order that the differences in performance between the current status of the SST and the developed status at the end of Phase II be made perfectly clear, it is pointed out that the improvements which are expected by continued research and development during this period are confined primarily to the cruise regimes. The take-off and landing performance and the inoperative engine climb performance presented in this report are equally applicable to the current status and the Phase II developed SST airplane.

The payload-range capabilities of the current status and the developed SST are shown in Figure 5-1. At the design range of 3,470 nautical miles, the developed SST, at its design take-off gross weight of 450,000 pounds, has a payload capability of 30,000 pounds as compared to a payload of 10,000 pounds for the current status airplane. The improvements in range and payload capability indicated for the developed SST are achieved on the basis of improvements that can be obtained by continued development in the areas of aerodynamic drag, structural weight, equipment weight, and engine specific fuel consumption and weight. The expected improvements in these areas are all modest, realistic values that do not require any significant extension of the present state-of-the-art to accomplish. For example, the expected improvement in supersonic L/D at Mach 3.0 is only .25 and the improvement in subsonic L/D is .60. Further work on structural and equipment weights is expected to yield a 5 percent improvement in weight empty. In addition, due to the conservative approach taken by the engine manufacturer in regard to engine turbine operating temperatures and engine weights, an improvement in cruise specific fuel consumption in the order of 1.5 to 2.0 percent appears feasible and a weight improvement of 5 percent is a possibility.

The airport performance capabilities of the SST, which are substantially the same as those classified as current status, are presented and discussed in detail in Paragraph 5.8.

5.2 DESIGN FLIGHT PROFILE

The design flight profile and detailed flight segment information is presented in Figure 5-2 for the design range of 3470 nautical miles (4000 statute miles) with 30,000 pounds of payload. The ramp weight is 453,000 pounds and 3000 pounds of fuel are consumed during taxi and holding prior to take-off.

The noise abated take-off is conducted at a weight of 450,000 pounds at a thrust setting corresponding to 79 percent of the maximum available thrust which is slightly greater than minimum duct heating value and will limit the airport noise so that 112 Pndb is never exceeded at any point one mile from the runway. The FAA take-off airport length required at this power setting is 9750 feet for a standard

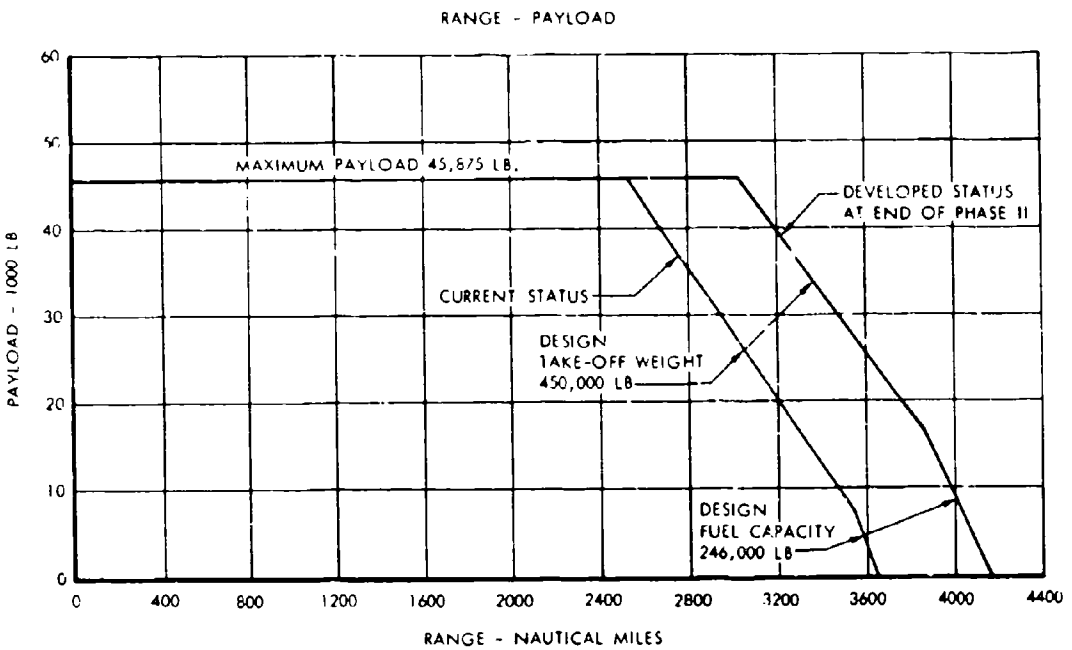

FIGURE 5-1 PAYLOAD-RANGE CAPABILITY, CURRENT STATUS VS PHASE II DEVELOPED STATUS

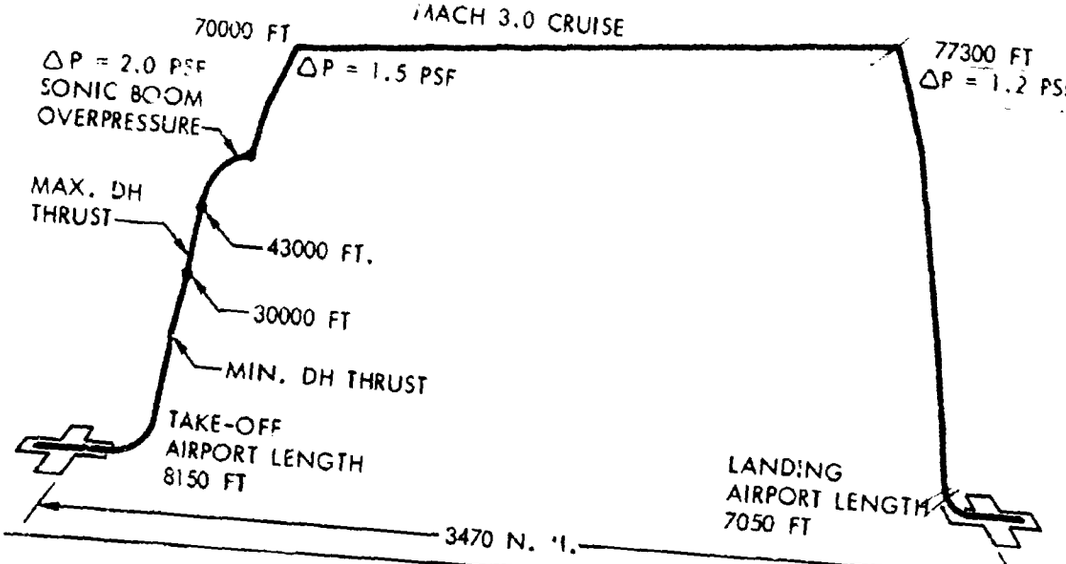

Flight Segment	Initial Weight (Lb.)	Initial Altitude (Ft.)	Initial Mach No.	Power Setting	Segment Fuel (Lb.)	Segment Time (Hr.)	Segment Distance (N. Mi.)
Taxi	453,000	Sea Level	—	Req'd	1,880	.10	—
Ground Idle	451,120	Sea Level	—	Idle	1,120	.15	—
Take-Off	450,000	Sea Level	—	79% Max.	2,660	.02	—
Climb Out to 2,500 Ft. Altitude	447,340	Sea Level	.27	79% Max	3,100	.02	—
Climb (1)	444,240	2,500	.575	Min. DH	19,248	.19	87
(2)	424,992	36,000	1.065	Max. DH	51,501	.30	311
Cruise	373,491	69,985	3.0	Part. DH	112,759	1.55	2,680
Decelerate	260,732	77,294	3.0	Min. DH	1,825	.08	125
Descend	258,907	77,294	2.22	Max. DRY & Idle	4,290	.42	267
Landing Weight	254,617	Sea Level					
Total					198,383	2.83	3,470
Reserves							
260 N. Mi. Diversion	254,617	77,878	3.0	Part. DH	8,868	.15	261
Loiter	245,749	15,000	.49	DRY	11,568	.50	—
7% × Block Fuel	234,181	—	—	—	14,097	—	—
					34,533		

FIGURE 5-2 DESIGN FLIGHT PROFILE

+15°C day. This compares to a maximum thrust FAA take-off distance of 8150 feet for the same operating conditions.

The climb-out is continued at the take-off thrust setting to an altitude of 2500 feet. This thrust setting is maintained during a brief acceleration at 2500 feet to the operational climb speed of 360 knots calibrated airspeed. This speed is maintained during the climb up to 43,000 feet and Mach 1.2. Minimum duct heat thrust is employed for climb below 30,000 feet and maximum duct heat thrust is employed at all higher altitudes.

At 43,000 feet and Mach 1.2 the condition for a sonic boom overpressure of 2.0 psf at the ground is reached and the airplane is accelerated with maximum thrust along the 2.0 psf sonic boom line shown in Figure 3-8 to 550 knots CAS at an altitude of approximately 52,000 feet. The climb is continued at 550 knots CAS and along the duct pressure limit line shown in Figure 3-8 to Mach 3.0 at cruise altitude. The initial cruise altitude for maximum range operation is reached at approximately 70,000 feet. A climbing cruise at Mach 3.0 is conducted with partial duct heat thrust to a final cruise altitude of approximately 77,000 feet. Sonic boom overpressures during cruise range from 1.5 psf at the initial altitude to 1.2 psf at the final altitudes.

As the destination is approached the SST is decelerated at cruise altitude with minimum duct heat thrust to a Mach number of approximately 2.2 corresponding to a calibrated airspeed of 330 knots. The descent is then initiated and is continued at 330 knots CAS with maximum dry thrust to an altitude of 55,000 feet at which point the thrust is reduced to the flight idle setting and is maintained at this setting at all lower altitudes. Between 55,000 feet and 45,000 feet the descent speed is reduced slightly to 320 knots CAS to limit the boom overpressure to 1.5 psf. The time required for the descent is approximately 24 minutes, so that the cabin rate of descent is less than 300 feet per minute.

The landing is accomplished at a weight of approximately 255,000 pounds including normal fuel reserves and the required FAA landing airport length is 7050 feet. The reserve fuel for normal operation is computed as 7 percent of the block fuel plus the fuel required to continue the cruise an additional 260 nautical miles and hold for one-half hour at 15,000 feet altitude.

Additional details of the climb profile are illustrated in Figure 5-3 which shows that the changes in flight path angle required to follow the operational climb and boom profiles are small and can easily be accomplished by the pilot without discomfort to the passengers. During the initial part of the climb at the constant speed of 360 knots CAS and constant power setting at minimum duct heat, the flight path angle varies gradually from 7.6 degrees at low altitude to 1.8 degrees at 30,000 feet where the thrust is increased to maximum duct heat and the flight path changes smoothly to 6.1 degrees. The part of the climb path controlled by the sonic boom requirment is reached at an altitude of 43,000 feet. At this point the flight path angle has reduced to 1.4 degrees and continues to decrease as the SST follows the boom path. It is anticipated that this boom path can be flown manually by maintaining constant rates of climb and breaking the boom path into two straight line segments.

At the end of the boom path corresponding to Mach 2.14 at 51,000 feet the climb path changes in order to follow the operational climb speed of 550 knots CAS and the flight path angle is increased by 1.5 degrees in a mild pull-up maneuver. The normal acceleration forces experienced by the passengers can be limited to approximately 0.05g if the 550 knot CAS speed is anticipated by as little as 6 knots or 0.01 in Mach number. In this way the pull-up is initiated early and the flight speeds remain slightly less than the 550 knot CAS design speed.

During the remaining climb to cruise altitude the flight path angle decreases slowly from 1.7 degrees to 1.1 degrees as shown in Figure 5-3. As the cruise altitude is approached the thrust is reduced so that the flight path approaches the horizontal. This roundout maneuver can begin at 68,000 feet where the rate of climb is 3300 feet per minute and 36 seconds are available to the pilot before the initial cruise altitude of 70,000 feet would have been reached. A gradual reduction in thrust to the cruise setting coupled with a mild push-over to an incremental normal acceleration of less than 0.02 g will enable the SST to reach cruise altitude without overshoot or discomfort to the passengers. Sufficient time is available for the pilot to adjust the altitude and thrust level manually.

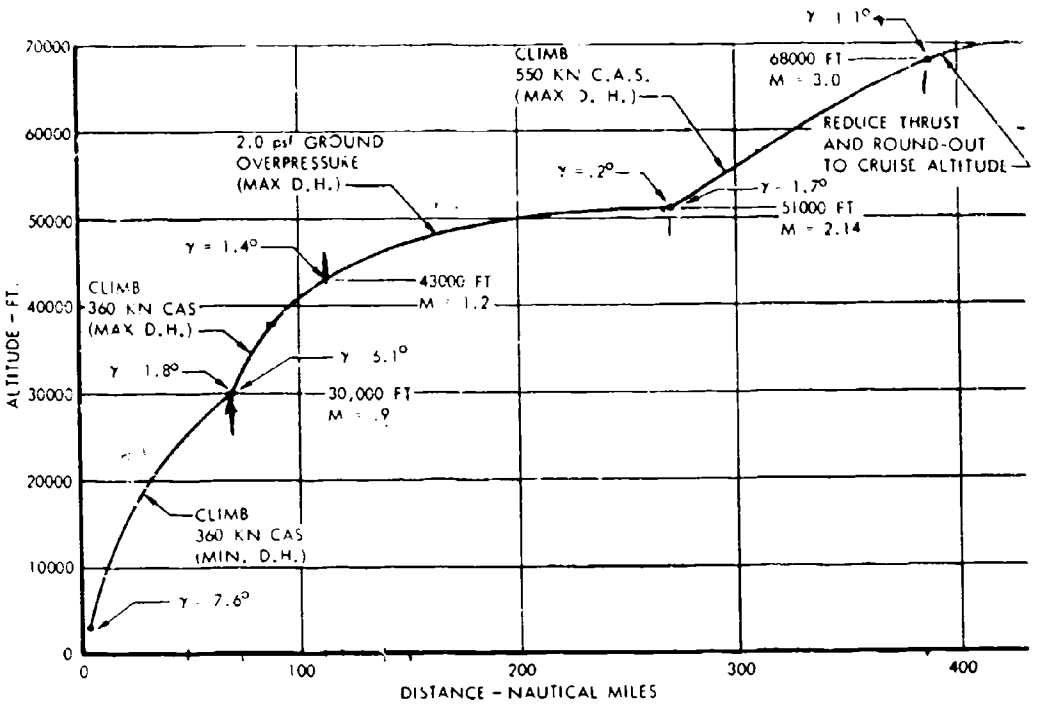

FIGURE 5-3 CLIMB-ACCELERATION FLIGHT PATH

5.3 MACH 3.0 RANGE-PAYLOAD CHARACTERISTICS

The range-payload characteristics of the SST for Mach 3.0 cruise-climb operation are shown in Figure 5-4. At the design range of 3470 nautical miles a payload capability of 30,000 pounds is realized which corresponds to 125 passengers and baggage plus 5000 pounds of cargo. This flight is accomplished at a block speed of 1240 knots including the assumption of 15 minutes ground maneuver time, and the corresponding block fuel is 198,383 pounds including 3000 pounds of fuel consumed prior to take-off. The maximum international payload of 45,875 pounds can be carried to a range of 3020 nautical miles, and a ferry range of 4000 nautical miles is available with approximately 10,000 pounds of payload.

The effect on range and payload of operation at Mach 3.0 at constant altitudes rather than in the cruise-climb mode is shown in Figure 5-5. A constant altitude of 74,000 feet yields the greatest range for this type of operation. With 30,000 pounds of payload the available range is reduced approximately 40 miles with respect to the cruise-climb mode of operation. For transcontinental flights with maximum payload, a wide latitude is possible with no measurable effect on the operating economics. A comparison of Figures 5-4 and 5-5 shows no discernible change either in block speed or block fuel for constant altitude operation as compared to cruise-climb operation.

The effect on the range-payload characteristics of ambient temperatures above and below the standard values is indicated in Figure 5-6. For the purpose of illustration, a temperature variation of 10 degrees centigrade above and below the standard temperature is chosen and these temperatures are assumed to apply throughout the flight. Examination of weather records shows that at the high altitudes, the temperature variation from standard will be less than 10 degrees centigrade over 99 percent of the time, so the probability of the occurrence of these extreme temperatures throughout the entire flight is very remote. Temperature variations will be encountered during the climb more frequently than during the cruise. The effect of temperature variations encountered only during the climb phase on total range is approximately 10 nautical miles per degree centigrade.

Under actual operating practice, the scheduled range can be maintained regardless of the ambient air temperature. The effect of temperature may be compensated for by the use of a small part of the normal reserve fuel. The SST will fly the standard day range values at temperatures 10 degrees centigrade above standard by using only 7,050 pounds of the normal reserve fuel which is only one-half of the 7 percent of block fuel contingency reserve specified by the FAA Request for Proposal. Use of the entire 7 percent of the contingency reserve makes the hot day range capability coincident with the cold day values as shown in Figure 5-6.

The SST airframe and engine are designed structurally for temperatures corresponding to operation at Mach 3.0 on a standard day. For ambient temperatures less than standard the maximum operational speed remains at Mach 3.0. For ambient temperatures greater than standard, however, the operational Mach number is reduced to maintain the total temperature at the design value. At 10 degrees centigrade above standard, for example, the Mach number is reduced to 2.9. Since the speed of sound increases with increasing temperature the true airspeed is affected to a less degree than the Mach number. Figure 5-6 shows that for temperatures 10 degrees centigrade above standard during the entire flight, the block speed is affected only slightly. For temperature variations occurring only during the climb phase the effect on block speed is negligible.

The effect of wind on the Mach 3.0 range is shown in Figure 5-7. An average headwind of 25 knots is the maximum expected 80 percent of the time and affects the range by 60 nautical miles.

The basic range-payload data presented thus far includes a climb schedule which prevents the sonic boom overpressure from exceeding 2.0 psf at ground level. For flights originating at points for which the sonic boom restriction need not be a consideration an increase in maximum range is available. Figure 5-8 shows that an increase in payload of approximately 4000 lbs can be realized or an increase in range of more than 100 nautical miles results when the ground overpressure is limited to 2.5 psf rather than to 2.0 psf. The corresponding increase in block speed is 40 knots or more than three percent. The use of climb schedules which limit the ground over-

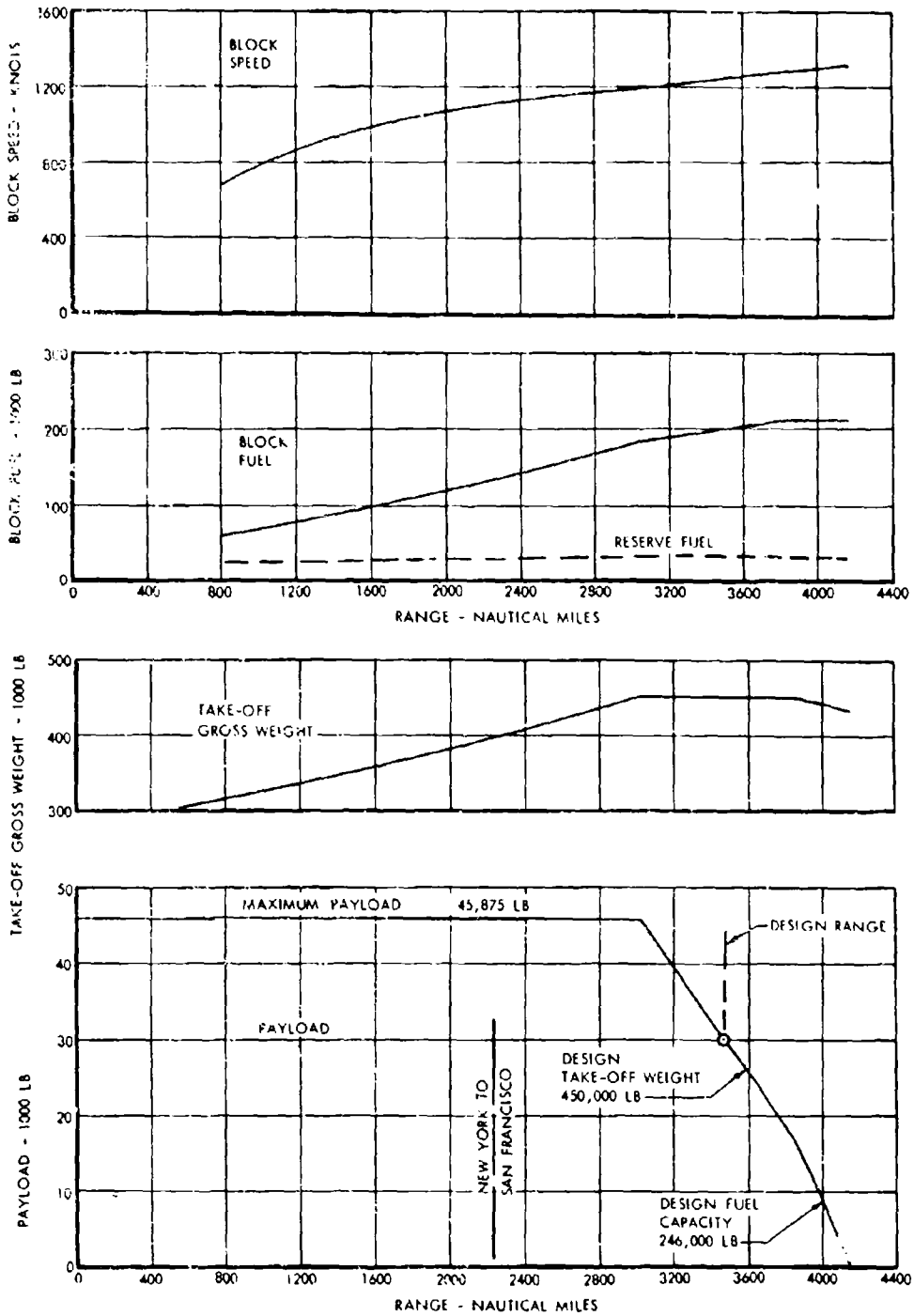

FIGURE 5-4 RANGE-PAYLOAD FOR MACH 3.0, CRUISE-CLIMB

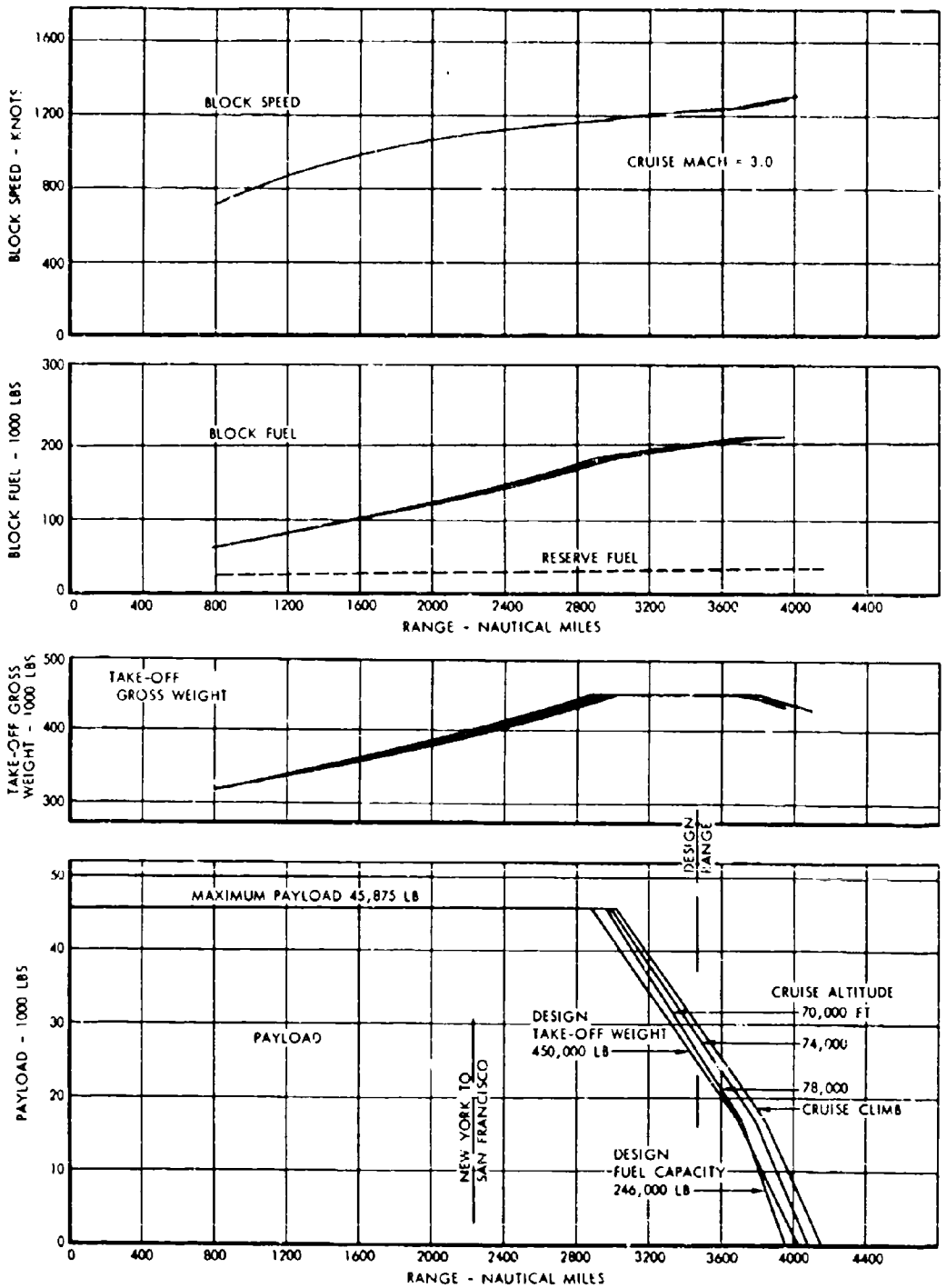

FIGURE 5-5 RANGE-PAYLOAD FOR MACH 3.0, CONSTANT ALTITUDE CRUISE

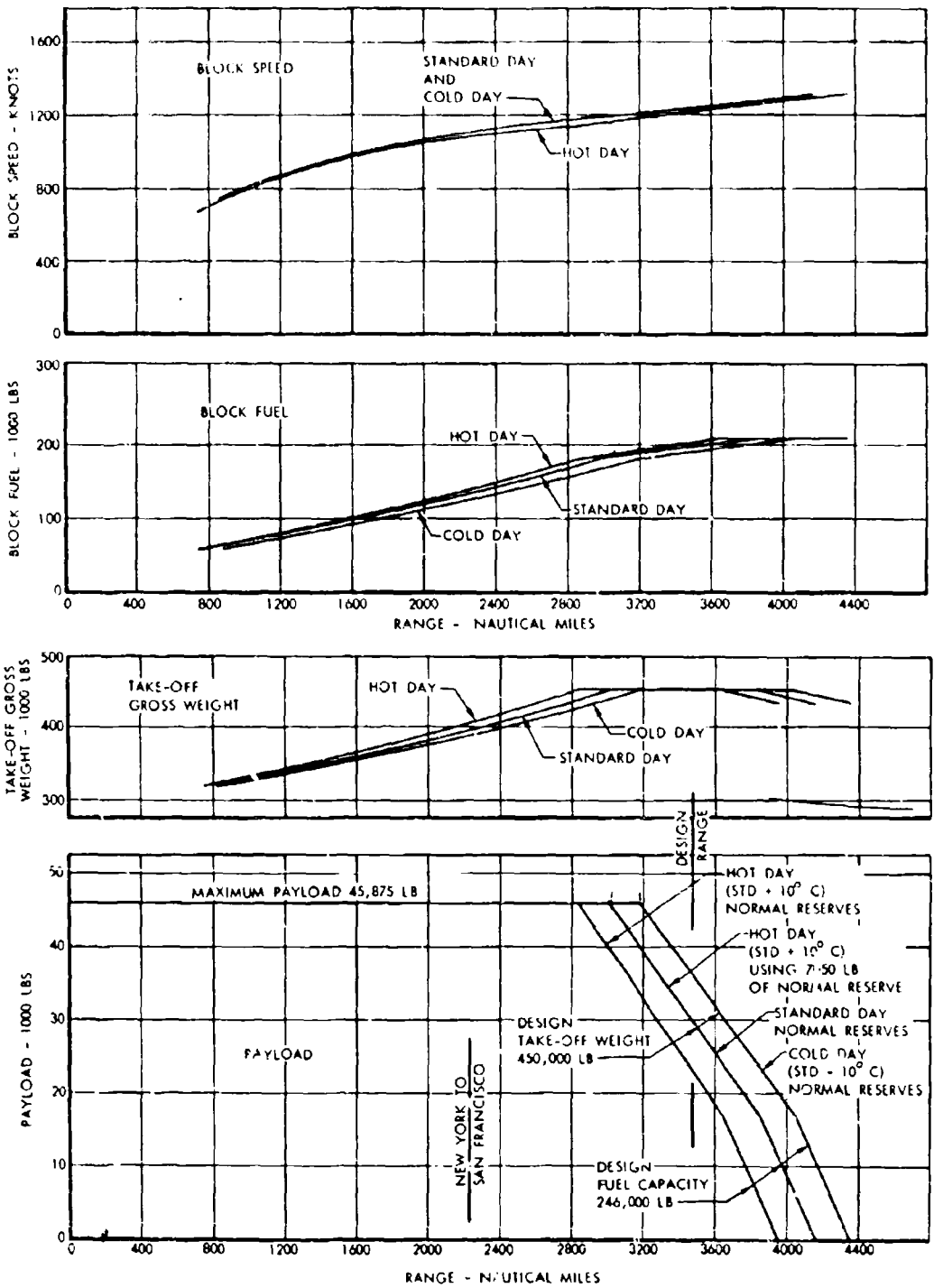

FIGURE 5-6 EFFECT OF ENROUTE TEMPERATURE ON MACH 3.0 RANGE-PAYLOAD

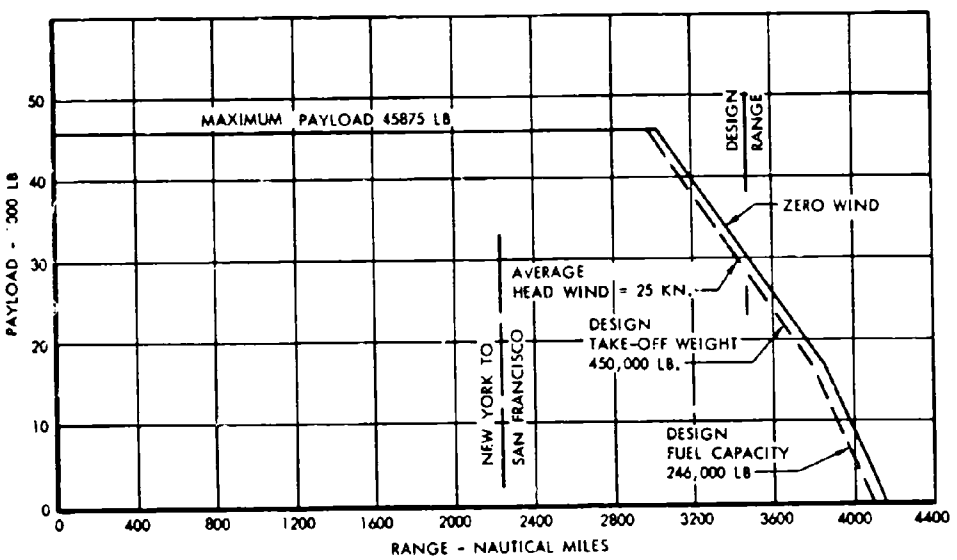

FIGURE 5-7 EFFECT OF WIND ON MACH 3.0 RANGE-PAYLOAD

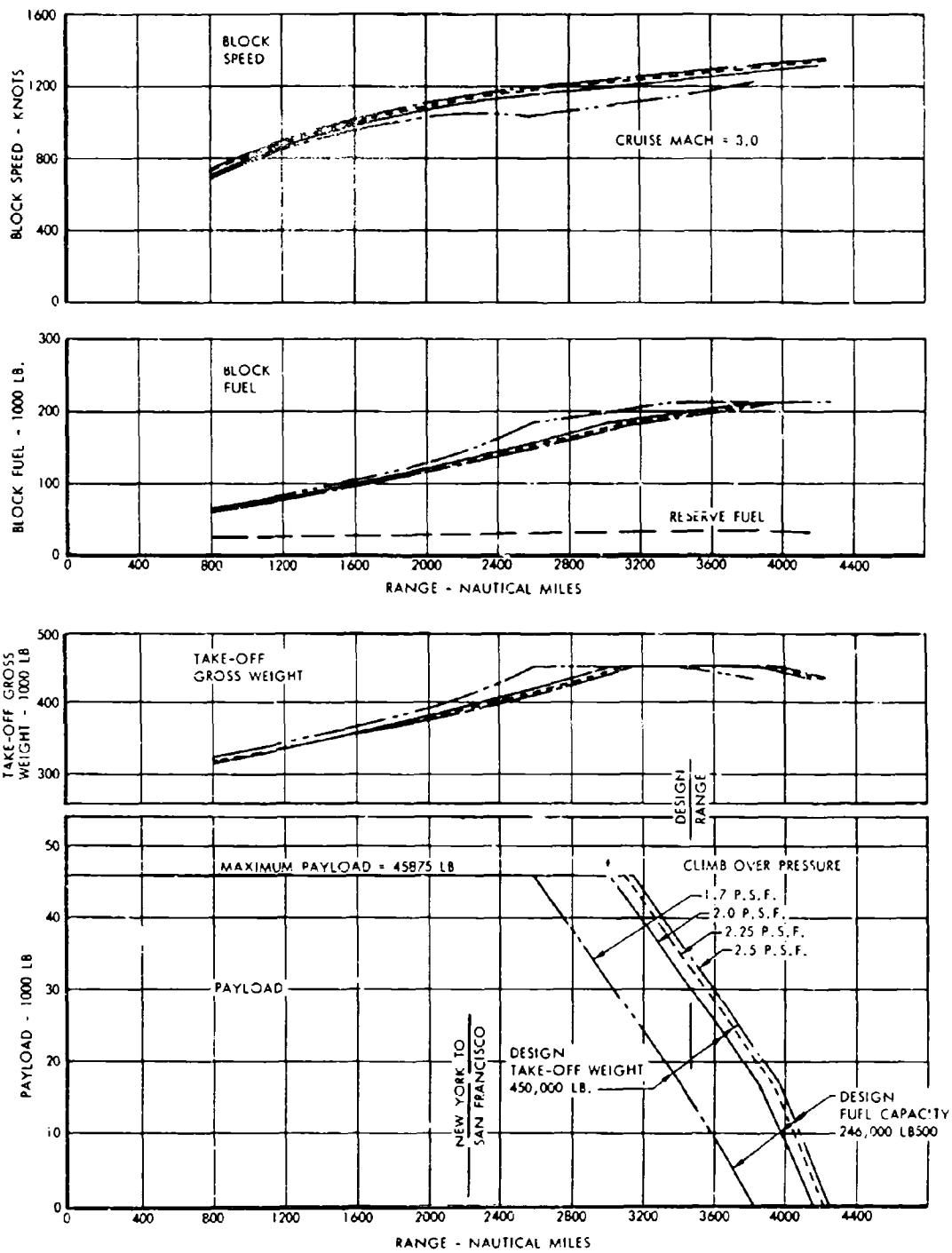

FIGURE 5-8 EFFECT OF CLIMB SONIC BOOM OVERPRESSURE LIMITS ON MACH 3.0 RANGE-PAYLOAD

pressure to less than 2.0 psf would penalize the long range performance, but will have only a small effect for shorter range flights. Figure 5-8 shows that for transcontinental ranges with maximum payload relatively small changes in block speed and block fuel result from reducing the ground overpressure to 1.7 psf. It is possible that some of the above gains can be realized if refined knowledge of the sonic boom and estimation techniques permitted reduced altitudes for acceleration.

The effect of variations in empty weight on the Mach 3.0 range capability is illustrated in Figure 5-9 for a take-off weight of 450,000 lb and a payload of 30,000 pounds. The range is seen to vary linearly with empty weight at a rate of 29 nautical miles for each 1000 pound change in empty weight. The effect of using reserve fuel to extend the Mach 3.0 range capability is shown in Figure 5-10. For the design flight of 3470 nautical miles with 30,000 pounds of payload the reserve fuel specified by the FAA Request for Proposal definition is 34,600 pounds. The range varies by approximately 29 nautical miles for each 1000 pound change in reserve fuel.

5.4 SUBSONIC RANGE-PAYLOAD CHARACTERISTICS

When subsonic cruise operation is intended, the climb to cruise altitude is conducted at the thrust setting corresponding to the maximum dry thrust rating of the engine. The subsonic cruise Mach number for maximum fuel economy is 0.91 corresponding to the foot of the transonic drag rise and the cruising altitude varies from 30,000 feet to 40,000 feet as a function of weight.

The range-payload characteristics for subsonic cruise-climb operation are shown in Figure 5-11. The maximum payload can be carried to a range 2820 nautical miles which is far more than adequate for any conceivable subsonic application. It is of interest that this range is 200 nautical miles less than is available at Mach 3.0. Block speeds at transcontinental ranges are approximately 490 knots. At a shorter range of 500 nautical miles the block speed is approximately 400 knots. The subsonic range-payload analysis employs the same allowances for ground maneuver fuel as for the supersonic case and the descent procedure and reserve fuel definitions are identical.

The effect on range-payload of constant cruise altitude operation as compared with cruise-climb operation is illustrated in Figure 5-12. The constant altitude for best long range flights is 35,000 feet and the maximum range with full payload is 2780 nautical miles which is approximately 40 nautical miles less than is available for the cruise-climb case. Examination of Figure 5-12 shows that both block speed and block fuel are very insensitive to the choice of operating altitude, so that complete flexibility with respect to traffic control demands is possible without an economic penalty.

The effect of wind on the subsonic range capability is shown in Figure 5-13. The average winds used for illustration are a 50 knot headwind and a 25 knot tailwind corresponding to the maximum average effective winds expected 80 percent of the time for subsonic operation. These winds are applied throughout the entire flight.

5.5 EMERGENCY OPERATING CHARACTERISTICS

The total range capability of the SST in emergency operation following the failure of a single outboard engine at various points during a Mach 3.0 cruise-climb flight is illustrated in Figure 5-14 for the maximum payload of 45,875 pounds and for the design range payload of 30,000 pounds. The boundary showing the point of no return is indicated. To the left of this boundary the pilot may elect either to return to the point of departure, or to continue the flight. To the right of the boundary he must continue to the destination. The decision to return or to continue may be deferred until well past the midpoint.

In the event of such an emergency it is permissible to use a part of the basic reserve fuel in order to reach the destination. The minimum reserve fuel for emergency operation is defined by the FAA Request for Proposal as that required for 15 minutes holding at 15,000 feet altitude before landing. Figure 5-14 shows that in the event of failure of a single outboard engine at any point during the cruise, the flight may be continued at Mach 3.0 to a range greater than the destination range. The SST will arrive at the destination on schedule with fuel reserves in excess of the minimum requirement.

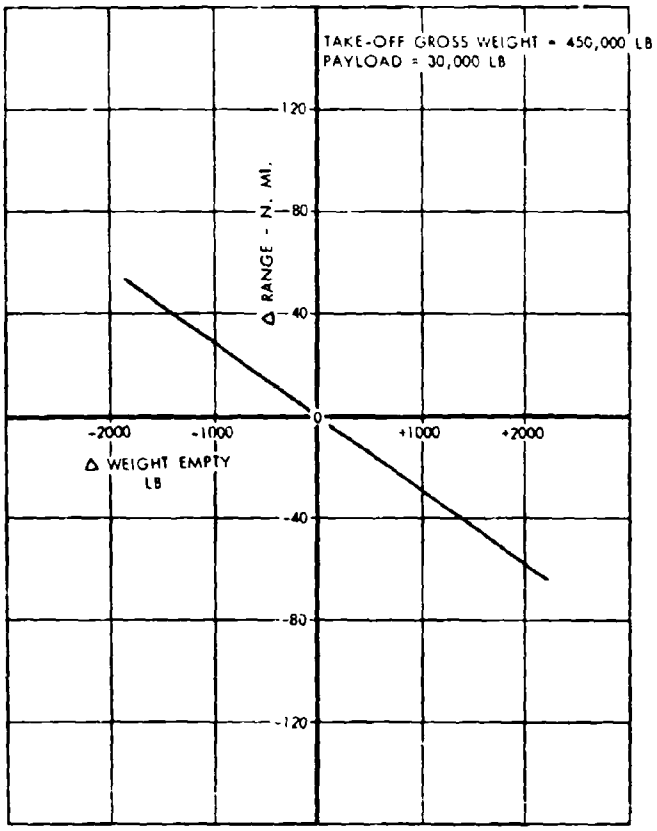

FIGURE 5-9 EFFECT OF EMPTY WEIGHT VARIATION ON RANGE

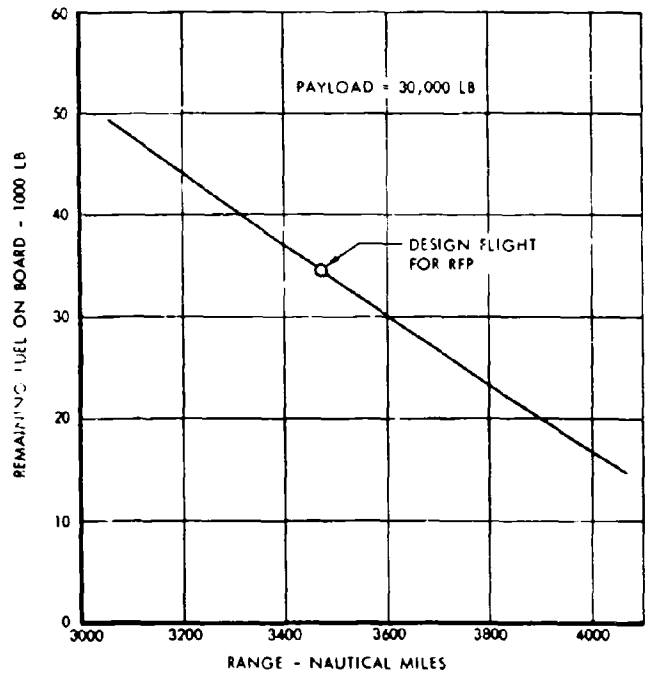

FIGURE 5-10 EFFECT OF RESERVE FUEL VARIATION ON RANGE

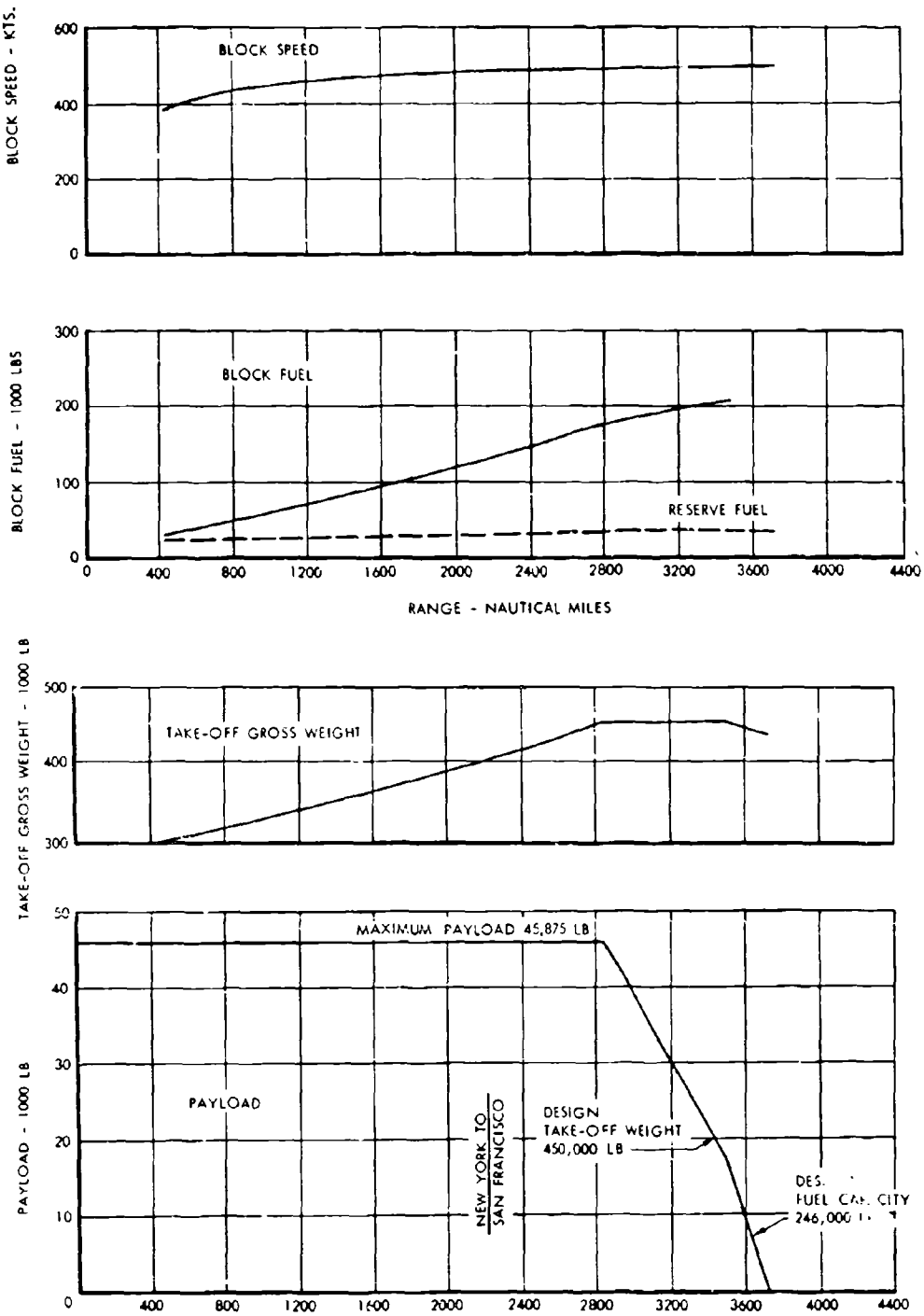

FIGURE 5-11 RANGE-PAYLOAD FOR MACH 0.91 CRUISE CLIMB

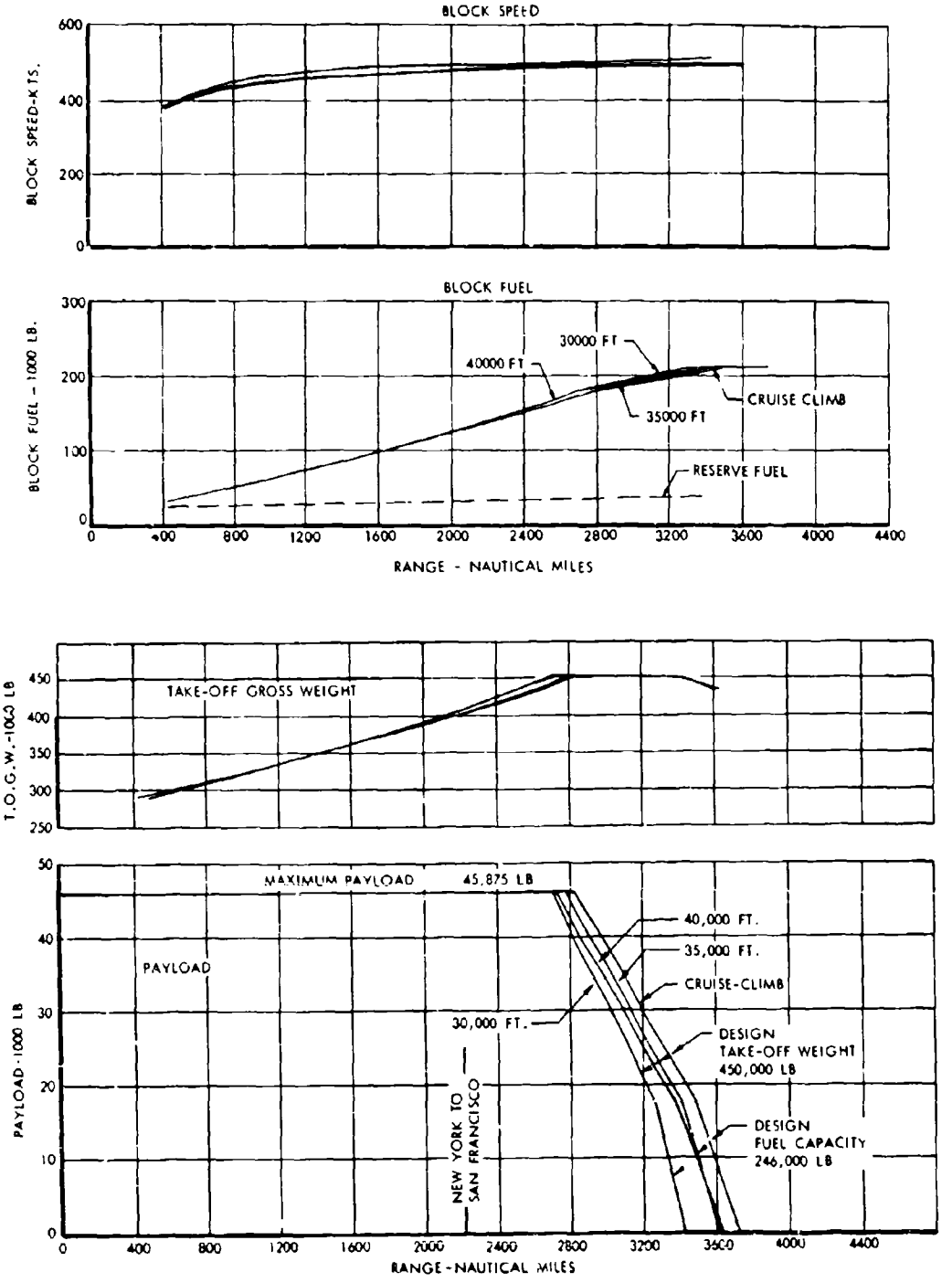

FIGURE 5-12 RANGE-PAYLOAD FOR MACH 0.91 CONSTANT ALTITUDE CRUISE

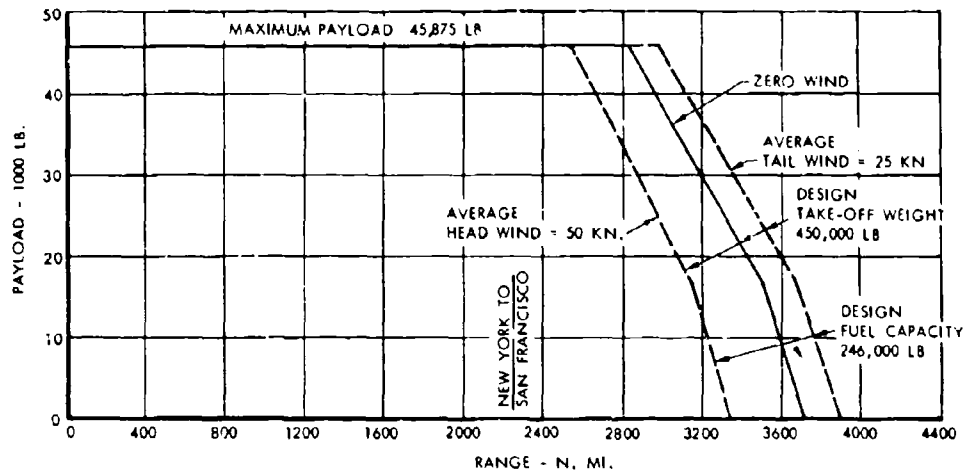

FIGURE 5-13 EFFECT OF WIND ON MACH 0.91 RANGE-PAYLOAD

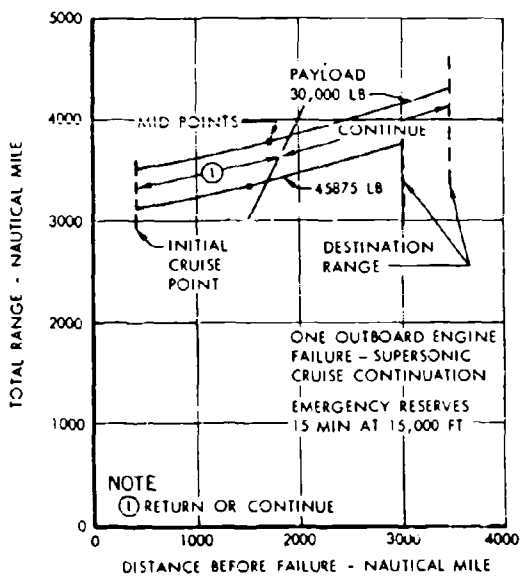

FIGURE 5-14 EMERGENCY CAPABILITY WITH AN INOPERATIVE ENGINE, MACH 3.0 CONTINUATION

Supersonic flight at Mach 3.0 with an inoperative engine does not impose any hazard, since the SST is easily controllable in the event of a second engine failure on the same side. Should such a second failure occur, however, it is necessary to continue the flight at subsonic speed after a normal descent to a lower altitude in order to reach the destination. The lower part of Figure 5-15 shows the total range capability following the simultaneous failure of two engines on the same side. Over the majority of the cruise segment the destination range can be exceeded.

The upper part of Figure 5-15 shows for comparison the total emergency range available following failure of a single outboard engine wherein the remainder of the flight is conducted at subsonic speed. A comparison of these results with those of Figure 5-14 shows that the available emergency range for continuation at subsonic speed is essentially equal to that available for continuation at Mach 3.0.

The SST can also reach its destination range following cabin depressurization even under the most improbable sequence of failures resulting in the complete loss of the cooling capability. This would require a simultaneous failure of both independent systems which are in themselves multiply protected.

Should this occur, however, the SST can make an emergency descent to an altitude of approximately 20,000 feet and fly at the design speed which corresponds to 0.8 Mach number at that altitude. Under these conditions ram air from the engine air inlets is sufficient to maintain the cabin pressure at the equivalent of 10,000 feet. At Mach 0.8 the ram air entering the cabin will be at a temperature of approximately 45 degrees Fahrenheit and cooling is not required.

At 20,000 feet altitude and Mach 0.8 the engines are operating at relatively low power settings resulting in relatively high specific fuel consumption. More economical flight is possible if one engine is shut down and the flight is continued on three engines. This type of operation is required in this case to reach the destination. As a conservatism an outboard engine is assumed shut down. The total range available with three engines operating from the mid-point the destination is shown in Figure 5-16 as a function of cruise altitude for the design range payload of 30,000 pounds. At 20,000 feet with emergency reserves the destination range is attained exactly.

In the extremely remote event of a failure of a cabin window the SST makes an emergency descent to 10,000 feet. With the cabin at ambient pressure at that altitude the hole is sealed with a plug which is carried for this contingency. The cabin is repressurized and the airplane climbs to altitude and continues to the destination in four-engine long-range cruise operation. The emergency range available in this case is 3720 nautical miles assuming a window failure at mid-point.

5.6 RANGE-PAYLOAD ANALYSIS DATA

All of the basic data required for the analysis of the range-payload characteristics of the SST are presented in this section. The fuel required for ground maneuvering prior to take-off and the fuel required to take-off and climb out to an altitude of 2500 feet totals 8760 pounds as tabulated in Figure 5-2. The time, distance, and fuel required to accelerate at 2500 feet to the operational climb speed of 360 knots CAS and to climb and accelerate to Mach 3.0 at cruise altitude is presented in Figure 5-17 for standard day conditions. Similar data for ambient temperatures 10 degrees centigrade above standard and 10 degrees centigrade below standard are presented in Figures 5-18 and 5-19, respectively. Minimum duct heating thrust is employed below 30,000 feet and maximum duct heating thrust is employed above 30,000 feet. The Mach number-altitude relationship on which the climb to cruise altitude is based is shown for the three temperature conditions in Figure 5-20. The time, distance, and fuel to climb to cruise altitude on subsonic flights is presented in Figure 5-21 and corresponds to operation at the maximum dry thrust rating.

Cruising fuel-economy data are shown in Figures 5-22 and 5-23 for supersonic and subsonic operation at standard day conditions and for temperatures 10 degrees centigrade above standard. The effects of constant altitude operation and cruise-climb operation is included for both Mach ranges.

The time, distance, and fuel required for normal descents from the final Mach 3.0 cruise altitude are shown in Figure 5-24. The time for deceleration from Mach 3.0 to the initial descent speed of 330 knots CAS is included on this Figure as is indicated. The actual normal descent time from 80,000 feet altitude is found to be 28 minutes. The descent speed

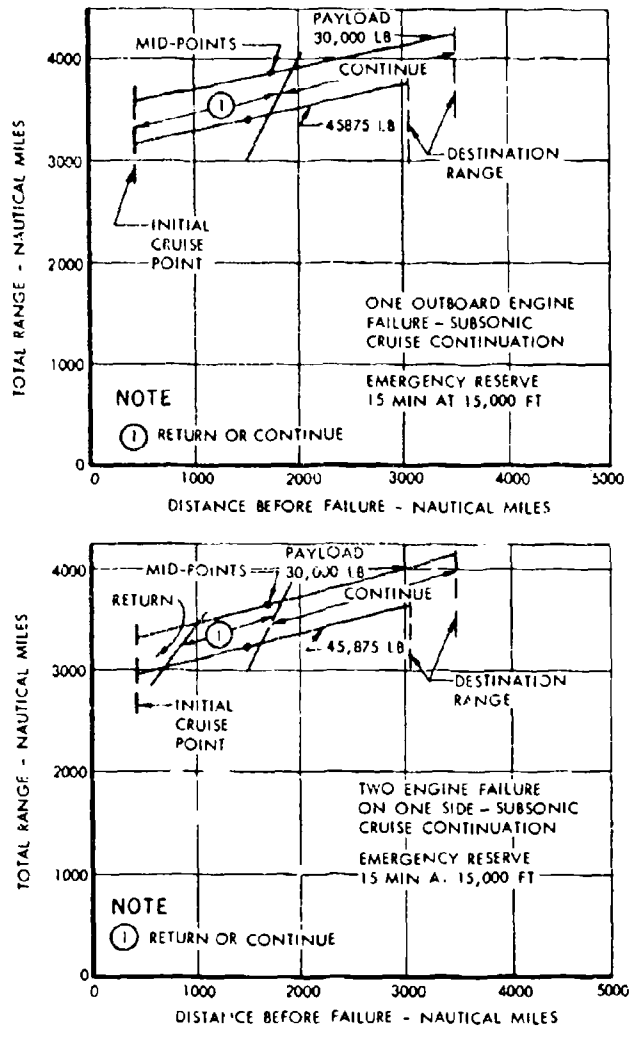

FIGURE 5-15 EMERGENCY RANGE CAPABILITY WITH INOPERATIVE ENGINES, SUBSONIC CONTINUATION

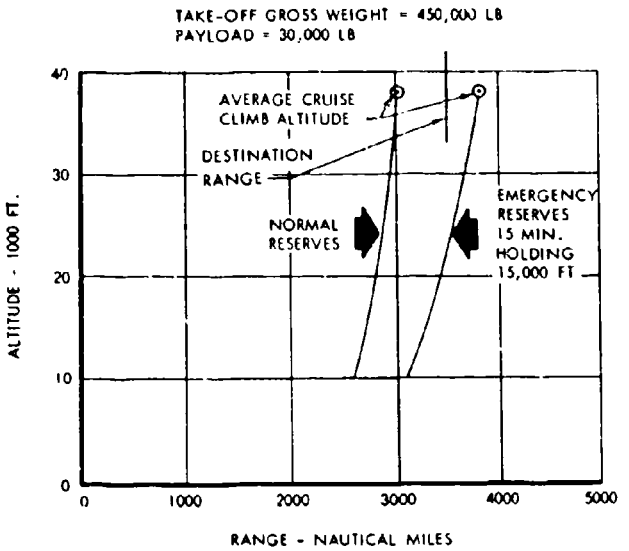

FIGURE 5-16 EFFECT OF CRUISE ALTITUDE ON EMERGENCY RANGE CAPABILITY WITH AN INOPERATIVE ENGINE

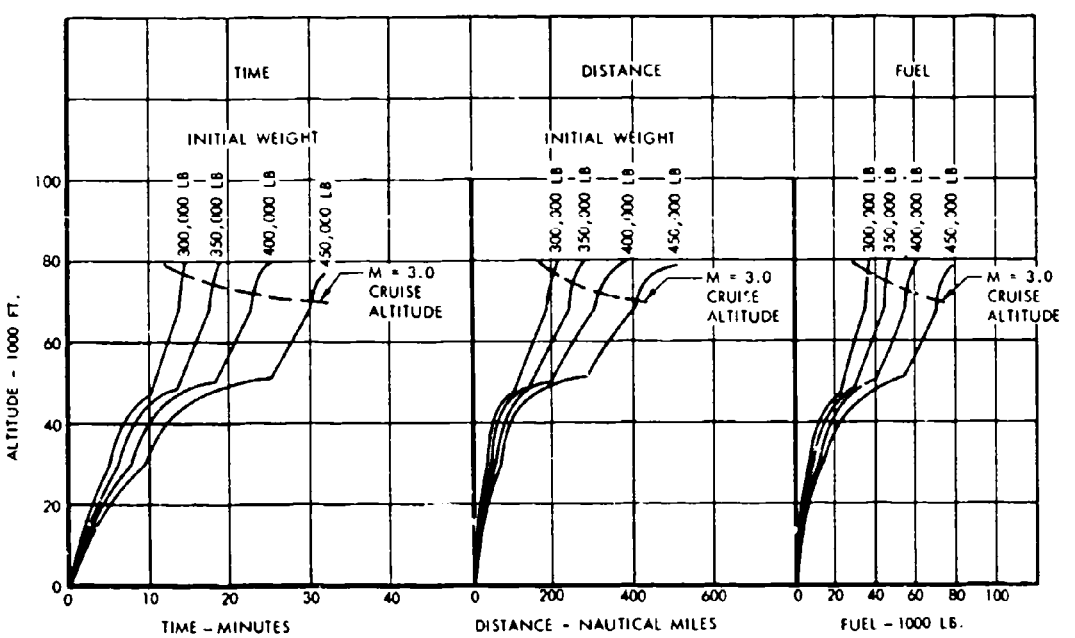

FIGURE 5-17 WEIGHT REDUCED CLIMB PERFORMANCE FOR SUPERSONIC FLIGHTS, STANDARD DAY

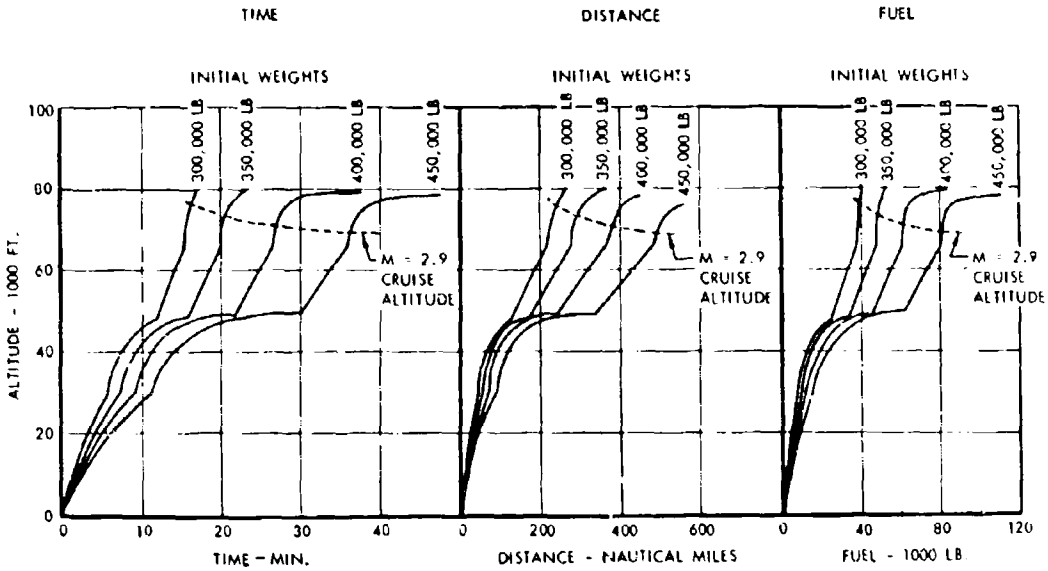

FIGURE 5-18 WEIGHT REDUCED CLIMB PERFORMANCE FOR SUPERSONIC FLIGHTS, HOT DAY (STD +10°C)

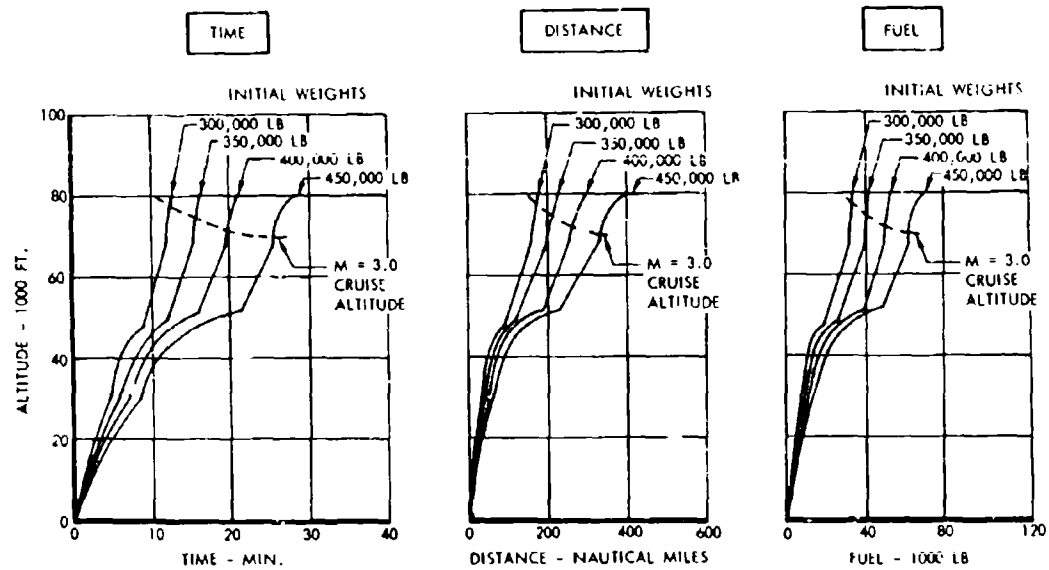

FIGURE 5-19 WEIGHT REDUCED CLIMB PERFORMANCE FOR SUPERSONIC FLIGHTS, COLD DAY (STD −10°C)

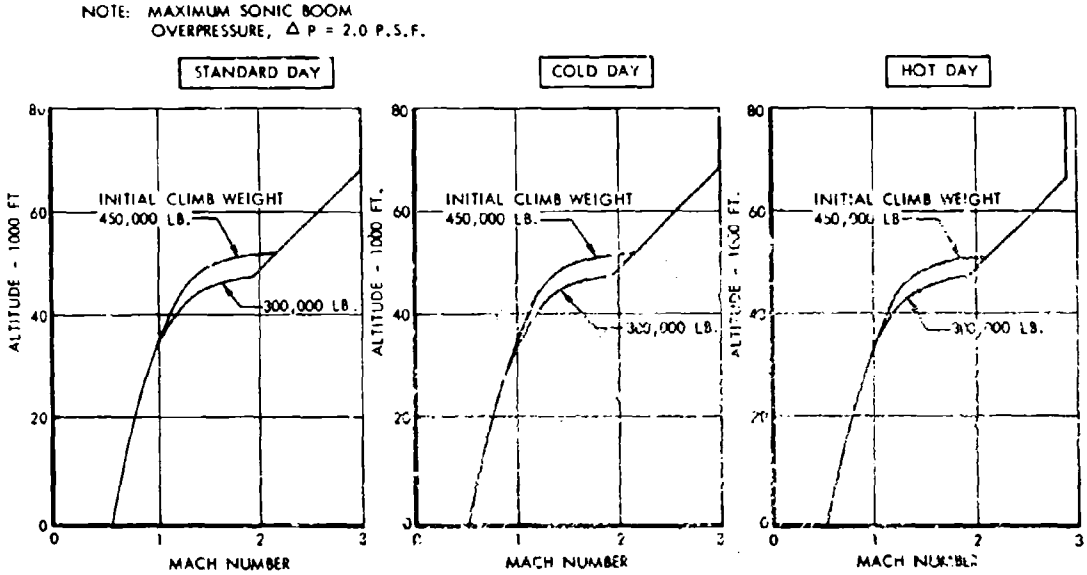

FIGURE 5-20 MACH-ALTITUDE CLIMB PROFILE FOR SUPERSONIC FLIGHTS

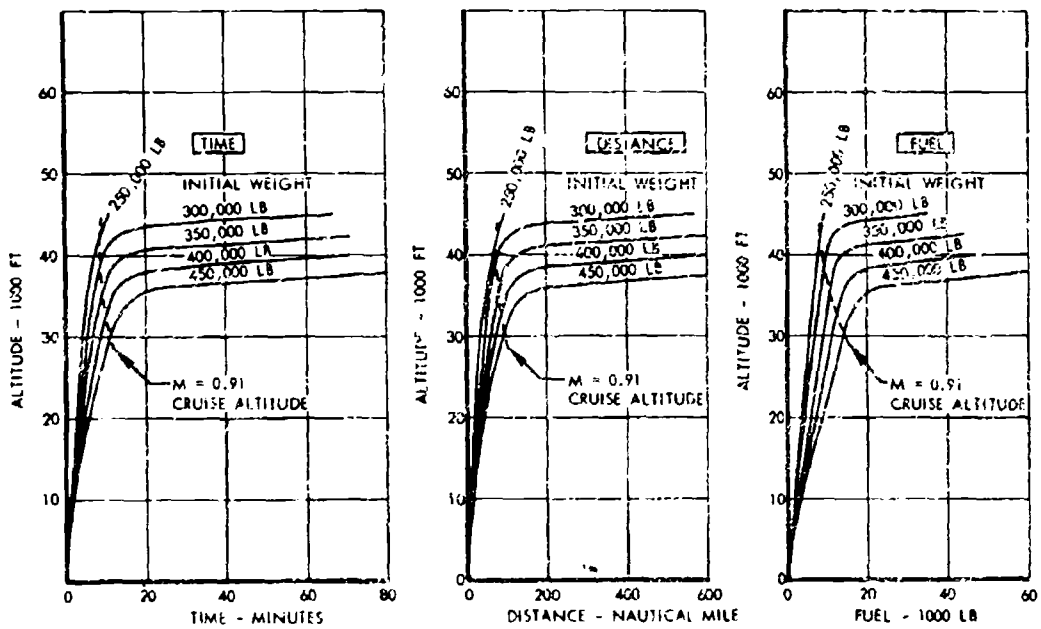

FIGURE 5-21 WEIGHT REDUCED CLIMB PERFORMANCE FOR SUBSONIC FLIGHTS, STANDARD DAY

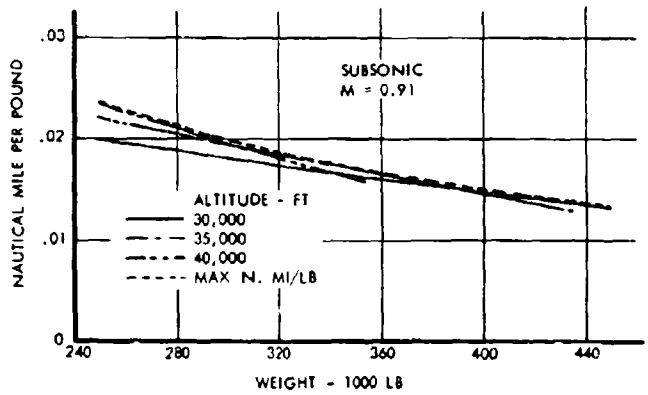

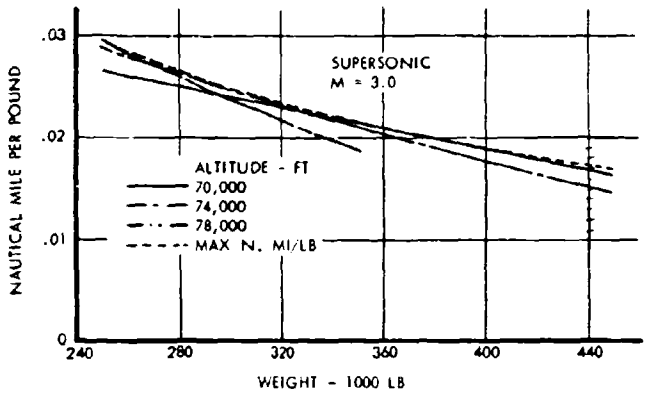

FIGURE 5-22 CRUISE FUEL ECONOMY, STANDARD DAY

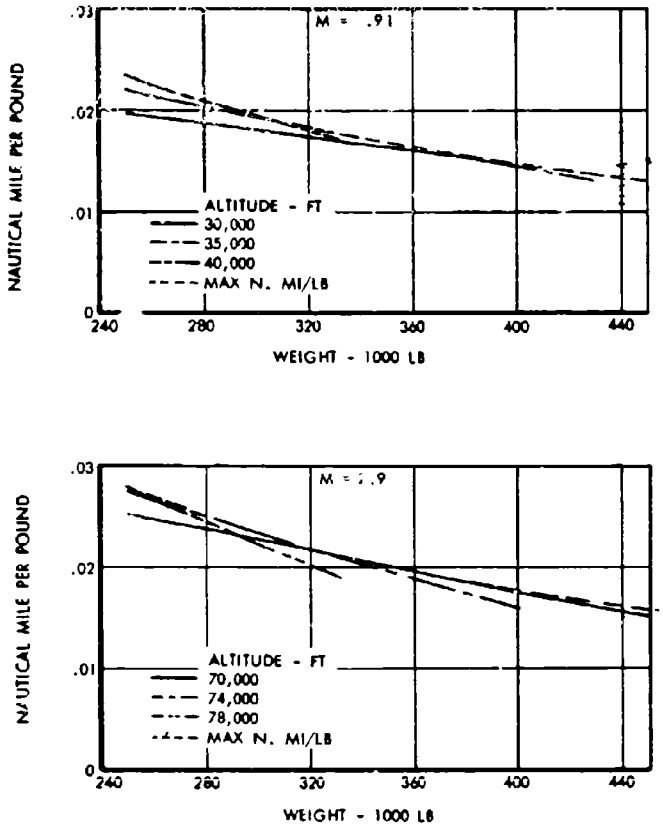

FIGURE 5-23 CRUISE FUEL ECONOMY, HOT DAY (STD +10°C)

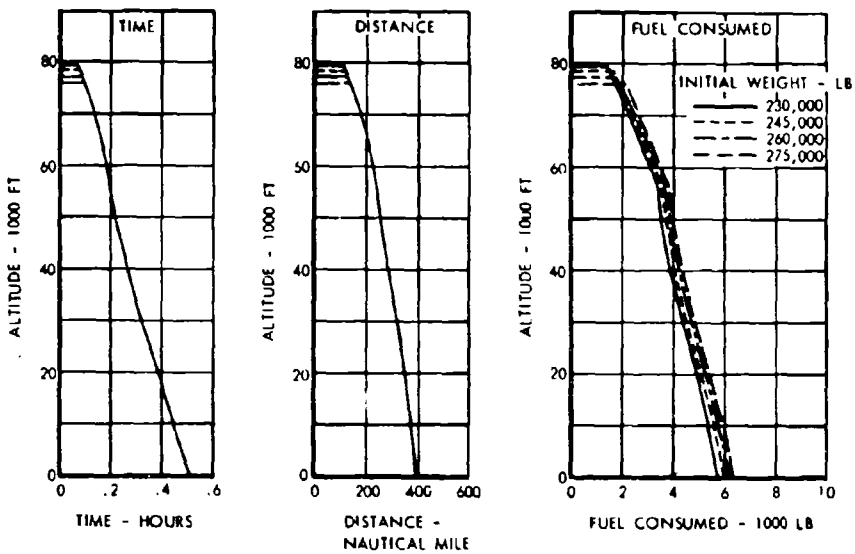

FIGURE 5-24 NORMAL DESCENT PERFORMANCE

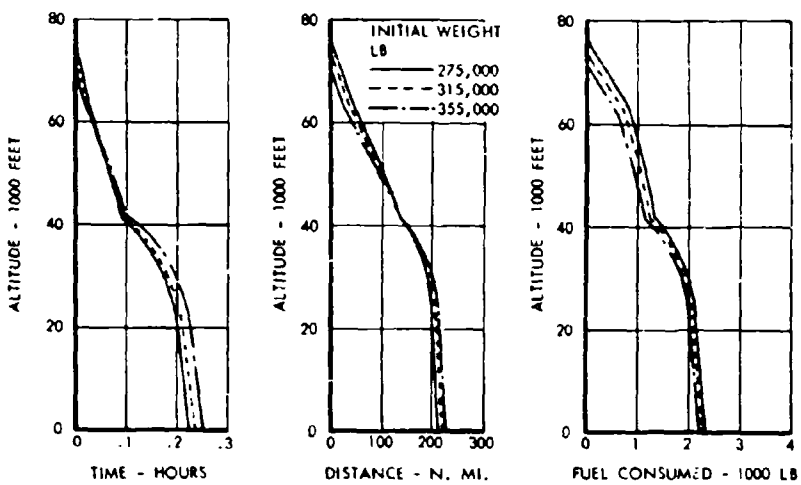

FIGURE 5-25 EMERGENCY DESCENT PERFORMANCE

at lower altitudes is reduced to 320 knots CAS to meet the required ground overpressure limit of 1.5 psf. This same speed of 320 knots is used for normal descents from the final subsonic cruise altitudes as well. Therefore, the descent segment for subsonic flights can be determined incrementally from Figure 5-24 with the aid of the final subsonic cruise altitude information furnished in Figure 5-32. The emergency descent characteristics are presented in Figure 5-25 and are computed at the structural design speeds shown in Figure 3-8. The landing gear is extended to increase the rate of descent at the gear design speed of 360 knots which is equivalent to 0.9 Mach number at approximately 25,000 feet. It is seen that the time to descend from the supersonic cruise altitudes to 10,000 feet is approximately 13 minutes.

Fuel flow information from which holding performance can be computed is presented in Figures 5-26 and 5-27 as a function of Mach number, weight and altitude for standard day conditions. Holding fuel consumption for the range-payload analyses herein are computed on the basis of operation at 15,000 feet altitude at the speed for minimum drag.

5.7 FLIGHT PERFORMANCE DATA

The rates of climb along the operational climb schedule for supersonic flights are presented for several temperature conditions in Figures 5-28 through 5-30. Minimum duct heat thrust is used at altitudes below 30,000 feet and maximum duct heat thrust is used at all higher altitudes. The rate of climb with maximum dry thrust used for subsonic flights is shown in Figure 5-31. The operational climb speed for subsonic flights corresponds to 360 knots CAS below 30,000 feet and 0.9 Mach number above 30,000 feet. Service ceiling capabilities at Mach 3.0 with maximum duct heat thrust and at Mach 0.91 with maximum dry thrust are shown as a function of weight in Figure 5-32. The altitudes corresponding to cruise-climb operation at Mach 0.91 and Mach 3.0 are included for comparison. The cruise altitudes are well below the ceilings indicating that adequate thrust margin is available for altitude control. The transonic acceleration characteristics along the flight path for a typical 2 psf overpressure climb profile are shown in Figure 5-33 as a function of Mach number, weight, and altitude.

5.8 AIRPORT PERFORMANCE (3.2.7.1)

Analysis of airport performance, in terms of FAA take-off and landing field lengths, operating speeds, climb gradients, and airport noise, is presented in this section in accordance with the considerations and requirements of references 5-1 and 5-2. It is shown that the proposed SST can satisfactorily meet all take-off objectives at maximum take-off weight using proper take off noise abatement power procedures, and will easily accomplish landing requirements. The proposed airplane is not over demanding with regard to operating techniques and conditions, having inherent performance margins that will allow for errors in rotation and climb out speed, and operation on wet runways. Use of high altitude airports or hot day ambient temperature conditions is possible without need for off loading of fuel or payload. A miss-set longitudinal trim setting at take-off does not result in any loss of control effectiveness and can be overpowered with a relatively small force (± 15 pounds) and does not represent an operational hazard. Take off and landing speeds reflect greater margins over minimum speed than do the current supersonic jet airplanes and the SST thereby offers greater safety margins when maneuvering or when encountering turbulence at low speed. During approach, there are no large trim shifts and drag changes due to adjustment of high lift devices requiring continual thrust monitoring. Approach visibility is better than realized with current jets, because of the weather-vision nose. After touchdown, landing spoilers are not required to destroy wing lift and improve braking capability. The six wheel bogey landing gear, equipped with individual modulated anti-skid devices, provides improved braking characteristics on wet as well as dry runways. In the following sections, consideration of airport noise as it affects airport performance is presented. A further discussion of noise is given in Section 7.2.

5.8.1 TAKE-OFF FIELD LENGTHS

The power plant for the SST, which is sized for transonic acceleration and cruise thrust, has the potential of providing extremely high static thrust for take-off operation, using full duct heating augmentation. At design take-off gross weight, the thrust/weight ratio is .40 for standard day conditions. Required balanced field length take-off distances for various weights using this maximum thrust level are given in Figure 5-34. Effects of operating airport altitudes and temperatures are also shown. For a

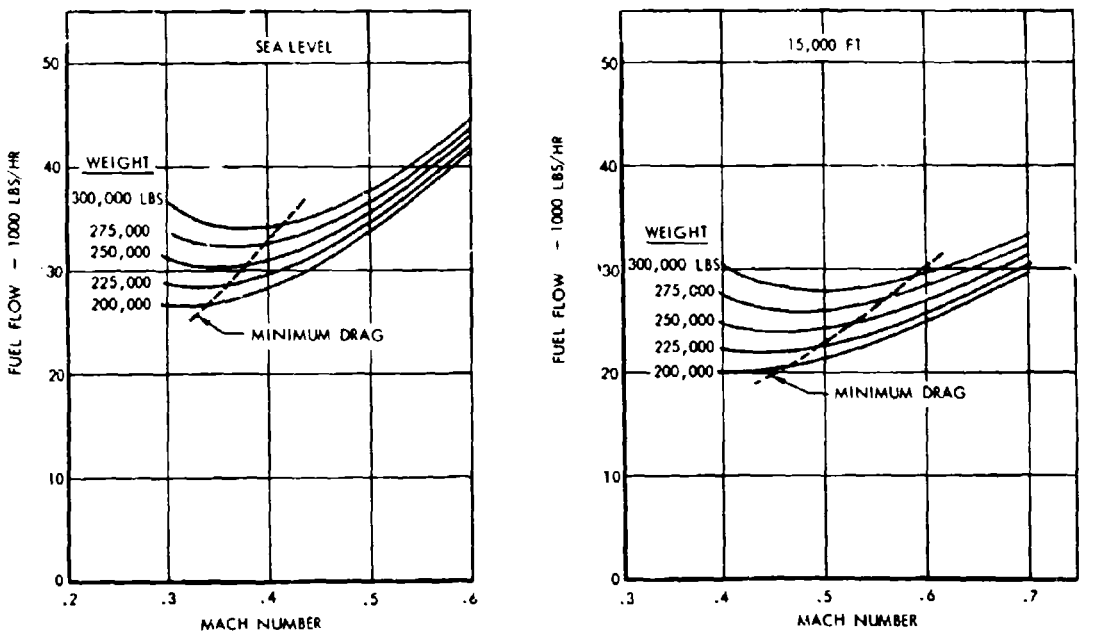

FIGURE 5-26 HOLDING PERFORMANCE, SEA LEVEL AND 15,000 FEET

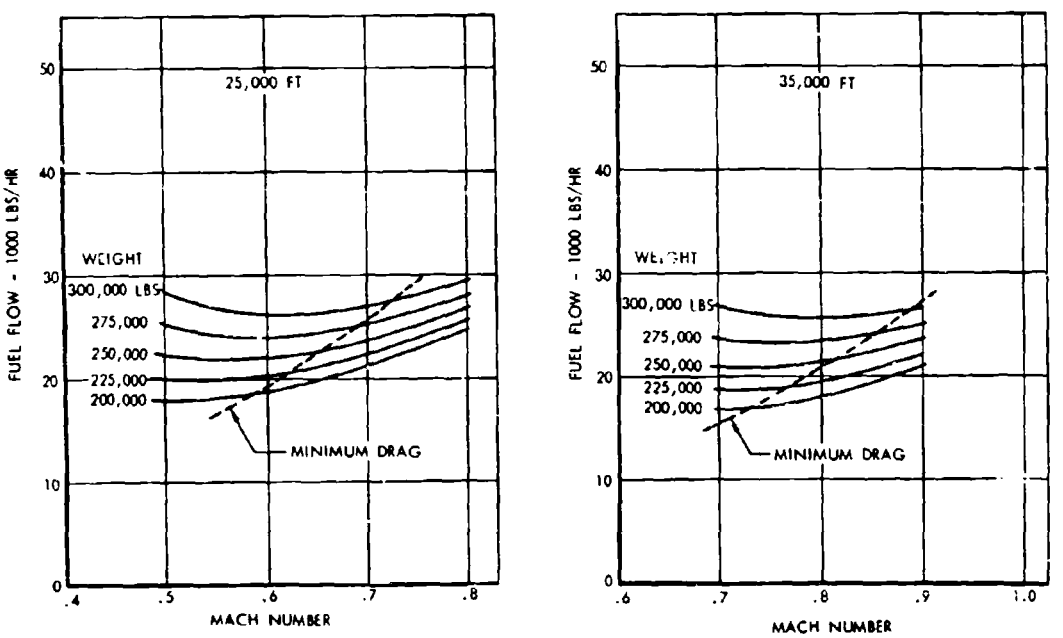

FIGURE 5-27 HOLDING PERFORMANCE, 25,000 FEET AND 35,000 FEET

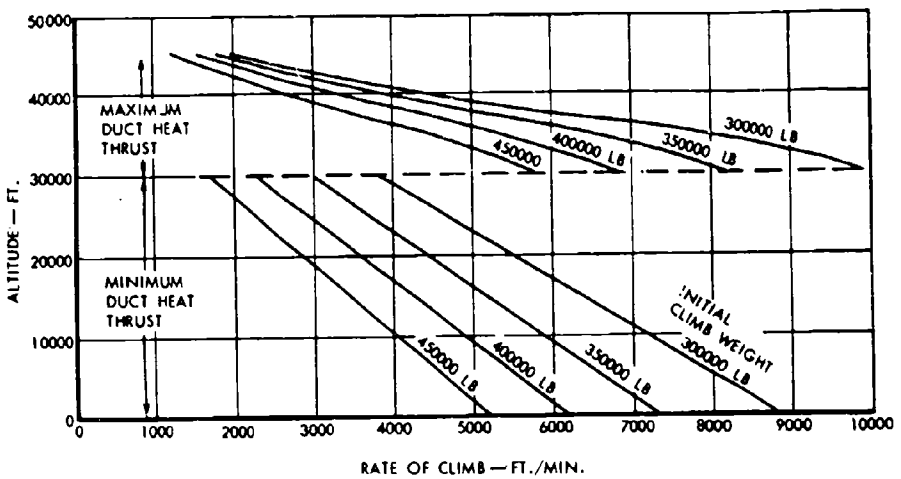

FIGURE 5-28 RATE OF CLIMB WITH DUCT HEAT THRUST, STANDARD DAY

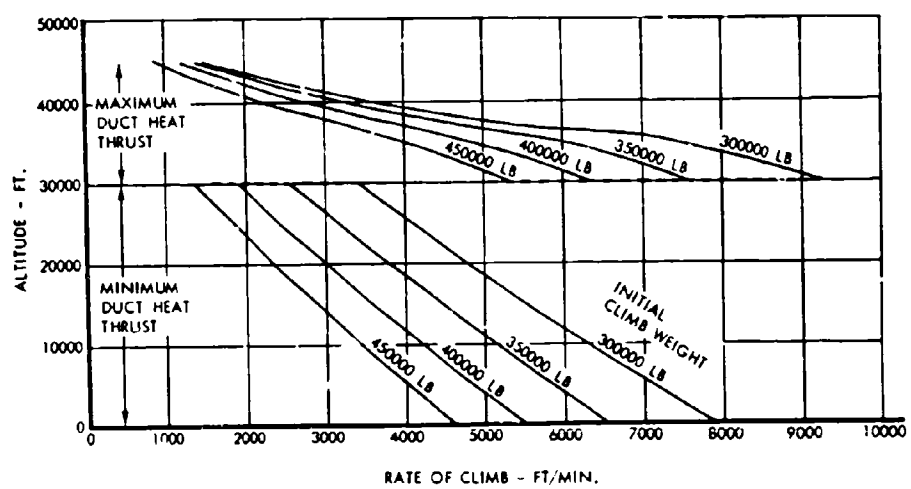

FIGURE 5-29 RATE OF CLIMB WITH DUCT HEAT THRUST, HOT DAY (STD +10°C)

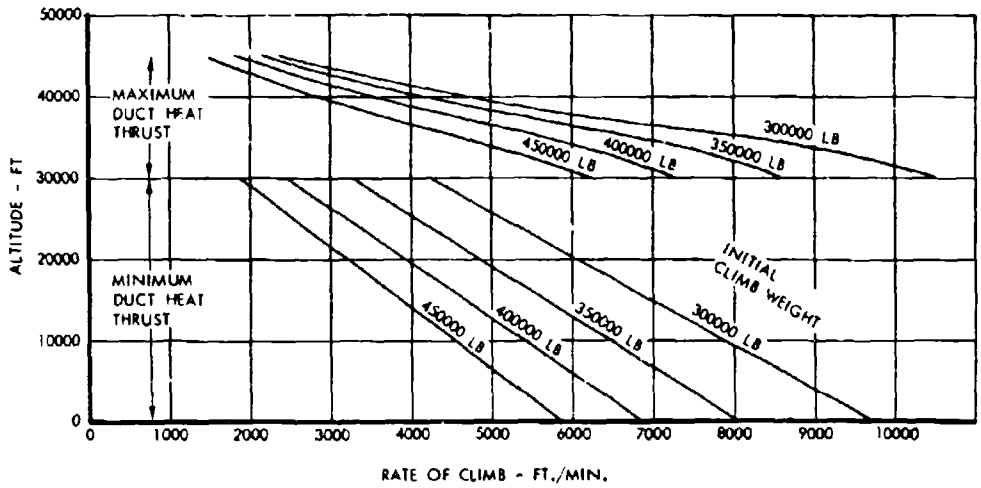

FIGURE 5-30 RATE OF CLIMB WITH DUCT HEAT THRUST, COLD DAY (STD −10°C)

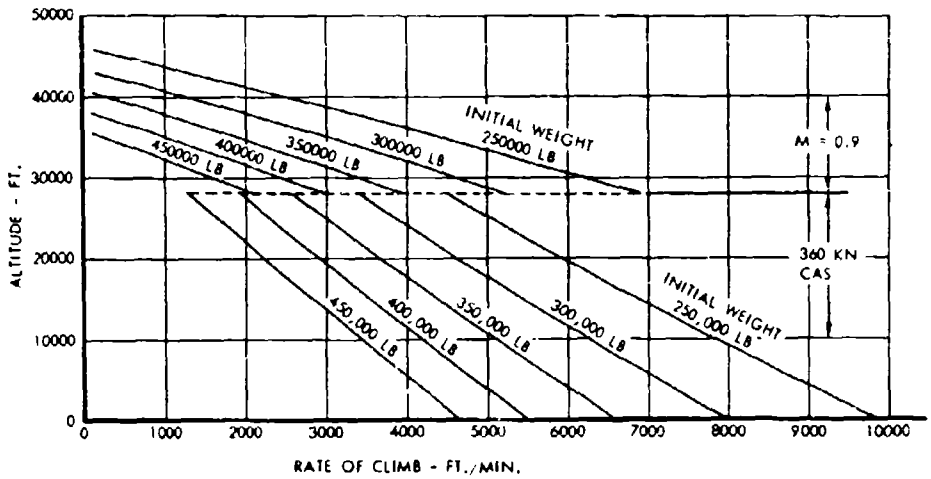

FIGURE 5-31 RATE OF CLIMB WITH MAXIMUM DRY THRUST, STANDARD DAY

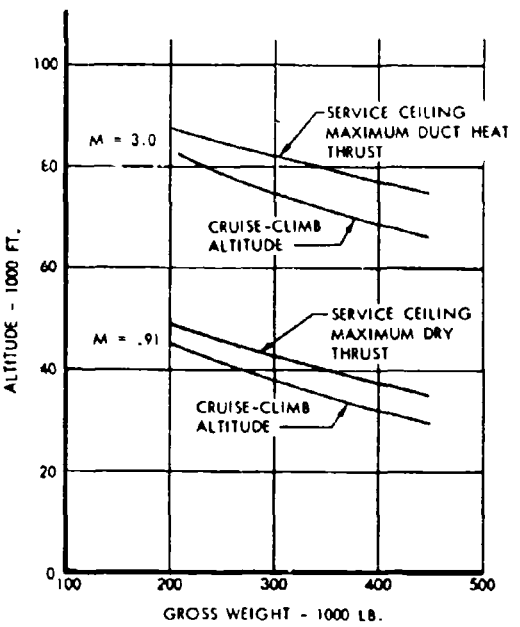

FIGURE 5-32 SERVICE CEILING AND CRUISE ALTITUDE, STANDARD DAY

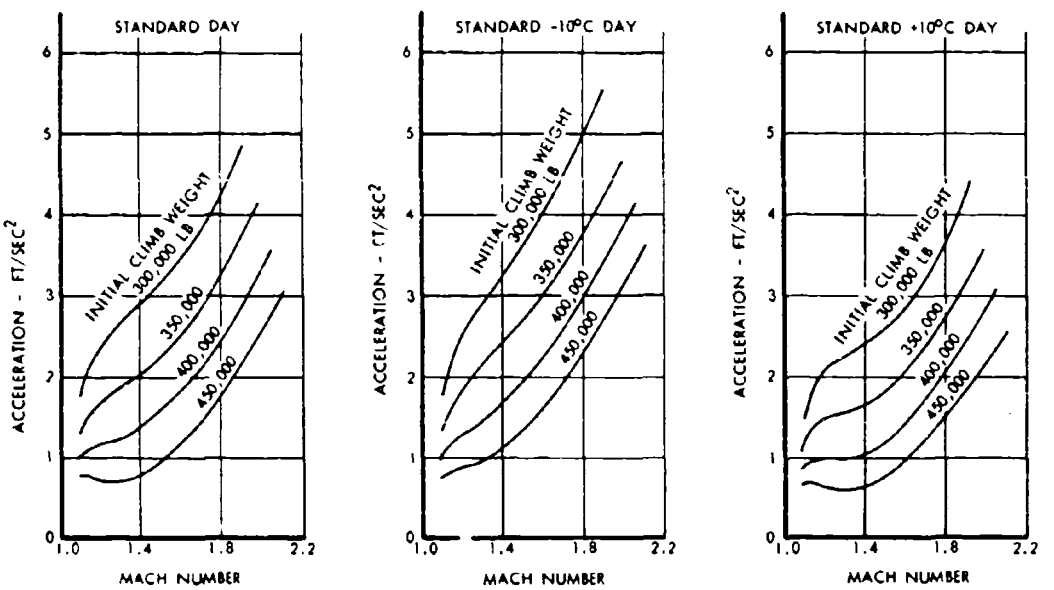

FIGURE 5-33 TRANSONIC ACCELERATION ALONG 2.0 PSF OVERPRESSURE CLIMB PATH

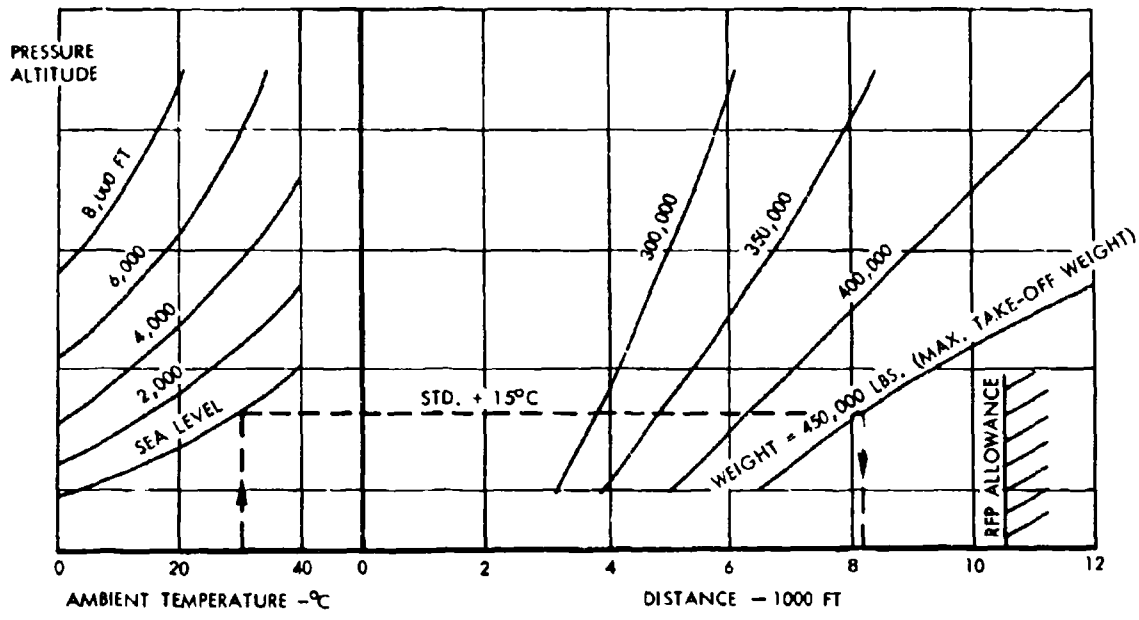

FIGURE 5-34 FAA TAKE-OFF FIELD LENGTH, MAXIMUM DUCT HEAT

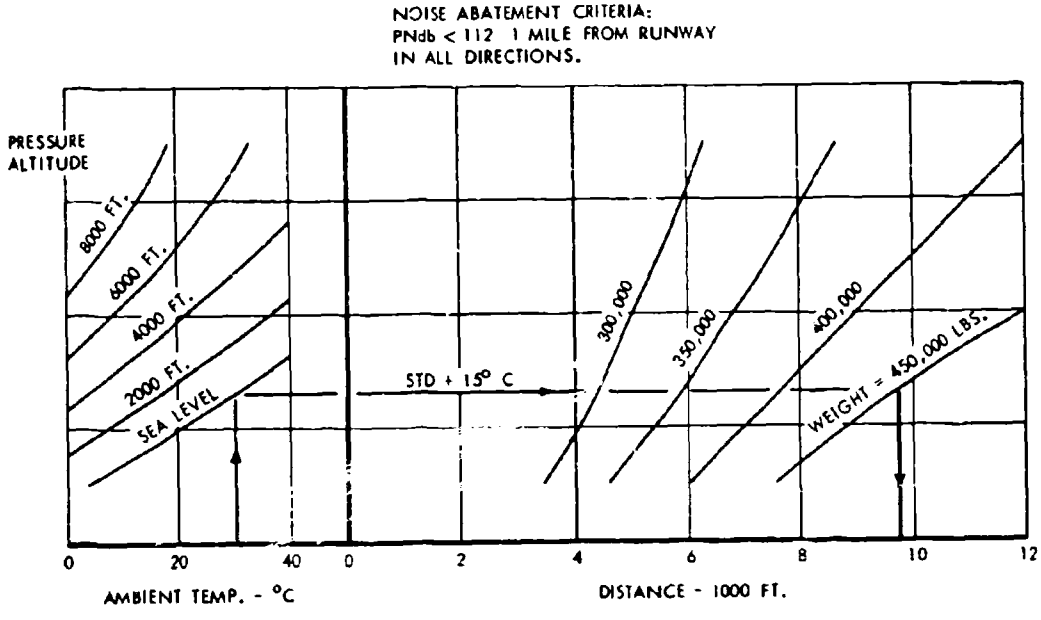

FIGURE 5-35 FAA TAKE-OFF FIELD LENGTH, NOISE ABATED

standard plus 15°C hot day at sea level, the take-off distance is 8,150 feet at 450,000 pounds design take-off gross weight. For the 10,500 foot field length stipulated in the FAA Request for Proposal, the proposed SST can operate from 6,400 foot altitude airports under standard day conditions, or take-off from sea level runways at standard plus 30°C hot day conditions without need for off-loading fuel or payload. First and second segment climb gradients exceed minimum requirements for all these conditions.

The elevon control power is capable of rotating the aircraft to the take-off attitude in 3.0 seconds at speeds above 140 knots. In the normal take-off performance data shown, an actual rotation time of 4.0 seconds was used and is reflected in the speed increase of approximately 20 knots between rotation and lift-off speeds.

For many airport facilities, community reaction to engine noise must be considered during the climb out phase of the take-off operation. For the proposed SST, four engine climb out profiles achieved using maximum reheat thrust will place the aircraft over the one mile runway point at a relatively high altitude.

When nearing the one mile control point, thrust can be cut back and the perceived ground noise level can be lowered below the 112 pndb criteria level and still maintain high climb gradients.

For some airport facilities, use of maximum augmented thrust will be undesirable because of the noise levels generated during the ground roll phase of the take-off procedure. The proposed SST can operate from these facilities by adopting a reduced thrust schedule operation. Partial duct heating is employed for normal four engine take-offs out to the one mile from runway point, where thrust is cut back to minimum duct heating. This reduced thrust take-off increases field lengths slightly, but reduces the engine noise levels to the extent that 112 pndb is never exceeded at any point one mile from the runway centerline, in any direction. In the event of an engine failure above the decision speed V_1, full duct heating is applied to the remaining engines with a four second time allowance to reach maximum thrust and this thrust utilized for the remainder of the take-off operation. Rudder pedal nose wheel steering provides adequate directional control to allow for the increased duct heating thrust.

Balanced field length performance attainable using this noise abatement procedure is presented in Figure 5-35. Effects of airport altitude and ambient temperature are given for various take-off gross weights. For particular operating conditions where the engine out field length requirement gives runway distances shorter than four engine field lengths increased 15 percent, the latter distances have been used to establish the curves in Figure 5-35, in accordance with FAA regulations. The data of this figure indicate that the proposed SST can operate from a 9750 foot sea level runway for standard plus 15°C conditions at maximum take-off gross weight. Using a 10,500 foot runway with standard day conditions, airport altitudes up to 4800 feet can be utilized without off loading fuel or payload.

The take-off profile and pndb ground contours for a maximum gross weight take off using the noise abatement thrust schedule is shown in Figure 5-36 for sea level standard day conditions.

The effect of wind on FAA take-off field lengths is shown in Figure 5-37. For head winds, 50 percent accountability is assumed and for tailwinds 150 percent. A ten knot tail wind is shown to increase the 3 engine distance by 1100 feet at design take-off gross weight.

The small range of operating centers of gravity indicated in Figure 3-6 will not have an effect on take-off performance.

The effects of runway slush on take off ground roll are given in Figure 5-38. One inch of slush is shown to increase the ground roll distance by 1200 feet. The six-wheel three-axle main landing gear minimizes this value by virtue of minimizing the tire frontal area exposed to the slush.

The proposed SST is not sensitive to early and over rotation abused take-off procedures, because of high thrust to weight ratio and low wing loading. The effects of abused rotation for standard +15°C conditions are shown in Table 5-1. For a 3 engine take-off with 5 knots early rotation and maximum attainable lift off attitude achieved with maximum rotation rate, total field length decreases. The distance penalty for the higher drag due to early rotation is more than compensated by the reduction in acceleration distance up to the lift off speed of 162 knots. Air distance over the 35 foot obstacle is not appreciably increased because of the low operating wing loadings and lift coefficients.

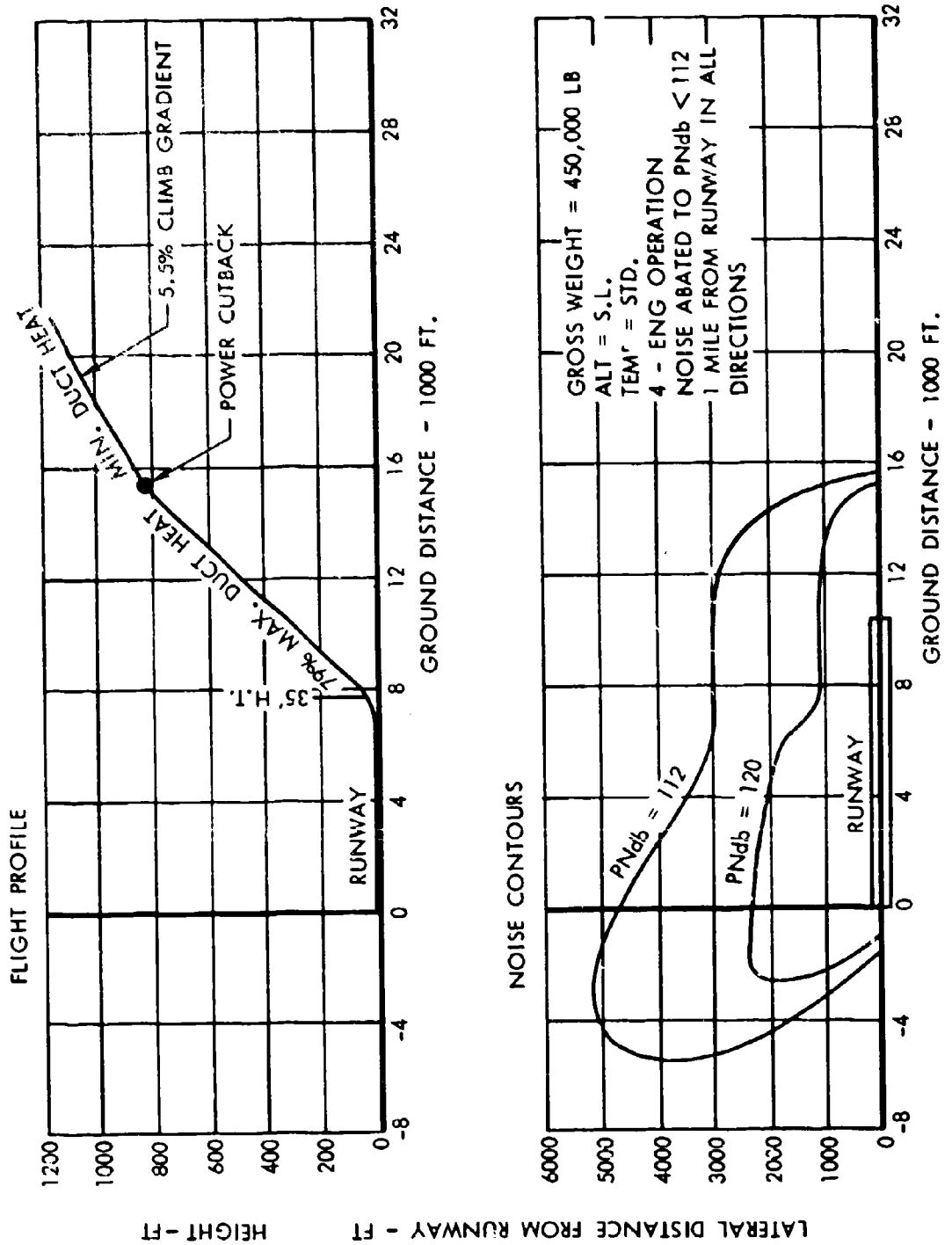

FIGURE 5-36 FLIGHT PROFILE AND PERCEIVED NOISE LEVELS, NOISE ABATED TAKE-OFF

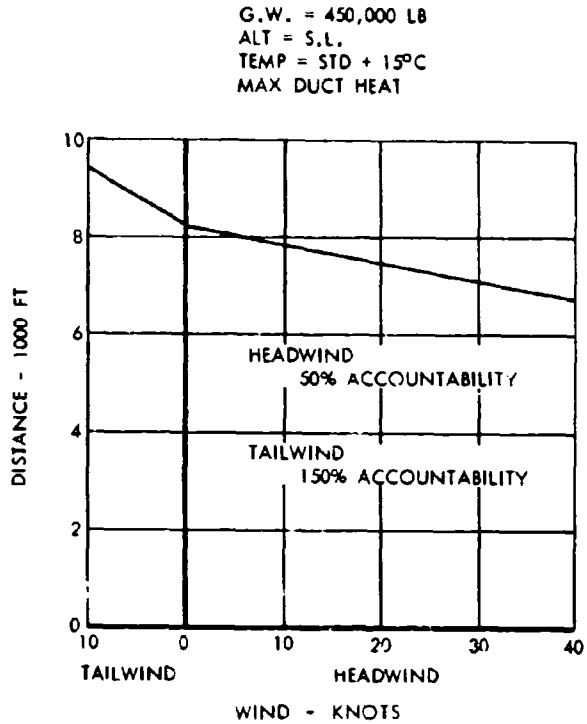

FIGURE 5-37 EFFECT OF WIND ON FAA TAKE-OFF FIELD LENGTH

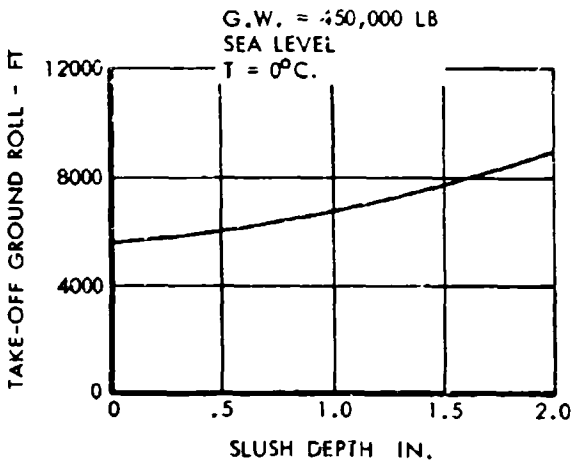

FIGURE 5-38 EFFECT OF SLUSH ON TAKE-OFF GROUND ROLL

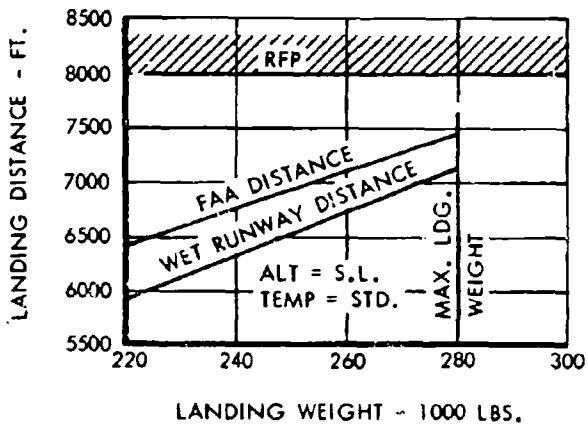

FIGURE 5-39 FAA LANDING FIELD LENGTH AND WET RUNWAY LANDING DISTANCE AT SEA LEVEL

Similar reductions in field length are experienced during a 4 engine take-off when early and over rotation occurs 10 knots below normal rotation speed. When rotation is postponed until 10 knots beyond normal V_R and the airplane is under rotated by 2 degrees, increased distance to accelerate up to the higher lift off speed is required. The total field length is less than the normal V_R 3 engine take-off distance, however.

TABLE 5-1 ABUSED TAKE-OFF EFFECTS

G. W. = 450,000 Paunds
Alt. = S.L.
Temp. = Std. + 15°C

Criteria	*Rotation Speed knots*	*Lift Off Speed knots*	*FAA Field Length feet*
Basic—3 engine	151	169	8150
Early and Over Rotation—3 engine	146	162	7650
Basic—4 engine	151	168	6410
Early and Over Rotation—4 engine	141	163	5650
Under and Late Rotation—4 engine	161	186	7680

The effects of wet runways, tire wear, and reverse thrust on accelerate-stop distance are shown in Table 5-2. Reverse thrust operation consists of two engines operated at 40% of the no-duct heat forward thrust and reduces the wet runway accelerate-stop distance by 1,000 feet.

Worn tires have no appreciable effect on dry runway braking distance but may extend the wet runway distance.

TABLE 5-2 ACCELERATE-STOP DISTANCE VS. BRAKING FRICTION COEFFICIENT

G. W. = 450,000 Pounds
Alt. = S.L.
Temp. = Std. + 15°C
Max. Duct Heat

Criteria	*Distance—ft.*
Basic Distance	6600
Wet Runway, Brakes only	10,400
Wet Runway, Brakes plus reverse thrust (2 engines)	8980
Wet Runway, Worn Tires, plus reverse thrust (2 engines)	9820

5.8.2 LANDING FIELD LENGTHS

Landing performance capabilities for the proposed SST will permit operation out of domestic as well as international airports at normal landing operating weights. Estimated landing distances as a function of airplane weight are given in Figure 5-39. Shown are the normal FAA dry runway field length requirements which include the 0.60 accountability factor, and distances required for landing on wet runways without reverse thrust. At maximum landing weights, field lengths required are less than the 8000 foot objective of the FAA Request for Proposal.

The landing ground roll reflected in these data includes a four second time allowance before the brakes are applied to permit the airplane attitude to be reduced from that at touchdown to the ground roll attitude. The elevon control at landing is sufficient to prevent the aircraft from pitching down and will, in fact, maintain nose high attitudes to speeds well below 100 knots if desired. Air distances are calculated assuming negligible change in airspeed during the 2.5° glide slope and flare maneuver from 50 feet to touchdown. Stopping distances are based on conservative braking coefficients, and do not reflect anticipated gains in effective braking that will be realized using a fully modulated anti-skid system. This system will also feature individual anti-skid sensors and a locked wheel protection device. This combination of braking devices will provide for the day to day operator the following features:

- Insensitivity to bank angles through the individual skid sensors.
- Insensitivity to hydroplaning because of the six wheel tandem bogey and individual skid sensors.
- Ability to apply brakes immediately after touchdown, provided by the locked-wheel protection device.
- Elimination of need for spoilers, because of absence of high lift devices.
- Insensitivity to excessive pilot foot pedal pressure, provided by the modulated brake system.

For these reasons, the estimated landing distances are believed to be conservative, and reflect discances which can be reproduced by the average airline pilot.

The effects of airport altitude on landing distance is presented in Figure 5-40. Distances increase approximately 200 feet for each 1000 foot increase in airport altitude.

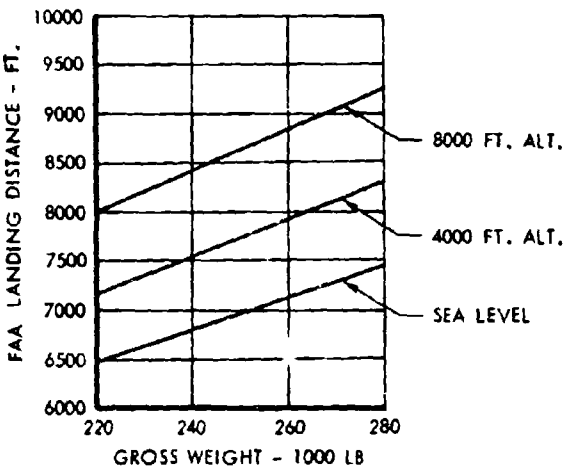

FIGURE 5-40 FAA LANDING FIELD LENGTH AT ALTITUDE

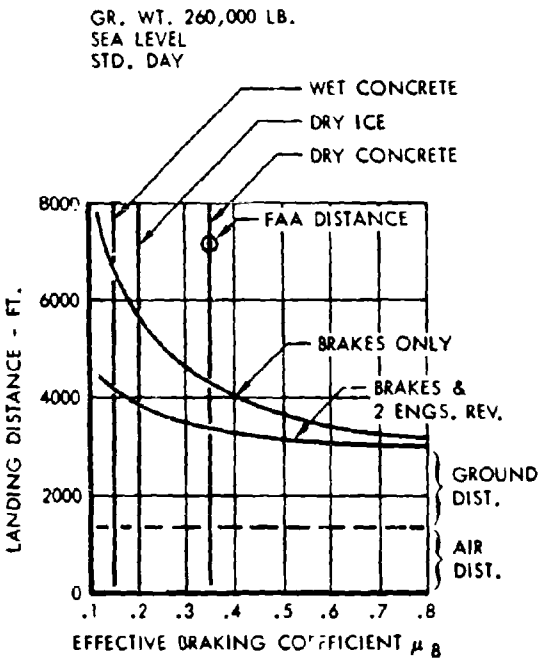

FIGURE 5-41 LANDING DISTANCE AS A FUNCTION OF EFFECTIVE BRAKING COEFFICIENT

Landing distance as a function of effective braking coefficient is presented in Figure 5-41. Effects of using two engine reverse thrust are also noted.

Ground pndb contours during landing approach are presented in Figure 5-42; the noise levels are well within acceptable values. Landing approach noise for current jet transports is greatly influenced by the thrust adjustments required when the drag and high lift devices are extended on the approach. The SST offers a single configuration change, gear down, which automatically establishes the 2.5° glide slope from level flight without throttle change. This eliminates excessive and random thrust adjustments and their associated noise levels.

5.8.3 AIRPORT OPERATING SPEEDS

Airport operating speeds for the SST are summarized in Table 5-3, showing take off characteristics at maximum design take-off gross weight, and landing values at normal landing weight. The speeds are compared with airport speeds employed by current subsonic jets also presented on the table. The subsonic jet speeds represent operational data obtained from the airlines and their operating manuals. The similarity in speeds indicate that the proposed SST will utilize operational procedures very similar to those currently employed.

Some concern has been expressed that airline operation of the supersonic transport will require increases in speed beyond those used for design, demonstration, and certification, since this situation came to pass during the acceptance of the subsonic jets. Therefore, in establishing target speeds for the SST design, the argument continues that it is desirable to establish low SST target speeds that will allow for this contingency.

Previous increases in operational speed were adopted so as to provide greater margins above stall speed, operation at speeds where greater potential excess thrust margins would be realized, and at lower lift coefficients where lateral and directional stability characteristics were improved above marginal levels. None of these reasons will form a basis for wanting to increase the speeds of Table 5-3 for the proposed SST when it goes into operation.

It is noted that the speed defined as "minimum speed" for the SST is based on a maximum angle of attack of 20 degrees and does not represent a physically limited minimum speed. The lift characteristics above this angle are still linear and lift coefficients 40 to 50% greater than at 20° can be obtained. This means that even at minimum flight speed it will be possible to achieve maneuver load factors of 1.5 g's, whereas current transports have no maneuver capability at

TABLE 5-3 SEA LEVEL TAKE-OFF & LANDING SPEEDS

Aircraft	*Lockheed "SST" JT11F-4 D/B*	*DC-8F JT3D-3*	*DC-8 JT4A-12*	*707-321B JT3D-3(w)*	*707-321C JT3D-3(w)*
Max. T. O. Wt., lbs.	450,000	325,000	315,000	324,500	324,500
Field Length @ 15°C, Ft.	7050/(8400)**	10,400	9,650	11,200	10,700
@ 30°C, Ft.	8150/(9750)**	11,600	10,800	11,900	11,300
Flaps	None	15°	25°	17°	14°
V_1 kts. (EAS)	151	142	139	152	147
V_R kts.	151	159	151	158	152
V_{LO} kts.	169	165	157*	168*	161*
V_2 kts.	174	170	162	173	166
Landing Weight, Lbs.	254,600	240,000	207,000	207,000	247,000
Field Length, Ft.	7,050	6,130	6,800	6,400	6,250
Flaps	None	50°	50°	50°	50°
Approach Speed ($1.3V_s$) kts.	135	144	133	134	137
Touchdown Speed kts.	134	140	128	128*	130*
V_s kts.	105***	110	102	103	105

**Estimated* ****Noise Abated Take-Off* ******Stick Shaker Speed*

Data provided by airlines from current operating manuals.

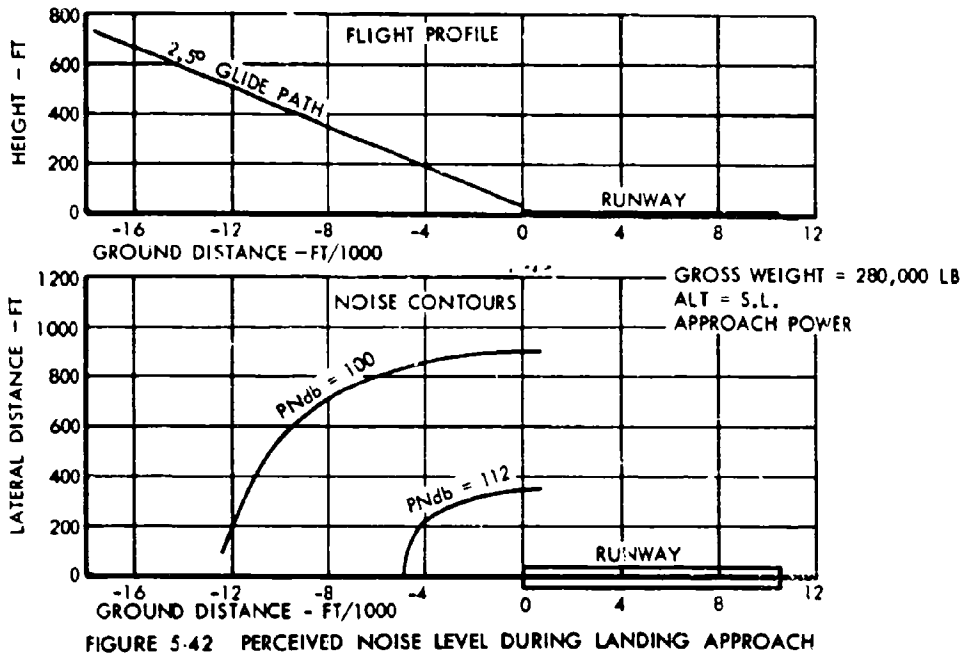

FIGURE 5-42 PERCEIVED NOISE LEVEL DURING LANDING APPROACH

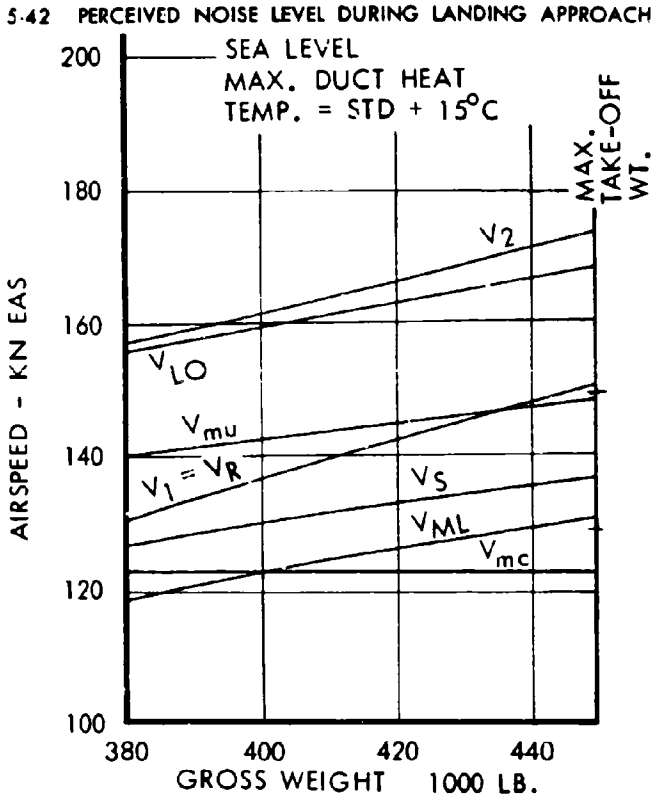

FIGURE 5-43 FAA TAKE-OFF SPEEDS

stall speed, and only 1.5 g capability at normal approach speeds. A stick shaker with a setting of 20° angle of attack is provided to inform the pilot of the approach of the minimum speed.

Take off and landing speed margins above the actual stall speed are therefore substantially greater than those used today. Thrust to weight ratios are considerably higher than for the current jets. Lateral and directional stability characteristics of the proposed SST do not become deficient at take-off and landing attitudes, as verified in Section 4.

The speeds shown for the SST in Table 5-3 are slightly greater than the target speeds listed as goals in the FAA Request for Proposal. However, on the basis of the similarity of these speeds to those of currently operational subsonic jets, and considering the wide speed margin over minimum useable speeds, these operating speeds are believed to be practical and acceptable.

The variations in operational airport speeds with gross weight for the proposed SST are presented in Figures 5-43 and 5-44.

5.8.4 CLIMB PERFORMANCE

Compliance with climb gradient requirements after take-off and during landing approach are easily met by the proposed SST. In the absence of high lift devices, light wing loadings and high thrust/weight ratios provide more than adequate climb margins.

The first segment climb gradient achievable with one engine inoperative at take off gross weight is presented in Figure 5-45 as a function of airspeed. It is seen that even at speeds less than normal lift-off speed, minimum requirements can be exceeded and even with gear down, positive rates of climb can be maintained down to minimum flight speed. The use of a low aspect ratio wing does not therefore lead to marginal climb performance which will make the climb characteristics sensitive to operational procedures.

First segment climb gradients realized and required for various airport altitudes and ambient temperatures are shown in Figure 5-46, for speeds corresponding to lift off speed.

Second segment climb performance, gear up at climb speeds equal to V_2 speed, are given in Figure 5-47. Adequate margins are available to permit operation at high altitude airports and high ambient temperatures without need for off loaded payload or fuel.

Similar margins are noted for final take off climb at climb speeds equal to 1.25 V_{MIN} and are shown in Figure 5-48.

Figures 5-49 and 5-50 summarize climb gradient performance for engine out approach and landing conditions. These performance requirements are easily met because of the large thrust levels available from the JT11F-4 engines.

5.8.5 TAKE-OFF LOAD FACTOR CAPABILITY

The normal load factor available on take-off at lift-off and climb speeds is shown in Figure 5-51 for four-engine operation. Because of the high thrust level of the SST engine, adequate load factor increments can be attained without causing longitudinal deceleration at both lift off and V_2 speeds.

5.8.6 METHODS OF ANALYSIS

The take-off field lengths have been calculated by a digital computer program. This program determines the critical engine failure speed, V_1, which will give the shortest CAR distance. In so doing, it calculates the following distance elements:

1. A 4-engine acceleration from zero velocity to a velocity, V_1, at which point an outboard engine failure occurs. During this segment the nose wheel is on the ground and the four engines are operating at take-off thrust.
2. A 3-engine acceleration from V_1 to a velocity, V_R, at which point the rotation is initiated. At V_1 it is assumed that the failed engine thrust instantaneously reduces to zero and full engine windmilling drag develops. This drag and the corresponding rudder trim drag are shown in Figure 5-52. During this segment the nose wheel remains on the ground. For the noise abated take-off the thrust is increased to maximum at V_1 with a time allowance of 4 seconds to reach maximum take-off thrust.
3. A 3-engine acceleration from V_R to V_{LOF} (lift-off). During this segment, the airplane rotates from ground roll attitude to the angle-of-attack required for lift-off. Elevon trim drag is considered. The lift and drag coefficient varies with velocity between V_R and V_{LO}.

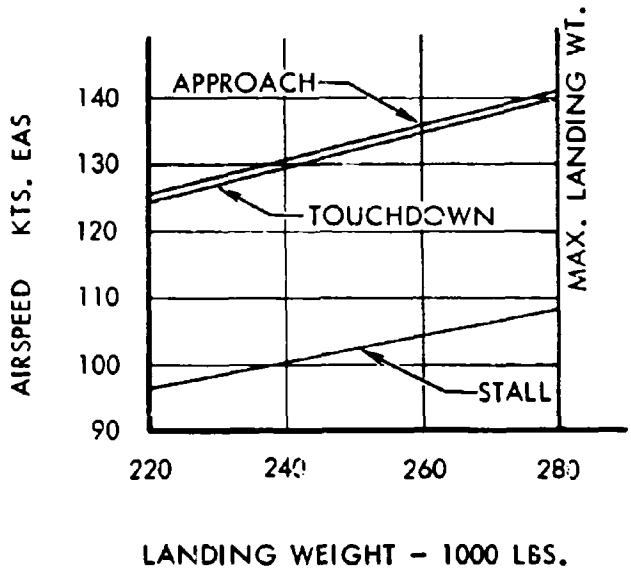

FIGURE 5-44 FINAL APPROACH AND TOUCHDOWN SPEEDS

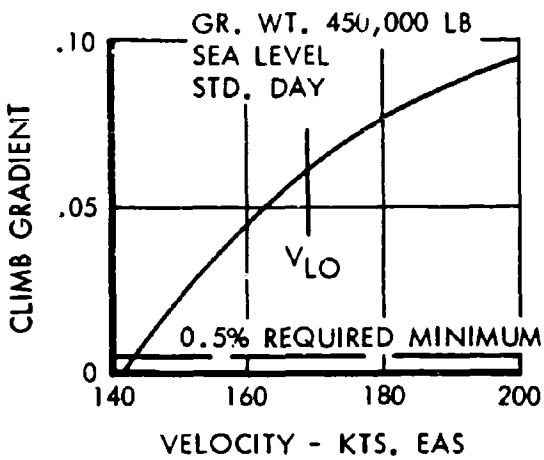

FIGURE 5-45 FAA FIRST SEGMENT CLIMB GRADIENT AT SEA LEVEL (ONE ENGINE INOPERATIVE—GEAR EXTENDED)

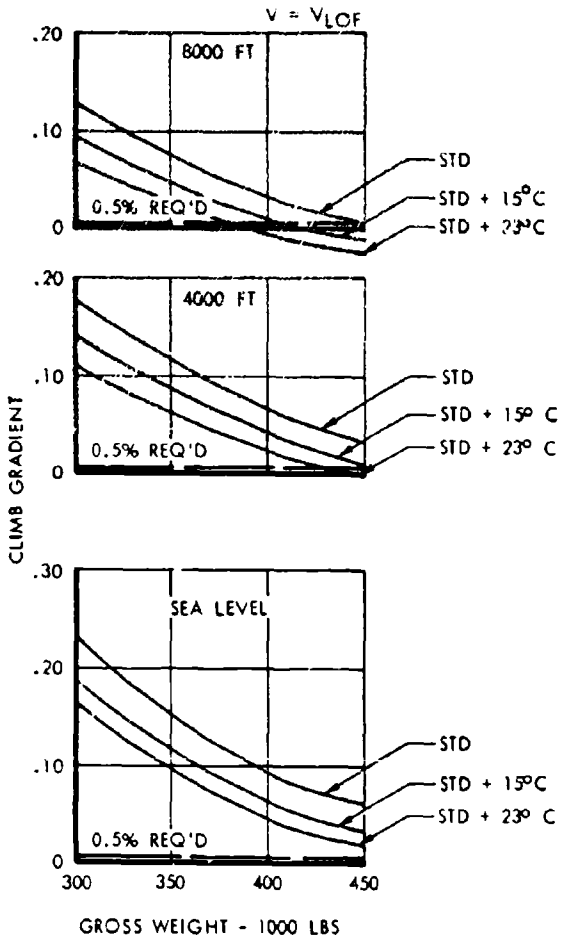

FIGURE 5-46 FAA FIRST SEGMENT CLIMB GRAL NT
(ONE ENGINE INOPERATIVE—GEAR EXTENDED)

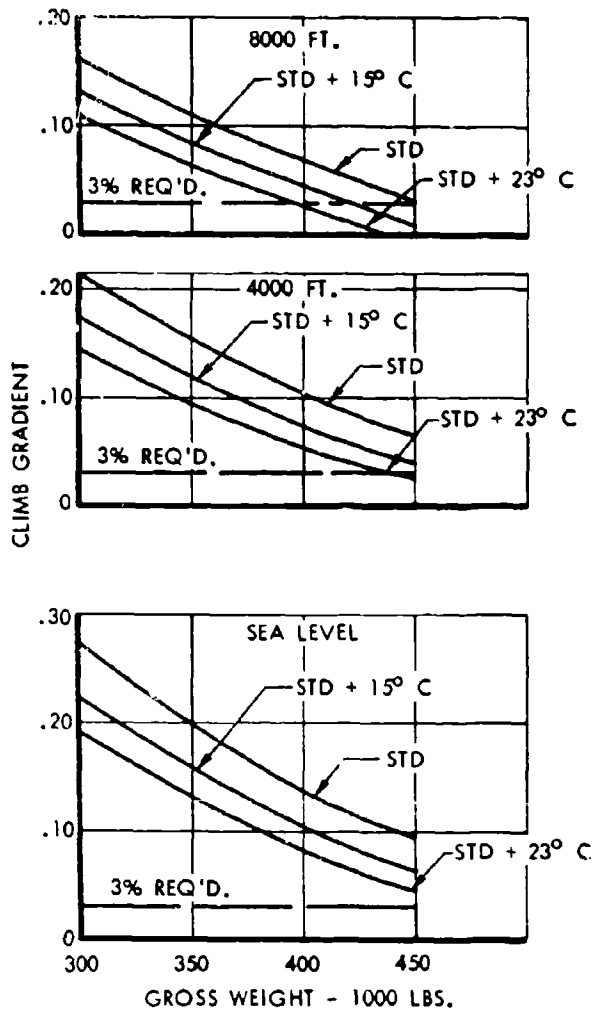

FIGURE 5-47 FAA SECOND SEGMENT CLIMB GRADIENT
(ONE ENGINE INOPERATIVE—GEAR RETRACTED)

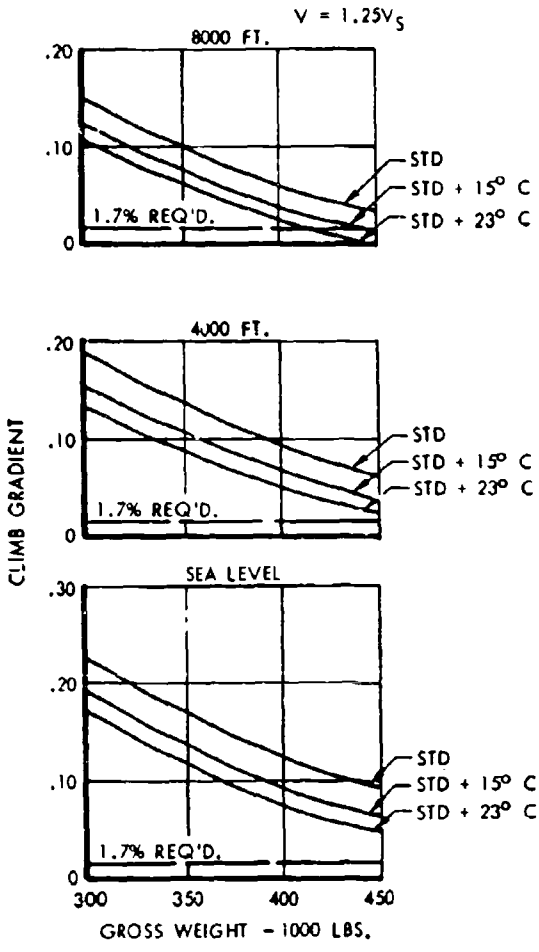

FIGURE 5-48 FAA FINAL TAKE-OFF CLIMB GRADIENT (ONE ENGINE INOPERATIVE—GEAR RETRACTED)

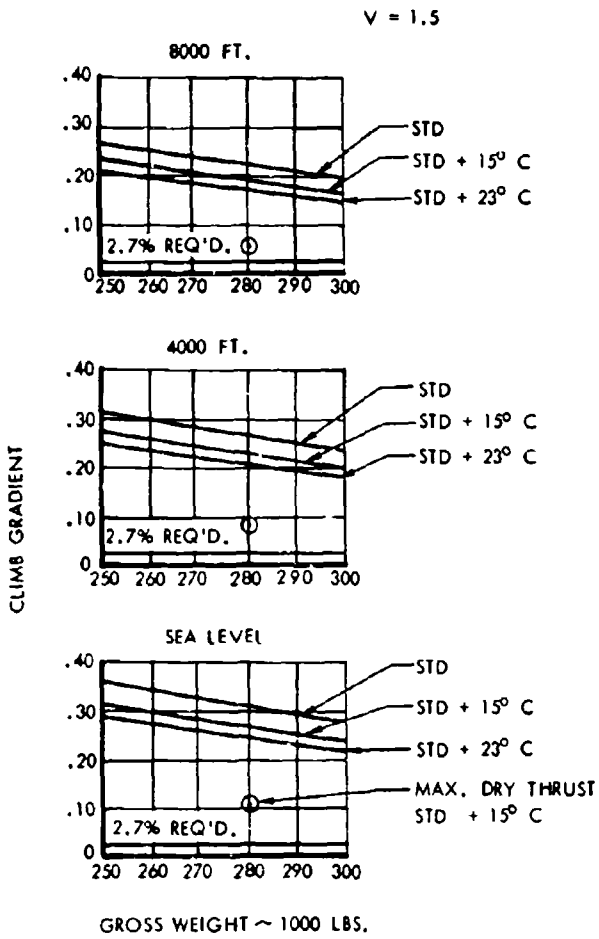

FIGURE 5-49 FAA APPROACH CLIMB GRADIENT (ONE ENGINE INOPERATIVE—GEAR RETRACTED)

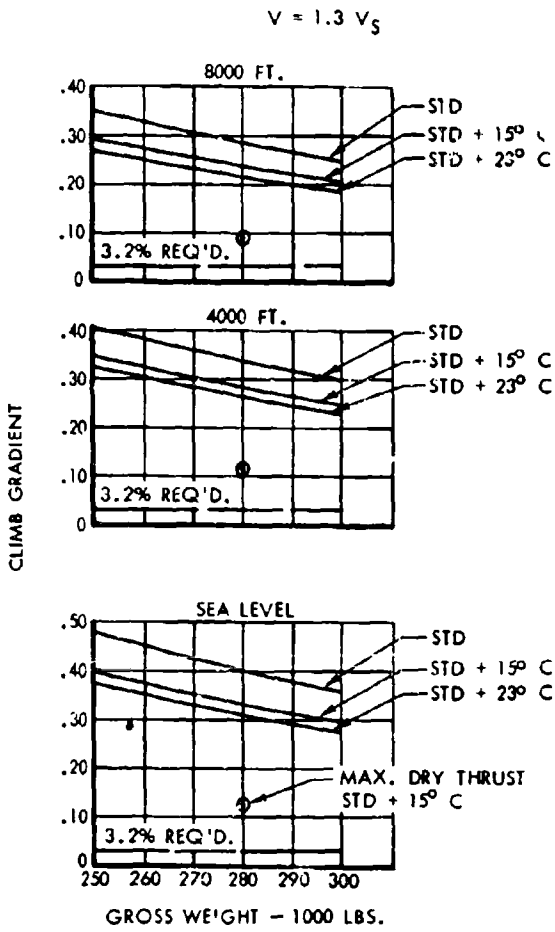

FIGURE 5-50 FAA ALL-ENGINE-OPERATING LANDING CLIMB (GEAR EXTENDED)

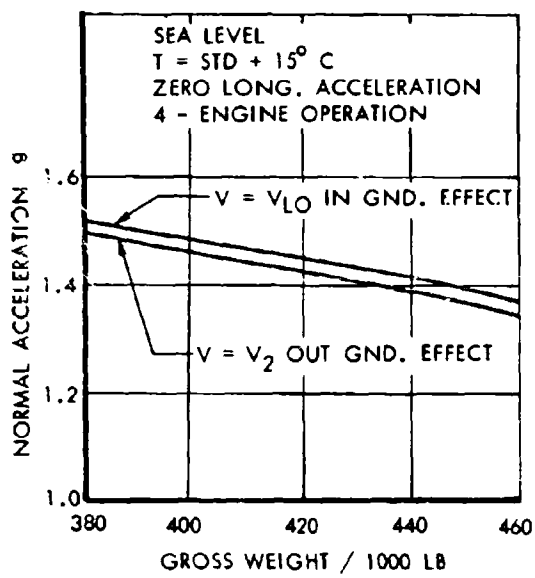

FIGURE 5-51 NORMAL LOAD FACTOR AVAILABLE ON TAKE-OFF

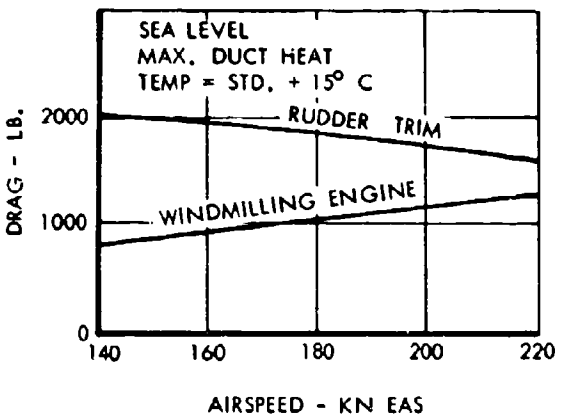

FIGURE 5-52 INCREMENTAL DRAG WITH ONE OUTBOARD INOPERATIVE ENGINE

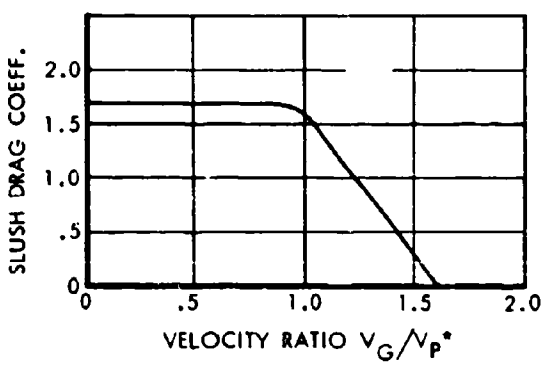

* V_G = GROUND SPEED
V_P = HYDROPLANING SPEED = $9\sqrt{\text{TIRE PRESS}}$

FIGURE 5-53 SLUSH DRAG COEFFICIENT

4. A 3-engine airborne acceleration from the point of lift-off to a height of 35 feet. During this segment, the airplane attempts to maintain a constant lift coefficient, and as the speed increases to the take-off safety speed, V_2, a curvilinear flight path develops. As the climb path and velocity increase, longitudinal acceleration decreases. If it becomes zero the lift coefficient is reduced and constant velocity and climb gradient are held.

Ground effects on lift and drag, and elevon trim drag effects are included in the calculations. The landing gear drag is held at its full value for the total retraction time of 12 seconds.

The abort portion of the balanced field lengths is computed by assuming engine failure at V_1 followed by two second free roll, after which brakes are applied. Three engines are at idle thrust and one is windmilling during this segment.

The computer program iterates on V_1 until the field length is balanced between the accelerate-climb and accelerate-stop distance, or the minimum rotation speed is reached. If the minimum rotation speed tends to be exceeded by V_1, the field length becomes unbalanced and the accelerate-stop distance becomes shorter than the accelerate-climb distance. This occurs over certain portions of the take-off spectrum because of the high acceleration capability of the SST. Four-engine take-offs are computed using the same V_1 and V_R speeds. If 1.15 times the four-engine distance exceeds the three-engine distance it becomes the CAR field length.

Rolling and braking friction coefficients employed in the analysis are:

Rolling	$\mu_R = 0.025$
Braking	
Dry runway	$\mu_B = 0.35$
Wet runway	$\mu_B = .15$
Wet runway, worn tires	$\mu_B = .12$

These coefficients have been developed from data presented in reference 5-3 and are achievable with an an anti-skid system.

The effects of slush on the take-off distance have been considered as follows: (1) slush drag from the main gear has been calculated assuming no slush impingement on the aircraft due to the aft location of the gear, (2) slush drag from the nose gear has been calculated assuming a 25% increase in drag due to impingement against adjacent structure, and (3) slush drag coefficients employed are shown in Figure 5-53 and have been taken from reference 5-4.

The total CAR landing distance is made up of the air distance required to touchdown from 50 feet altitude and a ground roll distance required to bring the airplane to a stop. The air distance has been estimated by the Controlled Sinking Speed Method. With this method the approach airspeed is set at 1.3 V_{MIN} with power sufficient to maintain a steady 2.5° glide path. Power is maintained at this setting during the flare maneuver. Sinking speed at touchdown is established conservatively at 4 feet/second. This method has been shown to correlate well with flight test data on several aircraft. The ground distance is made up of a four second free roll (to get nose wheel down and brakes on) followed by full brake application to zero velocity.

5.9 ENGINE PERFORMANCE CHARACTERISTICS

The performance characteristics of the Pratt and Whitney JT11F-4 engine as defined by the engine manufacturers model specification 2674 and including all installation effects and the bleed and power extraction values associated with normal operation of the SST are presented in Figures 5-54 through 5-69. These data encompass all thrust settings and are presented for the speed, altitude, and temperature ranges for which airplane performance information is calculated.

All of the engine performance data presented in Figures 5-54 through 5-69 are representative for the present status of the SST airplane performance, and are completely substantiated in the Propulsion Report, Volume A-VI. At the end of the Phase II period it is anticipated that further engine development will result in a nominal reduction in the specific fuel consumption at supersonic speeds. The performance analysis of the SST presented herein includes a reduction in the supersonic specific fuel consumption of 1.75 percent which is not reflected in the data in Figures 5-54 through 5-69.

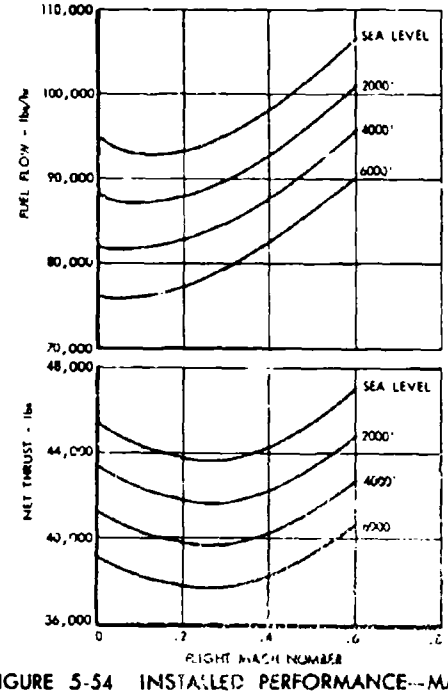

FIGURE 5-54 INSTALLED PERFORMANCE--MAXIMUM DUCT HEATING--PRATT & WHITNEY JT11F-4, U. S. STANDARD ATMOSPHERE, 1962

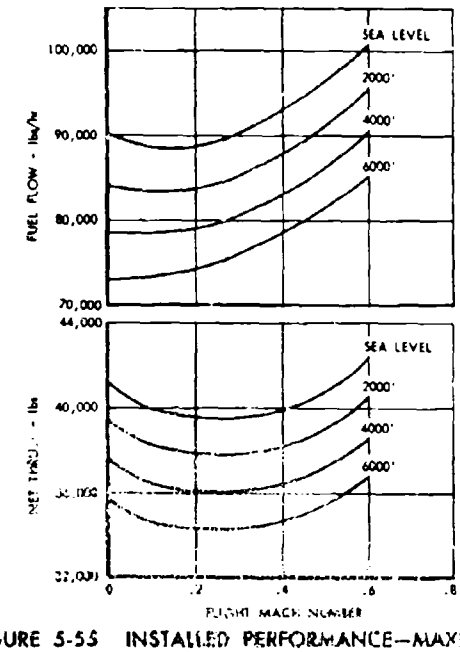

FIGURE 5-55 INSTALLED PERFORMANCE--MAXIMUM DUCT HEATING--PRATT AND WHITNEY JT11F-4, U. S. STANDARD ATMOSPHERE, 1962 (+15°C)

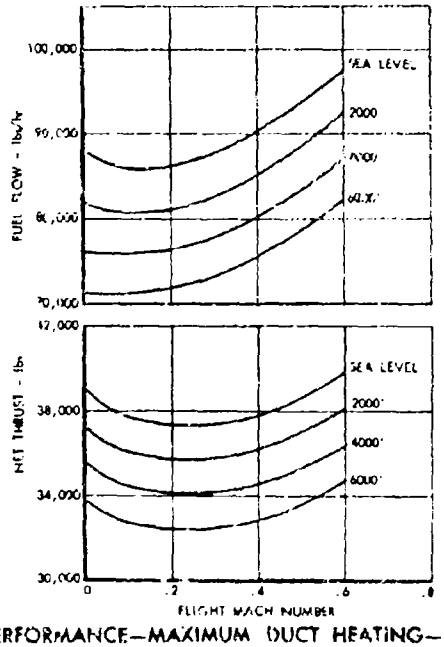

FIGURE 5-56 INSTALLED PERFORMANCE--MAXIMUM DUCT HEATING--PRATT AND WHITNEY JT11F-4, U. S. STANDARD ATMOSPHERE, 1962 (+23°C)

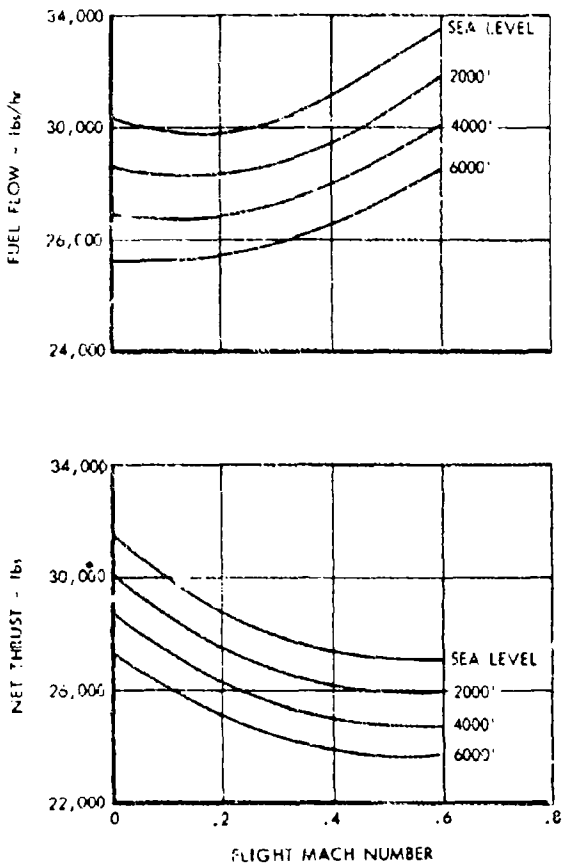

FIGURE 5-57 INSTALLED PERFORMANCE—MINIMUM DUCT HEATING—PRATT AND WHITNEY JT11F-4, U. S. STANDARD ATMOSPHERE, 1962

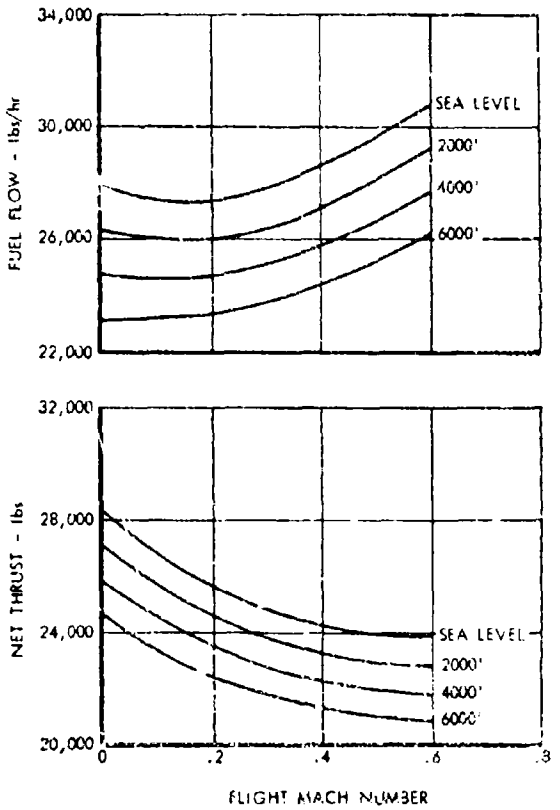

FIGURE 5-58 INSTALLED PERFORMANCE—MINIMUM DUCT HEATING—PRATT AND WHITNEY JT11F-4, U. S. STANDARD ATMOSPHERE, 1962 (+15°C)

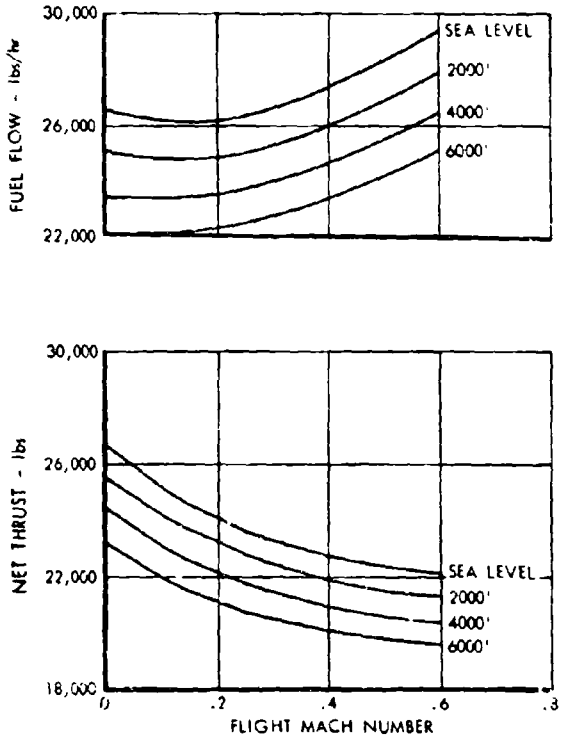

FIGURE 5-59 INSTALLED PERFORMANCE—MINIMUM DUCT HEATING—PRATT AND WHITNEY JT11F-4, U. S. STANDARD ATMOSPHERE, 1962 (+23°C)

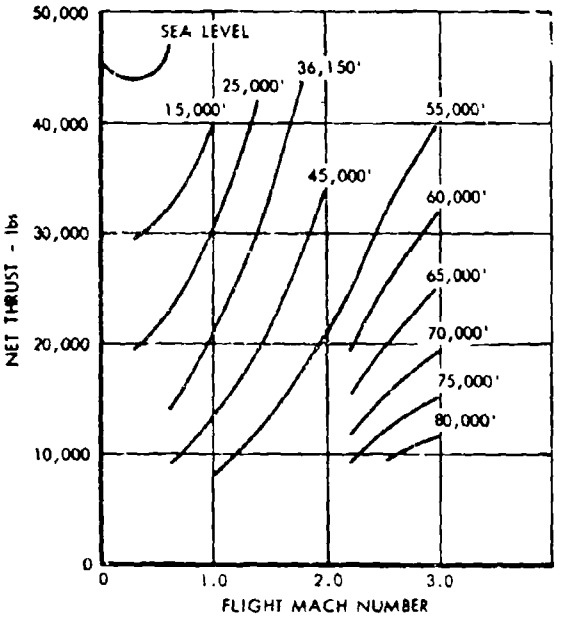

FIGURE 5-60 INSTALLED THRUST—MAXIMUM DUCT HEATING—PRATT AND WHITNEY JT11F-4, U. S. STANDARD ATMOSPHERE, 1962

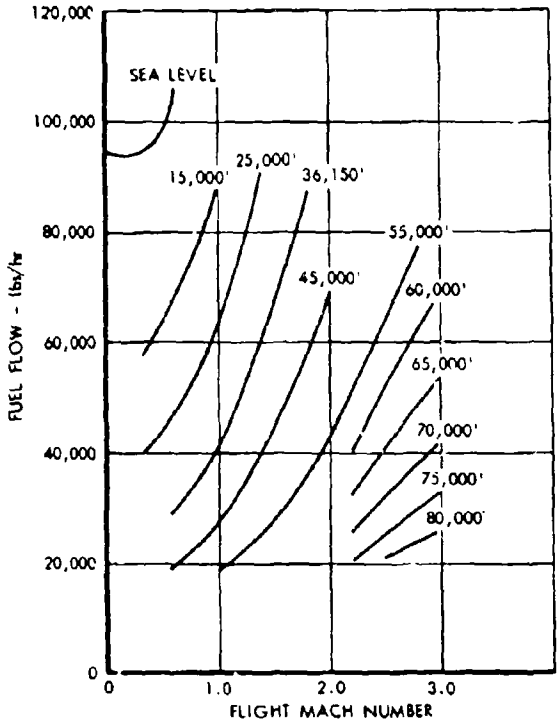

FIGURE 5-61 INSTALLED FUEL FLOW—MAXIMUM DUCT HEATING—PRATT AND WHITNEY JT11F-4, U. S. STANDARD ATMOSPHERE, 1962

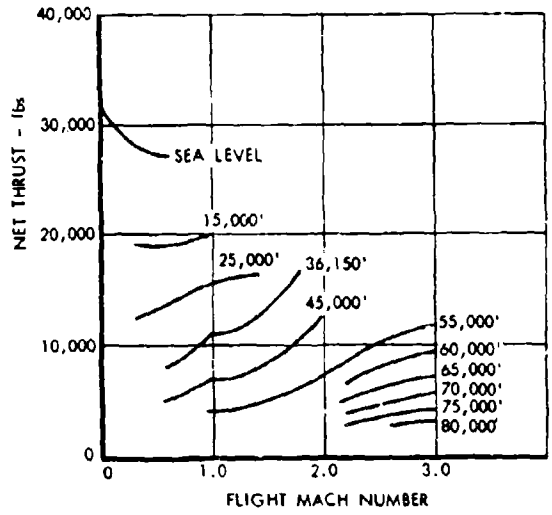

FIGURE 5-62 INSTALLED THRUST—MINIMUM DUCT HEATING—PRATT AND WHITNEY JT11F-4, U. S. STANDARD ATMOSPHERE, 1962

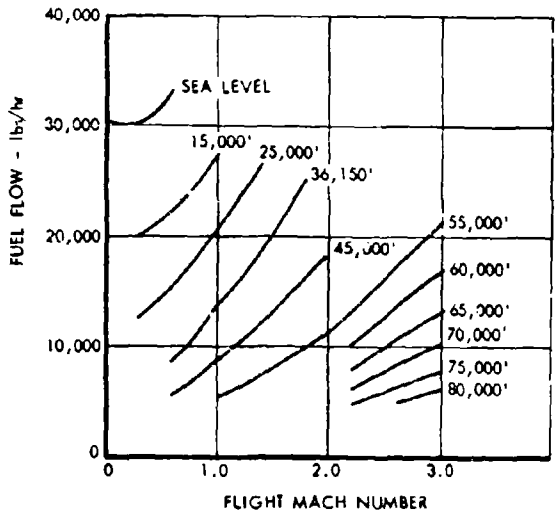

FIGURE 5-63 INSTALLED FUEL FLOW—MINIMUM DUCT HEATING—PRATT AND WHITNEY JT11F-4, U. S. STANDARD ATMOSPHERE, 1962

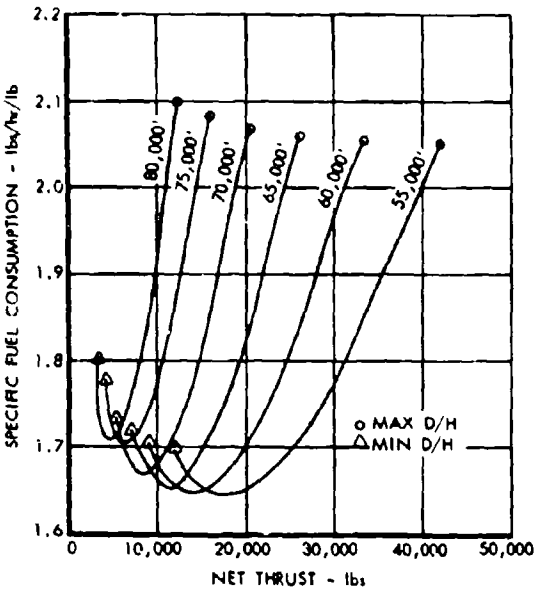

FIGURE 5-64 INSTALLED MACH 3.0 PERFORMANCE—PARTIAL DUCT HEATING—PRATT AND WHITNEY JT11F-4, U. S. STANDARD ATMOSPHERE, 1962

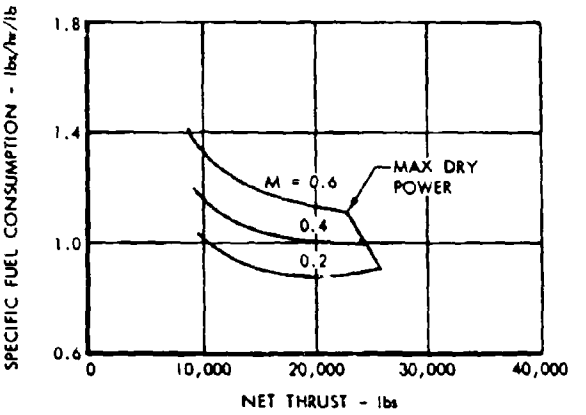

FIGURE 5-65 INSTALLED DRY PERFORMANCE—SEA LEVEL—PRATT AND WHITNEY JT11F-4, U. S. STANDARD ATMOSPHERE, 1962

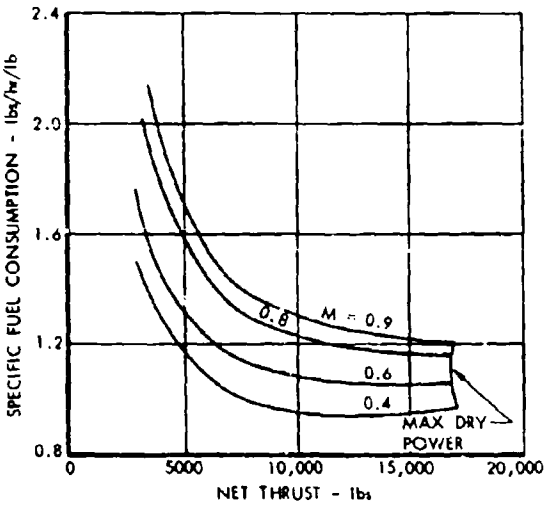

FIGURE 5-66 INSTALLED DRY PERFORMANCE—15,000 FEET—PRATT AND WHITNEY JT11F-4, U. S. STANDARD ATMOSPHERE, 1962

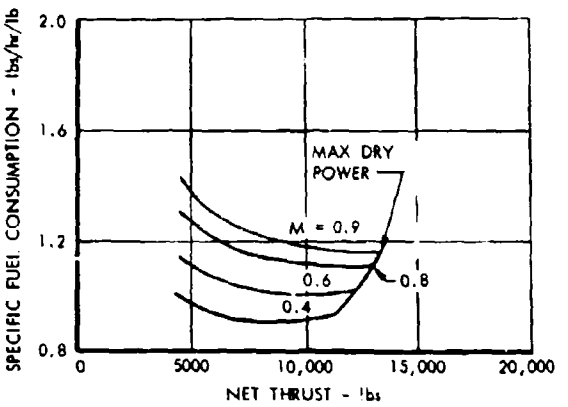

FIGURE 5-67 INSTALLED DRY PERFORMANCE— 25,000 FEET—PRATT AND WHITNEY JT11F-4, U. S. STANDARD ATMOSPHERE, 1962

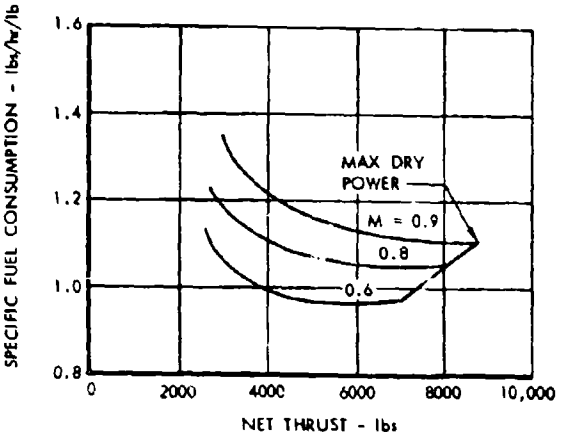

FIGURE 5-68 INSTALLED DRY PERFORMANCE— 36,150 FEET—PRATT AND WHITNEY JT11F-4, U. S. STANDARD ATMOSPHERE, 1962

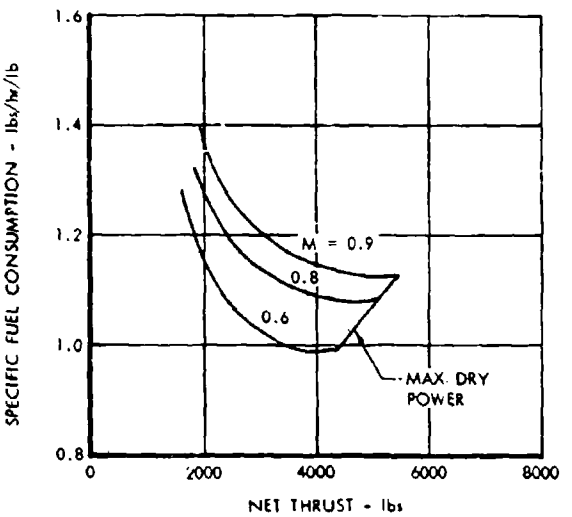

FIGURE 5-69 INSTALLED DRY PERFORMANCE— 45,000 FEET—PRATT AND WHITNEY JT11F-4, U. S. STANDARD ATMOSPHERE, 1962

5.10 SECTION 5 REFERENCES

5-1. Special Civil Air Regulation SR-422B, dated July 9, 1959.

5.2 Anon. Tentative Airworthiness Objectives and Objectives for Supersonic Transport Design Proposals. Flight Standards Service. FAA. August 15, 1963.

5-3. Horne, Walter B.; Leland, Trafford J. W. Runway Slipperiness and Slush. Journal of the Royal Aeronautical Society. Sept 1963.

5-4. Horne, Walter B.; Leland, Trafford J. W. Prediction of Slush Drag on Aircraft Performance. FAA and NASA Joint Technical Conference on Slush Drag and Braking Problems. Dec. 1961.

SECTION 6 STABILITY AND CONTROL ANALYSIS (3.2.8)

The stability and control analysis summarized in this section is the result of more than eight years of continuous study and wind tunnel testing as part of the supersonic transport research program. In addition, the broad background of analytical and flight experience gained in the F-104 program is, in many cases, directly aplicable. The stability and control analysis is based on the substantiating and correlating summary data of the basic aerodynamic characteristics presented in Section 4.

Static stability characteristics are determined in complince with CAR 4b and it will be shown that the aircraft as proposed requires no deviations. MIL-F-8785 is used in providing standards for acceptable dynamic stability characteristics. These are supplemented, where applicable, by additional criteria such as those provided by Cornell Aeronautical Laboratory and NASA studies and the SAE's "Airworthiness Recommended Practice Draft Bulletin." The experience gained in the high speed, high altitude F-104 program is also used for general guidance.

Particular consideration is given to aircraft handling qualities without stability augmentation to provide a definitive statement of requirements for the simplest control system capable of achieving a high level of flight line availability and minimizing the incidence of aborted flights.

The airplane demonstrates positive static stability margins both longitudinally and directionally under all flight conditions.

Longitudinal control is adequate to bring the airplane to the take-off attitude well before the take-off speed. Lateral and directional control are sufficient to provide a minimum engine out control speed of 123 knots as compared with a landing approach speed of 138 knots and a take-off rotation speed of 147 knots. Sufficient margins on control capability are available in all flight conditions in conjunction with adequate control system redundancy such that flight safety is retained even in the event of a dual control system failure. The reliability analysis indicates that a dual control system failure on a single flight is estimated to occur once in 50,000,000 flight hours.

The dynamic stability characteristics of the aircraft without damping augmentation of any kind are such that the aircraft is safely flyable dampers off, under all flight conditions. A damper failure, therefore, should not result in an aborted flight. A pitch damper and a yaw damper are desirable, however, to enhance passenger comfort and to minimize crew fatigue in cruise. A roll damper may prove desirable to minimize the roll to yaw ratio during the landing approach. F-104 experience indicates that a roll damper will enhance rough weather operation notwithstanding the fact that the Dutch roll mode in the landing approach is heavily damped without damping augmentation of any kind.

The following paragraphs provide a presentation of the handling qualities of the supersonic transport. The comprehensive low speed and high speed wind tunnel test data, which provides the basis for these estimates, are presented in Section 4. The aeroelastic corrections to the wind tunnel data are included. Future programs to further define aircraft handling qualities and refine the control system design are described. These include additional wind tunnel test analyses and both a ground based and flight simulator program.

6.1 CONTROL SYSTEM

Control of the SST is provided by conventional wing trailing edge flap type elevator and aileron surfaces and a conventional rudder. Provision for full time 3 axis damping augmentation is included.

The two middle wing flap surfaces provide both pitch and roll control. The wing tip surface provides only roll control and is deactivated when the landing gear is retracted. The inboard surface provides only pitch control.

The SST incorporates triple primary flight control hydraulic systems. These are irreversible, simul-

taneously-operating hydraulic systems; each one supplying one-third of the power required by each surface.

The fully irreversible system has longitudinal pilot forces provided by an artificial feel system with the force-rate varied as a function of stick position and airspeed. Maneuvering force gradients are provided by a bob weight installation. Feel characteristics for roll and directional control are provided artificially as a function of control position.

The variation of control force with control position is shown on Figure 6-1. The bob weight provides an incremental 30 pounds per "g" force. Figure 6-2 presents the linkage characteristics of wheel position and angle with pitch and roll control. Combined elevon control surface envelope is presented on Figure 6-3. Rudder pedal force versus rudder angle is presented on Figure 6-4.

Trim is effected through the main actuating cylinders by knobs on the pilots' wheels and the main console. Since the system is responsive to knob position it is fully modulated and the pilot may demand trim at the rate he desires up to the maximum rate of the trim motors. Maximum trim rate is one-half degree per second. Since the trim system does not effect movements of the control surfaces, but only provides forces at the control wheel and pedals, a mis-set or runaway trim system will not result in any loss in available control capability. For example, a runaway failure of the longitudinal trim system will only require a 14 pound force at the control wheel to overpower the system. Maximum available hinge moments from the three hydraulic systems as a function of elevator, aileron and rudder angle are presented in Figures 6-5 and 6-6.

An automatic stick shaker system is used, to provide minimum desired speed indication at high angles of attack. The minimum speed warning is provided by a device which shakes the control wheel when the normal operating boundary is exceeded. The system contains two angle of attack sensing elements. The stick shaker starts at an angle of attack of 17 degrees with increasing shaker actuation to a maximum amplitude at 20 degrees angle of attack. The speed V_{min}, associated with 20 degrees angle of attack, is a "minimum practicable speed" rather than a stall speed. At this speed there is a substantial lift margin and there is no significant departure from normal flight characteristics in longitudinal or directional stability as opposed to the case of previous transport configuration types. Similarly, the aircraft retains substantially full aileron, elevator, and rudder control effectiveness at the V_{min} shaker speed. Takeoff and landing operations, therefore, are conducted with safety margins which substantially exceed those provided by specification requirements. At supersonic speeds the stick shaker is actuated at an angle of attack of ten degrees.

The 3 axis damper configuration consists of the use of the three inboard sections of the wing trailing edge control for pitch dampers with ±2 degrees of authority, the two middle sections for roll dampers with ±5 degrees of authority, and the two lower sections of the rudder for yaw dampers with ±10 degrees of authority. In the gear down configuration the wing outboard trailing edge control surface also has the function of a roll damper.

The gain factor used for all damper surfaces is 2.5 degrees per degree per second in phase. The use of lag rate damping for pitch and yaw has also been considered.

6.2 LONGITUDINAL FLIGHT CHARACTERISTICS

6.2.1 STATIC LONGITUDINAL STABILITY

The static longitudinal stability characteristics are shown in Figures 6-7 through 6-12 for landing, approach, climb and cruise conditions for the critical airplane weight and center of gravity positions. The flexibility effects on aircraft characteristics are included.

In all conditions the airplane meets the CAR 4b requirement that the slope of the stick force-speed curve be in excess of one pound per six knots, and that the elevator-speed curve have a stable slope. For all conditions the speed range is that required by the Civil Air Regulations.

The transonic characteristics shown in Figure 6-11 are for the airplane without Mach trim compensation of any kind since the "tuck" characteristics occuring between Mach 1.0 and 1.1 are very mild. Aircraft characteristics with the landing gear extended as shown in Figure 6-12 are identical to those with the gear up as determined from wind tunnel tests.

6.2.2 SPEED THRUST STABILITY

The glide slope angle and the thrust to weight ratio for a typical landing approach on a constant 2½-

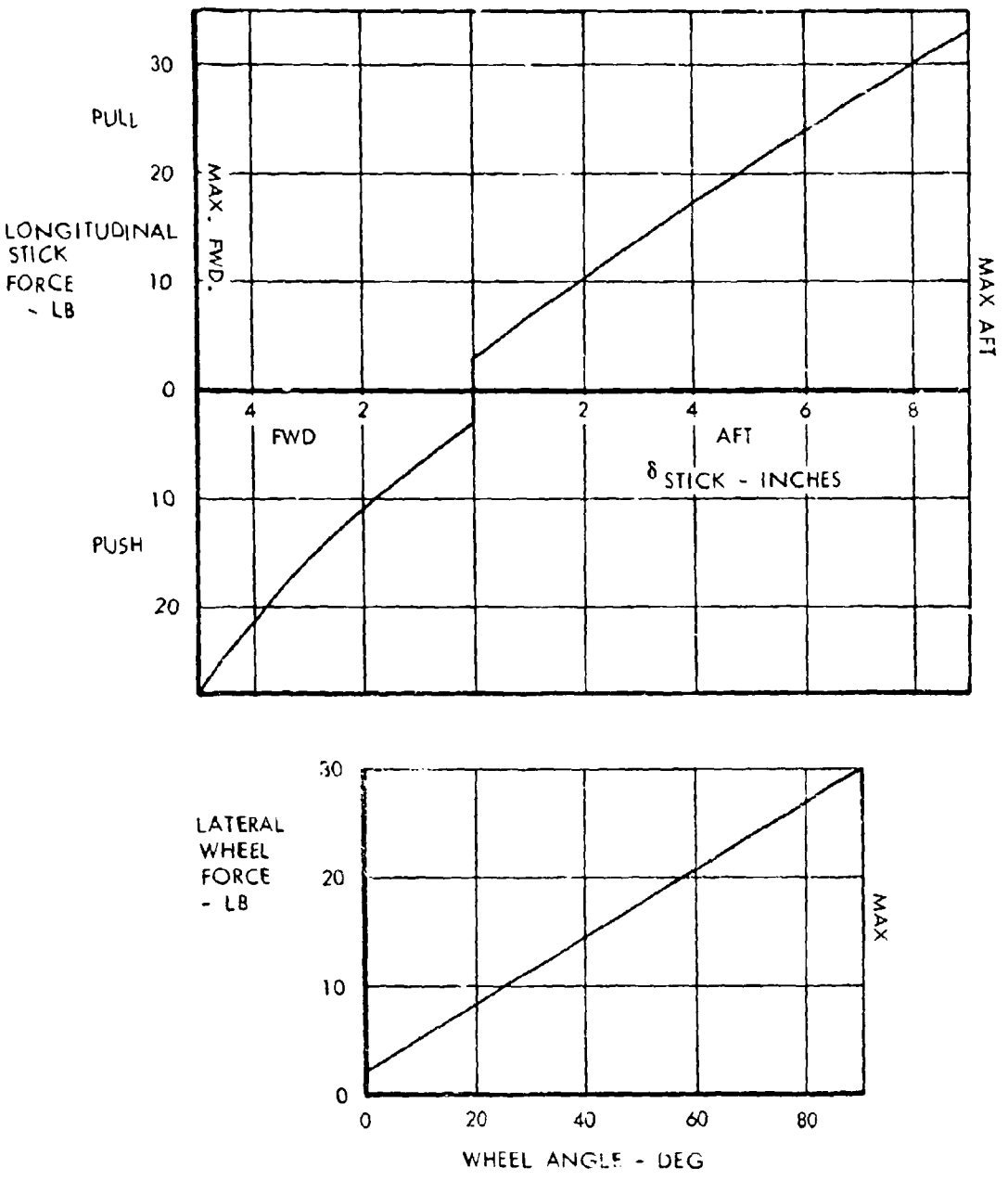

FIGURE 6-1 ELEVATOR-AILERON CONTROL FORCES

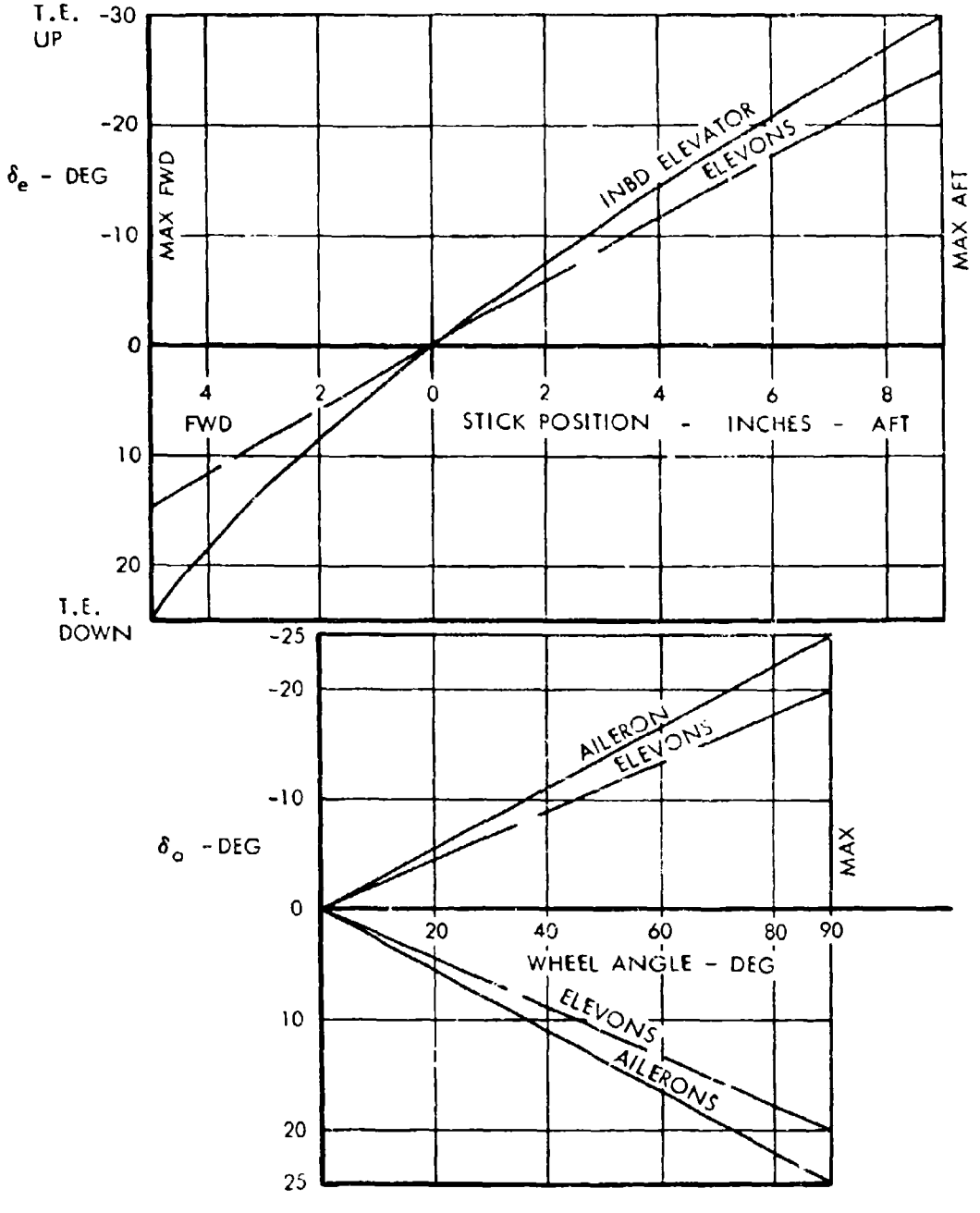

FIGURE 6-2 LONGITUDINAL LATERAL CONTROL SYSTEM CHARACTERISTICS

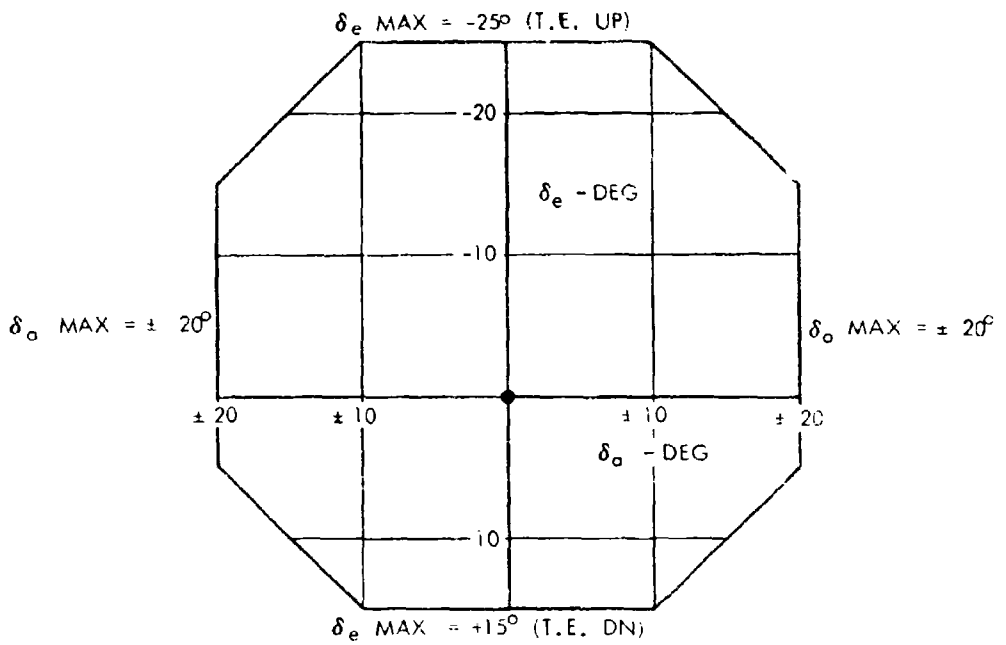

FIGURE 6-3 COMBINED ELEVON CONTROL SURFACE ENVELOPE

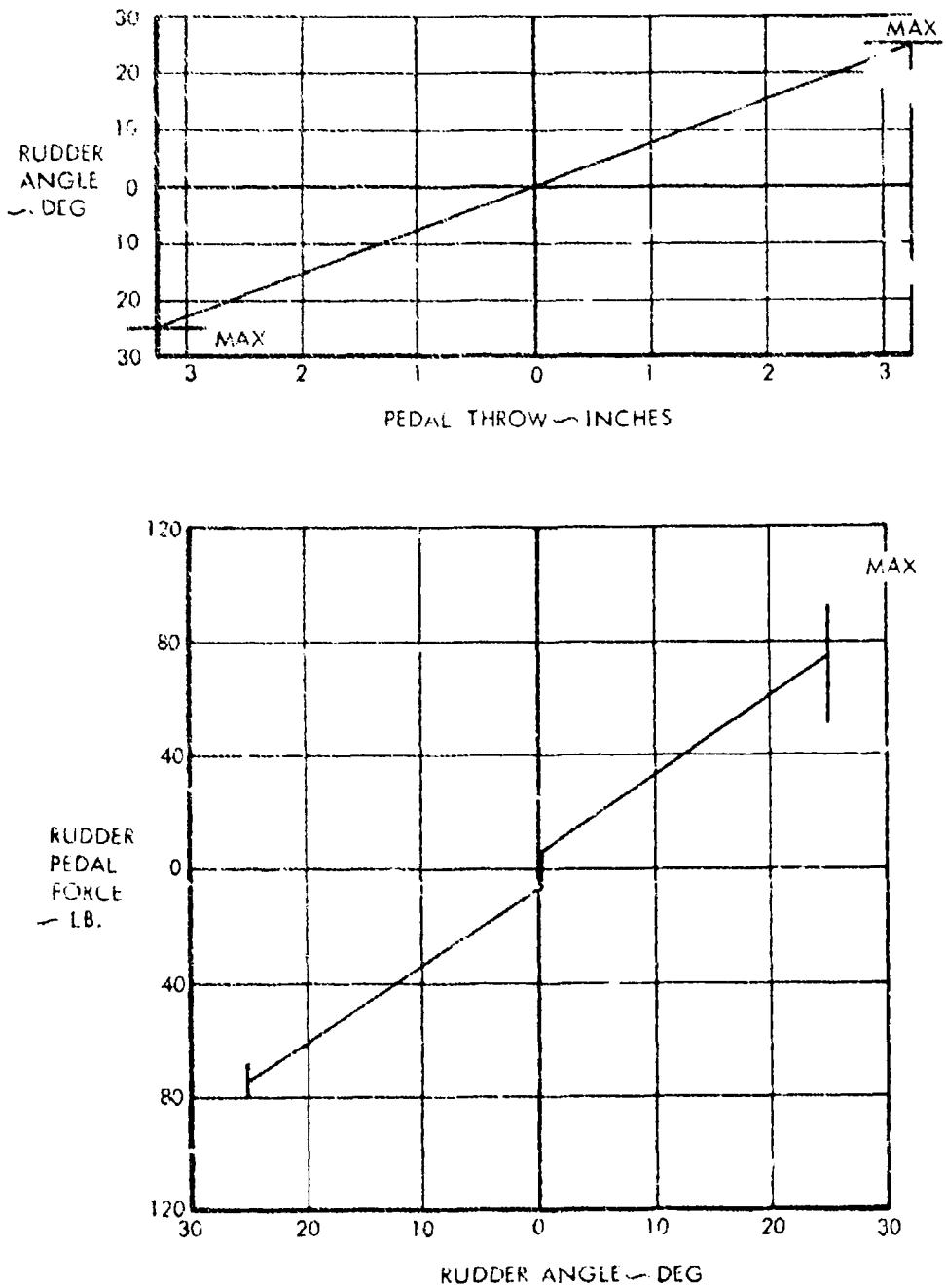

FIGURE 6-4 RUDDER PEDAL FORCE

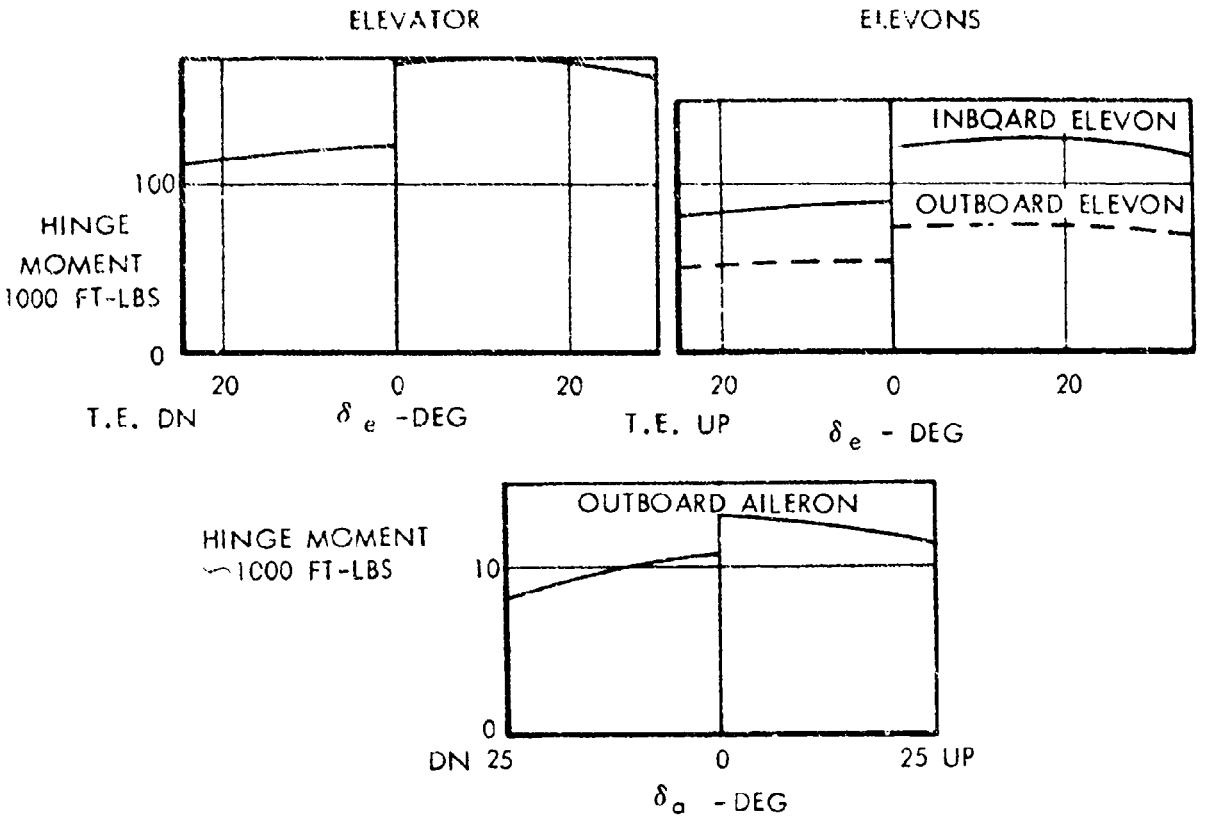

FIGURE 6-5 AVAILABLE ELEVATOR AND AILERON HINGE MOMENTS

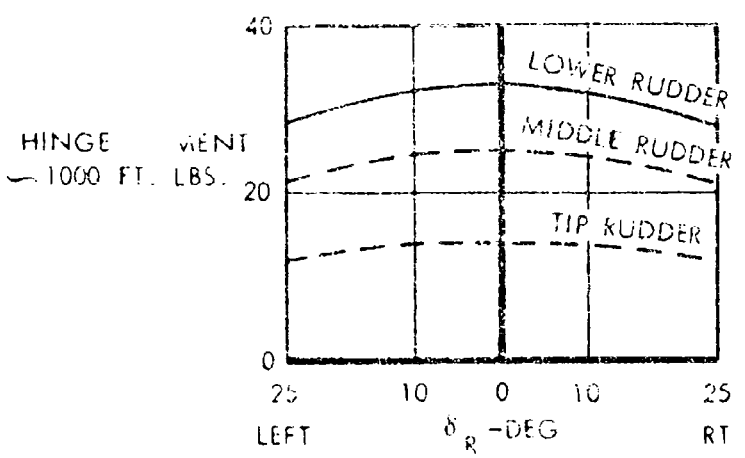

FIGURE 6-6 AVAILABLE RUDDER HINGE MOMENTS

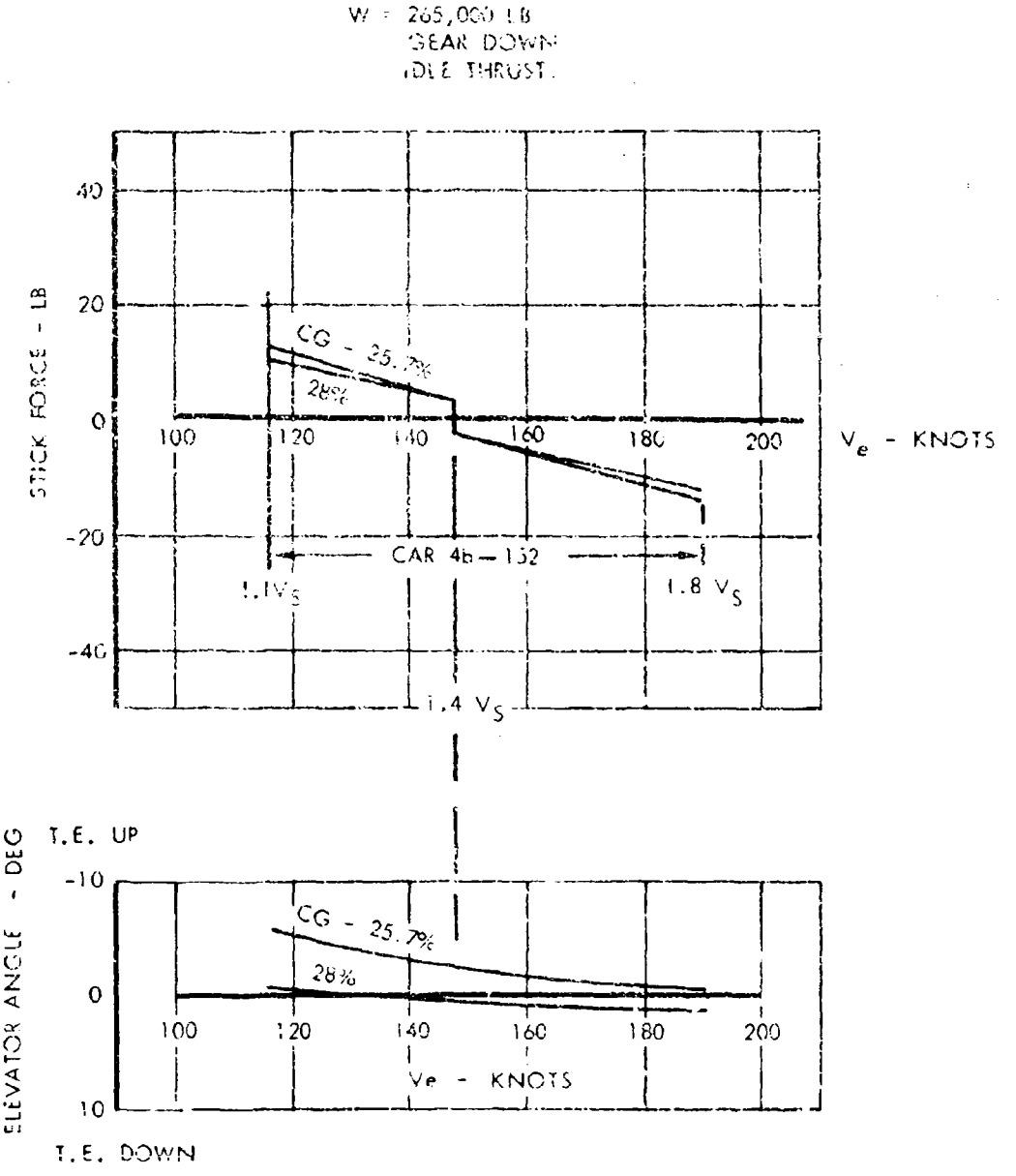

FIGURE 6-7 STATIC LONGITUDINAL STABILITY--LANDING

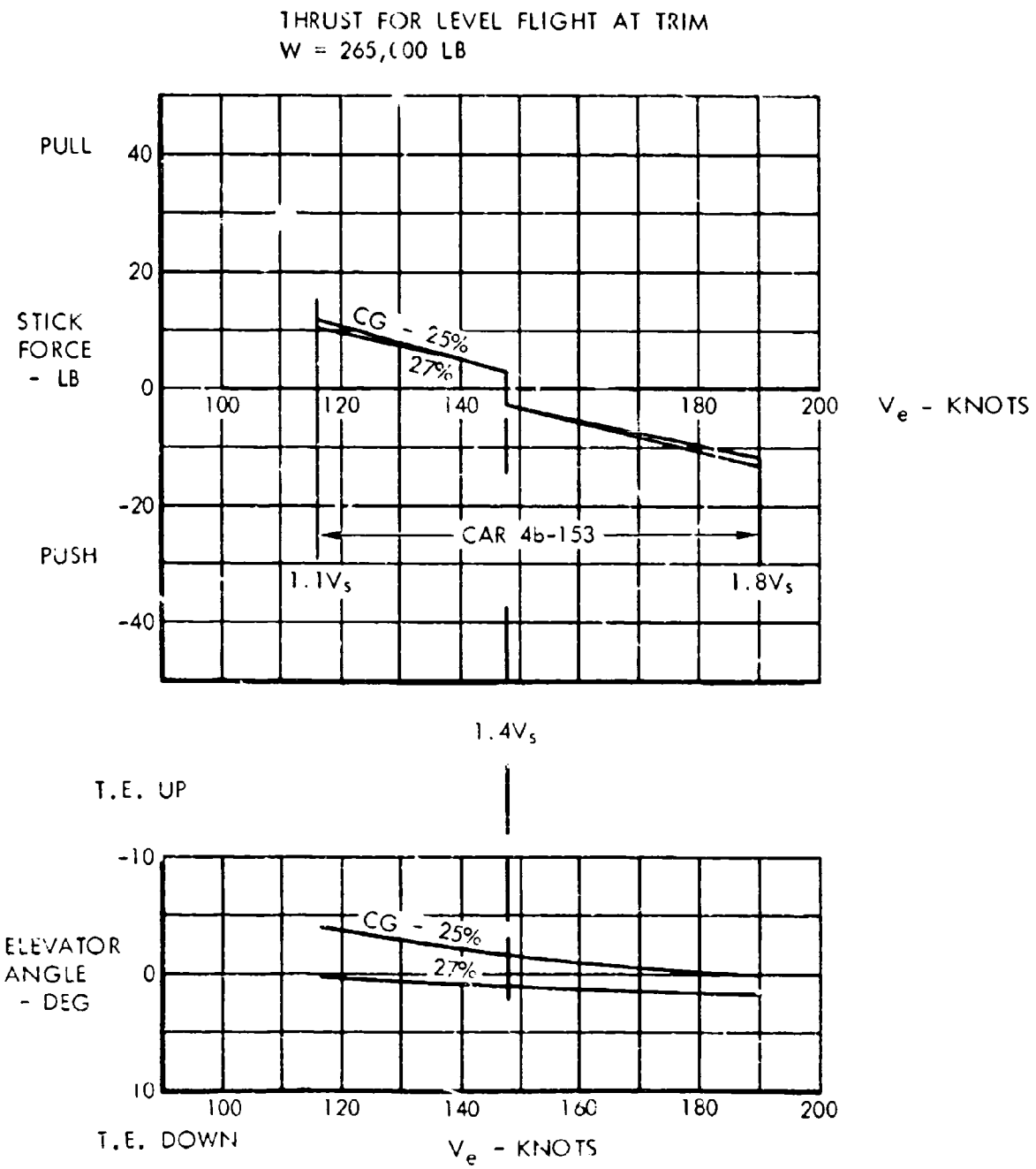

FIGURE 6-8 STATIC LONGITUDINAL STABILITY—APPROACH

W = 442,000 LB
H = 3,000 FT

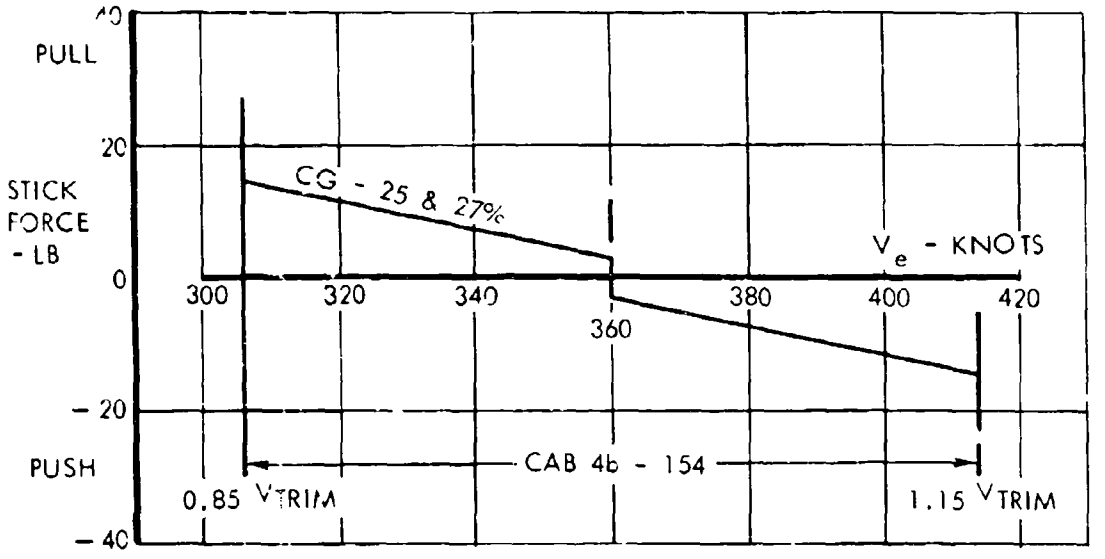

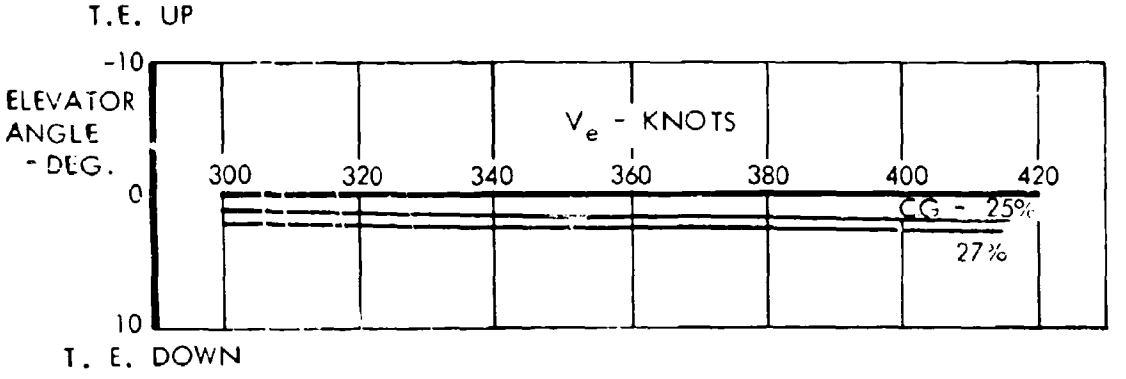

FIGURE 6.9 STATIC LONGITUDINAL STABILITY—CLIMB

W = 380,000 LB
H = 70,000 FT

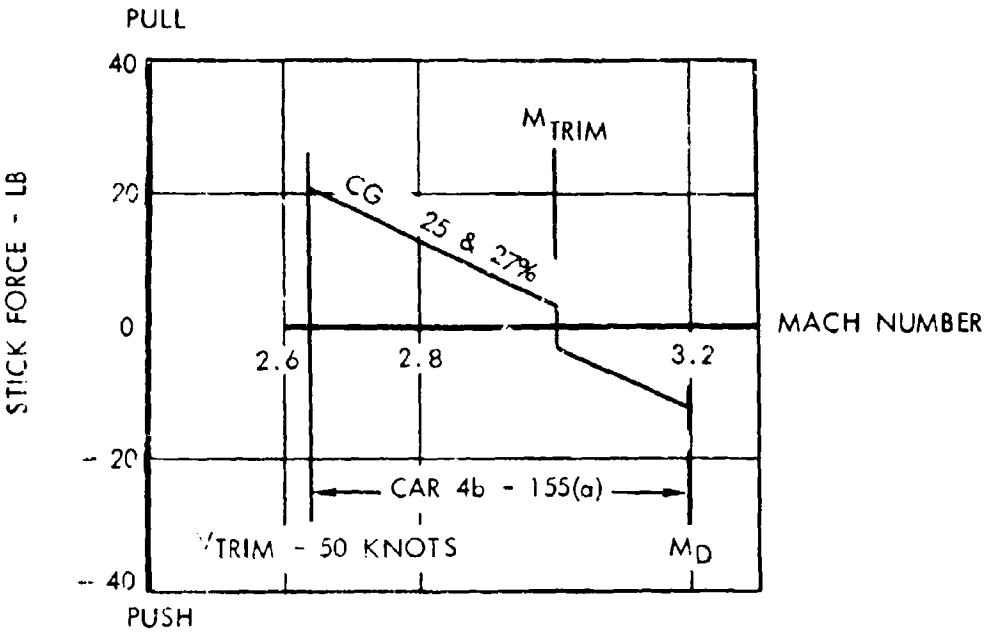

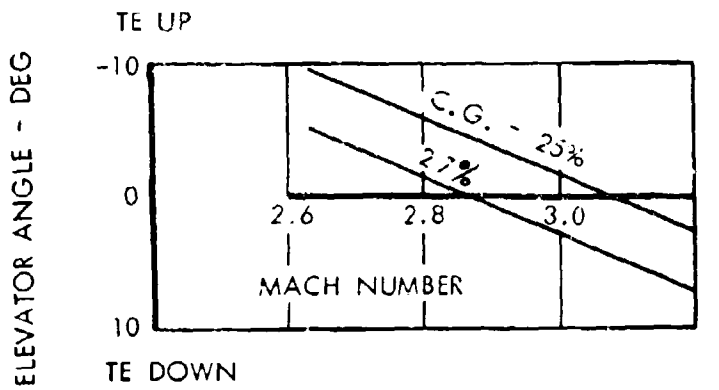

FIGURE 6-10 STATIC LONGITUDINAL STABILITY—MACH 3.0 CRUISE

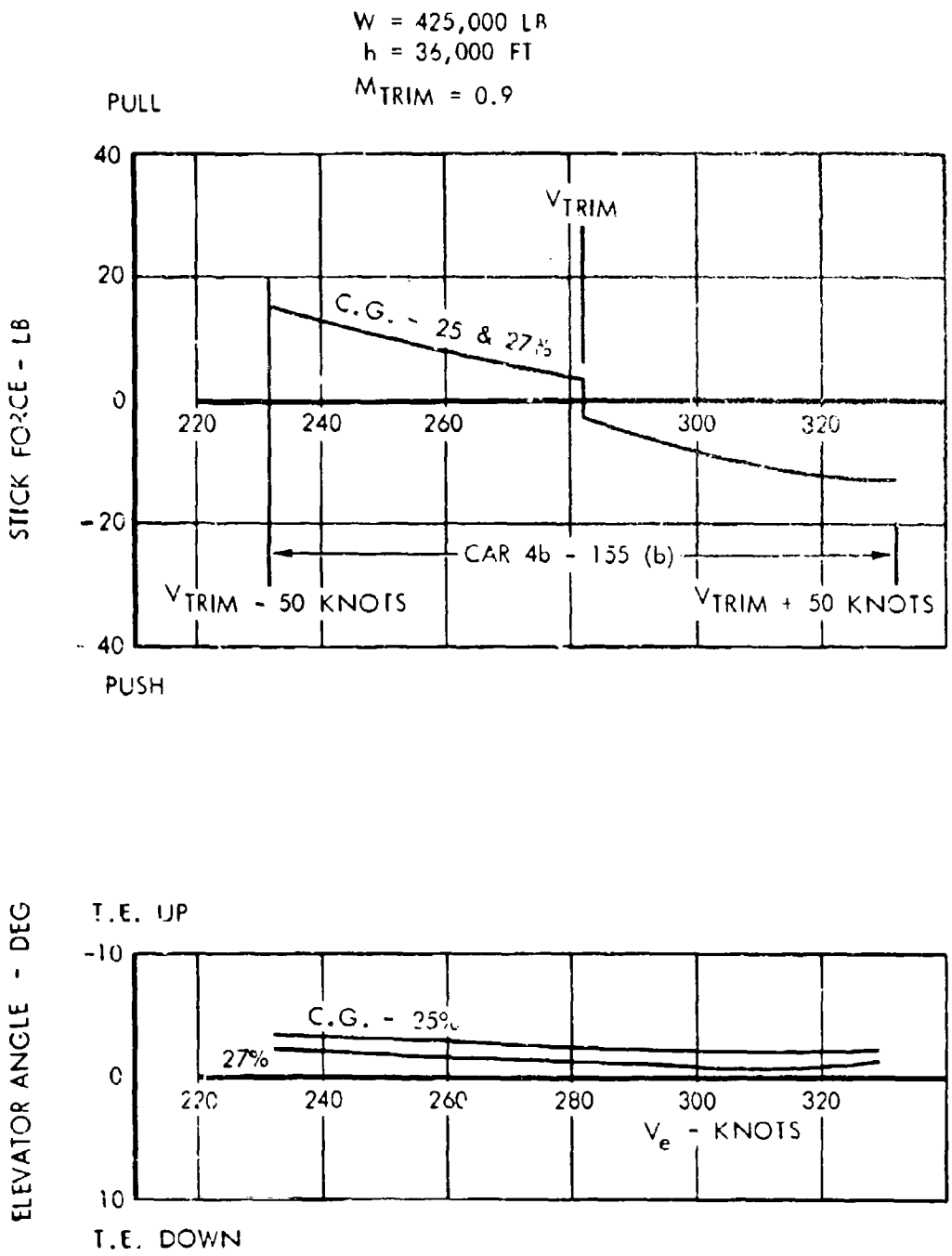

FIGURE 6-11 STATIC LONGITUDINAL STABILITY—SUBSONIC CRUISE

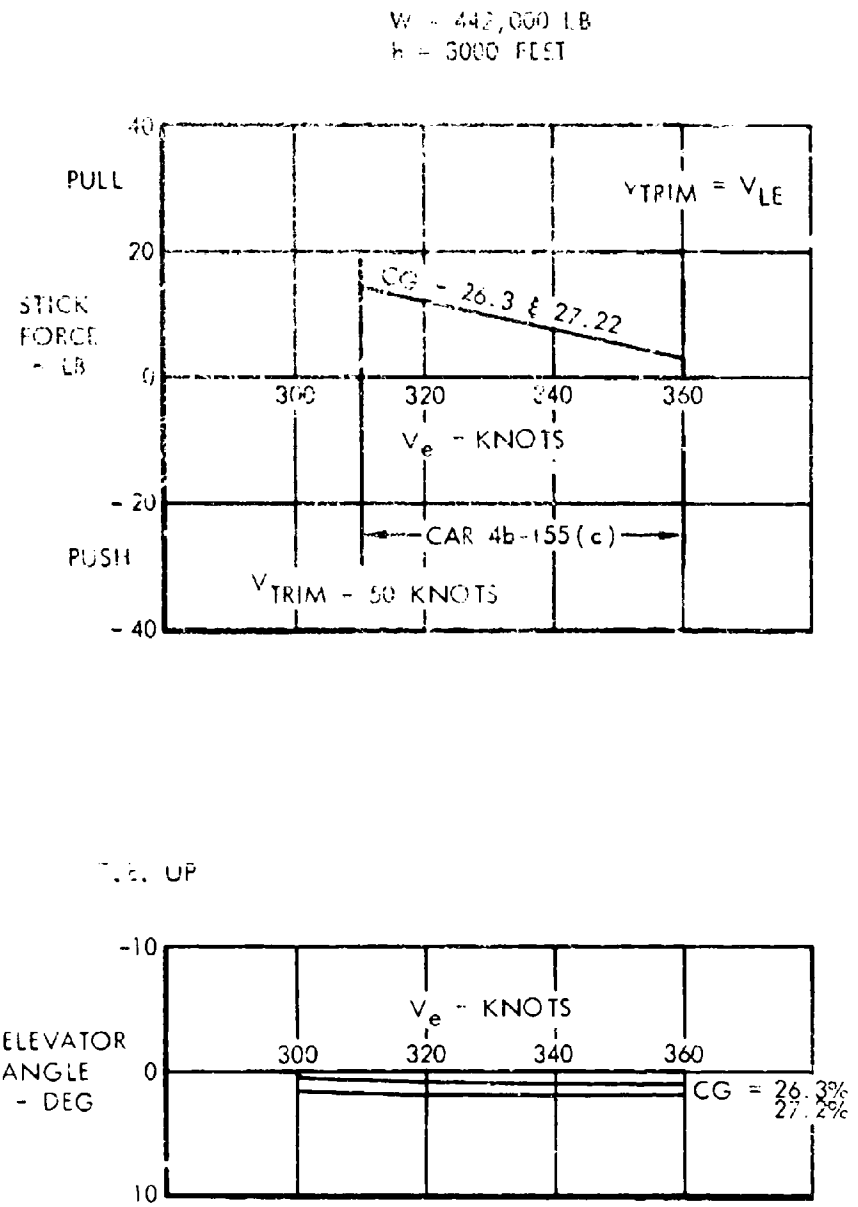

FIGURE 6-12 STATIC LONGITUDINAL STABILITY – CRUISE LANDING GEAR EXTENDED

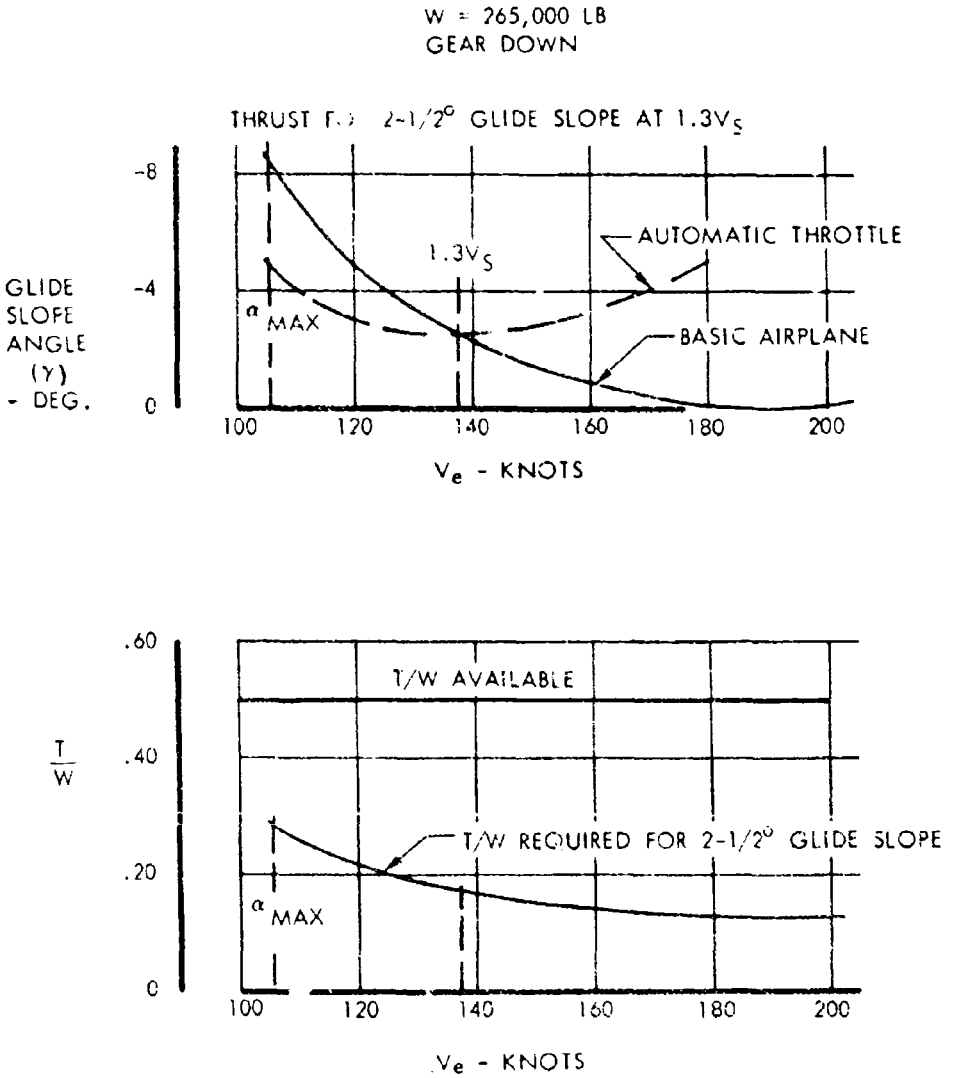

FIGURE 6-13 SPEED-THRUST STABILITY

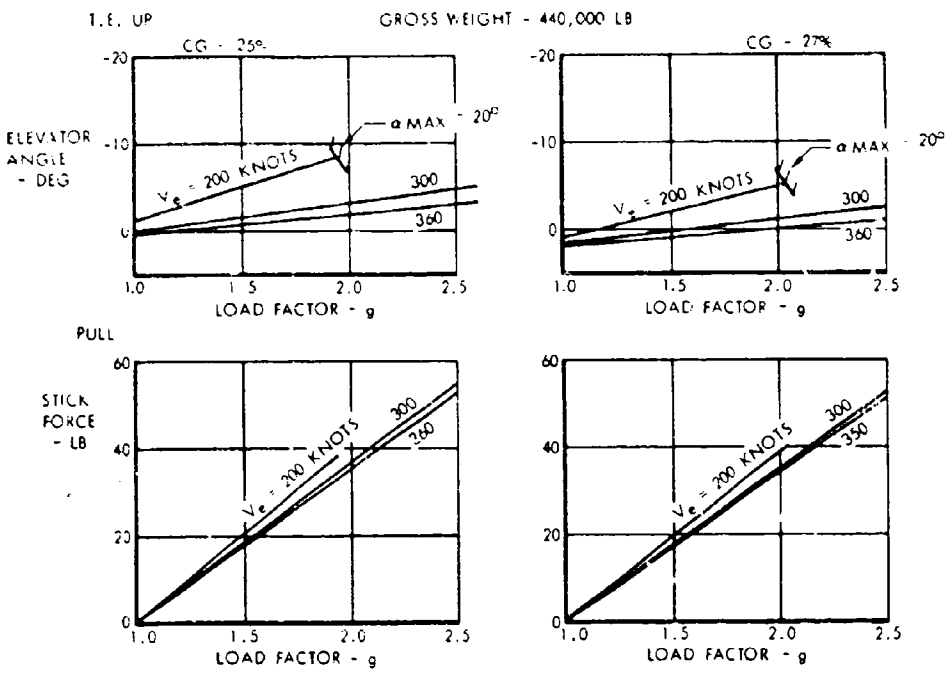

FIGURE 6-14 MANEUVERING CAPABILITY—SEA LEVEL

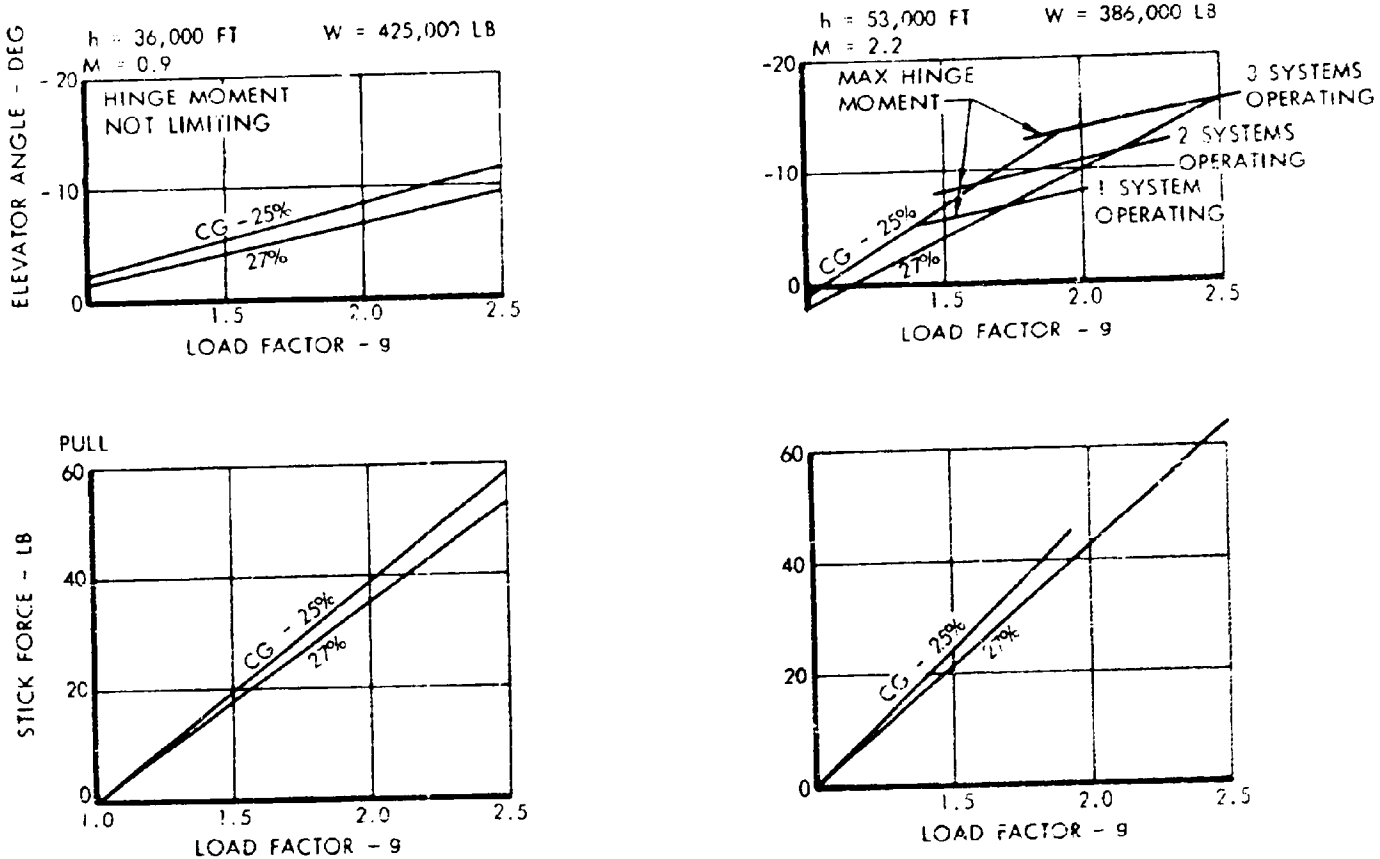

FIGURE 6-15 MANEUVERING CAPABILITY DURING CLIMB OUT

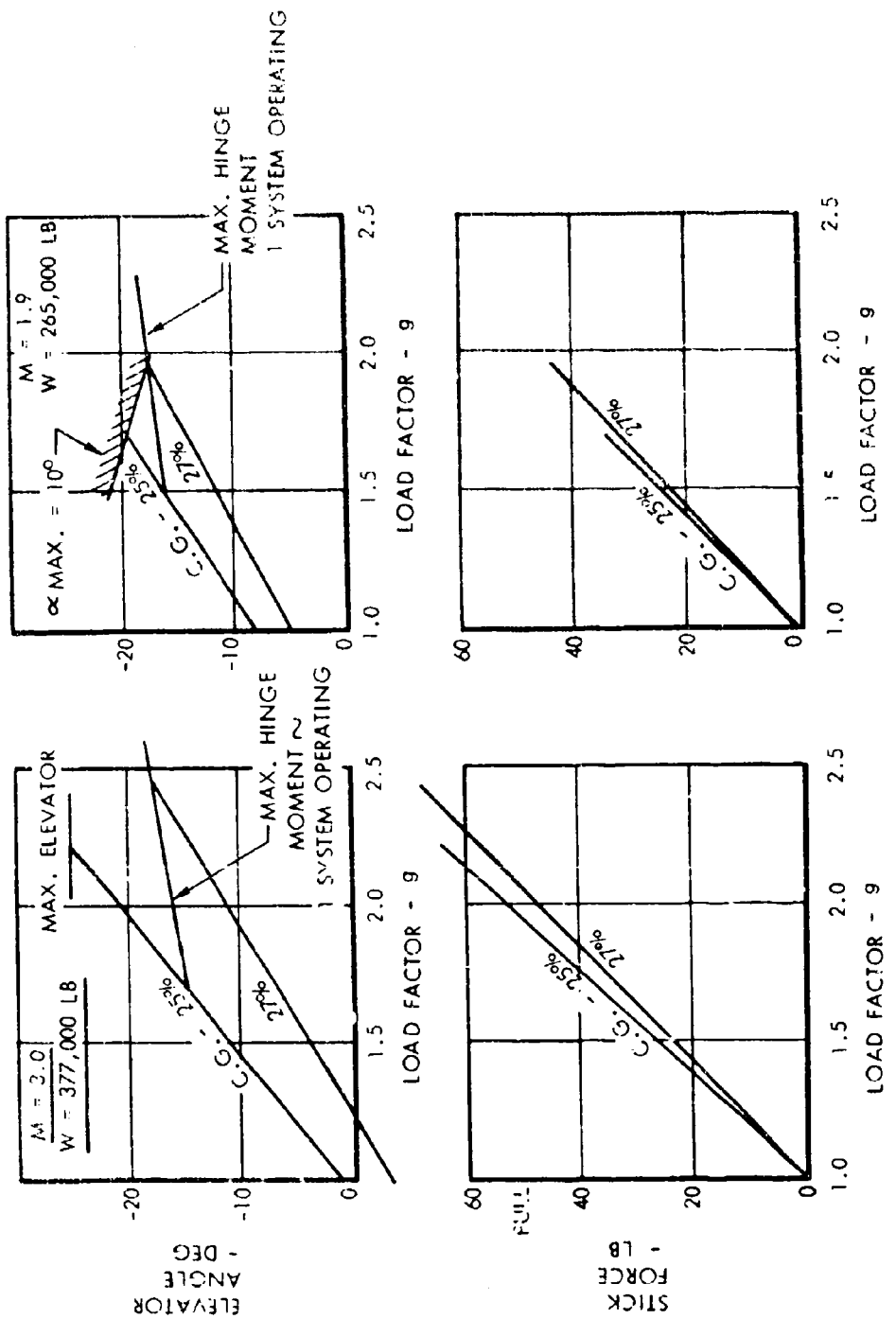

FIGURE 6-16 MANEUVERING CAPABILITY—70,000 FEET

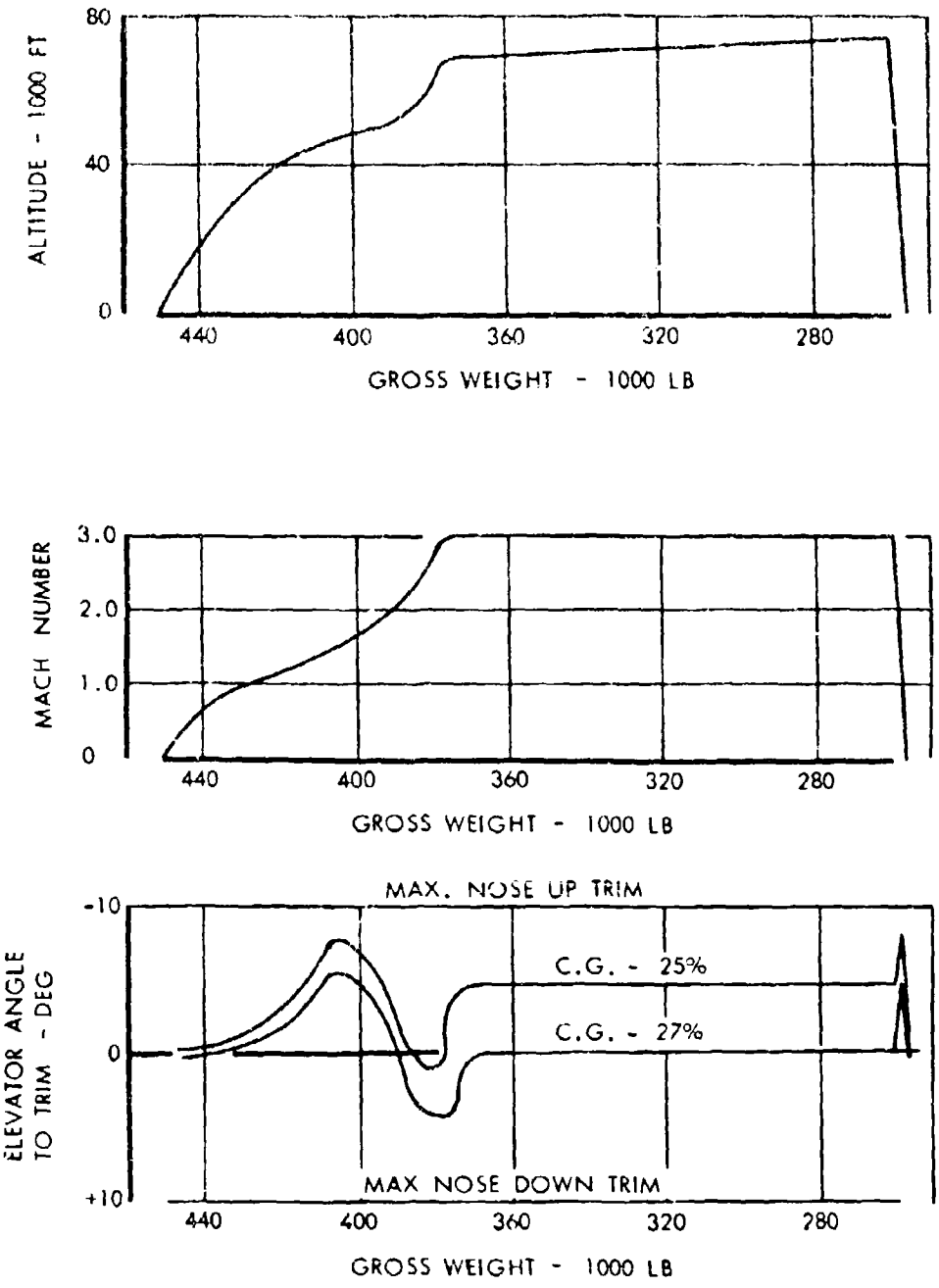

FIGURE 6.17 LONGITUDINAL TRIM CAR 4b - 140 THRU 142

FIGURE 6-17 LONGITUDINAL TRIM

approach conditions. All the trim changes are readily controlled by the pilot with one hand as required by the Civil Air Regulations. Lowering or retracting the landing gear results in a negligible trim change. A comparison is made on Figure 6-18 showing the elevator and stick force to trim the airplane at and away from the ground. It is assumed that the airplane is initially trimmed at 138 knots away from the ground. A conventional pull force of between 10 and 15 pounds is required to maintain trim as the airplane descends into ground effect.

6.2.5 LONGITUDINAL CHARACTERISTICS IN TAKE-OFF

Figure 6-19 shows a time history of a conventional four engine take-off ground roll for sea level standard day conditions with maximum duct heat at the maximum take-off weight and most forward c.g. The rotation speed is 147 knots, the nose wheel lifts off at 149 knots, and the airplane is airborne at the take-off speed of 168 knots.

Figure 6-20 shows a time history of a minimum unstick ground roll with four engines at maximum duct heat at sea level standard day conditions. With full up elevator the nose wheel lifts off at 119 knots and the airplane rotates to the maximum available angle with the oleo struts fully extended at 148 knots. The airplane will lift off at 152 knots. A speed of 152 knots is demonstrated, therefore, as V_{MU} under the design conditions.

6.2.6 DYNAMIC LONGITUDINAL CHARACTERISTICS

The short period longitudinal characteristics are presented for the entire flight profile in Figure 6-21. The augmentation used in the "damper on" curves represent the simplest form of pure rate damping using a surface gain of 2.5 degrees of surface travel for one degree per second pitch rate. This form of augmentation provides damping to 1/10 cycle in 1 second or less throughout the flight range in accordance with military specification. It is also shown that the basic unaugmented airplane damps to ½ cycle in approximately one second or less throughout the flight range. The aircraft, therefore, meets the pitch damper on and off requirements of MIL-F-8785. The basic unaugmented airplane is heavily damped in all subsonic conditions including approach and landing which implies maximum safety in the event of damper failure.

Figure 6-22 presents a more detailed summary of the short period characteristics as represented by natural frequency and damping ratio for the cruise and approach conditions and a comparison with current subsonic jet and prop-jet transports. The figure illustrates that pitch damping augmentation will improve cruise operation. Two criteria are shown; the MIL-F-8785 requirement (Reference 6-1) and NASA boundaries resulting from SST simulator studies (Reference 6-2). The effect of simple rate damping for the cruise case is shown with a near horizontal solid line indicating increasing damping ratio at constant frequency for gains increasing from 2.5, as incorporated in Figure 6-21, to a maximum of 5.0.

By both criteria the aircraft with this form of damping would appear acceptable or better than current jets for normal operation. Higher frequencies can be attained by a lagged-rate damper producing both increased frequency and damping as shown by the broken line on Figure 6-22 and representing the same gains as the simple rate damper.

Damping characteristics on approach at 135 and 148 knots are also presented in Figure 6-22. The aircraft in both speed conditions is heavily damped and with the pitch dampers inoperative is comparable to current subsonic tranports. Using simple rate damping, as for the cruise condition, the dynamic characteristics are superior to current subsonic jets.

The phugoid mode is stable throughout the entire flight profile. The damping is light and the periods vary from a minimum of about 40 seconds during takeoff and landing to a maximum of about 400 seconds during cruise.

An important consideration is the consequences of a pitch damper failure. As discussed above, the aircraft is safely flyable under all conditions with the damper system inoperative. The three channel damper system as discussed in Section 3 of Volume A-VII will not be subject to hard-over failures since the malfunctioning channel would be automatically identified and disengaged. Since the safe flying qualities of the aircraft are not dependent on the damper system, a simple 2-channel system and a single channel system will also be considered in Phase II as possible alternates.

W = 265,000 LB
C.G. = 25.7%
GEAR DOWN

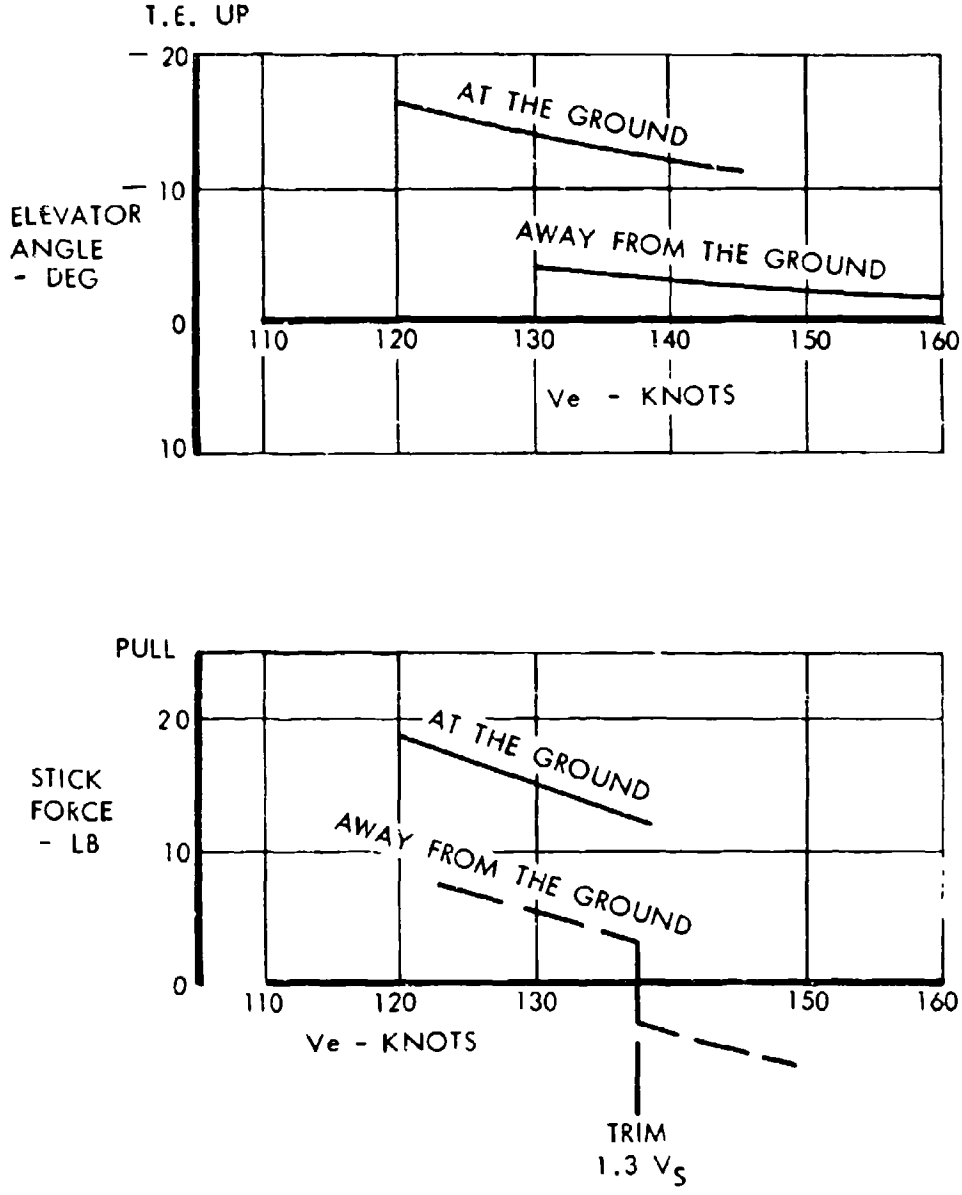

FIGURE 6-18 LONGITUDINAL CONTROL AT THE GROUND

W = 450,000 LB
C.G. = 26.3%
ST'D DAY, S.L. ALL ENGINES OPERATING

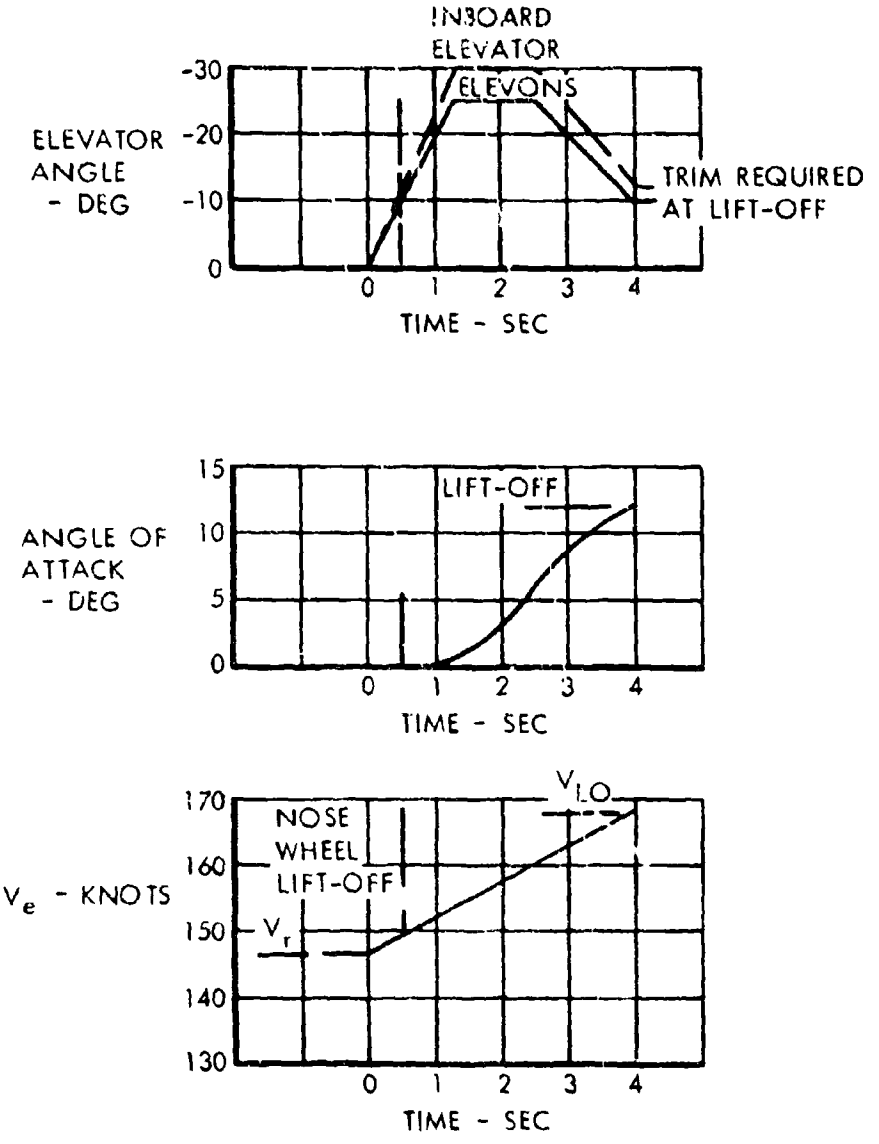

FIGURE 6-19 LONGITUDINAL CHARACTERISTICS IN NORMAL TAKEOFF

W - 450,000 LB
C.G. = 26.3%

S.L. ST'D DAY - ALL ENGINES OPERATING

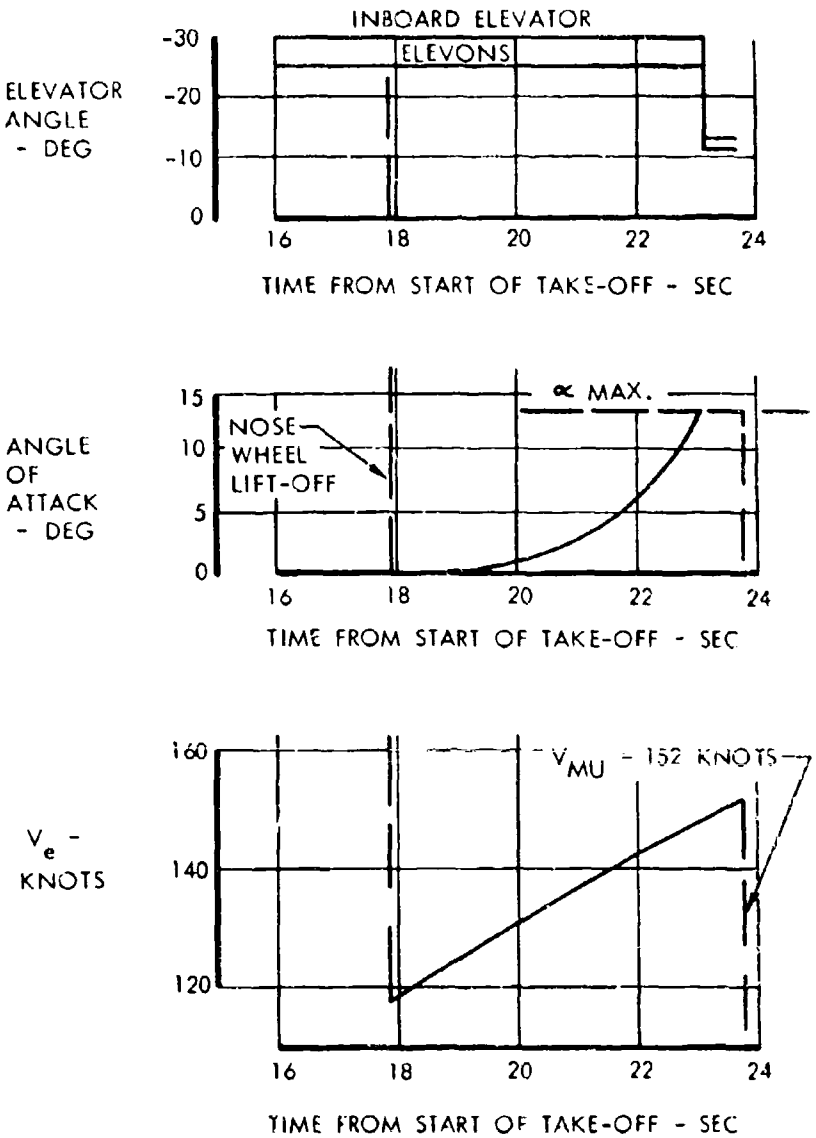

FIGURE 6-20 MINIMUM UNSTICK SPEED

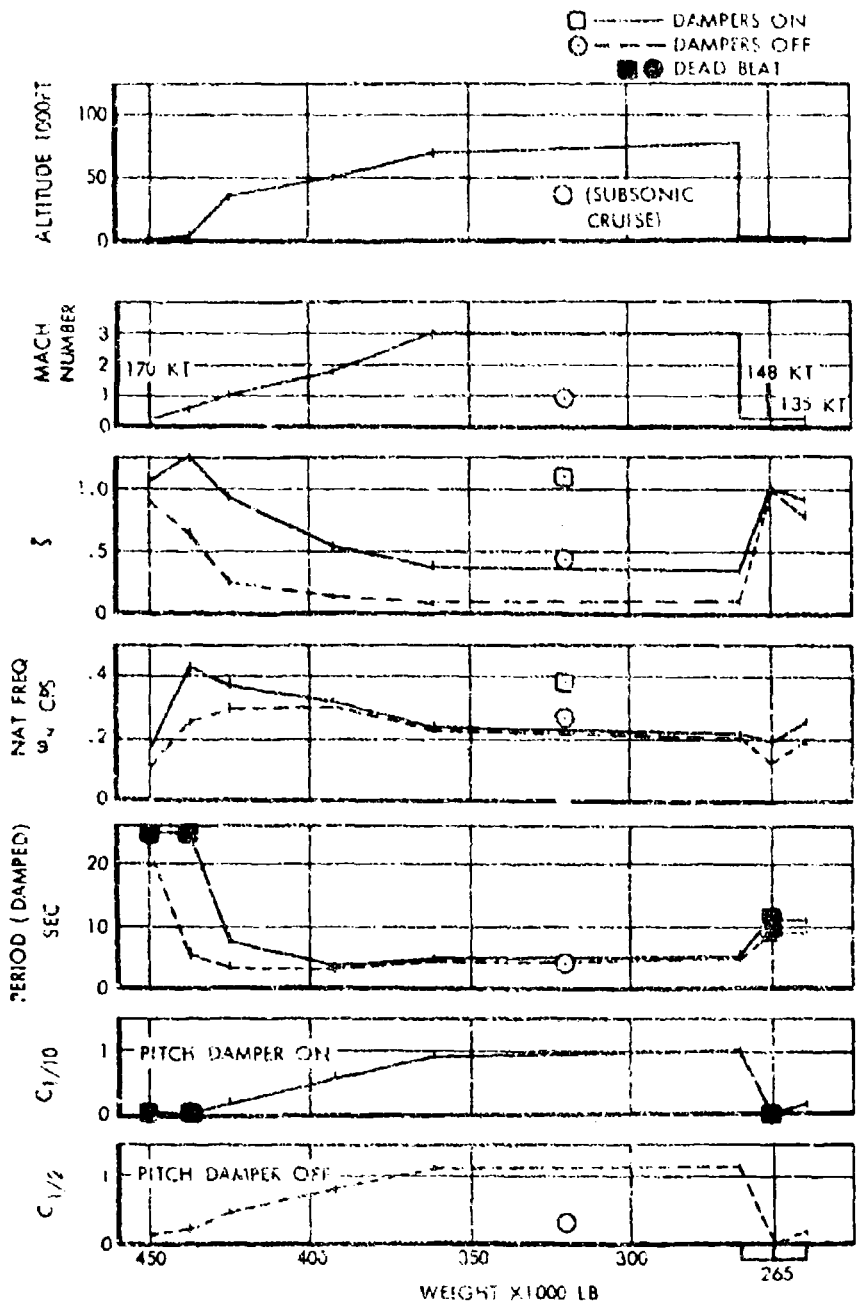

FIGURE 6-21 LONGITUDINAL DYNAMIC CHARACTERISTICS THROUGH THE FLIGHT PROFILE

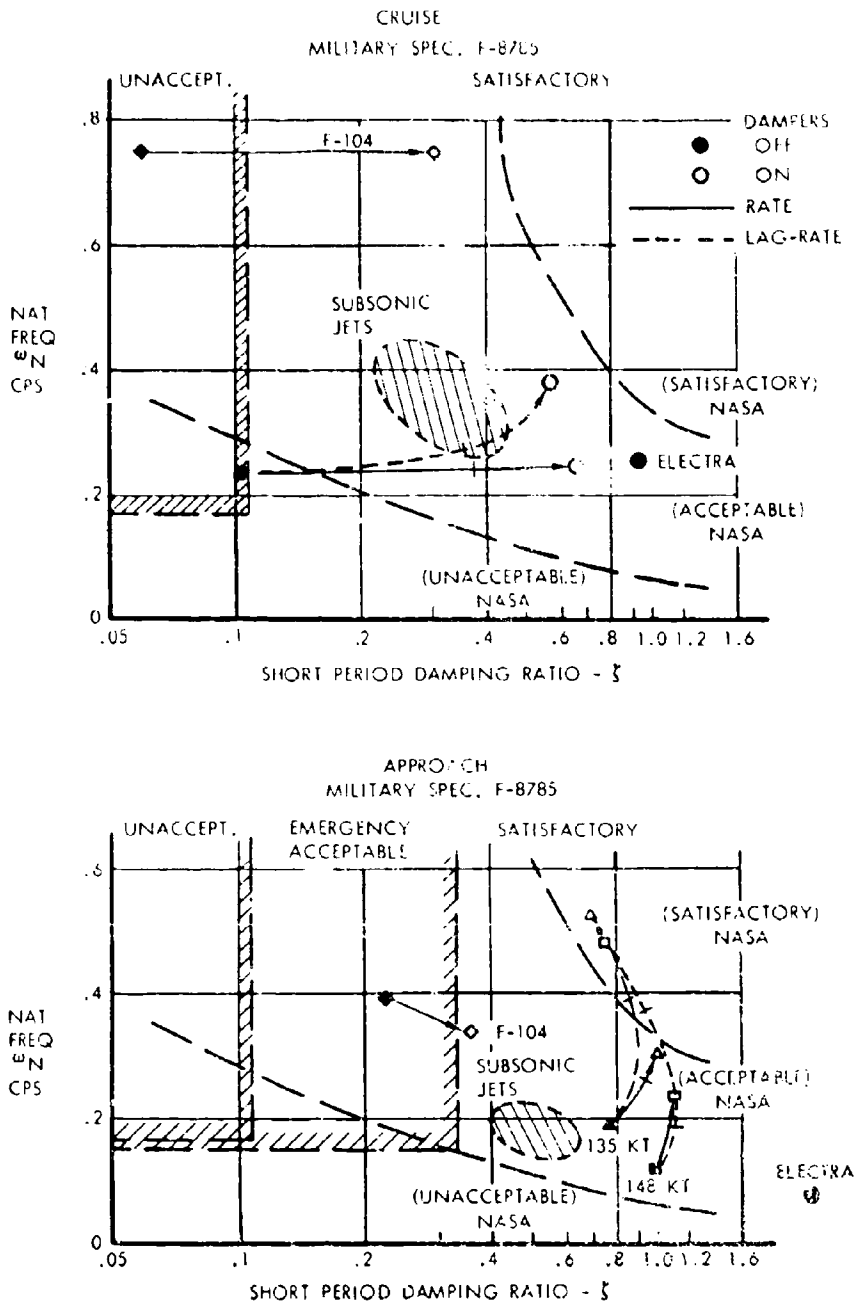

FIGURE 6-22 LONGITUDINAL DYNAMIC CHARACTERISTICS—APPROACH AND CRUISE

6.3 LATERAL-DIRECTIONAL FLIGHT CHARACTERISTICS

6.3.1 STEADY SIDESLIP AND CROSS WIND LANDING CAPABILITY

Figure 6-23 shows that rudder and aileron control movements and forces are proportional to sideslip angle over the range of sideslip angles attainable. Increased rudder deflections up to maximum rudder available produce increased sideslip angles and the rudder pedal forces do not reverse.

The ability to touch down on the runway heading during a cross-wind has been computed for a landing speed of 135 knots. Current practice with swept-wing jets during landing is to crab with wings level on approach and "de-crab" with the use of rudder and aileron at touchdown. Since this is a dynamic maneuver, this capability is presented as a time history in Figure 6-24. The calculation includes 25 degrees of right rudder resulting in nose-right yaw. Dihedral effect producing right rolling moment is countered with about one-half left aileron. It can be seen that the airplane achieves approximately 12.5 degrees of sideslip (corresponding to a 30 knot cross-wind at 90 degrees) after approximately 5 seconds with time remaining for ground contact.

6.3.2 ENGINE OUT CONTROL

The minimum engine out control speed with maximum duct heat thrust as determined under the conditions of CAR 4b requirements is shown in Figure 6-25 to be 123 knots. This compares with a takeoff rotation speed of 147 knots. This speed is limited by the maximum aileron and rudder deflections available. V_{mc} can be demonstrated at a maximum weight of 345,000 pounds at the maximum angle of attack as limited by the stick shaker. The minimum control speed for all weights above 345,000 pounds is below the minimum stick shaker speed. It is also apparent from Figure 6-25 that 5 degrees of sideslip relieves the rudder requirements through most of the speed range shown. The rudder pedal forces in all cases are well within the 180-pound limit specified and the airplane maintains a bank angle of less than 5 degrees.

The minimum ground control speeds at the design takeoff weight with maximum duct heat thrust and using full rudder and nose wheel steering are 99 knots, 117 knots, and 159.0 knots for dry, wet, and icy runway conditions, respectively. These again compare with a takeoff rotation speed of 147 knots at the same takeoff weight.

The airplane lateral-directional trim capabilities with two engines inoperative on the same side and the remaining engines at flight idle are presented in Figure 6-26 for speeds and altitudes corresponding to a typical flight profile. The loss of one engine at Mach 3.0 need not abort the supersonic cruise since the aircraft would remain controllable even with the loss of a second engine on the same side. A check of conditions at Mach 3.0 shows that the airplane can continue its supersonic cruise if desirable from a cruise efficiency standpoint. One outboard engine inoperative and power for level flight on the remaining three engines requires approximately 5.8 degrees of rudder which is within the available directional control capability as shown in Figure 6-26. This figure shows that with the loss of a second engine on the same side the aircraft can be held throughout the flight profile with flight idle power on the remaining engines until a descent is made to approximately 0.9 Mach number. Power for level flight can then be added on two operating engines to finish the cruise subsonically.

The dynamic response of the aircraft to an engine failure was computed for all conditions in the flight profile. Typical results are presented in Figures 6-27 through 6-29. The calculations were made using a 5 degree of freedom digital computer program.

The most severe type of engine failure in the initial cruise flight condition is shown in Figure 6-27. Maximum reheat thrust is assumed on the operating engines. A complete blockage of the nacelle is also premised. The thrust and drag asymmetries were assumed to be applied instantaneously as a further conservatism. This case represents a bounding condition for all subsonic, transonic and supersonic speeds since the resulting thrust plus drag asymmetry is greater than that obtainable throughout the flight profile with any compounding of engine and inlet system failures. Figure 6-27 shows that if the dampers have also failed, the aircraft would experience a maximum sideslip angle of 4½ degrees which would result in less than limit load on the vertical tail. The damper system, if operative, reduces the peak sideslip angle to approximately 3 degrees.

The aircraft response in a more common type of engine failure during Mach 3.0 cruise is shown in

LAN .NG APPROACH CONFIG. - WEATHER VISION NOSE AT - 15°

W = 265,000 LB. 1.4 V_S = 148 KNOTS

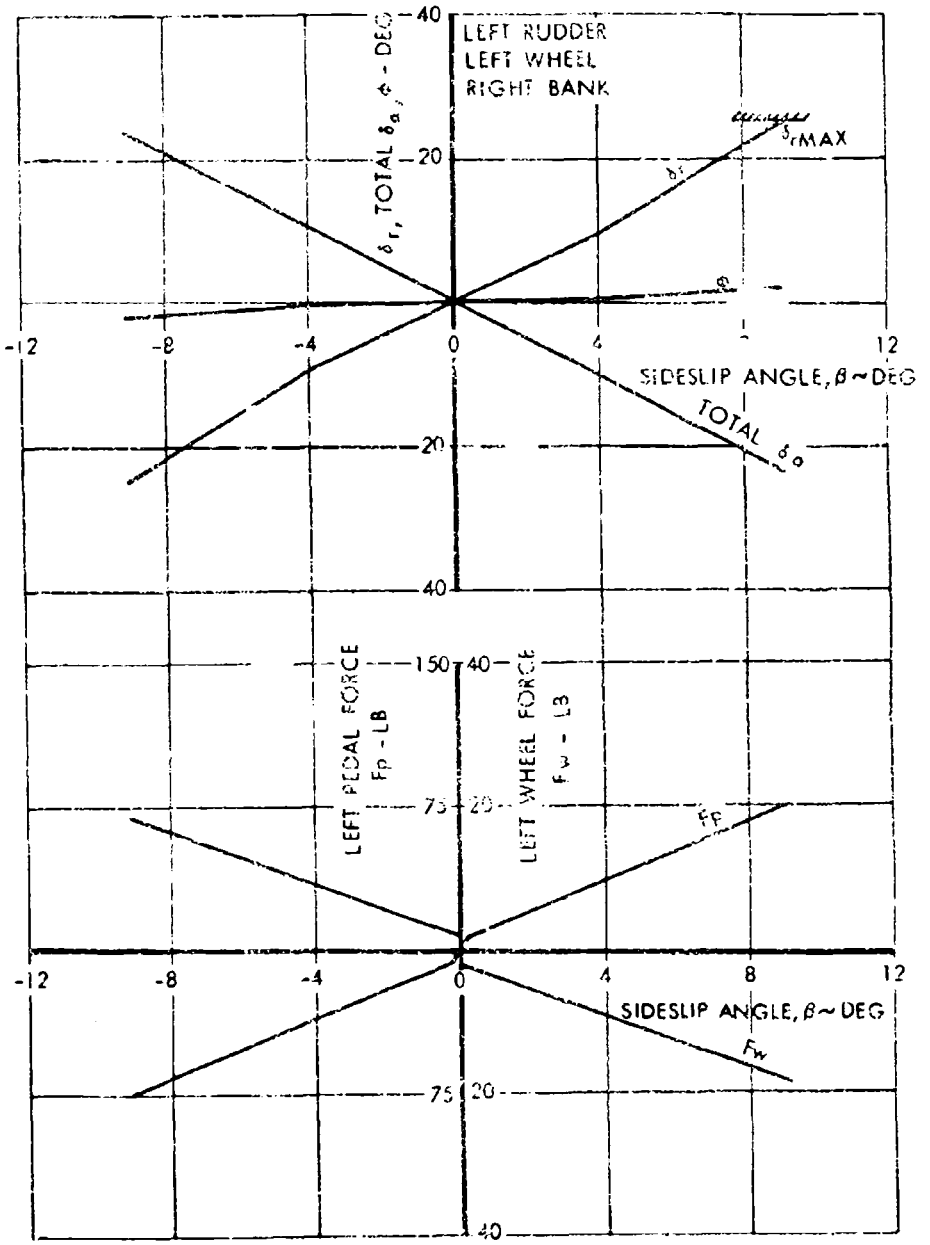

FIGURE 6-23 CHARACTERISTICS IN STEADY SIDESLIP

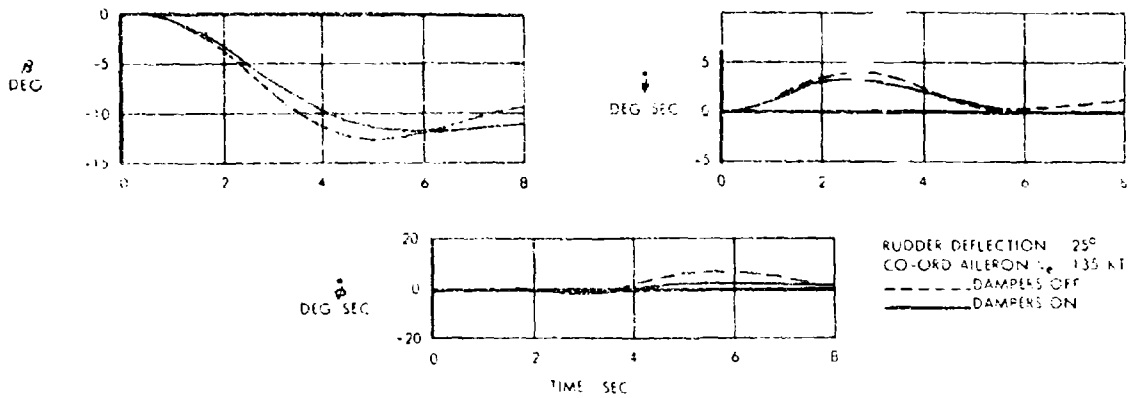

FIGURE 6-24 SIDESLIP CAPABILITY AT TOUCHDOWN

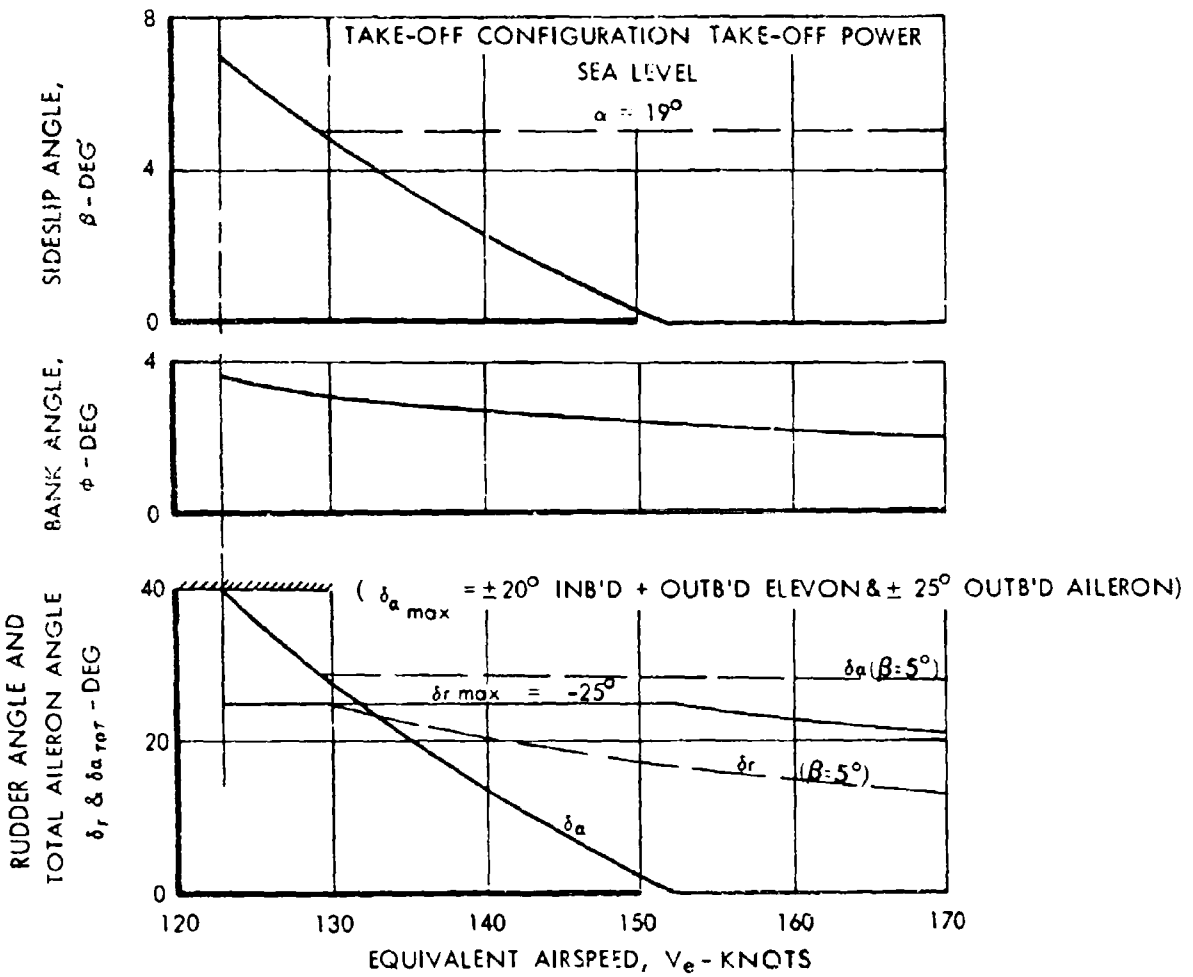

FIGURE 6-25 LATERAL-DIRECTIONAL CONTROL WITH ONE ENGINE INOPERATIVE

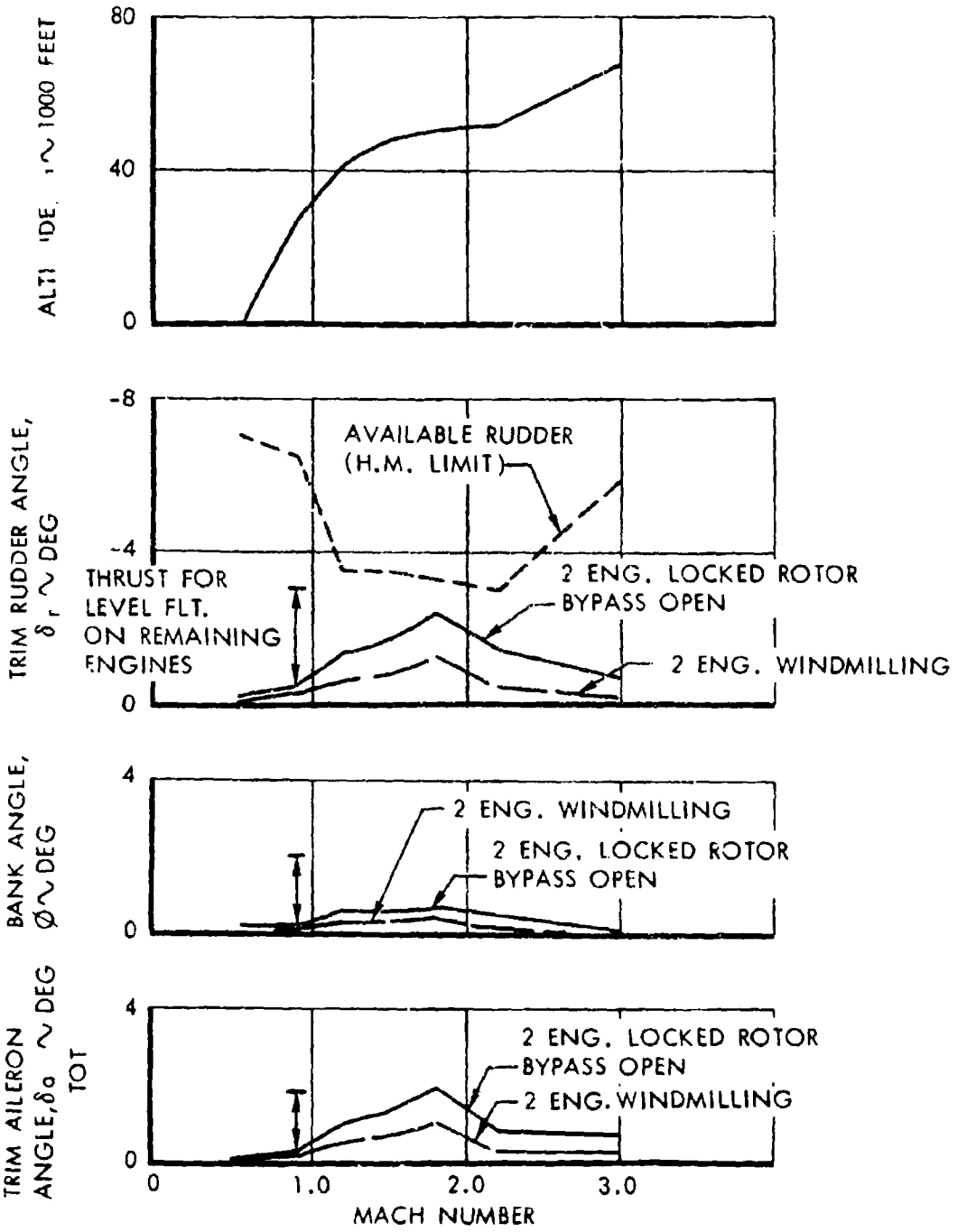

FIGURE 6-26 LATERAL-DIRECTIONAL TRIM CAPABILITY—TWO ENGINES INOPERATIVE

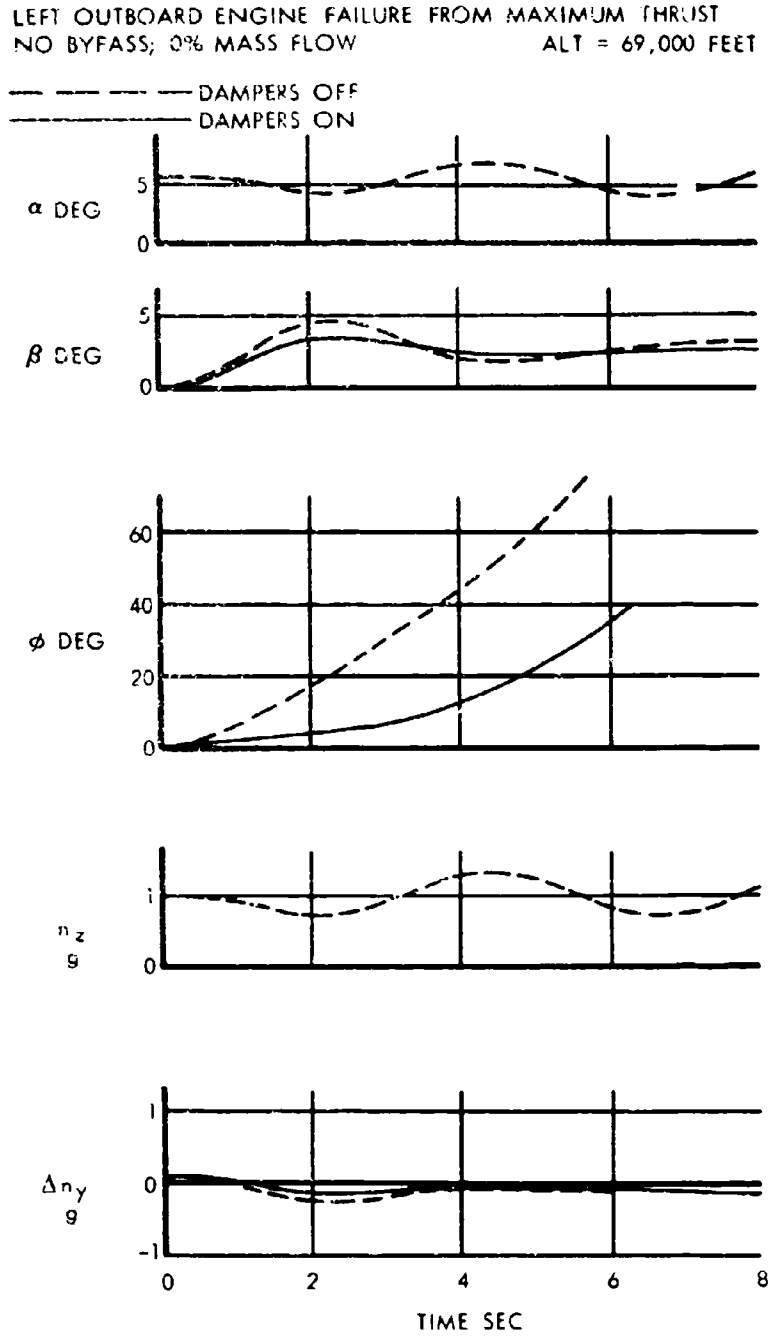

FIGURE 6-27 ENGINE FAILURE DYNAMIC RESPONSE CRUISE—NO INLET BYPASS

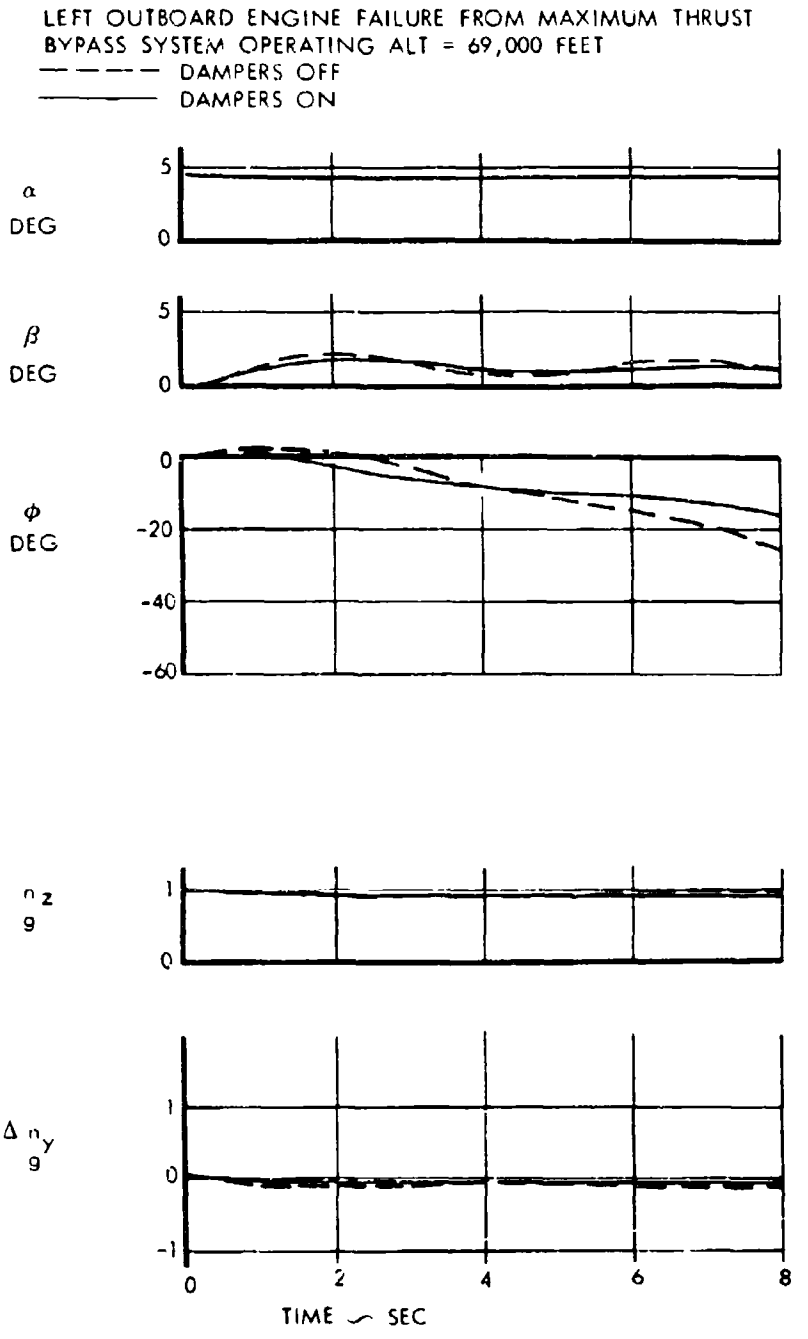

FIGURE 6-28 ENGINE FAILURE DYNAMIC RESPONSE WITH INLET BYPASS

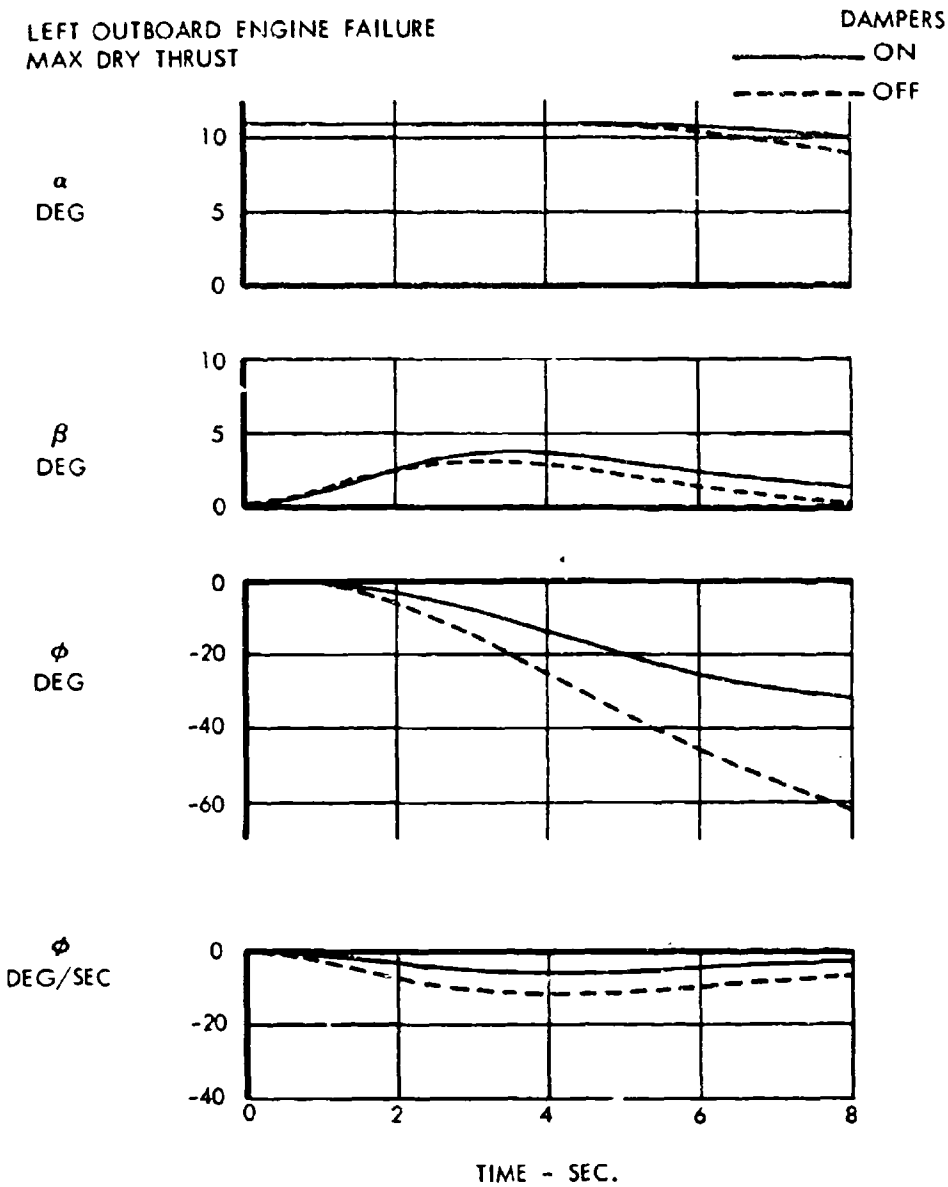

FIGURE 6-29 ENGINE FAILURE DYNAMIC RESPONSE--APPROACH

Figure 6-28. In this case again, a maximum thrust condition is premised. The drag asymmetry, however, is representative of the case of a fuel system failure with the failed engine windmilling, or alternatively a locked rotor condition with the inlet bypass operative. In this case again, the thrust and drag asymmetry are premised to be applied instantaneously for purposes of conservatism. In this case the peak sideslip angle is less than 2 degrees and the maximum lateral load factor experienced by the passengers is less than 0.1 g either dampers off or dampers on.

Additional supersonic flight conditions were studied including higher dynamic pressure but the combinations of thrust, altitude and stability produced lower disturbance levels than those cited above.

Of considerable interest is the response to an engine failure on approach which is shown on Figure 6-29. It was assumed for this condition that maximum dry thrust is used for a wave-off and simple rate-damping is included where noted. The significant feature of this response is that the engine thrust moment which produces the sideslip causes a roll displacement which is controllable by the pilot even assuming a 3-second delay. The characteristics of this response will be satisfactory as a result of good lateral-directional stability and high lateral controllability during approach.

It is concluded therefore that the normal type of engine failure can be easily controlled and will result in little, if any, passenger discomfort. The most extreme type of engine failure resulting from compounding engine failure, inlet bypass door failure, and damper failures will result in an aircraft dynamic response well within the structural design capability of the aircraft. In neither case is the aircraft dependent on the damper augmentation system.

6.3.3 ROLL PERFORMANCE

The aileron roll performance of the SST was determined for all conditions in the flight profile of the aircraft. The computations were made with 5 degrees of freedom equations utilizing a digital computer and including the effects of flexibility and the aerodynamics data as presented in Section 4. Engine angular momentum was included but found to be insignificant.

Figure 6-30 presents the roll capability of the SST in terms of time to bank to 30 degrees and roll rate at 30 degrees throughout the flight profile. It is significant from this figure that the roll capability during cruise compares quite favorably with subsonic jets, as reported for example in Reference 6-4. The time to bank also compares favorably.

Figure 6-31 presents time histories of rolls during landing at 135 knots including the effect of dampers and rudder coordination (ten degrees of rudder). The ailerons are applied at a rate of 20 degrees per second per surface and reversed at 30 degrees bank angle at the same rate. It is shown that roll rates in excess of 20 degrees per second are attainable and 30 degrees of bank achieved in a little over 2 seconds. The excellent roll capability is evident in the time to bank to 10 degrees which is about 1.2 seconds. This is quicker than current subsonic jets at comparable speeds as reported in Reference 6-5. It is shown that if co-ordinated rudder is desired, either mechanically or by pilot input, roll performance will not be penalized.

Figure 6-32 presents time histories of rudder-fixed aileron rolls executed at cruise conditions with and without 3-axis rate dampers. Roll rates in excess of 20 degrees per second are available. The time to bank to 30 degrees compares very favorably with current subsonic jets as reported in Reference 6-6.

The absence of any significant excursions in either angle of attack or sideslip in the roll maneuvers with or without damper augmentation as shown in Figure 6-32 is indicative of the absence of any substantial inertia coupling tendency. This is in accordance with Phillips' Criterion since the peak roll rate is 24 degrees per second which is approximately ⅓ of the pitch and yaw natural frequencies.

Adverse yaw has been evaluated for the approach and cruise conditions. The parameter ω_ϕ/ω_d as formulated and discussed in Reference 6-7 has been computed with normal aileron control with and without rudder co-ordination and is tabulated in Figure 6-33. The criteria of Reference 6-7 are shown for comparison. The airplane without rudder coordination in the approach condition with relatively high roll-to-yaw ratio has an ω_ϕ/ω_d which is .569. If the criteria can be extrapolated, this is an acceptable value. The effects of linked rudder-aileron coordination ($\pm .25\delta_r/\delta_a$) are also shown which indicates the ability to modify the parameter if future simulator studies indicate the necessity. The effect of dihedral on the approach con-

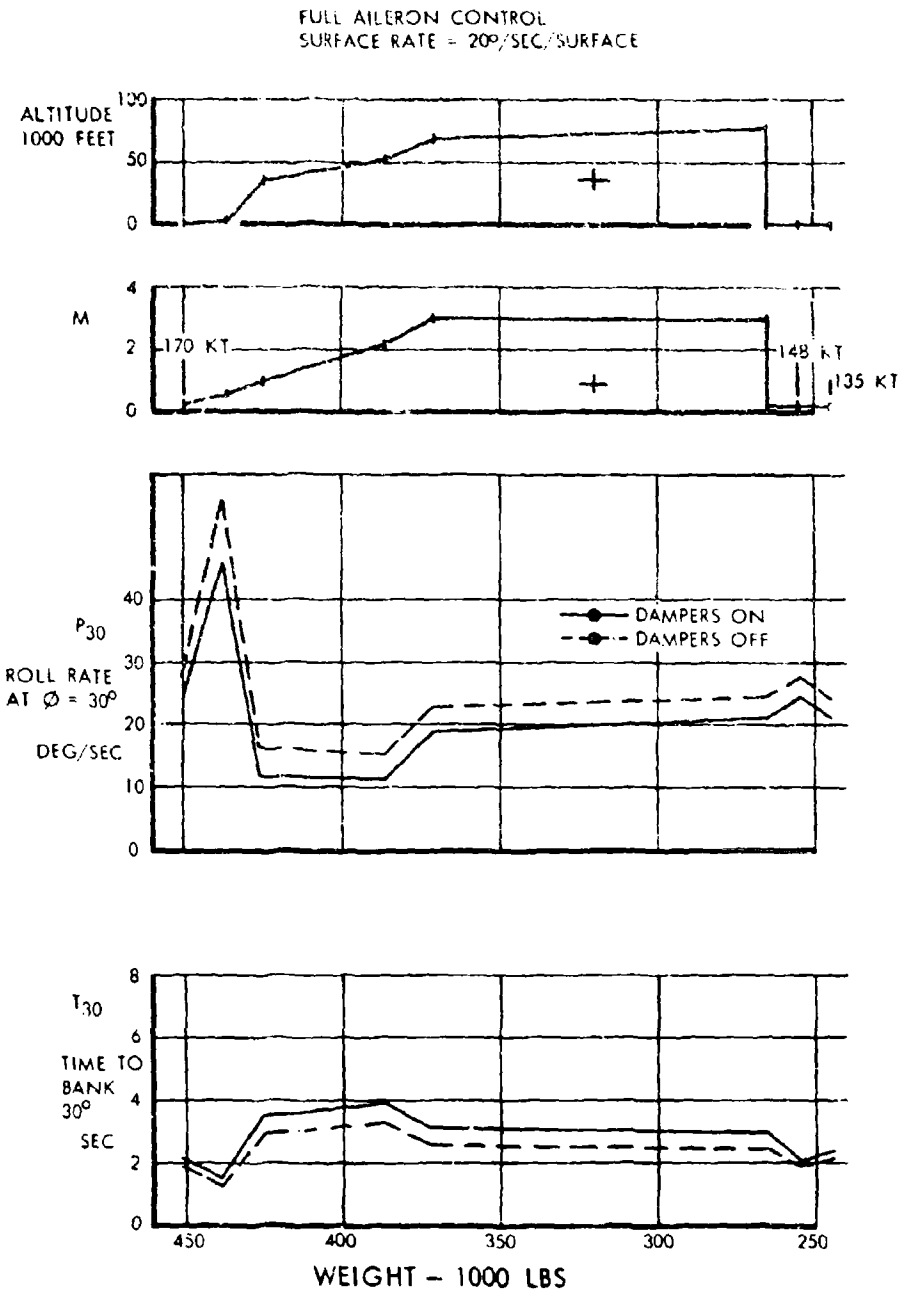

FIGURE 6-30 ROLL PERFORMANCE THROUGH THE FLIGHT PROFILE

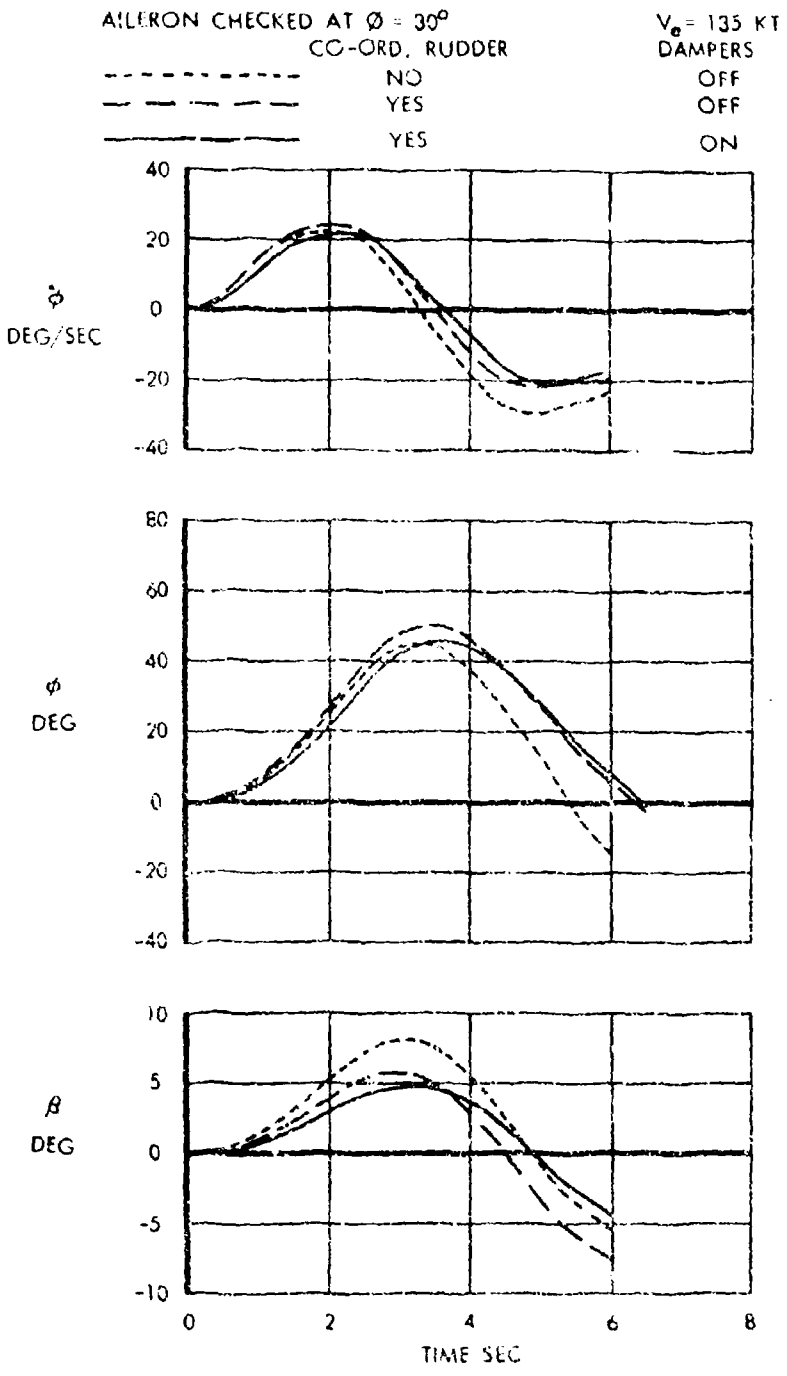

FIGURE 6-31 AILERON ROLL DURING LANDING

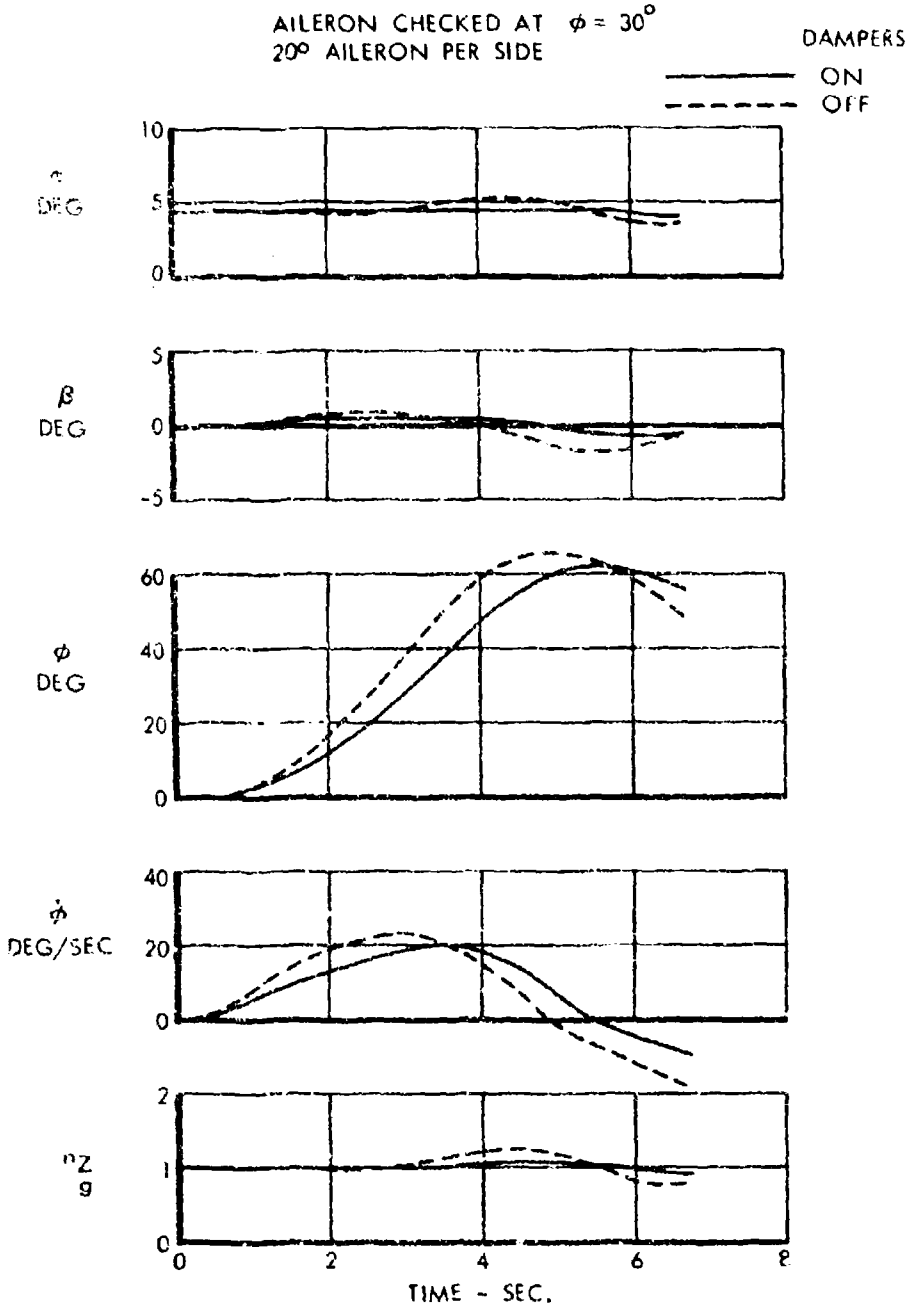

FIGURE 6-32 AILERON ROLL DURING CRUISE

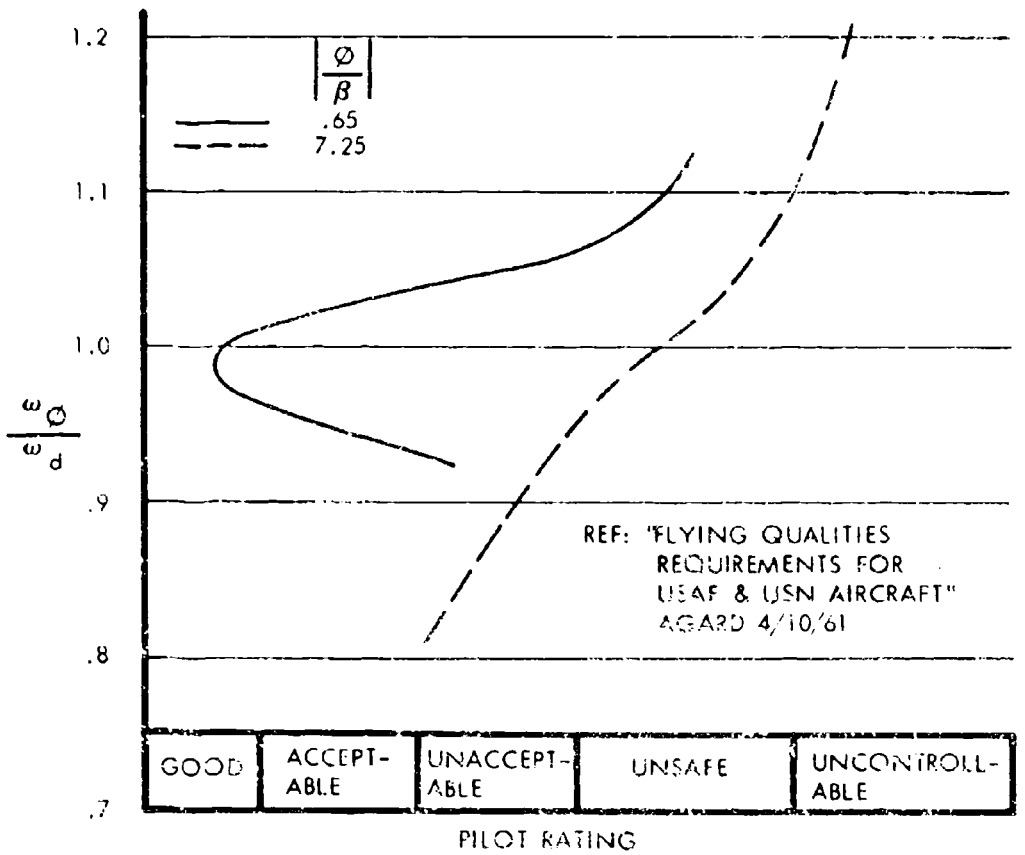

ADVERSE YAW PARAMETER $\frac{\omega_\phi}{\omega_d}$

RUDDER COORDINATION $\frac{\delta_r}{\delta_a}$	-.25	0	.25	$\left\|\frac{\phi}{\beta}\right\|$
APPROACH V = 135 KT	.481	.569 .610*	.660	4.0
CRUISE M = 3.0	.928	.936 .996*	.946	1.6

* 5° WING DOWN DIHEDRAL

FIGURE 6-33 ADVERSE YAW

dition is also shown for comparison. The cruise condition has an ω_ϕ/ω_d for the uncoordinated airplane of .936 and with low roll-to-yaw ratio would appear satisfactory compared to the criteria. In this case also, coordination of rudder motion with the aileron motion will vary the parameter ω_ϕ/ω_d in the region shown to be desirable in Reference 6-7.

The simulator studies described in a following section will be used to determine the desirability of linked aileron-rudder coordination and optimum parametric values.

6.3.4 DYNAMIC LATERAL DIRECTIONAL CHARACTERISTICS

The lateral directional dynamic characteristics have been evaluated for the SST throughout the flight profile and are presented in Figure 6-34. The calculations were made by digital computer using the classic 3-degree of freedom equations including the damper characteristics to obtain root solutions and the parameters as shown in Figures 6-34 and 6-35.

The results shown in Figure 6-34 indicate the desirability of the roll and yaw axis dampers through the flight envelope. It is shown that the subsonic speeds and lower altitudes (particularly at airport speeds) are characterized by high damping but moderately high roll-to-yaw parameter with dampers off. The low speed damper function then is primarily to reduce roll-to-yaw ratio while maintaining good damping. The high speed conditions are characterized by light damping and low levels of roll-to-yaw parameter. The high speed damper function is to increase damping through the yaw damper while maintaining relatively low roll-to-yaw ratios. When compared with current military requirements for transport aircraft as found in Reference 6-1, MIL-F-8785, the airplane exhibits very satisfactory dutch roll characteristics with normal damper operation and more than adequate characteristics with all dampers off.

Figure 6-35 presents a more detailed analysis of each of the damper contributions in the approach and cruise conditions. The approach condition is characterized by very high damping inherent in the basic unaugmented airplane but having a fairly high roll-to-yaw ratio as might be expected with a highly swept wing. The roll damper is shown to reduce the roll/yaw ratio considerably to a value approximately similar to current jets. The addition of the yaw damper increases the damping. For comparison, the Electra (which has no augmentation) and the F-104 (which does) is shown which leads to the conclusion that the low speed dutch roll problems of the fixed-wing SST is not as severe as previously anticipated.

Figure 6-35 also presents the dutch roll characteristics in the cruise condition and the contribution of the roll and yaw damper systems. The basic, unaugmented airplane exhibits light damping in cruise but a low roll-to-yaw ratio as desired. The addition of yaw dampers improves the damping considerably with a slight increase in roll/yaw ratio resulting from roll due to yaw damper deflection. The addition of roll dampers serves to reduce roll/yaw ratio slightly but is retained primarily for the low speed approach condition. By comparison with MIL-F-8785, the SST in normal cruise with dampers operating will exhibit very satisfactory dutch roll characteristics and will surpass current transports. The F-104 is shown for a $M = 2.0$, 51,000 foot altitude condition as a comparison.

It is concluded from extensive dynamic studies on the SST that the normal operation dutch roll characteristics will surpass current transports in all flight regimes and the basic unaugmented airplane with all artificial damping failed will still be a very flyable airplane and will meet the requirements as known today.

The three channel roll and yaw dampers as described in Section 3 of Volume A-VII are not subject to hard-over failures. Since flight safety is not dependent on damper operation as discussed above, Phase II will consider dual channel and single channel dampers as well. As in the case of the pitch damper, a dual channel yaw damper may have large authority limits which is desirable from the standpoint of fatigue life of the aircraft since hard-over failures which are detrimental from the standpoint of passenger comfort may be precluded. The single channel yaw damper offers possible attractions from the standpoint of cost, simplicity and reduction in the incidence of failures. It is quite possible that a single channel roll damper will be satisfactory for the SST as the roll damper will not contribute appreciably to the fatigue life of the aircraft; therefore, large authority is not necessary.

The spiral stability of the SST has been evaluated concurrently with the dutch roll analysis and the

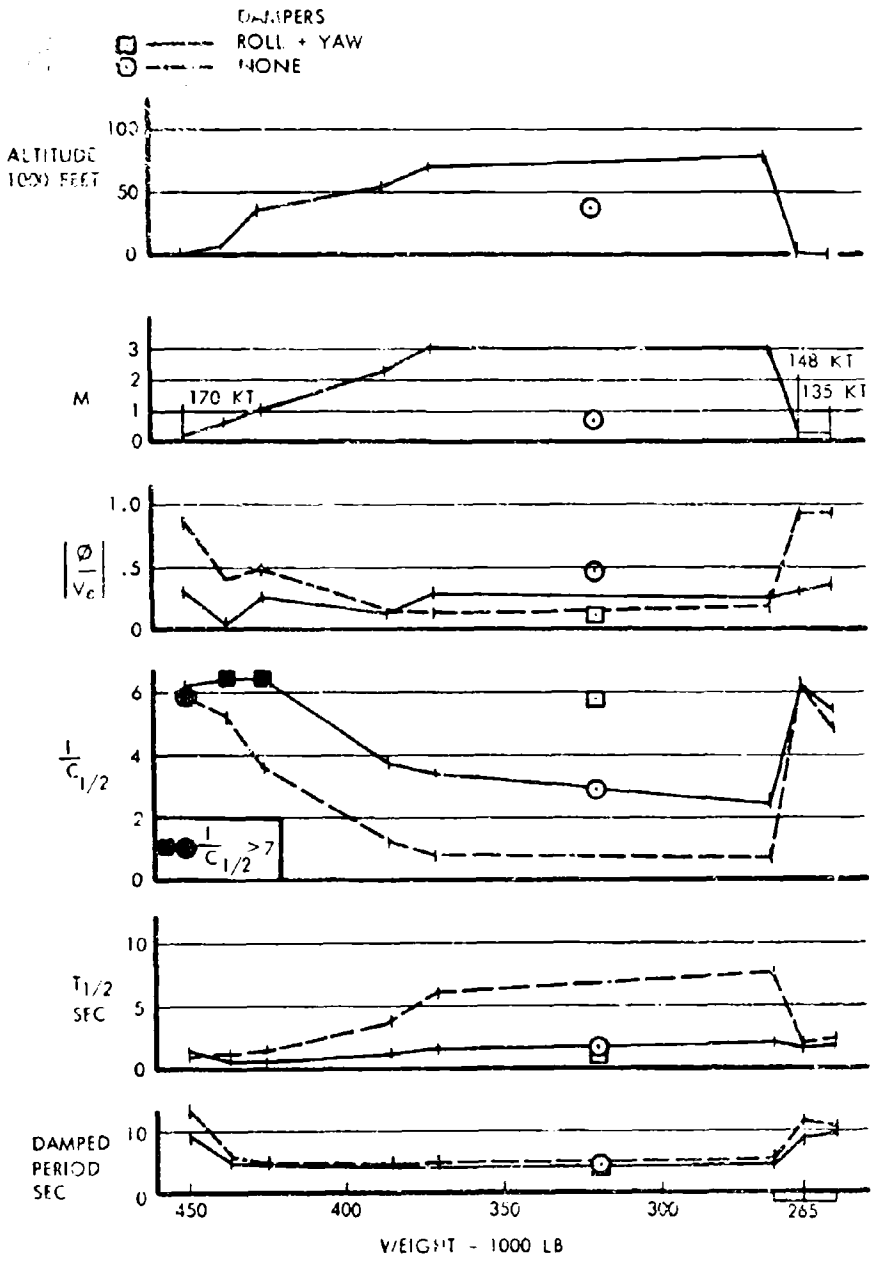

FIGURE 6-34 DYNAMIC LATERAL-DIRECTIONAL CHARACTERISTICS THROUGH THE FLIGHT PROFILE

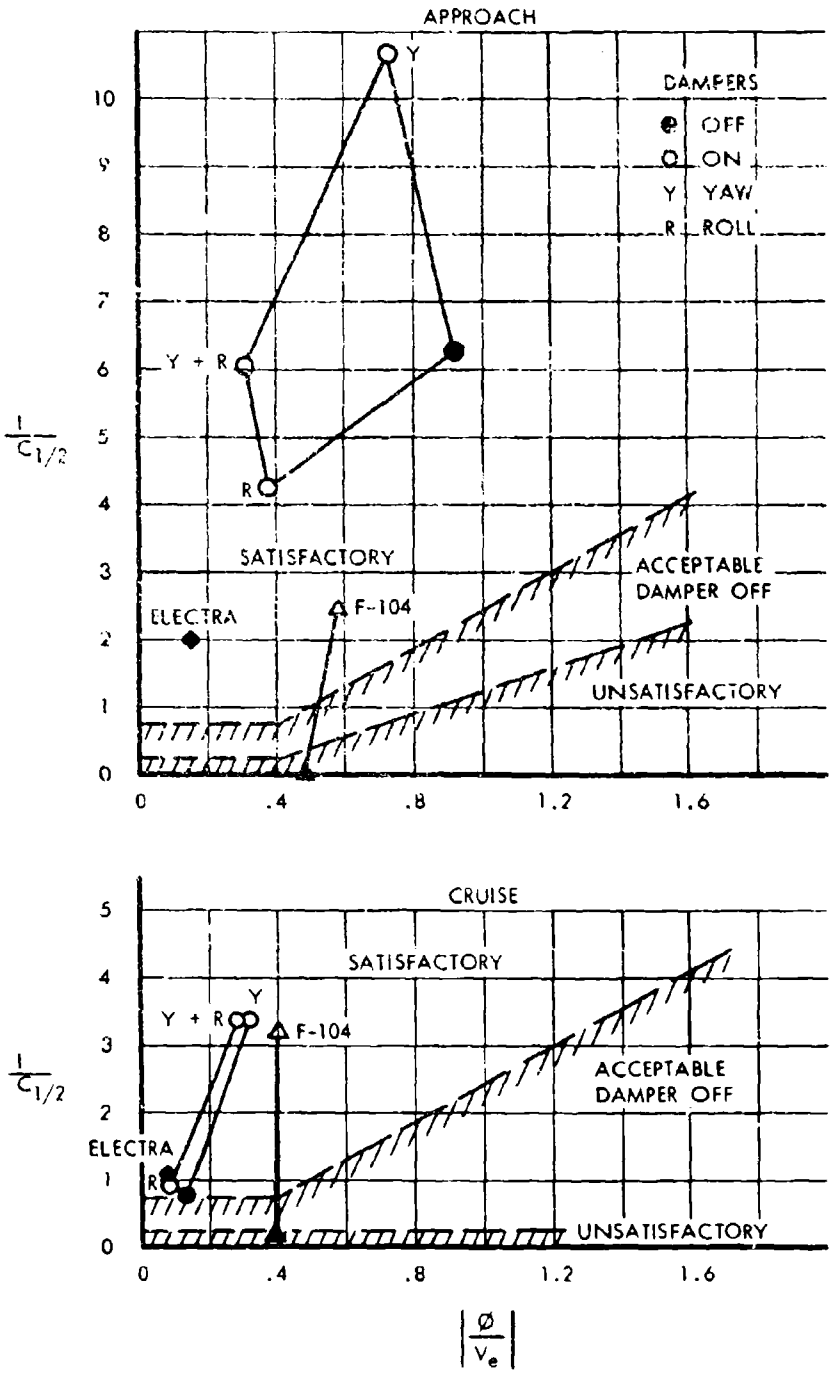

FIGURE 6-35 DYNAMIC LATERAL-DIRECTIONAL CHARACTERISTICS—APPROACH AND CRUISE

results indicate positive stability throughout the flight range with the exception of cruise. The divergence in cruise is very mild with greater than 20 seconds required to double amplitude. The spiral mode does not appear to be of any consequence.

6.4 HANDLING QUALITIES IN LANDING

The landing characteristics of the supersonic transport are comparable to those of subsonic jet transports. The optimum hold speed as indicated in Figure 6-13 is 200 knots at a representative landing weight of 265,000 pounds which compares favorably to the subsonic jets. The approach speed at $1.3V_{min}$ is 138 knots which also compares favorably with the subsonic jets. The time history of a transition into the approach condition is shown in Figure 6-36. Level flight at 148 knots ($1.4V_{min}$) gear up requires the same thrust setting as 138 knots ($1.3V_{min}$) gear down at a glide angle of 2.5 degrees. The pilot, therefore, can drop the gear without changing throttle setting to affect the transition to a 2.5 degree glide slope angle at the approach speed. Since there are no wing flaps and since the trim shift associated with dropping the landing gear is negligible, longitudinal control motions and forces during the transition are small. These simplifications of pilot functions will enhance the flying qualities of the aircraft.

At an approach speed of 138 knots the aircraft has a stable phugoid as discussed in Section 6.2.6. Undesirable speed divergency or flight path oscillations are not expected, therefore. The aircraft demonstrates a favorable static margin and a high damping ratio of the short period longitudinal mode. No undesirable longitudinal oscillations are anticipated. NASA simulator studies indicate the aircraft characteristics with no stability augmentation are acceptable for landing. The studies indicated, however, that a higher static margin and a positive variation of thrust required with forward speed is desirable for landing. A program of simulator and variable stability aircraft studies is recommended therefore in the following paragraphs to establish final design values. Provision has been made in the aircraft design such that automatic throttle controls (providing positive thrust required with forward speed) and phase lag in the pitch damper (raising the frequency of the short period mode and providing the equivalence of a higher static margin) are available if it is shown to be desirable in the simulator studies.

Lateral-directional characteristics at an approach speed of 138 knots are similarly acceptable. The supersonic transport demonstrates a capability to land in a 30 knot cross wind at this speed. As discussed in a previous section, the engine out minimum control speed is 123 knots. At 138 knots, therefore, there will be adequate directional and lateral control for flight path control adjustments. The dutch roll mode is heavily damped without damping augmentation in the landing approach. A roll damper is provided, however, since F-104 experience has shown that a low ratio roll-to-yaw is desirable in rough air even where the dutch roll mode is heavily damped.

In conjunction with the handling qualities, down vision capability over the nose is adequate for landing under conditions of ¼ mile visibility and a ceiling of 100 feet or the related runway visual range of 1300 feet. As shown in Figure 6-36 at an altitude of 100 feet the aircraft pitch angle with respect to the ground is 9 degrees. Since the down vision over the nose of the aircraft is 23 degrees, the pilot will have a down vision angle with respect to the ground of 14 degrees permitting him to see approximately 750 feet of the runway in front of the aircraft. Under the stated visibility conditions this will permit him to see approximately 7 or 8 approach and/or touchdown zone lights, spaced at 100-foot intervals, which is sufficient for orientation and completion of the landing.

6.5 PROPOSED PHASE II PROGRAM

The proposed program to insure acceptable handling qualities includes wind tunnel tests, elastic model tests, aeroelastic analyses and simulator studies.

Section 4.8 of Volume A-V describes the proposed program to provide all of the static aerodynamic data as well as damping derivatives. This program will obtain data for possible airframe refinements as well as data for the aircraft as currently conceived. The airframe refinements include minor modifications of the wing plan form to achieve a smaller aft movement of the aerodynamic center.

A comprehensive program of testing with an elastic model and aeroelastic analysis is also proposed to refine the aeroelastic data of Paragraph 6.6 as used in this report. This program is described in Section 3 of Volume A-IV.

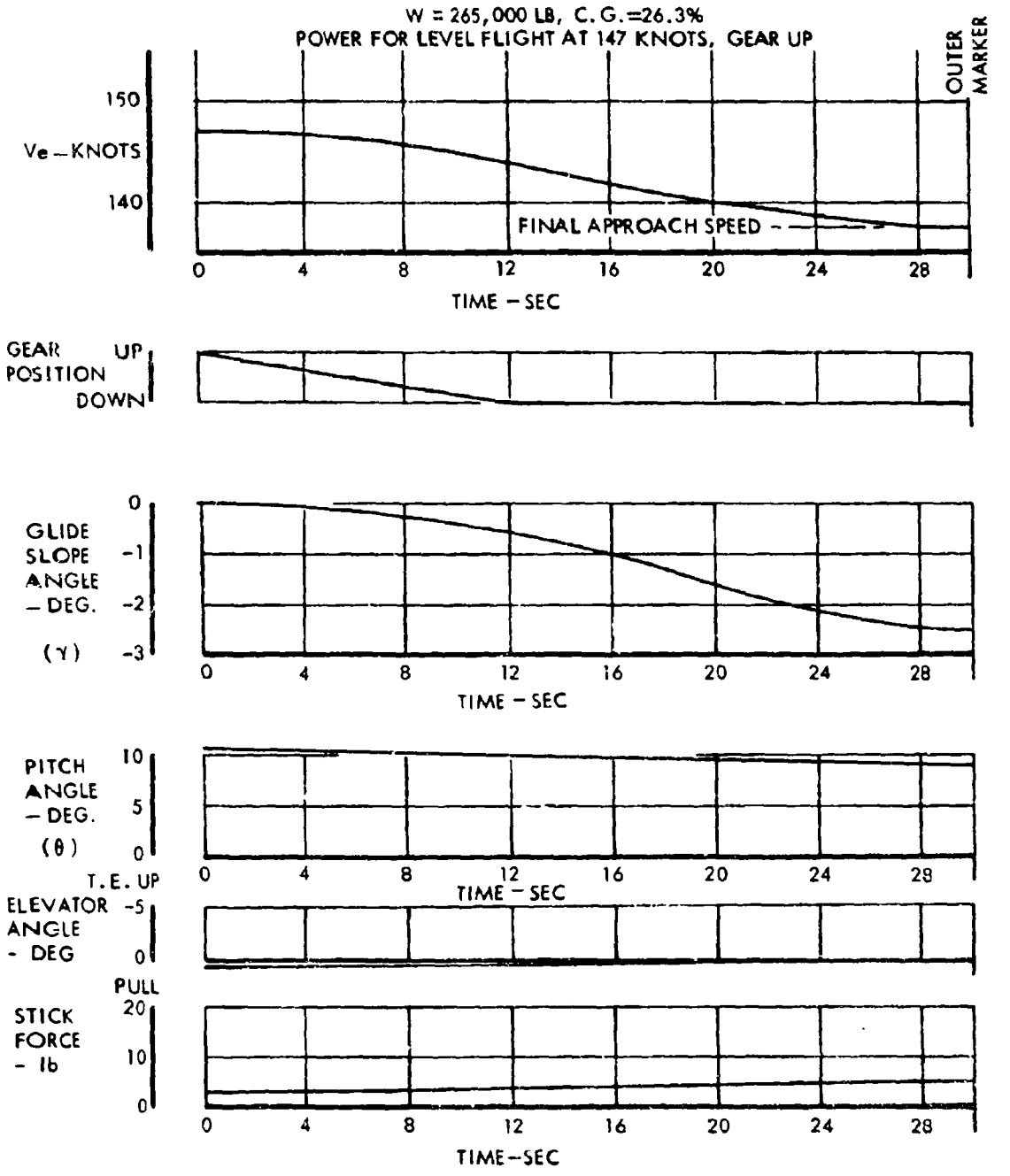

FIGURE 6-36 LANDING APPROACH DECELERATION

6.5.1 PHASE II, SIMULATOR STUDIES

6.5.1.1 Simulator Program Objective

Simulators will be used throughout the Phase II design period to accomplish several objectives.

- Provide guidance regarding the flight crew acceptance of the airplane handling qualities in and out of ground effect.
- Examine the results of control system malfunctions and the flight crew capacity for handling the abnormal and emergency situations.
- Establish the adequacy of the control system and handling qualities for the all-weather approach and landing system.
- Establish design criteria and optimum system characteristics for damper augmentation systems.
- Provide information regarding possible test techniques and FAA certification criteria to substantiate the development program proposed.

6.5.1.2 Handling Qualities and Control System Development—Simulator

The simulator program will make use of fixed base and motion simulators with and without visual aids. In general, the control system and handling qualities will be examined in the ground-based simulator until the regions of design are relatively well-defined. A variable-stability airplane will be used where real-life accelerations and turbulent air conditions are important to the program. Such tasks as the ILS approach and landing and low-speed handling qualities are particularly adaptable to the in-flight simulator. The expected motions of the airplane and controls, as derived by wind tunnel tests, calculations, and substantiated in the ground-based simulator, will be rapidly duplicated in-flight to see if the opinions and ratings will change in the actual environment. Such tasks as the ILS approach, wave-off, engine failures, stability augmentation inoperative, malfunctioning control system, altitude-hold and IAS hold capability, turn coordination, control force harmony, trim rates and power and location of controls and trim devices can all be accurately simulated quickly and economically by means of this combination of simulation devices.

6.5.1.3 Simulator Facilities

The ground-based simulators installed in the Lockheed research facility at Rye Canyon and at the Ames and Langley Laboratory facilities of the NASA will be utilized for the initial development effort. These include

- Lockheed limited moving base simulator with visual aid. Pitch, roll and heave. Artificial 3D visual.
- NASA moving base transport simulator. Dalto visual aid and motions to include pitch, roll and heave. C-130 cockpit.
- NASA five-degrees of freedom motion simulator. No visual aid. Motion includes roll, pitch, yaw, side force and limited normal acceleration.
- NASA six-degrees of freedom motion simulator. No visual aid. Motion includes roll, pitch, yaw, transverse accelerations (fore, aft and side) and limited normal accelerations.
- NASA landing height simulator. Possible Poltz visual. Vertical motion only for good normal acceleration.

The NASA simulation facilities will be contracted for on an as-available basis. Through judicious planning, the simulation requirements outlined in Paragraph 6.5.1.1 will be accomplished as an adjunct to the NASA's current SST simulator efforts. Cognizant NASA personnel in an informal contact have concurred that the NASA simulator facilities would be available for the program as described above. The in-flight simulation will include the three axis Cornell Laboratories' B-26. The airplane features frequency response ranges commensurate with most of the SST flight characteristic for all three axis. The ground-based simulation results or calculations of specific characteristics can be duplicated in-flight with ease by the variable-stability control system. The NASA High Speed Flight Research Center at Edwards AFB will provide an in-flight variable-stability C-140 Jet-Star with four engines for SST simulation efforts in mid 1965. This general purpose, airborne simulator (GPAS) features 3 axis variable stability and can vary drag and thrust characteristics. An automatic throttle control offers speed control. Blind-landing provisions and variable instrument panels are planned.

6.6 AEROELASTIC DATA

The effects of aeroelasticity on the static stability and control effectiveness are presented in this Section. The data was obtained using the IBM 7090 digital computer. The digital analysis is based on a general, matrix algebra system in which the basic numerical inputs for elasticity, inertia, and aerodynamics are used for static aeroelastic computations, and control effectiveness. Elastic characteristics are determined by a redundant structural analysis.

Section 3 of Volume A-IV describes the complete engineering approach to the aerothermoelastic problem.

The aerodynamic center shift, lift curve slope, and roll damping of the flexible airplane are presented on Figures 6-37 through 6-39. The flexible to rigid ratio for pitch and roll control are shown in Figures 6-40, 6-41 and 6-42.

Estimates of aeroelastic effects for the vertical tail were made by analogy to the results of the wing analysis. Figure 6-43 presents the flexibility correction to the vertical tail effectiveness and Figures 6-44 and 6-45 show the rudder and rudder damper corrections.

6.7 REFERENCES

6-1. MIL-F-8785 (ASG) Military Specification, Flying Qualities of Piloted Airplanes.

6-2. Aerospace Engineering, May 1962, "Assessment of Critical Problem Areas of the Supersonic Transport by Means of Piloted Simulators"--M. White, M. Sadoff, R. Bray, G. Cooper.

6-3. SAE-ARP 842 — Airworthiness Recommended Practice Bulletin (draft), November 11, 1963.

6-4. NASA Memo 3-2-59H, "Flight Studies of Problems Pertinent to High-Speed Operation of Jet Transports"—S. Butchart, J. Fischel, R. Tremant, G. Robinson.

6-5. NASA Memo 3-1-59H, "Flight Studies of Problems Pertinent to Low-Speed Operation of Jet Transports"--J. Fischel, S. Butchart, G. Robinson, R. Tremant.

6-6. USAF Stability and Control Methods, October 1960.

6-7. AGARD "Flying Qualities Requirements for United States Navy and Air Force Aircraft"—W. Koven and R. Wasicko.

6-8. NASA TN-842, "Normal Force and Hinge Moment Characteristics at Transonic Speeds of Flap Type Ailerons at Three Spanwise Locations on a 4 Percent-Thick Sweptback-Wing-Body Model and Pressure-Distribution Measurements on an Inboard Aileron"--Jack F. Runckel and Gerald Hieser.

6-9. NASA RM L51C22, "Comparison of the Effectiveness and Hinge Moments of All-Movable Delta and Flap Type Controls on Various Wings"—David G. Stone.

6-10. NASA RM L57B01, "Hinge Moment Characteristics for a Series of Controls and Balancing Devices on a 60° Delta Wing at Mach Numbers of 1.61 and 2.01"—Douglas R. Lord and K. R. Czarnecki.

6-11. NASA TM-X-643, "Large-Scale Low-Speed Wind-Tunnel Tests of a Delta Winged Supersonic Transport Model with a Delta Canard Control Surface"—James A. Brady, V. Robert Page, and David G. Koenig.

6-12. NASA TM-X-644, "Large-Scale Wind Tunnel Tests at Low Speed of a Delta Winged Supersonic Transport Model in the Presence of the Ground"—David G Koenig, James A. Brady, and V. Robert Page.

6-13. NASA TM-X-15, "Low-Speed Measurements of the Static and Oscillatory Lateral Stability Derivatives of a Model of a Canard Airplane Designed for Supersonic Cruise Flight"—Joseph L. Johnson, Jr.

6-14. NASA TM-X-781, "Dynamic Rotary Stability Derivatives of a Delta-Winged Configuration with a Canard Control and Nacelles at Mach Numbers from 0.25 to 3.50"—LeRoy S. Fletcher.

6-15. NACA Report 1098, "Summary of Methods for Calculating Dynamic Lateral Stability and Response and for Estimating Lateral Stability Derivatives"—John P. Campbell and Marion O. McKinney.

6-16. NACA Report 1052, "A Summary of Lateral-Stability Derivatives Calculated for Wing Planforms in Supersonic Flow"--Arthur L. Jones and Alberta Alksne.

6-17. "Airplane Performance Stability and Control"—Courtland S. Perkins and Robert E. Hage.

6-18. NASA TM-X-533, "Some Transonic Dynamic Longitudinal and Directional Stability Param-

eters of a Canard Airplane Model Designed for Supersonic Flight"—R. Kilgore and E. Hillje.

6-19. NASA TM-X-761, "Dynamic Stability Characteristics in Pitch and in Yaw for a Model of a Variable-Sweep Supersonic Transport Configuration at Mach Numbers of 2.40, 2.98, and 3.60"—B. Delaney and W. Thompson.

6-20. NASA TM-X-600, "Wind Tunnel Measurements and Estimated Values of the Rolling Stability Derivatives of a Variable-Sweep Airplane Configuration at Subsonic and Transonic Speeds"—W. Hayes, W. Kemp, and W. Thompson.

6-21. NASA Memo 11-30-58A, "Experimental Wind Tunnel Investigation of the Transonic Damping-In-Pitch Characteristics of Two Wing-Body Combinations"—H. Emerson and R. Robinson.

6-22. NACA TN 1423, "The Stability Derivatives of Low-Aspect-Ratio Triangular Wings at Subsonic and Supersonic Speeds"—H. Ribner.

6-23. NACA RM A52L04a, "Damping in Pitch of Low-Aspect-Ratio Wings at Subsonic and Supersonic Speeds"— M. Tobak.

6-24. NASA TM-X-658, "Effects of Off-Design Inlet Mass Flow Upon Static Stability of a Delta Winged Configuration with a Canard Control and Pylon-Mounted Nacelles for Mach Numbers from 0.65 to 3.50"—A. V. Gnos and R. L. Kurkowski.

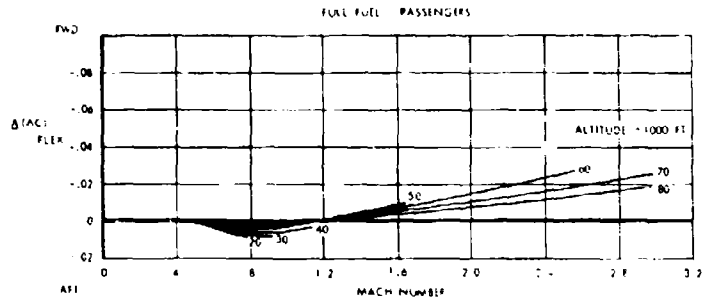

FIGURE 6-37 FLEXIBILITY CORRECTION TO AERODYNAMIC CENTER

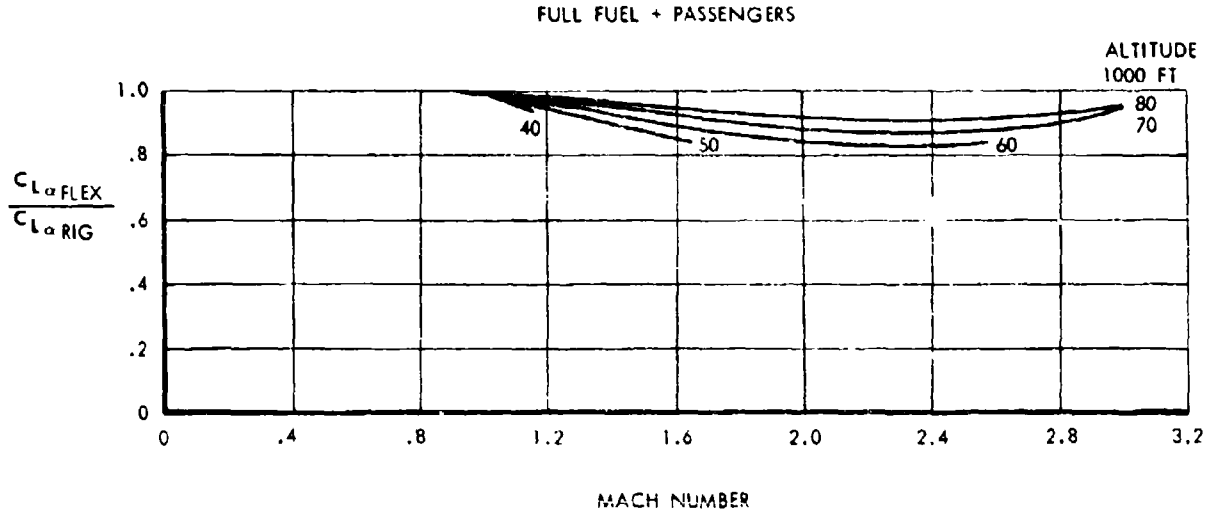

FIGURE 6-38 FLEXIBILITY CORRECTION TO LIFT CURVE SLOPE

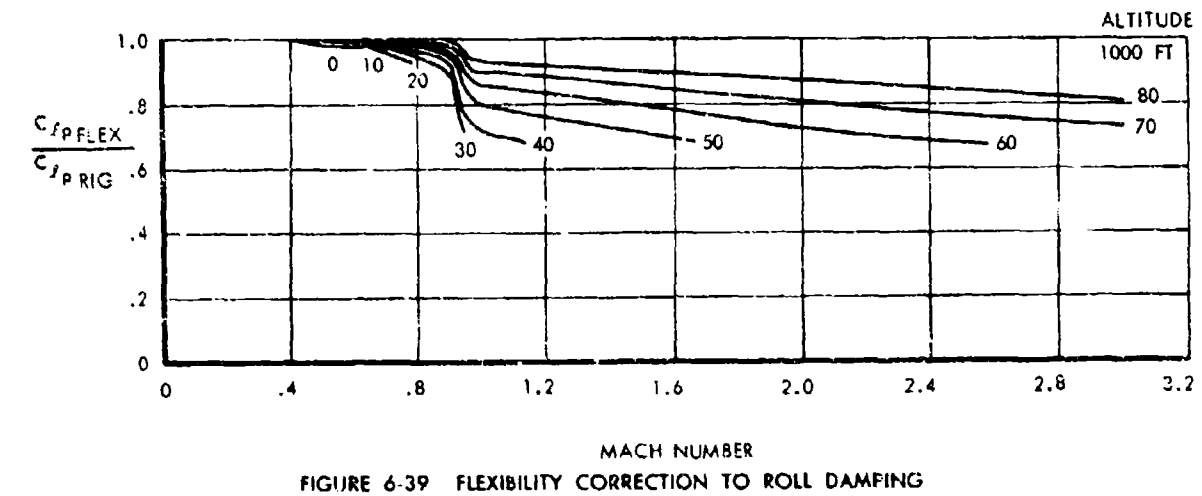

FIGURE 6-39 FLEXIBILITY CORRECTION TO ROLL DAMPING

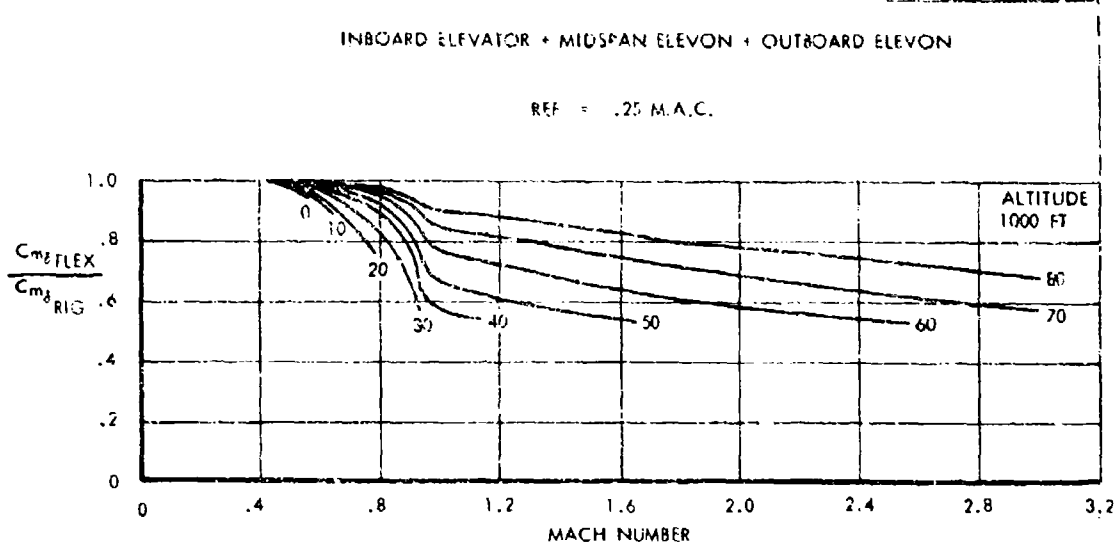

FIGURE 6-40 FLEXIBILITY CORRECTION TO ELEVATOR PITCH CONTROL

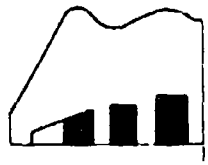

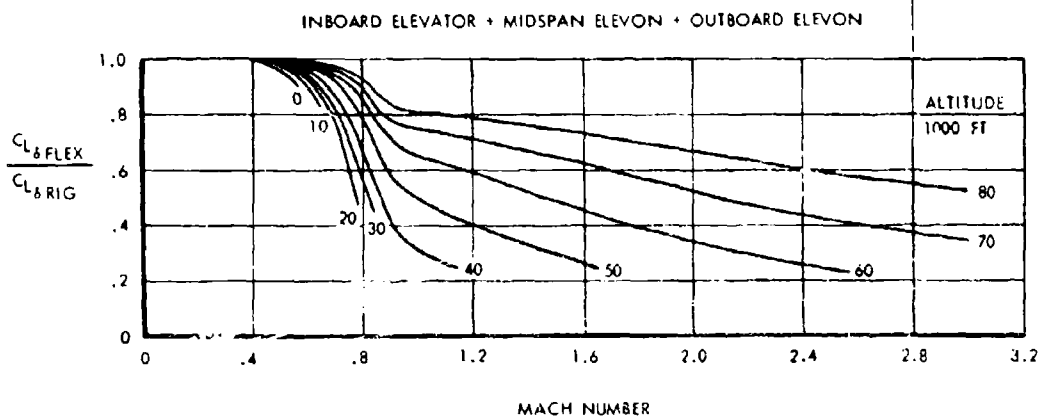

FIGURE 6-41 FLEXIBILITY CORRECTION TO ELEVATOR LIFT

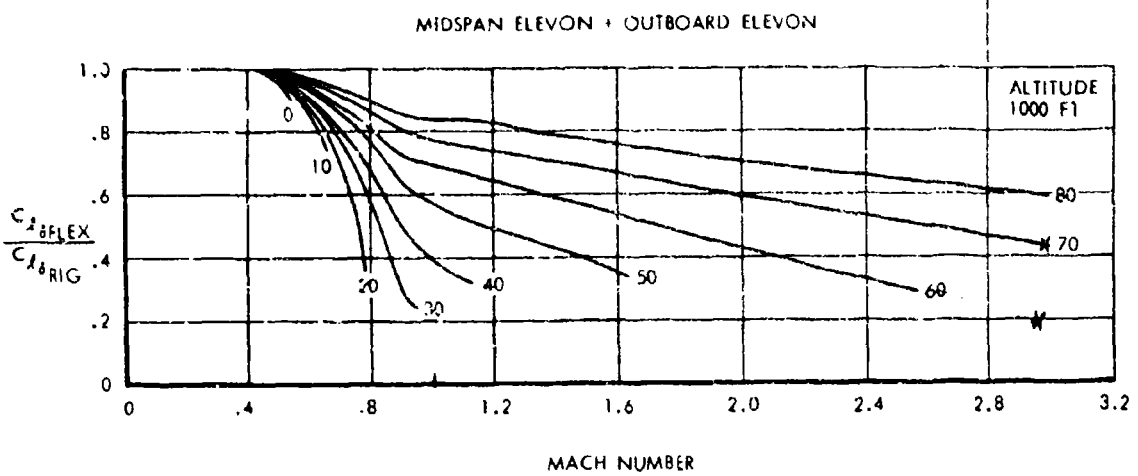

FIGURE 6-42 FLEXIBILITY CORRECTION TO ROLL CONTROL

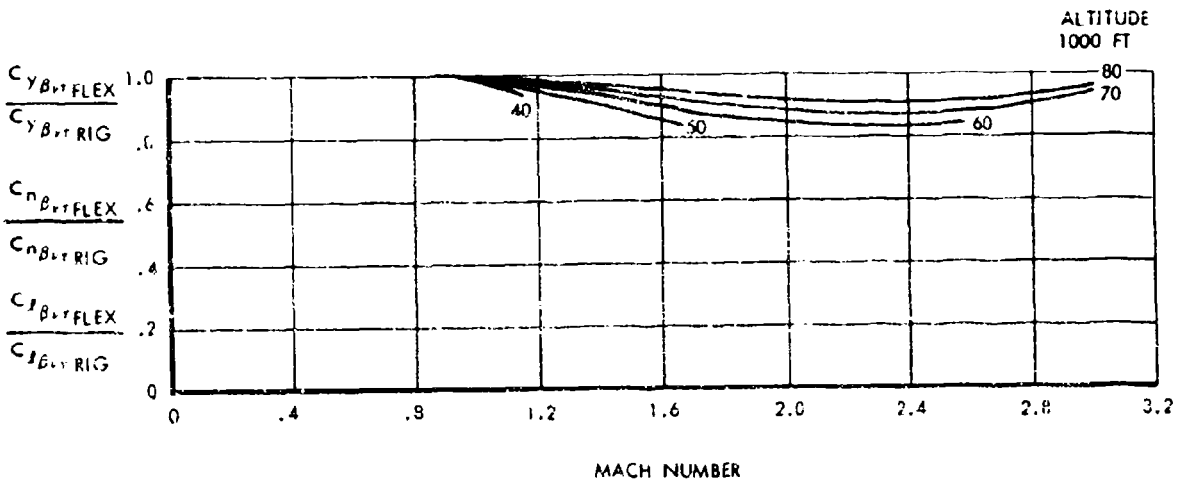

FIGURE 6-43 FLEXIBILITY CORRECTION TO VERTICAL TAIL EFFECTIVENESS

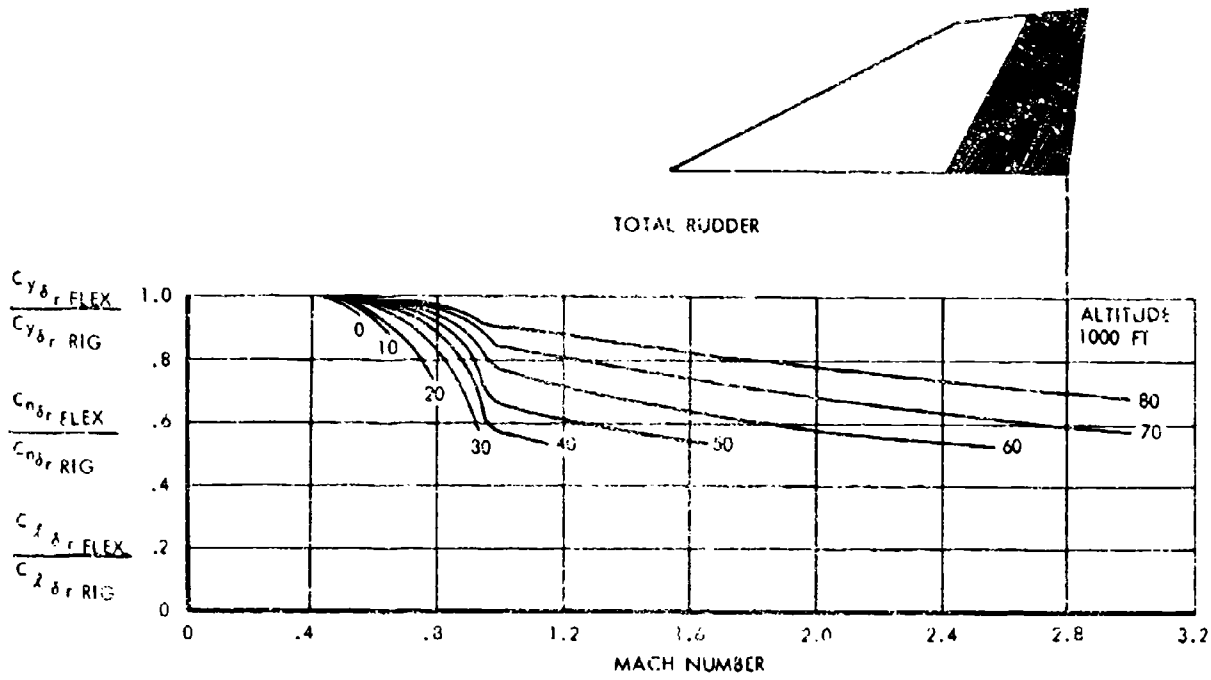

FIGURE 6-44 FLEXIBILITY CORRECTION TO DIRECTIONAL CONTROL

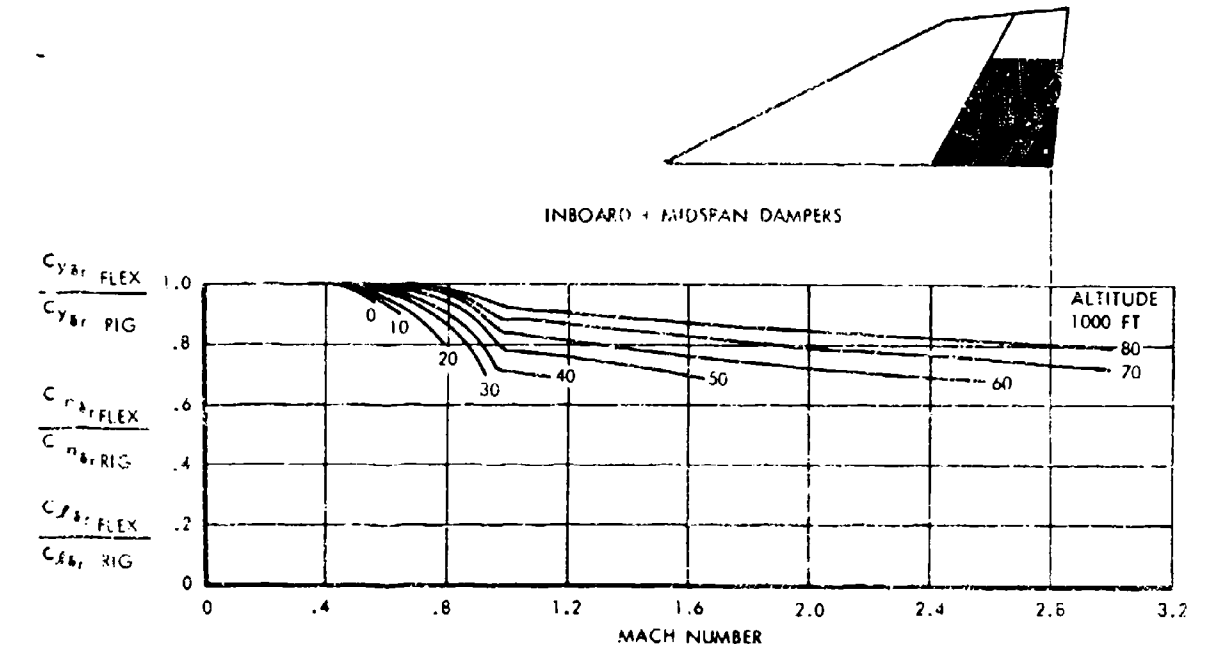

FIGURE 6-45 FLEXIBILITY CORRECTION TO YAW DAMPER EFFECTIVENESS

SECTION 7 SONIC BOOM AND AIRPORT AND COMMUNITY NOISE (3.2.7.1)

7.1 SONIC BOOM OVERPRESSURE CHARACTERISTICS (3.2.7.1)

Aircraft operating at supersonic speeds produce shock wave patterns and resultant sonic boom overpressures on the ground. Theoretical studies and correlation with limited flight test data and wind tunnel test results suggest that these overpressure intensities will increase with increasing airplane size. These observations give rise to concern regarding the sonic boom intensity generated by the SST which will be larger than any supersonic airplane in operation to date. The intensive studies devoted to this potential problem area have led to a clearer understanding of the phenomenon, and have indicated means for designing an airplane to alleviate the boom intensities that are generated. The double delta wing planform shape represents a major airplane configuration improvement from a sonic boom viewpoint. This planform shape provides a smooth airplane area progression curve, as noted previously. In addition, the long chords of the wing spread the distribution of lift along the length of the fuselage. The resultant volume and lift distribution characteristics are in the direction to reduce substantially sonic boom intensity.

Because of this improvement in airplane geometry, the SST airplane is capable of performing the design flight profile within the sonic boom overpressure limits established as guide lines by the FAA Request for Proposal. Notwithstanding, the sonic boom still assumes a vital role in establishing the climb flight profile. To meet the 2 psf climb overpressure requirement and utilizing present estimation techniques, the airplane must operate at higher than optimum acceleration altitudes from the standpoint of fuel consumption. If refined knowledge of sonic boom permitted reduced altitude acceleration as much as 4000 pounds payload could be added with takeoff at the same gross weight as a result of fuel savings.

This graphic illustration of the importance of sonic boom suggests that future efforts be expended to learn more about the boom problem, since the potential gains to be realized by further improvements are large. For a large low wing configuration, the disturbances generated by the upper fuselage will be shielded from the ground until the disturbances are propagated to the edge of the wing back along appropriate Mach lines. There will also be a change in the spanwise distribution of lift caused by the presence of the fuselage.

These effects are not now included in the sonic boom theory. Whether these refinements to the boom studies will indicate that further reductions in boom overpressures are possible is not known at this time. However, experimental measurements of overpressures generated by overflights of various aircraft at supersonic speeds have produced data with noteworthy amounts of scatter (Figure 7-1). The results may indicate that atmospheric effects alter the attenuation of the waves, or they may suggest that additional understanding of the complex wave pattern problem is needed. The importance of the boom characteristics emphasizes the need to continue exploring this area.

The sonic boom overpressures were predicted by the method developed by Carlson of NASA-Langley Research Center (Reference 7-1). Calculations were based on conditions of standard atmosphere, zero wind gradient, and non-maneuvering flight. A ground reflectivity factor of 1.9 was used for all sonic boom calculations.

Sonic boom overpressures for the SST airplane, for all pertinent flight regimes are presented in Figures 7-2 through 7-4. The carpet plot for each Mach number is the sonic boom spectrum for the configuration. Airplane operating points have been spotted on the carpets. These operating points were taken from the mission analysis program for the design mission. Throughout the supersonic climb the airplane sonic boom overpressure is slightly less than 2.0 psf and reduces to 1.5 psf at the start of cruise. During cruise the airplane's reduction in weight and gain in altitude result in a gradual lowering of the overpressure to a value of 1.2 psf at the end of cruise. Sonic boom overpressure rises during deceleration and descent, reaching a maximum value of 1.5 psf at Mach 1.2.

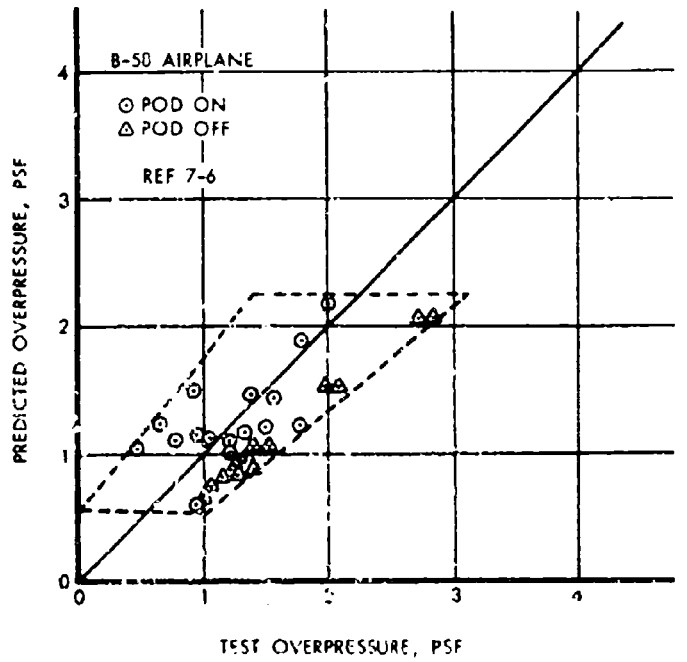

FIGURE 7-1 COMPARISON OF MEASURED AND PREDICTED SONIC BOOM OVERPRESSURES

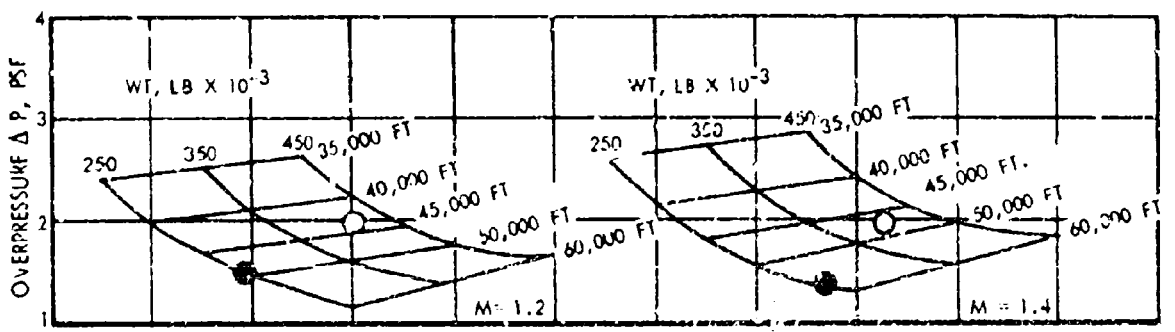

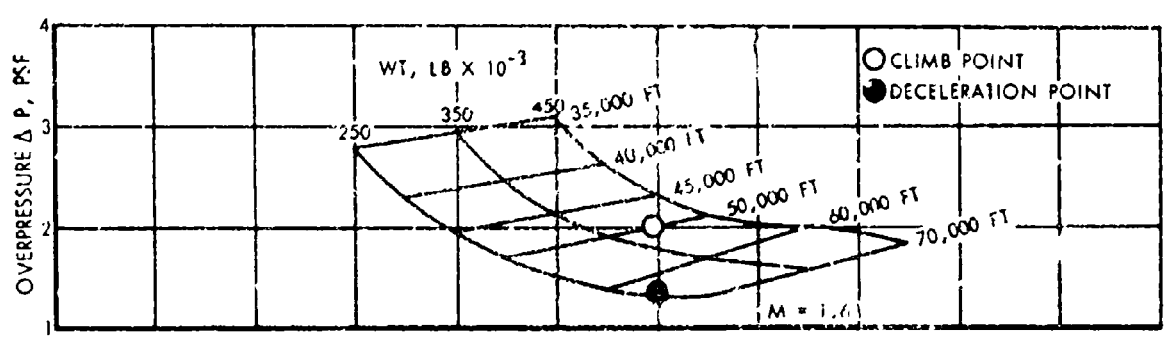

FIGURE 7-2 SONIC BOOM OVERPRESSURE, M = 1.2, 1.4, AND 1.6

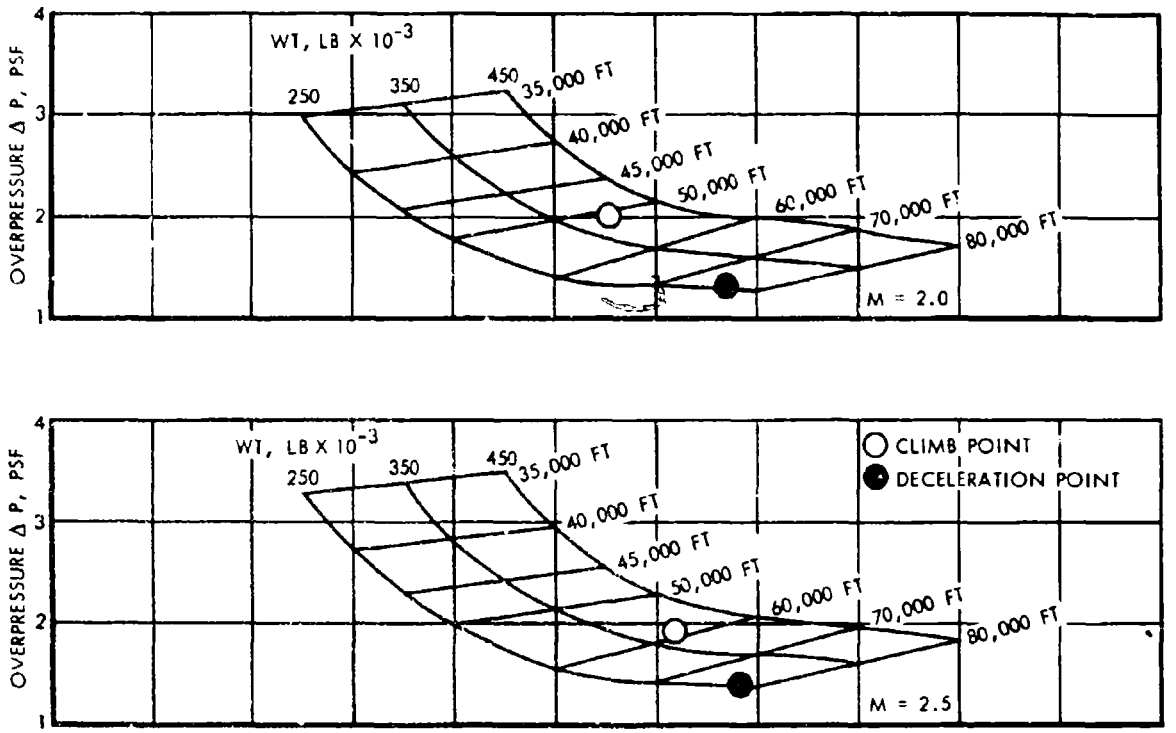

FIGURE 7-3 SONIC BOOM OVERPRESSURE, M = 2.0 AND 2.5

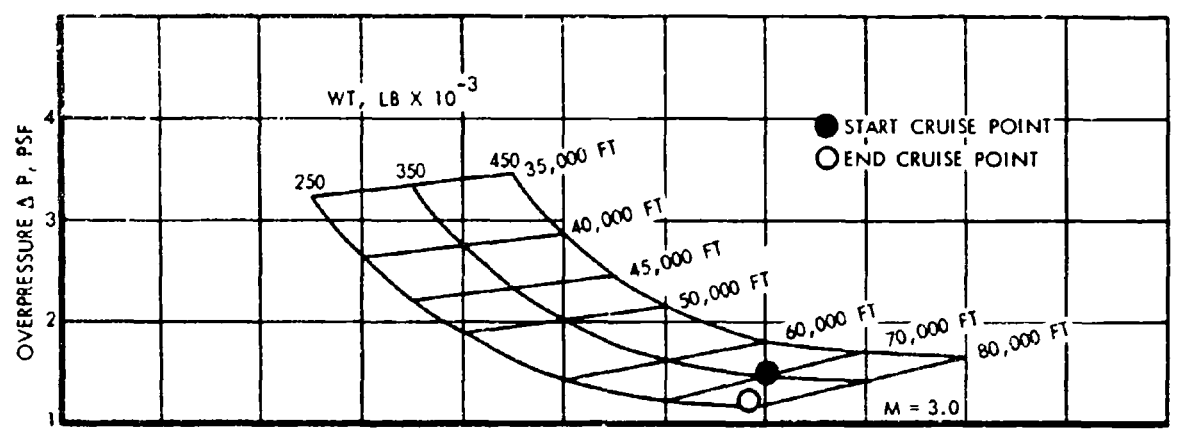

FIGURE 7-4 SONIC BOOM OVERPRESSURE, M = 3.0

Area distributions for volume inputs to the NASA sonic boom 7094 program are shown in Figure 7-5. The oblique cutting plane method of area generation was employed. A slight forward shift of area with Mach number was occasioned by the low position of the wing and nacelles relative to the fuselage. Figure 7-6 shows the lift input to the NASA program. Conical flow lift was assumed back to the leading edge break, then a smooth $B(t)$ curve was faired to the value of $B(t)$ at the trailing edge. A small lift allowance was made for the fuselage nose and afterbody. $B(t)$ maximum was calculated as $\beta W/2q$. Reference length was 220 feet.

Figure 7-7 is the airplane sonic boom parametric plot resulting from the NASA 7094 program. Solutions were obtained for both the Mach 1.4 area distribution case and the Mach 3.0 area distribution case. Differences in the two solutions were small and, as shown in the figure, were resolved by the representative solid line.

7.1.1 APPLICATION OF SONIC BOOM THEORY

Sonic boom, expressed in pounds per square foot of ground overpressure, is given by

$$\Delta P = K_r \frac{1.19\beta^{1/4}\sqrt{P_o P_A}}{h^{1/4}} \frac{\gamma}{\sqrt{\gamma+1}} \sqrt{\int_o^{T_o} F(\tau)\, d\tau} \qquad \text{(Equation 1)}$$

where

ΔP = Ground overpressure, psf

K_r = Reflection factor, 1.9

P_o = Ambient pressure at sea level, 2116 psf

P_A = Ambient pressure at airplane altitude, psf

h = Altitude, ft

γ = Ratio of specific heats for air, 1.4

$\beta = \sqrt{M^2 - 1}$

$F(\tau)$ = Function of airplane geometry and weight

T_o = Axial station for largest positive integral of $F(\tau)$

$F(\tau)$ is defined by Equation 2.

$$F(\tau) = \frac{1}{2\pi}\int_o^t \frac{A_E''(t)}{\sqrt{\tau - t}}\, dt \qquad \text{(Equation 2)}$$

where

t = Axial reference station

$\tau - t$ = Distance along the axis, from the reference station t

$A_E''(t)$ = second derivative of area $A_E(t)$ at reference station t

l = Airplane reference length

The area $A_E(t)$ is the sum of two parts: $A(t)$, the area due to volume, and $B(t)$, the area due to lift. The area due to volume corresponds to the frontal projection of the airplane oblique section areas formed by cutting planes inclined at the Mach angle. Maximum area due to lift, $B(t)_{max}$, is given by Equation 3.

$$B(t)_{max} = \frac{\beta W}{2q} = \frac{\beta}{2} C_L S \qquad \text{(Equation 3)}$$

where

W = Airplane weight, lb.

q = Dynamic pressure, psf

C_L = Lift coefficient

S = Reference area for lift coefficient

$B(t)$, at any axial station, is some percentage of $B(t)_{max}$ and depends on the integrated lift per unit length along the airplane's longitudinal axis. A typical $A_E(t)$ distribution is shown in sketch 1.

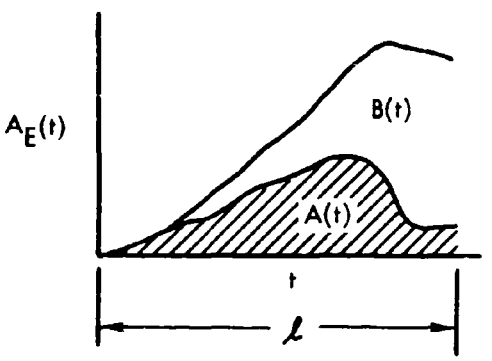

SKETCH 1.

For smooth $A_E(t)$ distributions, the $F(\tau)$ integral is influenced most strongly by the maximum value of $A_E(t)$. Ryhming and Yoler have shown the $F(\tau)$ integral to be a function of fineness ratio, length, and a shape factor:

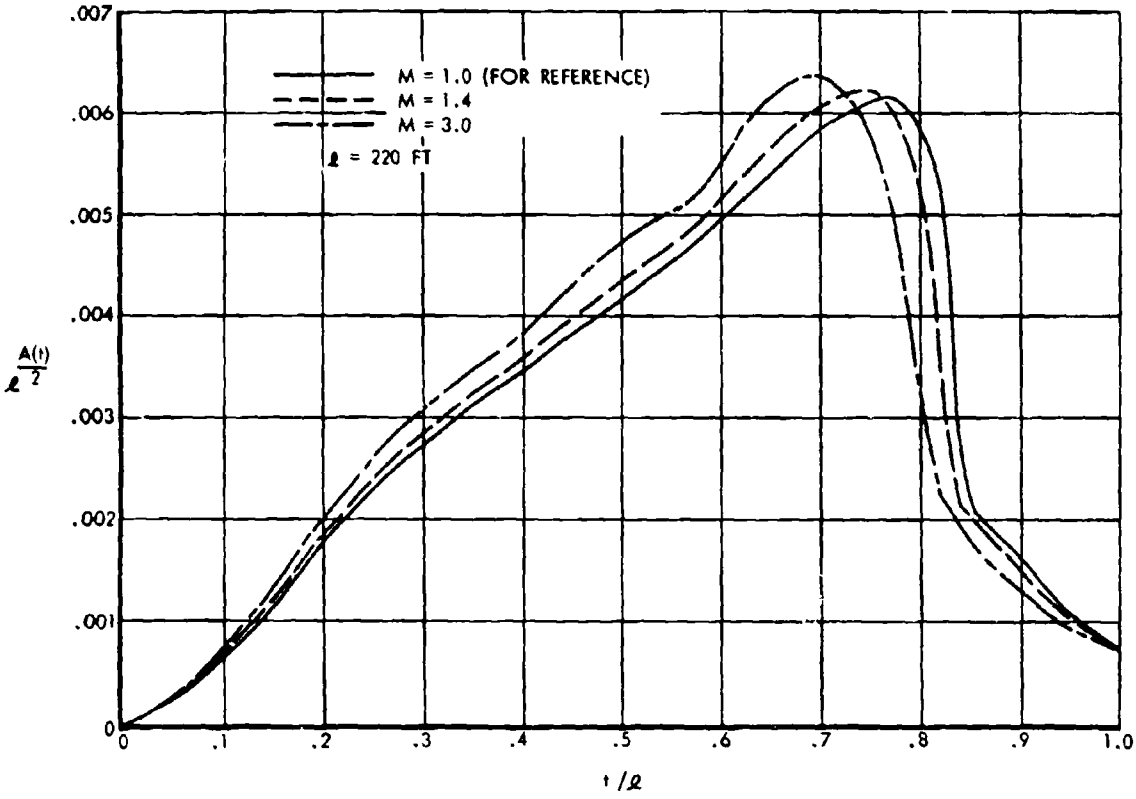

FIGURE 7-5 VOLUME FOR SONIC BOOM PROGRAM

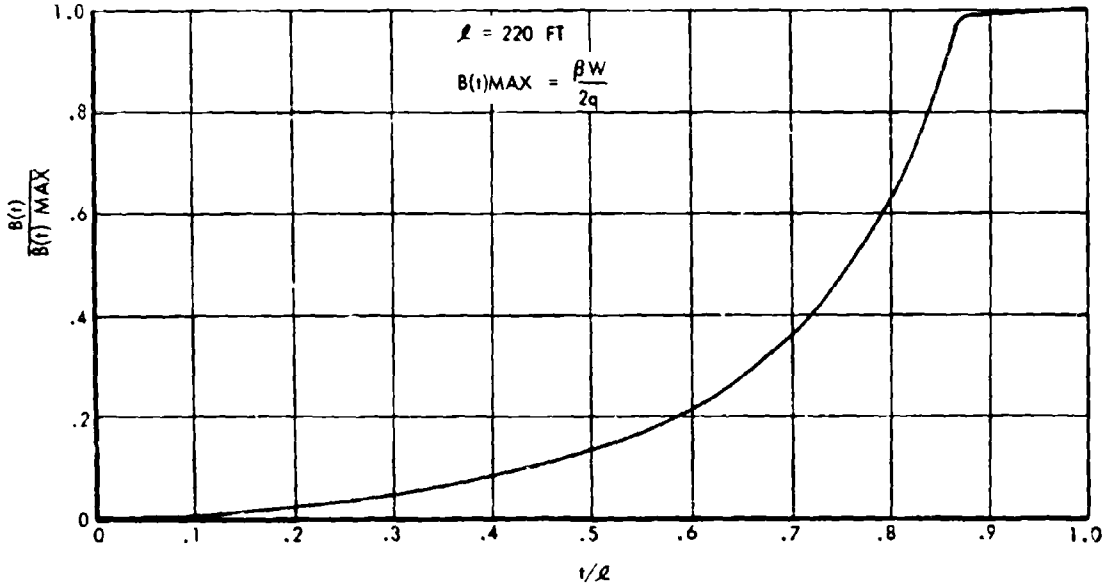

FIGURE 7-6 LIFT FOR SONIC BOOM PROGRAM

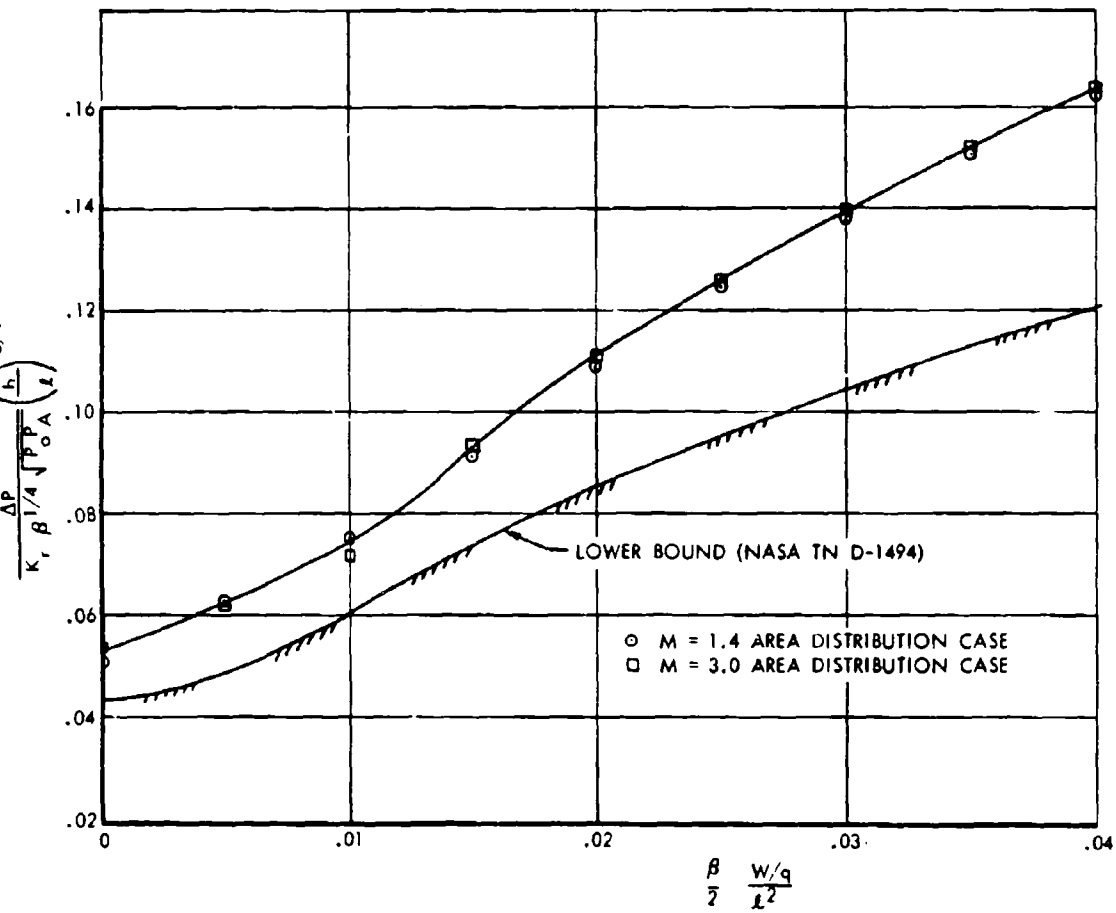

FIGURE 7-7 SONIC BOOM OVERPRESSURE PARAMETER

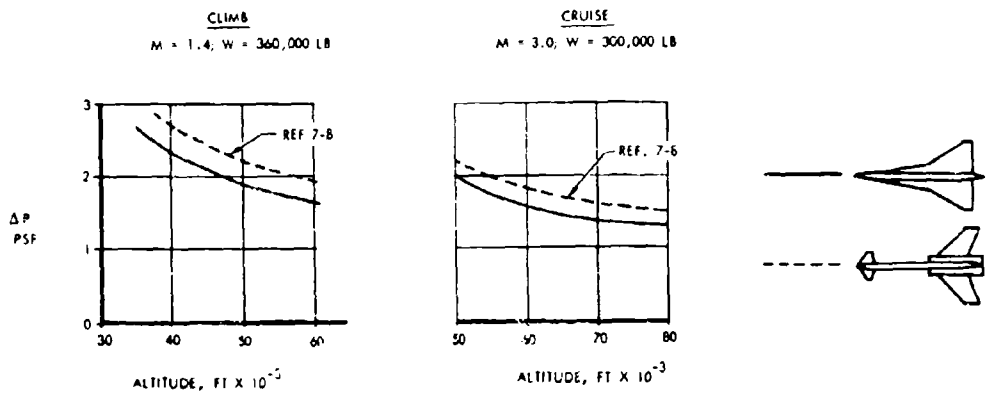

FIGURE 7-8 COMPARISON OF SONIC BOOM INTENSITY

$$\sqrt{\int_0^{\tau} F(\tau)\,d\tau} = g\left(\frac{R}{l}\right)^{1/4} \qquad \text{(Equation 4)}$$

where g is the shape factor and R is the radius corresponding to a circle of area $A_E(t)$ maximum. For a given R and l, the shape factor can influence $F(\tau)$ about 10 percent. As l appears as a multiplication factor, R becomes dominant when one is designing for low sonic boom. From sketch 1 it is seen that to hold $A_E(t)_{max}$ small, $A(t)$ must be small where $B(t)$ maximizes. Similarly, $B(t)$ must be small where $A(t)$ maximizes. The situation is very much like eating your cake and having it too. The playoff of $B(t)$ against $A(t)$ is useful only at climb Mach numbers and altitudes. At high Mach numbers and altitudes, $B(t)$ becomes overwhelmingly large, compared to $A(t)$, and renders shaping ineffectual (Sketch 2).

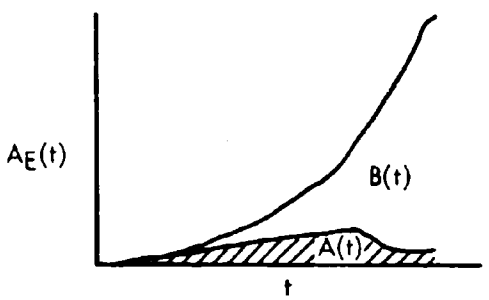

SKETCH 2.

The effect of diverging from a smooth area distribution can be shown by Sketch 3 and Equation 2.

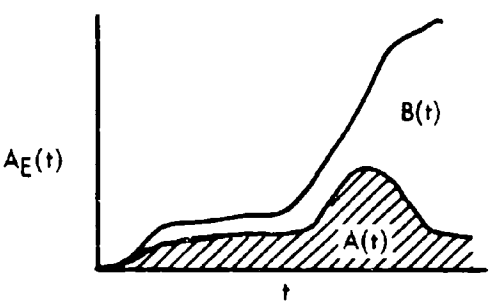

SKETCH 3.

Sketch 3 represents a "delayed-bump" configuration. The above distribution is typical of a short-chord wing located at the rear of a fuselage. Equation 2 suggests keeping $A_E''(t)$ small, when positive in sign, and negative wherever possible. For the smooth configuration of Sketch 1, the second derivative $A_E''(t)$ has a high positive value only at the nose, then goes quickly negative. For the "delayed-bump" configuration of Sketch 3, $A_E''(t)$ has a high positive value at the nose, at the start of the constant section, and again at the start of the wing.

Investigations by Carlson, of NASA-Langley, have demonstrated the sonic boom advantage enjoyed by the smooth configuration over the "delayed-bump."

Figure 7-8 demonstrates the overall sonic boom advantage of the double delta. In this figure, the sonic boom overpressures of the double-delta SST are compared to the overpressures of a "delayed-bump" airplane. Boom intensity values for the "delayed-bump" were taken from Reference 7-8 and compared to the double delta on the basis of the weight assigned in the reference. At the transonic climb condition as well as the supersonic cruise condition of Figure 7-8, the double delta shows markedly superior sonic boom characteristics. The SST was configured to give the smooth area distribution typified by Sketch 1. The double-delta wing, starting near the nose of the airplane, allows a smooth progressive build-up of volume and lift, thus providing acceptable sonic boom characteristics within a working design envelope.

Another advantage of the double delta is its low wing loading which lends important flexibility to the transonic boom-climb profile. Transonically, a highly loaded wing operates quite near the buffet limit C_L. The SST, with a lightly loaded wing can operate well below the buffet limit C_L, and can take advantage of its buffet altitude margin to adopt climb techniques tailored to meet specific community sonic boom problems.

Comparison of the SST boom parameter curve of Figure 7-7 with the minimum achievable or lower bound limit that is established in Reference 7-3 would suggest that further improvements in boom characteristics are possible. However, the lower bound limit of this reference represents a family of airplanes each designed to an optimum configuration, each at a given desired Mach number. Figure 7-9 presents a more meaningful comparison, showing the transonic acceleration and cruise sonic boom levels for the SST and

two airplanes of the lower bound family. For the SST, boom levels of 2 psf and 1.5 psf are indicated for acceleration and cruise, respectively. For a lower bound airplane optimized for Mach 1.4, the acceleration boom intensity can be lowered to 1.75 psf. However, this configuration would generate a cruise boom of approximately 1.9 psf. Similarly, another lower bound airplane optimized for cruise could reduce the cruise boom intensity to 1.1 psf, but at the expense of acceleration intensity, which would increase to 2.2 psf. It is seen, therefore, that only a moderate amount of configuration tailoring can be tolerated to minimize the boom intensity at a given Mach number, because improvements at one desired point give rise to penalties at other Mach numbers.

As noted in the introduction to this section, work must continue in the sonic boom area. Refinements of theory may lead to better understanding and indicate additional ways to tailor the airplane. Effects of longitudinal acceleration and climb flight path, as well as wind gradients, thermal gradients, and cloud formations, need to be considered. These factors could assume significant proportions that might affect flight procedures and suggest operating techniques that can alleviate the boom intensity, particularly during the transonic acceleration portion of the flight profile.

7.2 AIRPORT AND COMMUNITY NOISE

The airport and community noise problems resulting from operation of current subsonic jet transports have been sufficiently serious and extensive to make the acoustic output of any contemplated aircraft a major factor in its design and operation. This section describes the community noise aspects of the SST.

7.2.1 JET NOISE PREDICTION

All experience indicates an increase in acoustic power with an increase in mechanical power; Lighthill's theoretical derivation (References 7-9 and 7-10) of the sound power output of a jet shows a dependence on the eighth power of the exhaust velocity.

$$W = \frac{K\rho_j^2}{\rho_0}\frac{V^8}{C_0^5}d^2 \text{ watts}$$

where W = sound power radiated from jet

ρ_j = density in jet flow

ρ_0 = density of the atmosphere

V = jet velocity

d = jet nozzle diameter

K = acoustical power coefficient = constant

Laboratory measurements with cold jets and engine measurements generally have confirmed the eighth-power-of-jet-velocity law up to Mach numbers of about 2.78 and have provided values of K, the acoustical power coefficient (Reference 7-11); the reported values of K have been in the range of 3×10^{-5} to 15×10^{-5}. Rocket noise data indicate dependence on a lower power of exhaust velocity, possibly a sixth power, and some afterburner jet engine results seem to fall in a transition region between the eighth and sixth power functions.

For convenience in calculations, and in order to compress the large range of values of power that occurs, acoustic power output (W) usually is converted to a corresponding sound power level (PWL) with respect to a reference power (W_{ref}) by means of the relation

$$PWL = 10 \log_{10}\frac{W}{W_{ref}} \text{ decibels.}$$

A reference power of 10^{-13} watt is convenient to use when distances from the source are to be given in feet.

At large enough distances from the noise source so that it may be considered a point source (far field), sound pressure levels at any position may be computed from the source power level if the directional characteristics of the sound radiation and the absorption of sound in air are known. Sound pressure level, which may be measured, is defined as:

$$SPL = 20 \log\frac{P}{P_{ref}} \quad \text{decibels}$$

where P is the pressure due to the sound wave, and P_{ref} is a reference pressure, commonly 0.0002 dyne/sq. cm. The directionality of jet noise in the far field has been determined experimentally, and a composite of published results has been used for the engine noise predictions to be presented. The excess attenuation of sound with distance due to air absorption depends on the temperature and humidity of the air as well as on the sound frequency. Below about 1000 cps there is essentially no attenuation.

The effects of sound on both structures and people are dependent not only on sound pressure level, but

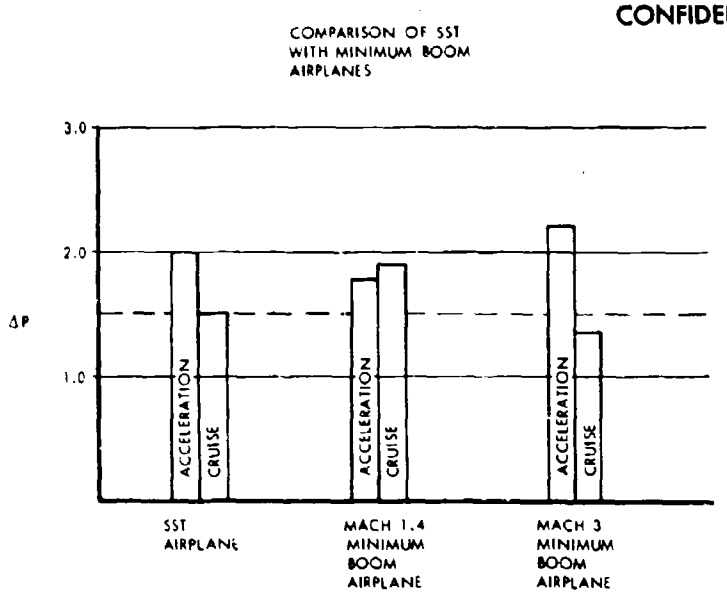

FIGURE 7-9 COMPARISON OF SST WITH LOWER BOUND AIRPLANES

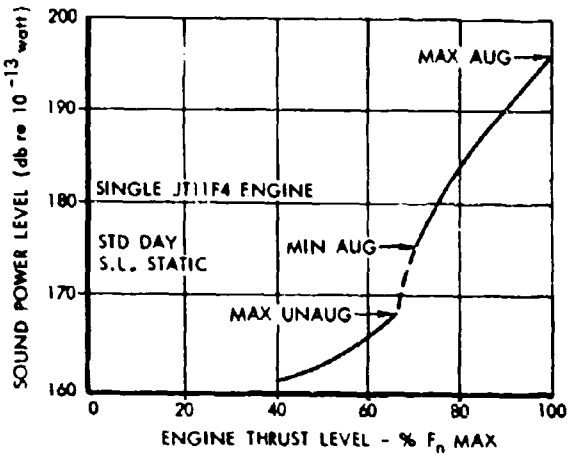

FIGURE 7-10 EFFECT OF ENGINE THRUST LEVEL ON SOUND POWER LEVEL

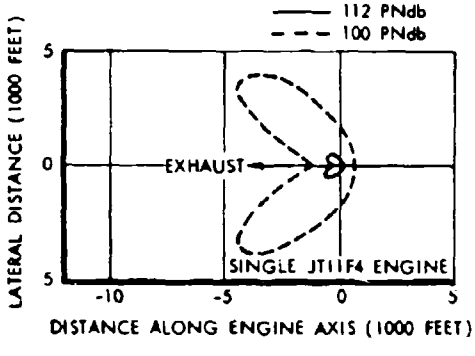

FIGURE 7-11 GROUND RUN-UP ISO-PERCEIVED-NOISE CONTOURS, MAXIMUM DRY THRUST

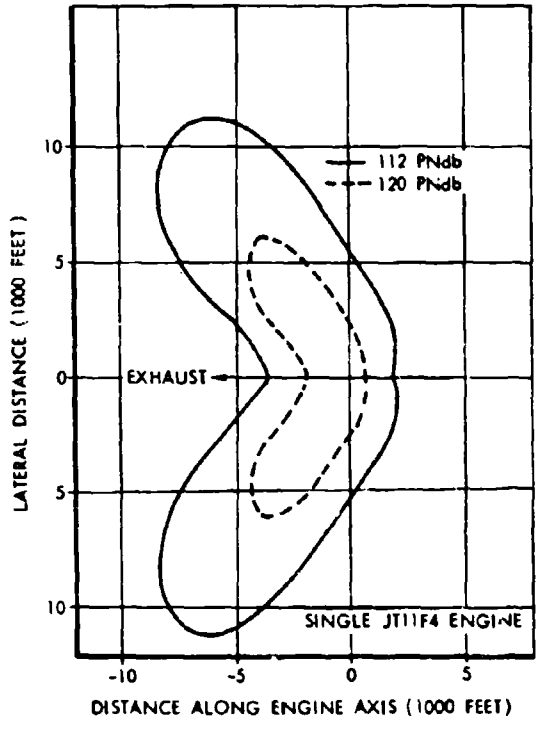

FIGURE 7-12 GROUND RUN-UP ISO-PERCEIVED-NOISE CONTOURS, MAXIMUM DUCT HEAT THRUST

aiso on the frequency distribution of the sound energy. For jet noise, which is broad band in character, frequency bands one octave wide are found to describe the frequency distribution adequately. Octave-bands have an upper frequency bound twice the lower, and a set of eight such bands, extending from 37.5 — 75 to 4800—9600 cycles per second, is commonly used to cover the major portion of the audible range. Prediction of the octave-band distribution of the noise from a particular jet may be done from an experimentally determined frequency distribution curve by fixing the position of maximum frequency from the peak Strouhal number.

$$S_0 = \frac{f_{max} D}{V}$$

where f_{max} = peak of sound spectrum

D = diameter of nozzle

V = jet exit velocity

The peak Strouhal number has been found to be approximately constant for a number of jets.

When the octave-band sound pressure levels are known for the noise at some location, it is possible to compute a quantity known as "perceived noise level," which is a measure of human reaction to sound (References 7-12 and 7-13). The unit of perceived noise level is the PNdb. At 1000 feet from a large propeller airliner at takeoff power the perceived noise level is about 103 PNdb; at 100 ft. from a 40 mph freight train it is about 93 PNdb. A noise requirement for the supersonic transport is stated in the Final FAA RFP of August 15, 1963 (Paragraph 2.6.1). The requirement is that takeoff noise shall be less than 112 PNdb at a point on the ground one statute mile from the departure end of a 10,500 foot runway. This point shall be referred to as the three-mile point. A perceived noise level of 112 PNdb has been set as a general goal for noise at a one mile distance in a racetrack pattern about the airport runway.

7.2.2 PREDICTED NOISE FOR THE JT11F-4 ENGINE

The techniques outlined above, with engine parameters supplied by the manufacturer, have been used to predict the acoustic output of the Pratt & Whitney JT11F-4 engine and the noise environment about an SST equipped with four such engines. Eighth-power law has been utilized, although it is felt that at high thrust levels the predicted sound power is appreciably higher than will actually be encountered. However, until at least model test data become available, there is no basis for determining sound power by other than the eighth power law. A change from an eighth power of velocity to a sixth power of velocity relationship would reduce the predicted sound power output at full sratic engine thrust by about 10 db. Another factor, not included in the computations, which would tend to lower the sound output is mixing of primary exhaust with duct exhaust and the mixing of ejector air with duct exhaust. Complete mixing of the ejector air could give an additional 2 db reduction in predicted sound power level and, because of change in spectrum, an even larger change in perceived noise level.

7.2.2.1 Acoustic Output of JT11F-4 Engine

The computed source-sound level for a single JT11F-4 engine as a function of engine thrust level for sea level static operation is shown in Figure 7-10. Four-engine sound power levels may be obtained by adding 6 db to single engine values (a 3 db increase for each doubling of sound power). Static operation gives the highest noise levels; relative velocity of the jet exhaust with respect to the ambient atmosphere decreases with forward motion of the aircraft and, consequently, generated noise decreases.

7.2.2.2 Ground Run-up Noise

The iso-perceived-noise-level contours of Figures 7-11 and 7-12 indicate the noise environment that will exist during ground run-up. For unaugmented engine operation, noise levels are moderate; one mile from the engine, noise is below 100 PNdb. With maximum duct heating, noise levels are much higher, with a value of 112 PNdb at a distance of two miles from the engine. To maintain desirable airport noise levels a ground run-up suppressor will be necessary in the engine maintenance areas. At least 10 db attenuation will be needed at maximum thrust operation to ensure 112 PNdb at a one-mile distance.

7.2.2.3 Take-off Noise

For many airport facilities, community reaction to aircraft engine noise must be considered during the

climb-out phase of the take-off operation. The SST utilizes a large fixed wing with very light wing loadings which, combined with a high thrust-to-weight ratio, results in a high level of take-off and climb performance. For a standard plus 15°C hot day at sea level, the take-off distance using maximum reheat thrust is only 8,150 feet at the maximum take-off gross weight of 450,000 pounds. This short take-off distance, coupled with the excellent four-engine climbout profiles achieved with full power, places the aircraft at a relatively high altitude when it reaches the one-mile point from the departure end of the runway. When nearing this point, thrust can be reduced and the perceived noise level can be lowered below the 112 PNdb criterion level specified in the FAA Request for Proposal. Climb gradients available after power cutback exceed CAR requirements.

For some airport facilities, the use of maximum augmented thrust may be undesirable because of the noise levels generated during the ground-roll phase of the take-off. The SST can operate from these facilities by utilizing a *"noise abated"* reduced thrust procedure for take-off. Partial duct heating is employed for normal four-engine take-offs to the one mile from the runway point, where power is reduced to minimum duct heating. This reduced power take-off increases field lengths somewhat, but reduces the engine noise levels to the extent that 112 PNdb is never exceeded at any point one mile from the runway, in any direction. In the event of an engine failure at or above the critical decision speed V_1, full duct heating is applied to the remaining engines with a four-second time allowance to reach maximum thrust and this power utilized for the remainder of the take-off operation. The FAA take-off distance using this noise abatement procedure for a standard plus 15°C day at sea level is 9,750 for the maximum take-off weight of 450,000 pounds. Available climb gradients exceed the FAA requirements.

The perceived noise level contours for a maximum augmented power take-off are shown in Figure 7-13 for a maximum-gross weight take-off on a standard day. For this type take-off the noise levels one mile to the side of the runway are in excess of 120 PNdb. The noise at one mile past the runway end is maintained at and below 112 PNdb by reducing engine thrust to 72 percent of maximum at an altitude of 1430 feet.

A standard noise abatement take-off, which keeps both airport noise and community noise at desirable levels, may be made at 79 percent of maximum duct heating. The maximum-perceived-noise-level contours of Figure 7-14 show 112 PNdb or less along the perimeter of a rectangle with sides one mile from the runway. Measured acoustic data (Reference 7-14) for an airliner with current type fan engine (JT3D-1) indicate similar noise levels although the current engine operates at a much lower take-off thrust. The reduced power take-off still requires a power cut-back, to minimum duct heating at an altitude of 850 feet, to meet the three mile point specification. The climb gradient after cut-back is still above 0.03 (see Section 5).

Octave-band sound-pressure-level spectrums are presented in Figure 7-15 for noise one mile from the runway center line at the point of maximum noise. Both maximum thrust and noise-abatement take-off are considered; the over-all sound pressure levels are 124 db and 109 db (re 0.0002 dyne/sq. cm.) respectively. The maximum-thrust spectrum gives a perceived noise level of 126 PNdb, the 79%-thrust spectrum, 112 PNdb.

A time history of the perceived noise at the three-mile point (Figures 7-16 and 7-17) shows the manner in which the noise drops at power cut-back and then rises again to a maximum of 112 PNdb. It is realized, of course, that the thrust cut-back will not be instantaneous, so that the drop in noise will not be as abrupt as shown. Too sharp a drop in noise would be as disturbing as higher levels. If no cut-back were resorted to, then perceived noise would be above 112 PNdb for about 16 seconds with a full power take-off and for about 8 seconds for a 79 percent thrust take-off.

7.2.2.4 Approach Noise

Noise in the vicinity of the airport during landing approach is expected to be determined by the acoustic output of the compressor radiated from the inlet. Compressor-generated noise is found to vary with blade-tip Mach number and, based on a current empirical relationship, the sound power output of the compressor for the JT11F-4 engine has been estimated at 174 db re 10^{-13} watt with the energy in the highest three octave-bands. It is expected that the compressor will be improved, so far as noise generation is concerned, over current models (Reference 7-15). In addition, it is expected that at least 20 db attenuation in the critical high frequency bands can be provided by the inlet. Further attenuation could be accomplished by the use of a sonic inlet. The duct burning

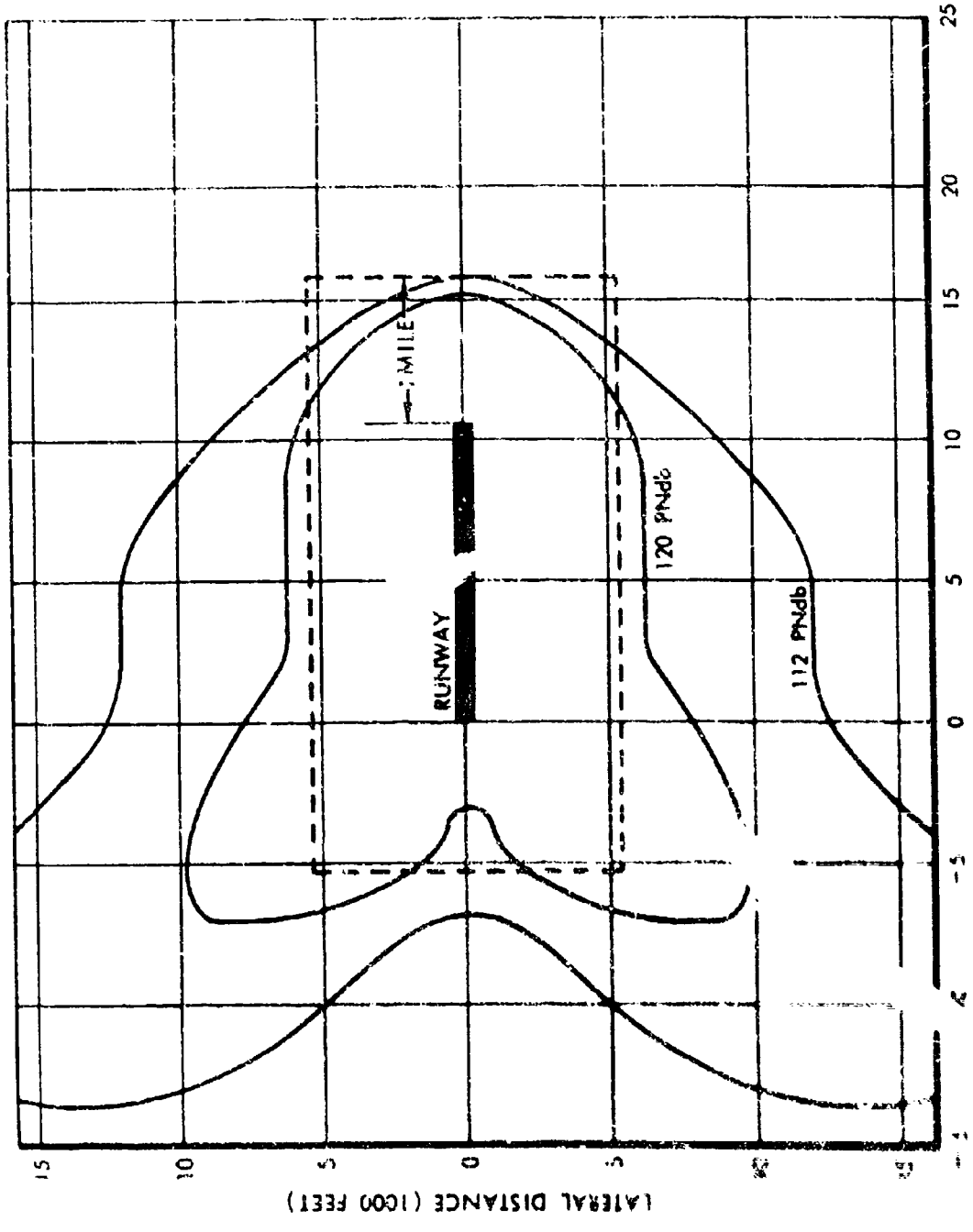

[illegible] CONTOURS FOR MAXIMUM THRUST TAKE-OFF WITH CUT-BACK TO 72 PERCENT THRUST AT 1430 FEET ALTITUDE

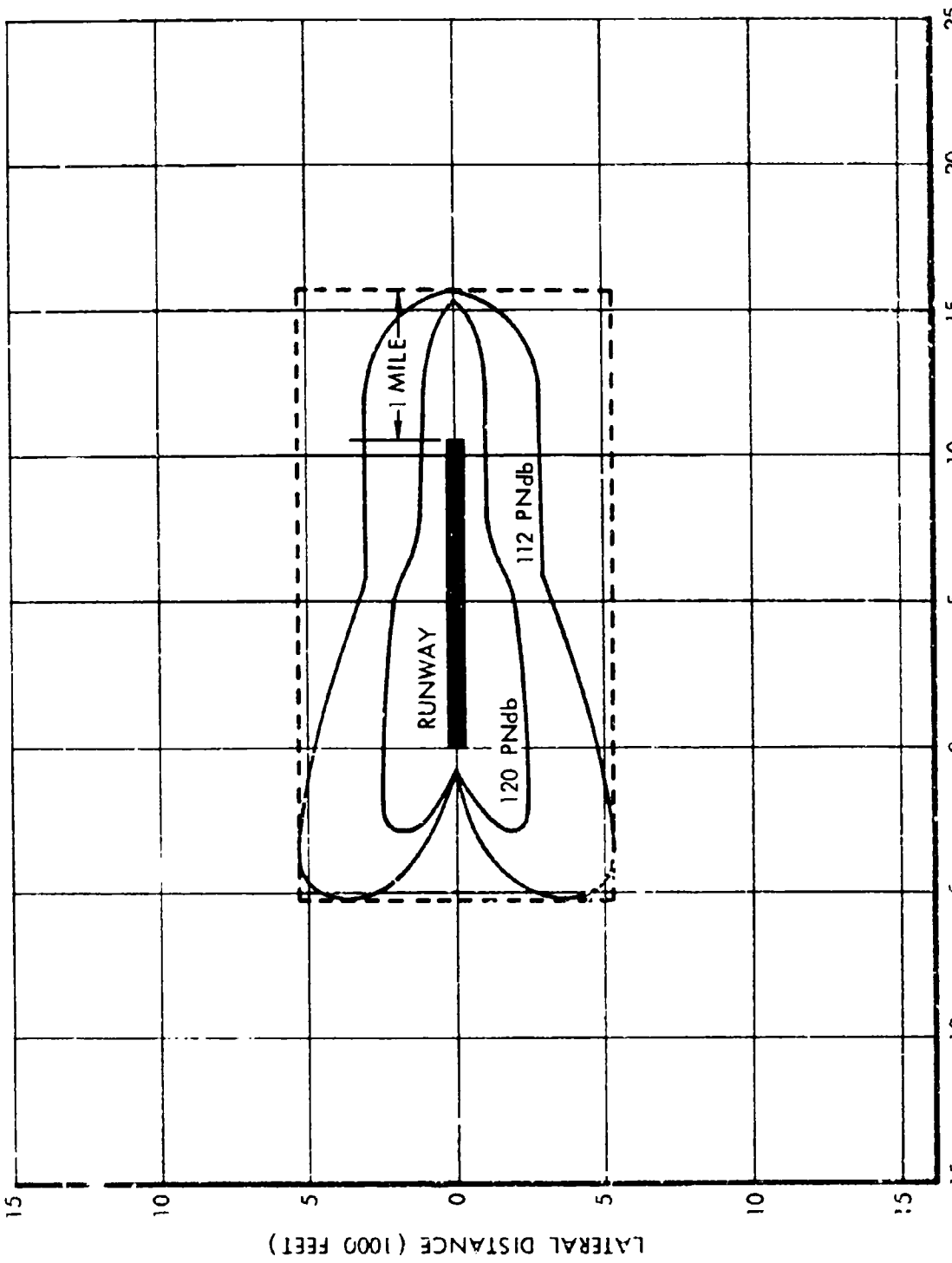

FIGURE 7-14 MAXIMUM-NOISE CONTOURS FOR NOISE ABATEMENT TAKE-OFF WITH CUT-BACK TO MINIMUM DUCT HEAT THRUST AT 850 FEET ALTITUDE

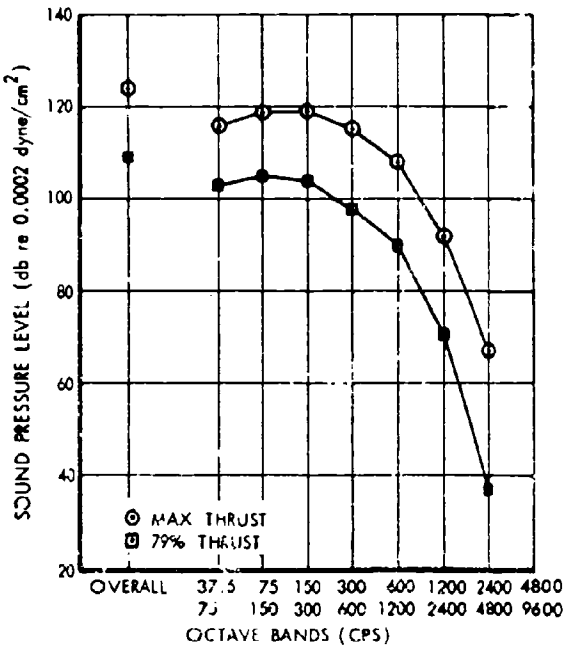

FIGURE 7-15 MAXIMUM JET NOISE ONE MILE FROM RUNWAY CENTERLINE DURING TAKE-OFF

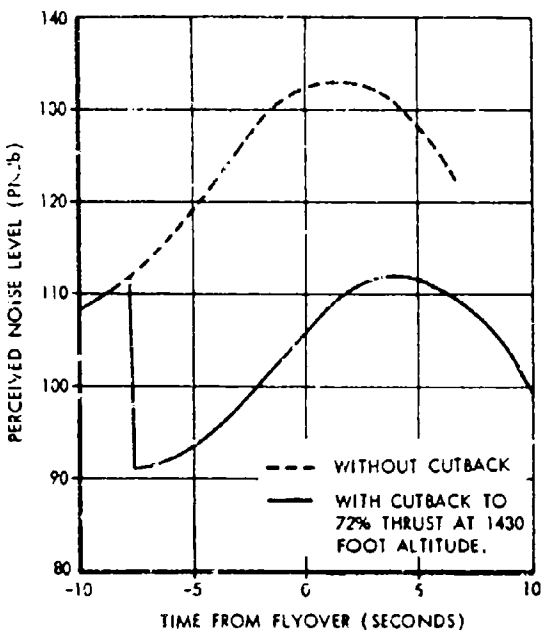

FIGURE 7-16 VARIATION OF NOISE WITH TIME AT POINT ONE MILE PAST END OF RUNWAY FOR MAXIMUM THRUST TAKE-OFF

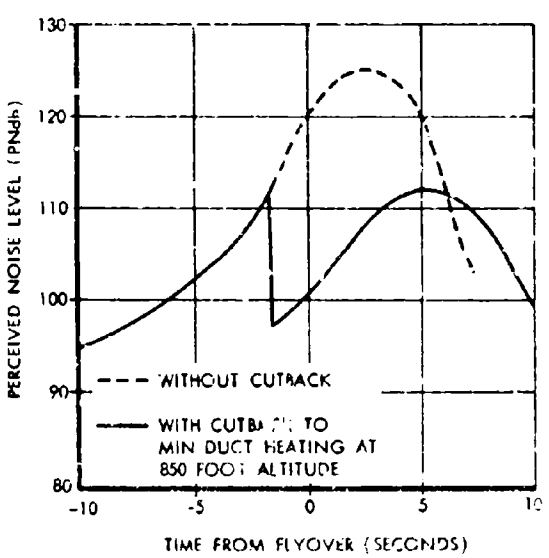

FIGURE 7-17 VARIATION OF NOISE WITH TIME AT POINT ONE MILE PAST END OF RUNWAY FOR 79 PERCENT THRUST, NOISE ABATEMENT TAKE-OFF

and exhaust systems are expected to reduce compressor noise from the nozzle to below exhaust noise.

For approach condition, the power level output of the exhaust from the four engines will be 158 db compared with 160 db for the four compressors. Because of the high frequency characteristic of the inlet-radiated sound, the perceived noise level at a point one mile from runway start will be appreciably higher for inlet noise than for exhaust noise. The octave-band spectrums of Figure 7-18—sound pressure levels at the one-mile point at flyover—show the relative levels of compressor noise, inlet-attenuated noise, and exhaust noise. Contours of maximum perceived noise on the ground below the approach path (Figure 7-19) show that a maximum of 112 PNdb will be heard at the one-mile point with the planned minimum inlet attenuation. This is at least 5 PNdb less than the noise computed from data on current airliners (Reference 7-14). A time history of approach noise at the one-mile point (Figure 7-20) shows both inlet noise and the limit that could be reached if compressor noise were reduced to levels below those of the exhaust noise.

7.3 REFERENCES

7-1. Carlson, Harry W.: An Investigation of the Influence of Lift on Sonic-Boom Intensity by Means of Wind-Tunnel Measurements of the Pressure Fields of Several Wing-Body Combinations at a Mach Number of 2.01. NASA TN D-881, 1961.

7-2. Carlson, Harry W.: Wind-Tunnel Measurements of the Sonic-Boom Characteristics of a Supersonic Bomber Model and a Correlation with Flight-Test Ground Measurements. NASA TMX-700, 1962.

7-3. Carlson, Harry W.: The Lower Bound of Attainable Sonic-Boom Overpressure and Design Methods of Approaching this Limit. NASA TN D-1494, 1962.

7-4. Ryhming, I. L.: The Supersonic Boom of a Projectile Related to Drag and Volume. Boeing Doc. D1-82-0023, 1959.

7-5. Ryhming, I. L. and Yoler, Y. A.: Supersonic Boom of Wing-Body Configurations. Boeing Doc. D1-82-0034, 1959.

7-6. Hutchinson, Herbert A.: Defining the Sonic-Boom Problem. *Astronautics and Aerospace Engineering*, December 1963.

7-7. Carlson, H. W.: A Numerical Evaluation of Sonic-Boom Theory. Presented at NASA SCAT Conference, Langley, Virginia, Sept. 17-19, 1963.

7-8. Carlson, H. W.: The Influence of Airplane Configuration on Sonic-Boom Characteristics. Presented at the AIAA-ASD Vehicle Design and Propulsion Meeting, Dayton, Ohio, Nov. 4-6, 1963.

7-9 Lighthill, M. J. "On Sound Generated Aerodynamically, Part 1: General Theory" Proc Roy Soc London 211A, pp 564-87 (1952).

7-10 Lighthill, M. J. "On Sound Generated Aerodynamically, Part II: Turbulence as a Source of Noise" Proc Roy Soc London 222A pp 1-32 (1954).

7-11 Sperry, W. C., Ramo, K., and Peter, A. "Experimental and Theoretical Studies of Jet Noise Phenomena" Report No. ASD-TDR-62-303, June 1962.

7-12 Beranek, L. L., Kryter, K. D., Miller, L. N., "Reaction of People to Exterior Aircraft Noise" NOISE CONTROL 5 No. 5, September 1959.

7-13 Kryter, K. D. and Pearsons, K. S., "Judgement Tests of the Sound from Piston, Turbojet, and Turbofan Aircraft" SOUND 1 No. 2 March–April, 1962.

7-14 Marsh, A. H. and McPike, A. L., "Noise Levels of Turbojet and Turbofan-Powered Aircraft" SOUND 2 No. 5 p 8, Sept.–Oct. 1963.

7-15 Private Communication, Pratt & Whitney Aircraft to Lockheed-California Company, November 18, 1963.

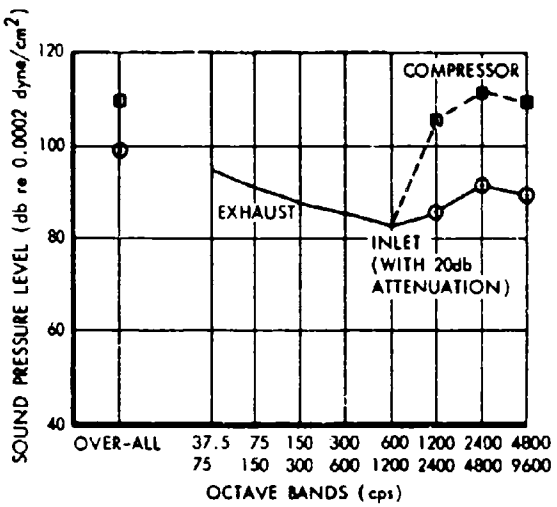

FIGURE 7-18 NOISE DURING LAND APPROACH AT POINT ONE MILE BEFORE START OF RUNWAY

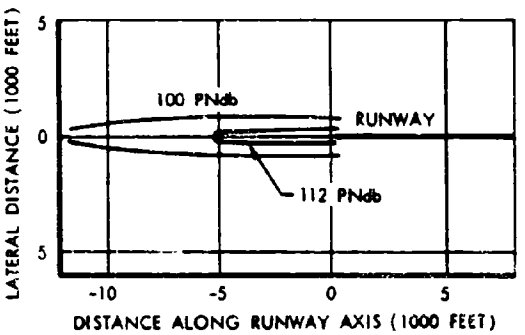

FIGURE 7-19 MAXIMUM-NOISE CONTOURS FOR LANDING APPROACH

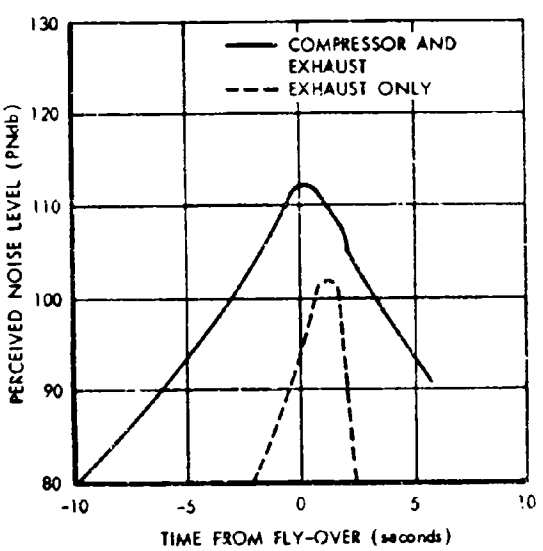

FIGURE 7-20 TIME HISTORY OF APPROACH NOISE AT POINT ONE MILE BEFORE START OF RUNWAY